Microbial Adaptation to Antibiotic Treatment Both in the Lab and the Clinic

Submitted by

Emily Wood

to the University of Exeter as a thesis for the degree of Doctor of Philosophy in Biological Sciences

March 2021

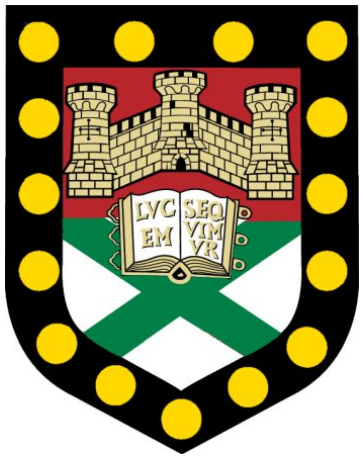

Signature .....

Abstract

Despite the use of antibiotics in modern medicine for nearly a century, there is still much to learn about how bacteria respond and adapt to these commonly used drugs. Furthermore, antibiotic treatments in patients can span weeks or even months, therefore it is crucial to understand how pathogens evolve to antibiotics within the human body over time. This thesis comprises two parts, with the first exploring the impact that antibiotics have on bacterial growth and viability during nutrient starvation through experimental evolution and the second investigating the genomes of multidrug-resistant pathogens acquired from patients suffering with chronic infection.

Initially in chapter two we demonstrate how ribosome-targeting antibiotics such as doxycycline and erythromycin can actually be beneficial for *Escherichia coli*, both through the stimulation of growth and improved long-term viability in an environment starved of nutrients. This is not true for all antibiotics though, as antibiotics with alternative cellular targets (rifampicin and penicillin) do not confer the same benefits. Given that antibiotics are primarily associated with negative impacts on bacterial growth, this is a surprising finding and we sought to identify the mechanism. Whole genome sequencing was performed on doxycycline-exposed populations of *E.coli* as they went through starvation, as well as the use of a GFP-tagged promoter library to study short-term metabolic changes occurring as nutrients are depleted. Following this, we demonstrate the influence that ribosome production has on long-term viability through the use of *E.coli rrn* knockout strains. Through doing so, we show that interference with ribosome functioning can improve long-term viability in nutrient starved environments, mirroring the effects of ribosome-targeting antibiotics.

Chapter four is dedicated to understanding the effects of genomic background on doxycycline-induced benefits in *E.coli*. Through the use of the keio library, over 2,500 individual growth curves were generated, consisting of growth data in both the presence and absence of doxycycline. Principle component analysis was subsequently

carried out, and groups of strains associated with particular phenotypes were assigned into functional categories. Through doing so we uncover some unexpected phenotypes, for example *E.coli* knockout strains that are only able to grow in media containing doxycycline.

Finally, chapters five and six explore the genomes of pathogenic bacteria during long-term antibiotic treatment. Bacteria evolve resistance towards antibiotics within laboratory experiments in a matter of days, but how do pathogens adapt to repeated antibiotic treatment within the human body? *Klebsiella pneumoniae* and *E.coli* isolates spanning 18 and 26 months respectively were acquired from two different patients and characterised through the use of nanopore sequencing and phenotypic studies. Nanopore sequencing allowed the resistomes of these pathogens to be elucidated, as well as genomic variations and structural changes. Whilst the *K.pneumoniae* isolates were found to be clonal, thereby allowing genomic changes to be tracked over time, the *E.coli* isolates were found to belong to different clonal groups. Comparative genomics was therefore carried out on these isolates to assess the genomic variability between isolates and determine the genetic basis for antibiotic resistance.

In summary, this thesis describes a novel, beneficial effect of ribosome-targeting antibiotics on long-term bacterial viability. Whilst an antibiotic may be effective in the short-term, over long periods it may actually stimulate bacterial growth. This has implications not only on the clinical use of antibiotics, but also on our understanding of natural antibiotic production in the environment. Additionally, this thesis builds upon our knowledge of within-host evolution of pathogens and demonstrates the ability of nanopore sequencing to elucidate resistomes. Alongside phenotypic data, genomics can be a powerful tool in determining the antimicrobial resistance profile of pathogens, particularly in complex clinical cases such as those presented here.

Acknowledgments

First I would like to thank my supervisors, Robert Beardmore and Ivana Gudelj for their constant support, guidance and patience over the course of this PhD. I have had the privilege of working alongside some wonderful people at Exeter - thank you to Carlos Reding-Roman, Lisa Butt, Richard Lindsay, Olga Nev, Phillipa Holder and Alys Jepson not only for your expertise and advice, but also for making these past few years so enjoyable.

Starting my PhD back in 2015, I couldn't have foreseen that my final stages of research and writing would coincide with a global pandemic. It has been challenging and seemingly impossible at times, and I am forever grateful to my friends, family and supervisors for the support that they have offered. I am particularly thankful to my son Finley. Fin has always been part of my academic journey, from attending undergraduate lectures whilst pregnant, to now finishing my PhD eight years later. There is no doubt that carrying out research whilst parenting is difficult, as I am sure many others will agree. This pandemic has brought with it the additional challenge of homeschooling for most of my final year, the thought of which initially filled me with terror! However, I feel incredibly lucky to have such a kind and considerate boy who has made the whole ordeal that much easier. There is nothing quite like his little smile to keep me grounded at the end of a stressful day.

These past few years would have been significantly harder if it wasn't for my mum and step-dad due to the never-ending childcare (and pep talks!). Thank you also to my wonderful dad for reminding me to stay curious about the world and inspiring me into a career in science.

Finally, my husband Dan. I am forever grateful to have had him by my side on this journey, celebrating my wins but also comforting me when life gets tough. I truly couldn't have done it without him.

Contents

List of Figures

List of Tables

Abbreviations

MIC : Minimal inhibitory concentration

OD : Optical density

CFU: Colony forming units

GFP: Green fluorescent protein

WT: Wild type

AMR: Antimicrobial resistance

Dox : Doxycycline

Ery : Erythromycin

Rif : Rifampicin

Pen : Penicillin

KPC: *Klebsiella pneumoniae* carbapenemase

M9 : M9 minimal media

LB : Lysogeny broth

MLST: Multilocus sequence type

ST: Sequence type

SNP: Single nucleotide polymorphism

Indel: Insertion/deletion

WGS: Whole genome sequencing

CNV: Copy number variation

TCA: The tricarboxylic acid cycle, otherwise known as the citric acid cycle

TEM: Temoneria β-lactamase gene

SHV: Sulfhydryl variable β-lactamase gene

CTX-M: Cefotaxime Munich β-lactamase gene

OXA: Oxacillinase β-lactamase gene

M9CAA : M9 minimal media supplemented with 0.1% casamino acids, and unless otherwise stated, 0.2% glucose i.e. defined minimal media.

ROS : Reactive oxygen species

461

CHAPTER ONE

INTRODUCTION

The discovery of antibiotics in the early 20th century marked a turning point for modern medicine. These so called ‘miracle’ drugs have since saved countless lives by allowing us to treat infections that would otherwise prove fatal. However, the surge in antibiotic use brought with it a bacterial counterattack - antibiotic resistance. Not only are effective treatment options limited by the increasing incidence of antibiotic resistance, but we also face the issue of a dwindling antibiotic pipeline. As a result, we are at great risk of entering a ‘post-antibiotic era’ in which very few, or ultimately no effective antibiotics remain in our arsenal against bacterial infection [1]. In working towards a solution to this crisis, we first must fully understand how antibiotics impact every aspect of bacterial growth, and indeed death. Furthermore, it is imperative that we not only carry out research on traditional laboratory strains of bacteria, but that we also use clinical isolates that have recently experienced the conditions of the human body. By doing so, we can accurately investigate microbial adaptation to antibiotic treatment in more clinically relevant bacteria, and over realistic infection timespans.

In this thesis we explore microbial adaptation to antibiotics over the course of long-term antibiotic treatment. Initially, we look at the impacts that ribosome-binding antibiotics have on bacterial death over the course of many weeks. Moving into the second half of this thesis, we will investigate the phenotypic and genotypic adaptation towards repeated antibiotic treatment in clinical isolates, with a focus on particularly complex infection case studies.

1.1 What are antibiotics?

Antibiotics negatively impact bacterial growth and clear infection, hence why they are so therapeutically useful [2, 3, 4]. Consequently, much attention is given to the detrimental outcomes of antibiotic treatment on microbes, with antibiotics classified loosely under two broad categories - bacteriostatic drugs that negatively impact microbial growth rate, and bactericidal drugs that induce cell death [5, 6]. Nevertheless, this is a rather simplistic view of antibiotic action, as we know that under certain conditions they can actually be beneficial. For example, doxycycline can simultaneously increase microbial growth rate and biomass yield [7]. It is not entirely unexpected that antibiotics would have unforeseen effects on microbial traits, given their large-scale impacts on bacterial metabolism and gene expression. Chlortetracycline, for example, is known to induce a global cellular response leading to the differential expression of various metabolic pathways [8], and chloramphenicol has been shown to slow down metabolic rate and decrease oxygen uptake, counteracting the effects of bactericidal drugs and reducing death rate [9]. Nonetheless, antibiotic-induced microbial benefits are rarely identified.

However, given that antibiotics have been shown to provide benefits towards the bacterial populations that they target, this raises the question - what is an antibiotic? Antibiotics are produced by a wide range of fungi and bacteria in the environment, for example *Streptomyces* naturally produce the aminoglycoside antibiotic streptomycin as a secondary metabolite. Traditionally, antibiotic production is thought of as a 'warfare strategy' to kill competitors in the surrounding environment, thus providing the space and nutrients needed for growth [10]. There is certainly plenty of evidence that antibiotics do play a role in competition in natural microbial communities [11, 12]. Nevertheless, in recent years it has been suggested that antibiotics in the environment may serve an alternative, peaceful purpose as signalling molecules [13]. This

is motivated in part by the suggestion that the concentration of antibiotics in the soil are mostly subinhibitory and so are unlikely to be detrimental to competitors. Furthermore, secondary metabolites are usually produced during the stationary phase of growth, when nutrients are becoming scarce. It has been suggested that the production of these secondary metabolites signals variations in resource availability and induces changes in gene expression to facilitate survival [14].

However, even very low concentrations of antibiotic can promote the development of antibiotic resistance and thus pose some level of selection pressure [15, 16]. Despite this, multiple studies have shown the range of alternative impacts that subinhibitory concentrations of antibiotics can have on bacterial cells, aside from the development of resistance. For example, low doses of antibiotic can result in changes in gene expression, resulting in increases in virulence [17] and biofilm production [18].

It is likely that the function of antibiotics as either a warfare or peaceful molecule is not mutually exclusive and that they function differently depending on the concentration of antibiotic present. This is termed 'hormesis' - in other words, whilst high concentrations of antibiotic such as that used clinically may induce cell death, the subinhibitory concentrations often found in the environment may play an alternative role. Indeed, antibiotic-induced hormetic effects on bacterial growth have been reported [19, 20]. This brings us back to our original question - what is an antibiotic? Despite our use of antibiotics as a treatment for bacterial infections, can they in fact confer microbial benefits, and how does this change the definition of an antibiotic?

1.1.1 The structure and function of doxycycline

In this thesis, there is a particular emphasis on doxycycline and its impact of the growth and survival of *E.coli*. Doxycycline is part of the commonly used tetracycline class of broad-spectrum antibiotics. Many antibiotics within this class are natural (i.e. naturally produced by microbes in the environment), for example oxytetracycline and

chlortetracycline that are produced by Streptomyces [21]. However, various semi-synthetic and synthetic derivatives of these antibiotics have been developed in the years since their discovery - doxycycline, for example, is a second-generation semi-synthetic tetracycline antibiotic first developed in the early 1960's by Pfizer [22]. It is now a commonly prescribed antibiotic, used to treat a range of infections such as sexually transmitted, respiratory tract and skin infections.

The chemical structure of tetracycline antibiotics is based on four aromatic rings, with various functional groups attached. The structure of doxycycline in particular is displayed in figure 1.

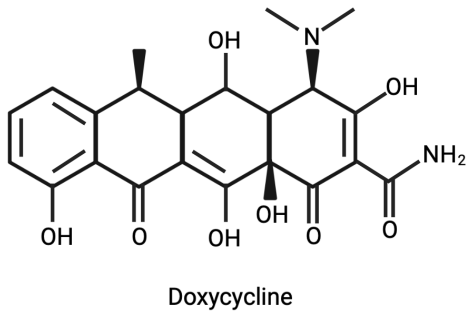

Figure 1: The chemical structure of doxycycline, created using BioRender.

Doxycycline is largely considered to be a bacteriostatic antibiotic, in that it inhibits the growth of bacterial populations rather than causing cell death. However, this is highly dose dependent, as large concentrations of bacteriostatic antibiotics can result in cell death [23]. Its primary mechanism of action is through binding to the 16S rRNA (a component of the 30S subunit of the ribosome), thereby inhibiting the binding of aminoacyl-tRNA and preventing protein synthesis [6].

Aside from its primary effect on the bacterial ribosome and consequent effects on growth, doxycycline can have other effects on bacterial cells and population dynamics. For example, doxycycline has been shown to result in increased growth rate and

cell yield of *E.coli* [7]. It has also been shown to alter the metabolism of both prokaryotes [24] and eukaryotes [25, 26], with some tetracycline antibiotics even prolonging the lifespan of certain organisms [27, 28]. The effect on longevity is partly due to the antioxidant properties of tetracycline antibiotics, and this is a property that will be further explored within this thesis. In particular, these antibiotics scavenge and inactivate superoxide molecules that could otherwise could result in cellular damage (such as DNA damage) [29, 30]. Furthermore, due to these antioxidant properties, tetracyclines have been shown to be effective in the treatment of inflammatory illnesses [31, 32]. Despite the existing knowledge on doxycycline and its mechanism of action, evidently there are still gaps in our understanding of its wider cellular effects.

1.2 The interaction between antibiotics and bacterial metabolism

Aside from the effects on the cellular target, antibiotics are also known to have a range of downstream impacts on bacterial metabolic pathways. Furthermore, antibiotics from different classes will interact with metabolism in different ways. Bactericidal antibiotics, for example, result in elevated metabolic rate, in contrast to bacteriostatic antibiotics which slow down the rate of metabolism [33, 5]. Indeed, it is thought that this disregulation of central carbon metabolism results in cell death after treatment with a cidal drug due to oxidative stress [34, 35]. Moreover, metabolism directly influences a cells susceptibility towards antibiotics. At the extreme end of the spectrum are persister cells that are effectively dormant and therefore tolerant towards antibiotics [36].

Indeed, antibiotic resistance can be conferred by genomic alterations in metabolic genes and these mutations can be detected in clinically relevant pathogens [37, 38, 39]. Here we sought to understand how doxycycline interacts with the expression of key carbon metabolism genes in *Escherichia coli* as glucose is exhausted, in ad-

dition to measuring the impacts of metabolic gene knockouts on the response to doxycycline.

1.3 The quantification of bacterial fitness : considering death as well as growth

The quantification of bacterial fitness is key to characterising microbial adaptation and evolution over time, as genotypes with greater fitness will produce a greater number of offspring and thus outcompete other microbes in the environment. Fitness itself is often quantified as the rate of bacterial growth [40, 41], however this is only one aspect of fitness. An alternative, and commonly used method for fitness quantification is the use of a competition assay in which one microbial strain is competed against another strain, and the relative frequency of both strains provides an indication of their relative fitness [42, 43, 44]. Although this method gives a broader view of fitness across multiple growth parameters, the media used is often rich in nutrients and thus promotes rapid growth. And yet, it is predicted that the natural environment is dominated by bacteria in an energy-limited state [45]. As such, rapid growth isn't necessarily the most preferable growth strategy in every environment.
Nutrients within the environment often fluctuate and form gradients [46, 47], and as a result microbes pass through multiple stages of growth and death as carbon availability changes [45, 48]. Moreover, it is inevitable that these nutrient fluctuations will impact on metabolic pathways. For example, upon entering a nutrient-poor environment microbes must adapt to use more 'thrifty', resource efficient strategies over the wasteful metabolic routes used in optimal conditions [49, 50]. Indeed, even in relatively nutrient-rich environments such as the mammalian gut, temporal fluctuations in nutrients occur with variations in feeding pattern [51]. Moreover, when nutrients *are* available the competition to acquire them will be fierce [52].
Given that death is such a ubiquitous life stage in the environment, it seems logical to

consider death as a crucial component of fitness alongside other growth parameters such as growth rate. Indeed, growth rate is known to directly influence death rate as *E.coli* with slower growth rate experience a delay in the onset of death [9]. Fitness should therefore be considered as both the ability to grow rapidly when nutrients are abundant, as well as the ability to endure periods of starvation.

In this thesis, we highlight the importance in measuring microbial responses to antibiotics in suboptimal environments. By doing so, we can understand the influence of antibiotics on the later stages of microbial life, and indeed on death. For the purpose of this study, we define death as the decline in cell viability over time (measured as colony forming units - CFU), with the eventual loss of $\sim$99% of the population. As such, we consider bacterial populations to have improved longevity when they maintain cell viability in environmental conditions that would otherwise result in death/the loss of cell viability.

1.4 Antibiotic resistance

Antibiotics have revolutionised medicine, allowing us to treat previously untreatable infections. However, the incidence of antimicrobial resistance are on the rise, and this is particularly concerning in life-threatening conditions, for example sepsis. Driving antimicrobial resistance is the widespread dissemination of antimicrobial resistance (AMR) genes, often carried on mobile genetic elements such as plasmids [53, 54]. This ultimately results in treatment complications, and consequently increases in morbidity and mortality.

Bacteria can develop resistance to antibiotics through a variety of mechanisms. For example, efflux pumps can be produced that actively pump the antibiotic out of the cell and into the external environment [55]. The antibiotic target may be modified, thereby preventing antibiotic-target binding [56]. Enzymes such as β-lactamases can be produced that hydrolyse the antibiotic, inactivating it. Finally, genomic variations

can result in modifications to outer membrane porins, resulting in decreased uptake of antibiotic into the cell [57]. We will now discuss two common classes of enzymes that confer resistance to antibiotics and that are particularly relevant to the clinical isolates that will be discussed in chapters five and six.

1.4.1 Extended-spectrum β-lactamases

β-lactam antibiotics such as penicillin are commonly used in the treatment of bacterial infections, however their use is threatened by the rising incidence of Extended-spectrum beta-lactamase (ESBL)-producing *Enterobacteriacaea* worldwide [56, 58]. ESBLs are able to hydrolyse a variety of β-lactam antibiotics, including third generation cephalosporins such as cefotaxime [56]. However, the vast majority are susceptible to β-lactamase inhibitors such as clavulanic acid and tazobactam, and so upon detection of ESBL production a β-lactam-β-lactamase inhibitor combination may be used. The most clinically relevant ESBLs are Temoneria (TEM), Sulfhydryl variable (SHV), Cefotaxime Munich (CTX-M) and Oxacillinase (OXA)-type β-lactamases, all of which are often located alongside other AMR genes on plasmids and are thus rapidly disseminated throughout populations [59].

TEM β-lactamases were the first chromosomally-located β-lactamase, initially described in the 1960's originating in Greece. TEM has since spread worldwide in a variety of pathogens. Furthermore, derivatives of TEM have arisen due to amino acid substitutions, resulting in changes to the enzymes action [60]. SHV β-lactamases are primarily identified in *K.pneumoniae* and *E.coli*, with the first identification occurring in *E.coli* in the 1970's [61]. 189 variants of SHV have since been identified both in the chromosome and plasmids of various *Enterobacteriacaea* and disseminated worldwide [62]. CTX-M producing bacteria have become particularly widespread, resulting in a so called 'CTX-M pandemic'. This is thought to be driven partly by the co-resistance to aminoglycosides and fluoroquinolones in CTX-M producing bacte-

ria, increasing selection for strains harbouring the $bla_{CTX\text{-}M}$ gene. Since their identification in the late 1980's, new variants have arisen and the CTX-M group of enzymes have steadily become more diverse, increasing resistance to a broader range of antibiotics such as cefotaxime and ceftazidime [63]. Finally OXA β-lactamases represent one of the earliest identified β-lactamase, first discovered in the 1970's [64] and primarily located on plasmids. Of the hundreds of OXA-type β-lactamases identified since, some such as OXA-48 are additionally found to hydrolyse carbapenem antibiotics and thus pose a significant clinical risk [65].

1.4.2 Carbapenemases

Carbapenems are often considered the antibiotic of last resort, particularly in ESBL-producing bacteria for which there are few treatment options. β-lactamase enzymes including ESBLs are generally ineffective against carbapenem antibiotics due to variations in their structure relative to other β-lactam antibiotics. Consequently, they are often the drug of choice for serious infections in which multidrug-resistance is suspected. This makes the rise of carbapenemase-producing *Enterobacteriacae*, driven by carbapenem use, particularly concerning [66]. Moreover, carbapenemases are not inhibited by β-lactamase inhibitors, and as such β-lactamase-β-lactamase inhibitor combination treatments such as pip/tazobactam are ineffective treatment options in carbapenemase-producing bacteria.

Carbapenem resistance is conferred by a group of enzymes called 'carbapenemases' that are able to hydrolyse a range of carbapenem antibiotics. The four main groups of carbapenemases include KPC, NDM, VIM and OXA-48. KPC are part of the class A group of carbapenemases first identified in *K.pneumoniae* in the US in 2001 [67]. It has since become one of the most widespread carbapenemases in the US, and indeed worldwide [68, 69] partially due to its dissemination on AMR plasmids. The risk posed by these carbapenemases is only heightened by the frequent

failure to identify them using standard AMR testing protocols.

Both VIM and NDM are class B carbapenemases, characterised by an active-site zinc [70]. VIM carbapenemases are found to be particularly prevalent in Europe, and were first identified in Italy in 1997, harboured by *Pseudonomas aeruginosa* [71]. NDM was first described in 2009, originating from New Delhi, India [72] and has since diversified into multiple different variants conferring resistance to a wide range of antibiotics, alongside carbapenems.

Finally, OXA β-lactamases are relatively weak class D carbapenemases [73]. Most of the early OXA β-lactamases are able to hydrolyse β-lactam antibiotics, including cephalosporins, but have no activity against carbapenems. However, later variants such as OXA-48 have a broader range and *are* able to hydrolyse carbapenem antibiotics, albeit weakly [74, 75].

In addition to carbapenemases, alterations in outer membrane porins such as OmpK36 can result in reduced susceptibility towards carbapenems. This results in further treatment complications due to difficulties associated with the detection of these porin variants using traditional AMR testing protocols [76, 77, 78].

1.5 Within-host adaptation to antibiotic treatment

There are a plethora of studies tracking the prevalence and spread of AMR genes within hospital environments, particularly in cases of infection outbreaks and with serious pathogens such as KPC-producing *K.pneumoniae*. Whole genome sequencing (WGS) is increasingly used in order to determine the AMR profile of pathogens that are identified, and track changes in AMR genes that occur both over time and between patients. For example, genomic and epidemiological data was used to trace a serious outbreak of *K.pneumoniae* back to the original patient in the US National Institute of Health Clinical Centre [79]. Furthermore, the use of rapid sequencing platforms such as the MinION from Oxford Nanopore allow outbreaks to be tracked

in real time, for example in the characterisation of ESBL strains within hospital wards [80]. An obvious recent example is the use of nanopore sequencing to rapidly track the global spread of COVID-19 [81].

Although studies across multiple patients are invaluable for tracking infection spread, only by sequencing serial isolates from individual patients can we appreciate microbial adaptation to antibiotic treatment over the course of a single infection. Despite this, there are limited studies of genomic adaptation within a single patient. Examples of within-patient adaptation include the use of WGS to track the emergence of mutations within *rpoA* and *rpoC* genes in a rifampicin-resistant strain of *Mycobacterium tuberculosis* within a single patient [82]. Blair et al. measured genomic changes retrospectively from a patient that failed antibiotic therapy and identified that a single amino acid change within an efflux pump protein was responsible for increases in drug resistance [83]. Furthermore, PacBio sequencing has been used to track the progression of a urinary tract infection in a single patient, ultimately failing to identify any genomic variants between multiple samples acquired from different body sites. The suggestion being that there are insufficient selective pressures in a single host over the short time period studied [84]. Given the rapid adaptation towards antibiotics in experimental systems [85, 7, 86], we sought to understand how bacteria would adapt over long periods of repeated antibiotic treatment within a patient. Moreover, we questioned if the large selective pressures posed by antibiotic treatment would result in structural changes within the genome, particularly in regions containing AMR genes. Large structural variations such as deletions and duplications can have a substantial impact on the antibiotic susceptibility of pathogens, for example duplications in a genomic region containing the doxycycline efflux pump operon *acr* have been shown to result in decreased susceptibility towards doxycycline [7]. As such, we sought to identify any structural variations present in the clinical pathogens acquired for this study, and explore if and how they change over a period of extensive antibiotic use.

1.6 Thesis aims

This thesis aims to explore the novel, beneficial effects that antibiotics can have on bacterial cells, as well as the development of antibiotic resistance over the course of bacterial infection within two patients. In chapter two we will investigate the impact of ribosome-binding antibiotics on both resource efficiency and longevity. For this, we study the growth dynamics of the model organism *E.coli* in starvation conditions, with the presence of antibiotics from different classes. This is followed by WGS and promoter expression measurments to elucidate the impact of antibiotics on the genome and metabolic gene expression during growth in suboptimal environments.

In chapter three, we identify the relationship between a cells capacity for ribosome production and long-term survival in suboptimal environments through the use of rRNA (*rrn*) knockout strains. We know that ribosome production is correlated with microbial growth rate, but what about death?

Next, in chapter four we utilise a subset of the keio collection, a library of almost 4,000 strains of *E.coli* with individual genes knocked out. Through the use of this library we explore the relationship between genomic background and phenotypic response to the antibiotic doxycycline, and in doing so uncover a number of highly unusual phenotypes.

Finally, in chapters five and six we track the progression of microbial adaptation to repeated antibiotic treatment across a time-course of patient samples. We acquired bacterial isolates from two patients, one of whom was infected with carbapenem-resistant *K.pneumoniae* over 18 months, and the other with multi-drug-resistant *E.coli* over 26 months. We aimed to use nanopore sequencing to rapidly identify both the presence of AMR genes, virluence genes and structural variations in the genome.

CHAPTER TWO

RIBOSOME-BINDING ANTIBIOTICS BENEFIT GROWTH AND LONG TERM VIABILITY

2.1 Overview

In this Chapter, we explore the impacts that antibiotics can have on the long-term growth of *E.coli*, and the effects on entry into death phase. Furthermore, we quantify the genomic impacts of starvation following doxycycline exposure, as well as the differential expression of key metabolic genes. The key findings are summarised below.

1. Pre-exposure to ribosome-binding antibiotics leads to improvments in the growth and long-term viability of *E.coli* populations.
2. These benefits to viability are lost in a doxycycline-resistant *E.coli* strain.
3. Doxycycline-exposed populations are better able to use cell debris as a nutrient source.
4. We show that doxycycline treatment results in differential expression of key carbon metabolism genes through the use of a GFP promoter library.

5. Starvation results in the accumulation of a large number of genetic polymorphisms, some of which are unique to antibiotic treatment.

Our understanding of antibiotic function is largely limited to studies exploring adaptation in conditions that are optimal for growth [16, 87]. However, this fails to reflect the conditions in which the majority of naturally occurring bacteria find themselves. The natural environment is harsh, with fierce competition for available nutrients by various microbes, and consequently death is a common life stage observed under these conditions [45]. Moreover, unlike the homogenous shaken cultures used in laboratory experiments, the human body consists of complex nutrient and drug gradients [88, 51], in addition to the intense competition for available carbon [52].
Antibiotic susceptibility is typically measured over the course of 24 hours, again in rich growth media. However, in reality the duration of antibiotic treatment can span weeks or indeed months in duration. Consequently, traditional tests do not capture the true range of microbial adaptation over clinically relevant time periods. Antibiotics have in fact been reported to have beneficial impacts on bacterial growth over extended growth periods [7], and it is therefore critical that all stages of bacterial growth are considered when measuring the microbial response to a drug.
By focusing purely on antibiotic-induced effects on the initial stages of growth, we are neglecting the dominant life stages observed in the environment (i.e death), and thus limiting our understanding of microbial adaptation to antibiotic treatment. Furthermore, we know that bacteriostatic antibiotics have a plethora of impacts on microbial metabolism, and this can impact not only on growth, but also reduce cell death caused by bactericidal antibiotics [9]. Nevertheless, the benefits conferred by antibiotics are rarely discussed in the literature.
In this chapter, we sought to investigate the impact that antibiotics from various classes have on *E.coli's* long-term viability and entry into death phase. Bacteria are subject to a 'growth-longevity' trade-off whereby slower growth results in a slower rate of death and rapid growth rates accelerate entry into death phase [9]. Moreover,

antibiotics that slow down growth have been shown to counteract the lethal effect of antibiotics that otherwise result in cell death [5]. We therefore hypothesised that a compound which slows down growth rates, such as certain antibiotics, would have beneficial effects on the long-term viability of a microbial population.

Alternatively, antibiotic-induced inhibition of cellular processes and changes in metabolic pathways could result in accelerated death, and therefore reduced long-term viability. The impact of various antibiotics on long-term bacterial viability was studied, and any effect on viability is shown to be specific to the antibiotics mechanism of action. Additionally, the genomic changes occurring over the course of starvation in doxycycline-exposed populations of *E.coli* will be discussed, as well as alterations in the expression of key metabolic genes over the initial stages of antibiotic treatment and nutrient exhaustion.

2.1.1 Interaction between doxycycline and the ribosome

In this chapter we will primarily focus on the antibiotic doxycycline. Doxycycline is part of the tetracycline class of antibiotics - a group of broad spectrum antibiotics used in the treatment of a range of diseases such as urinary tract and intestinal infections [6]. Tetracyclines carry out their antimicrobial action by binding to the 16S rRNA, thereby inhibiting the binding of aminoacyl-tRNA to the ribosome and consequently inhibiting the process of protein synthesis [6]. The interaction between tetracycline antibiotics and the ribosome is often transient, as the binding is reversible. Moreover, the reversibility of ribosome binding has been reported to impact the outcome on growth inhibition, with reversible ribosome-targeting antibiotics more effective in the inhibition of fast-growing bacterial populations than irreversible antibiotics [89].

Tetracyclines are generally considered to be bacteriostatic as they result in slower bacterial growth rates, unlike bactericidal antibiotics that result in bacterial death.

However, it should be noted that the distinction between bacteriostatic and bactericidal antibiotics is not clear cut as bacteriostatic drugs can behave as cidal drugs at sufficiently high concentrations [23], furthermore it has been suggested that the distinction of antibiotics into these two classes is not particularly useful or relevant to clinical treatment [90].

As proper ribosome functioning is so crucial to such a vast range of cellular processes, interference with translation has a multitude of downstream effects on the cell aside from simply the inhibition of protein production [8, 91]. For example, treatment with ribosome-binding antibiotics has been associated with reduced cellular respiration and metabolic rate [5] as well as impacts on gene expression [8]. Moreover, despite ribosome-binding antibiotics traditionally being viewed as detrimental compounds towards bacterial cells, we are now beginning to understand the range of beneficial impacts that they can have on bacterial growth [20], even at clinically relevant doses [7].

It should also be noted that aside from the intended effects on bacterial cells, tetracycline antibiotics are also known to have a range of unexpected side effects on eukaryotic cells. For example, clinically relevant doses of doxycycline can induce alterations in mitochondria functioning [92], as well as changes in oxygen consumption and metabolism in human cell lines [25]. There is also evidence that certain ribosome-binding antibiotics increase longevity in eukaryotic organisms, for example doxycycline exposure resulted in a dose dependent increase in longevity in *C. elegans* [28] and minocycline has been shown to extend the lifespan of *Drosophila* due to increases in oxidative stress resistance [93]. This raises the question - can ribosome-targeting antibiotics such as doxycycline also prolong the lifespan of prokaryotes?

2.1.2 Microbial death and survival

When grown in a media with sufficient quantities of a carbon source such as glucose, *E.coli* will pass through five key stages of growth - the first being lag phase in which bacteria adapt to their new environment, followed by a period of exponential growth with cells doubling approximately every 20 minutes. During this phase the available nutrients will rapidly deplete as they are utilised by cells for growth and the population will enter stationary phase, characterised by little cell turnover. After a short period of time the population will enter death phase and cell density will rapidly decline. This leads to the final stage, long term stationary phase in which 'growth advantage in stationary phase' (GASP) mutants arise and eventually dominate the population [94].

In the natural environment microbes often find themselves in nutrient poor, fluctuating conditions and consequently they are required to survive during periods of extended nutrient deprivation. It is unsurprising therefore that both stationary and death phase are common growth stages in the natural environment. Indeed, when these nutrient-poor conditions are replicated in a laboratory environment, *E.coli* adopt similar phenotypes to those seen in nature by slowing down their rate of metabolism, thus improving capacity for survival [95]. As bacteriostatic antibiotics have also been reported to reduce the rate of metabolism [5, 8], this leads us to question if they inadvertently prepare a bacterial population for the effects of nutrient deprivation.

Bacterial death is the process by which a population of bacteria rapidly loses cell viability, eventually resulting in the loss of 99% of viable cells. It has long been considered a consequence of the imbalance between incoming nutrients and the maintenance costs of the cell during starvation, ultimately resulting in cell death and lysis [96]. In addition, the build-up of toxic metabolic by-products as well as reactive oxygen species (ROS) in the media only act to accelerate the death process [97]. We can now appreciate microbial death as a complex and highly regulated process. For example, cells undergo multiple physiological and chemical changes on the ap-

proach to death such as a decrease in cell size [98, 99], ribosome degradation [100] and reductions in protein production [101].

Certain bacteria are able to withstand periods of starvation through the formation of dormant endospores [102], allowing them to survive harsh conditions for long durations of time, even thousands of years [103]. Although vegetative bacteria such as *E.coli* are unable to form spores to withstand stressful environments, they have been shown to survive in long-term stationary phase for many years in media, even once all available nutrients had been depleted [104]. But how do *E.coli* cells survive in media depleted of nutrients without the ability to form spores? Initially, one route to survival lies in the ability of cells to utilise alternative carbon sources in the environment, such as the acetate produced by overflow metabolism [105]. Furthermore, the nutrients released by dead cells can be recycled and used as a carbon source - as cells die and lose their membrane integrity, nutrients will leak out into the environment and be taken up by neighbouring cells [106, 107]. Ultimately, when a population has passed through death phase and entered long term stationary phase, a small portion of the population may survive in a balance between birth and death. GASP mutants may arise, often with *rpoS* mutations allowing the cells to better catabolise certain amino acids as a carbon source and thus giving them a competitive advantage [108, 109, 110].

2.2 Contributions

The experimental design, implementation of protocols, and data analysis were carried out by Emily Wood. Dr Carlos Reding-Roman provided support for the analysis of whole genome sequence data. Prof Ivana Gudelj assisted with experimental design and provided computational facilities. Prof Robert Beardmore provided funding (EPSRC), as well as assisting with experimental design and data analysis. Whole genome sequencing was carried out by Prof Hinrich Schulenburg (Evolutionary Ecol-

ogy and Genetics, Zoological Institute, Kiel, Germany). The *E.coli* GBc strain was gifted by Dr Remy Chait and Prof Roy Kishony.

2.3 Doxycycline improves the growth of *E.coli* in defined minimal media

To determine the impact of ribosome-binding antibiotics on long-term population dynamics, it is first important to understand changes to resource efficiency. In other words, how efficiently the cells can convert available carbon into ATP. Traditionally, the minimal inhibitory concentration of an antibiotic is determined by diluting the drug 2-fold and measuring changes in turbidity (optical density) at 24 hours, as set out by the clinical laboratory standards institute [111]. However, here we are interested in antibiotic-induced changes to bacterial growth over an extended time period, and consequently an extended antibiotic susceptibility test is required.

In order to illustrate the effects of long term incubation on the doxycycline dose response, a simple dilution series of doxycycline was set up as described in the materials and methods, and the wild type (WT) strain *E.coli* MG1655 was left to grow for 72 hours in M9CAA without the addition of fresh media. Note that, unless others stated, within this thesis M9CAA refers to M9 media supplemented with 0.2% glucose and 0.1% casamino acids. As figure 2 shows, the growth at 24 hours is consistent with our expectation of a traditional dose response in that the growth of *E.coli* is inhibited in a dose dependent manner. The minimum inhibitory concentration (MIC) was estimated to be 0.83mg/l doxycycline, as shown by the grey line in figure 2.

By 48 hours (blue line), we observe a deviation from the monotonic decrease in growth measured at 24 hours, rather we now find that exposure to subinhibitory doses of doxycycline results in a stimulation of growth. Moreover, by the end of the measurement period (72 hours - green line), the largest population densities are found in the concentration previously determined to be around the MIC (0.8mg/l). It

is clear that whilst doxycycline is inhibitory at 24 hours, there is an increase in population density relative to the control by both 48 and 72 hours, with $\sim$2.5 fold increase in cell density in 0.8mg/l doxycycline relative to the drug-free control. The raw growth curves for each doxycycline concentration are displayed in supplementary figure S2. To ensure the robustness of OD readings in the measurement of bacterial growth over the extended period of time used, colony forming units (CFU) were also quantified at both 24 and 72 hours for *E.coli* in drug-free conditions and those exposed to 0.4 and 0.8 mg/l doxycycline. These CFU counts mirrored the outcome obtained via OD measurements, thus confirming that this is a reliable measurement of cell density under the conditions used here (figure 3b).

The 'overgrowth' phenotype observed here in doxycycline has previously been reported [7, 112]. Although, in contrast to the data we present here, the overgrowth phenotype was not previously observed in *E.coli* MG1655, only in *E.coli* AG100. This antibiotic-induced stimulation in bacterial growth challenges the commonly held assumption that doxycycline, and indeed antibiotics in general, are purely detrimental molecules for bacteria.

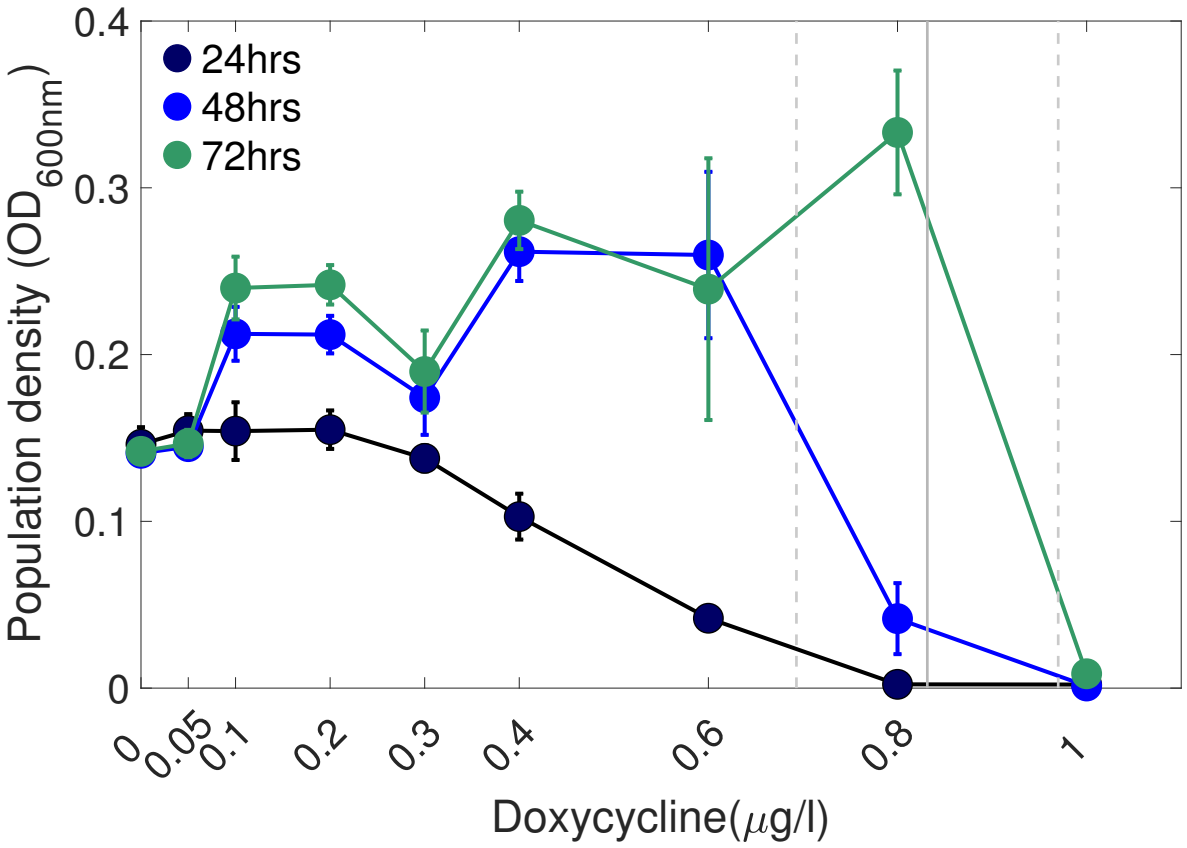

Figure 2: Experimental data on the growth of *E.coli*, shown as OD(600nm) on the y axis, as a function of doxycycline concentration shown on the x axis. The different coloured lines represent measurements at different times points, with the dark blue line representing 24 hours, light blue 48 hours and finally green for 72 hours. The vertical grey line represents the IC99, and the vertical dashed lines represent the 95% confidence intervals. The data shows a transition from a monotone dose response at 24 hours to a non-monotone dose response at 72 hours, indicating that doxycycline is no longer inhibitory. *(*n=3).

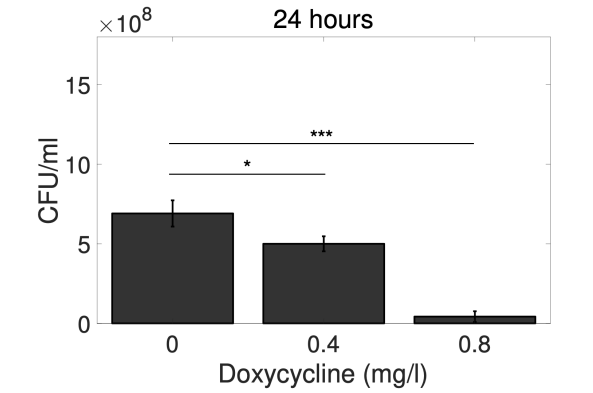

(a)

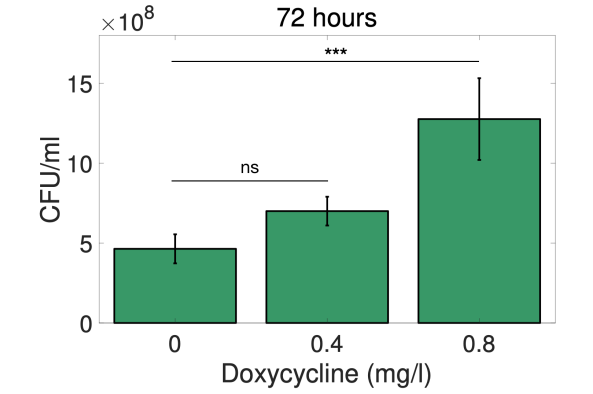

(b)

Figure 3: (a) CFU counts confirm that the growth of *E.coli* populations initially exposed to 0.8mg/l doxycycline is inhibited at 24 hours, (b) however they grow to significantly higher cell densities by 72 hours relative to the drug-free control. One way ANOVA with post-hoc tukey, ns = not significant, * = $p < 0.05$, ** = $p < 0.01$, *** = $p < 0.001$. *n=3*.

For the purpose of this study, we define K as the maximum population density (OD) within the measured time period. For details on the methods used to estimate the growth parameters, please refer to the methods and materials section 8.6. When the growth parameters of these populations are quantified, we find that there is a decrease in the growth rate of doxycycline-exposed cultures relative to the drug-free control, yet growth rate doesn't decrease further in a dose-dependent manner (figure 4a). However, microbial growth rate is highly dependent on resource concentration, and it is therefore possible that at different glucose concentrations a dose-dependent decrease in growth rate would be measured. Both K and lag (figure 4b-c) were found to increase significantly with increasing concentrations of doxycycline.

Next, the data was examined for trade-offs between the different growth parameters. In evolutionary biology, the term 'trade-off' refers to a phenomenon whereby the improvement of one trait negatively effects another trait [113, 114]. Figure 5a shows that doxycycline treatment results in a trade-off between the duration of lag and the final population density. In other words, drug-free populations have a short lag period but also a small K, whereas *E.coli* exposed to high concentrations of doxycycline (e.g. 0.8mg/l) have the 'cost' of a longer lag phase, but benefit from a larger K. A long lag phase can be considered costly as a longer period of no growth provides more time for competitors to exploit resources within the environment. This lag-K trade-off mirrors that reported previously in *E.coli* AG100 [7, 112]. Although growth rate is lower in doxycycline-exposed populations relative to the drug-free, there is no evidence of a trade-off between growth rate and K (figure 5b), or growth rate and lag (figure 5c).

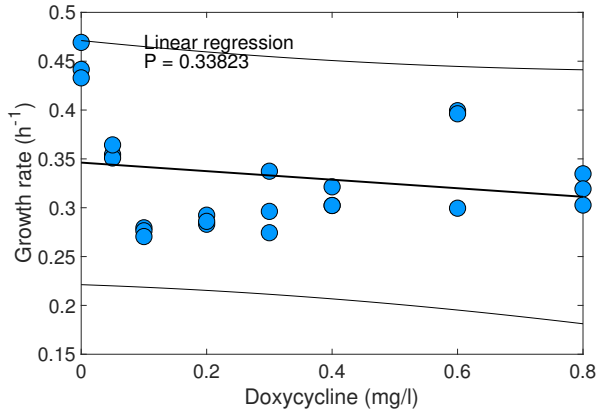

(a)

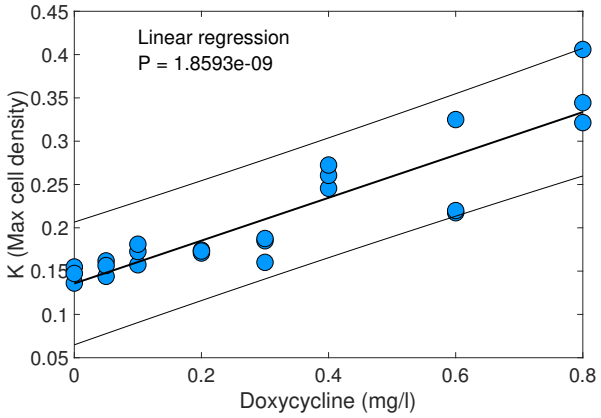

(b)

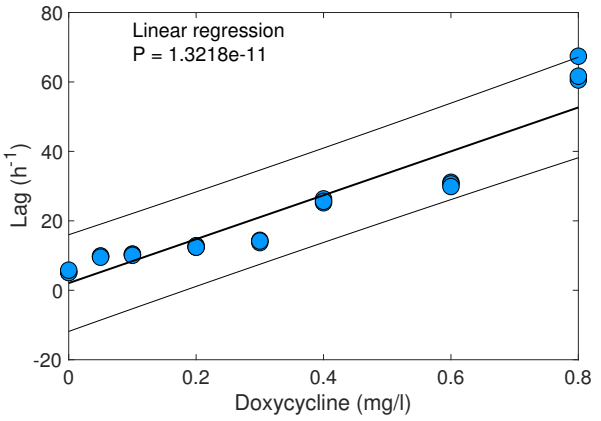

(c)

Figure 4: The effect of doxycycline on a) growth rate, b) K and c) lag is shown. There is a decrease in growth rate between drug-free and doxycycline-treated cultures, however this does not decrease further with increasing concentrations of doxycycline. Both K and lag increase in a dose-dependent manner. Linear regressions are shown as thick solid lines, with $\pm$ estimated 95% confidence intervals (CI, 3 replicates) shown as thinner lines. *n = 3*.

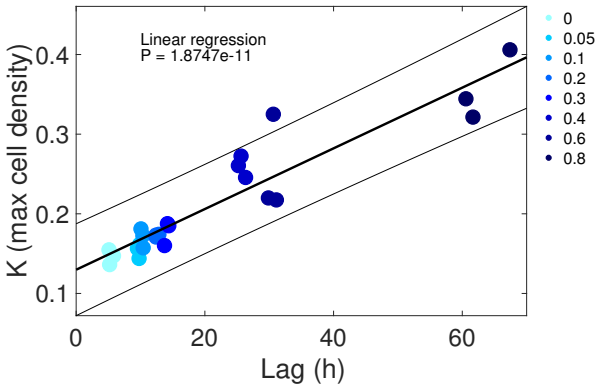

(a)

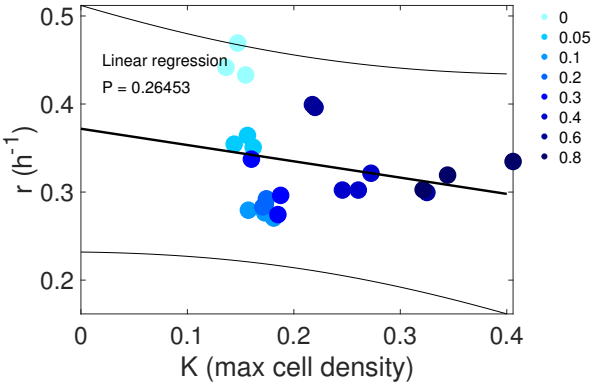

(b)

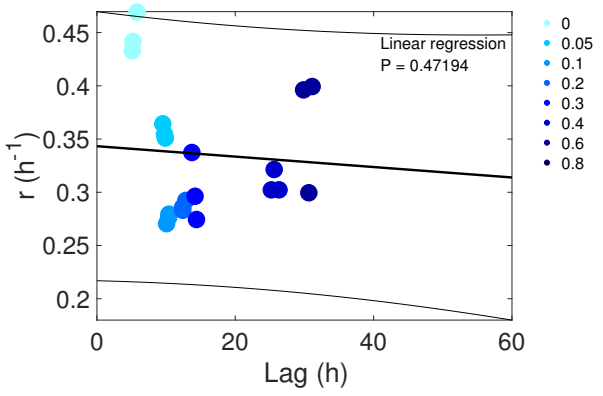

(c)

Figure 5: The final population density (K) is shown as a function of lag (a) and rate (b), and lag is shown as a function of rate (c). There is a significant, linear increase in K with lag time, however there is no significant relationship between rate and K, or rate and lag. Linear regressions are shown as solid lines, with $\pm$ estimated 95% confidence intervals (CI, 3 replicates) shown as thinner lines. *n=3*

2.4 Doxycycline-induced changes to growth parameters are resource-dependent

Microbial growth is highly dependent on the richness of carbon source in the environment and as such there exists a metabolic trade-off between the yield and rate of ATP production. For example, at low growth rates when nutrients are limiting, *E.coli* cells tend to perform respiratory metabolism, a highly efficient process that results in large ATP yields. On the other hand, when resources are abundant and growth rates are rapid, cells switch to inefficient fermentative metabolism with lower ATP yields [115, 116, 117]. Given the relationship between nutrient availability and resource efficiency, we next asked if varying the amount of carbon in the environment would alter the doxycycline-induced improvements to cell density.

During a 72 hour time period, separate populations of *E.coli* were grown in defined minimal media containing 1mg/ml^{-1} casamino acids and glucose ranging from 0.2 - 20mg ml^{-1}. Three cultures were left drug-free whilst the remaining cultures were exposed to either 0.2, 0.4 or 0.8mg/l doxycycline. Growth was measured as optical density every 20 minutes and the raw growth curves are shown in supplementary figure S3. Figure 6 shows the relationship between K (maximum cell density) and the concentration of glucose supplied in the media for populations exposed to doxycycline, normalised to the drug-free control. In populations treated with the lowest dose of doxycycline (0.2mg/l), we find that there is only a marginal increase in K with increasing glucose supply. However, in those cultures treated with 0.4 and 0.8mg/l doxycycline, K is maximised at intermediate glucose concentrations relative to the drug-free population. The benefits to efficiency provided by doxycycline are likely to be lessened at high glucose concentrations due to the toxic effects of surplus glucose supply. Furthermore, growth is found to be relatively poor at low glucose concentrations, resulting in this humped geometry. Both linear and quadratic regressions were applied to the data to test the robustness of the quadratic fit.

The lag-K trade-off is found to be robust across varying glucose availability, as show

in figure 7. The data suggests that doxycycline exposure enhances the cells ability to efficiently use the glucose that is available in the media, as a higher K is achieved in doxycycline-exposed cultures than in drug-free conditions with the same supply of glucose. We can further quantify this by showing the relationship between K and yield (OD per mg of glucose) over the range of glucose and doxycycline concentrations used - it is evident that K is maximised in the most resource efficient populations, that is those populations exposed to the highest concentrations of doxycycline (figure 8). Moreover, doxycycline-induced changes in growth rate are also found to be mediated by glucose supply, as shown in figure 9. Growth rate is known to be influenced by glucose availability [7], and so it is perhaps not surprising that glucose availability also influences the growth rates of doxycycline-exposed *E.coli*.

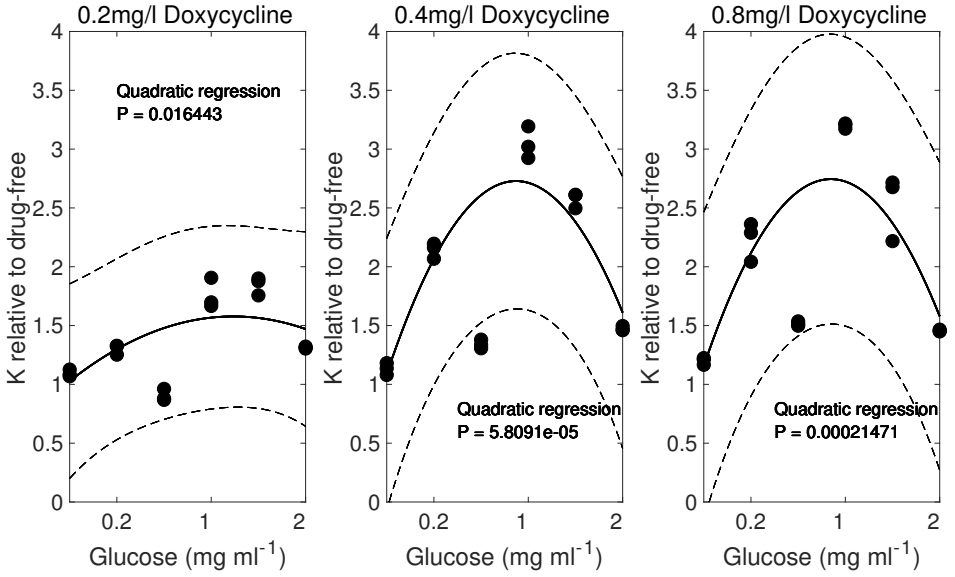

Figure 6: The variation in K (OD at carrying capacity), relative to the drug-free control and as a function of glucose concentration. We find that K is maximised at intermediate glucose concentrations at larger doses of doxycycline. Quadratic regressions are shown as solid lines, with $\pm$ estimated 95% confidence intervals (CI, 3 replicates) shown as dashed lines.

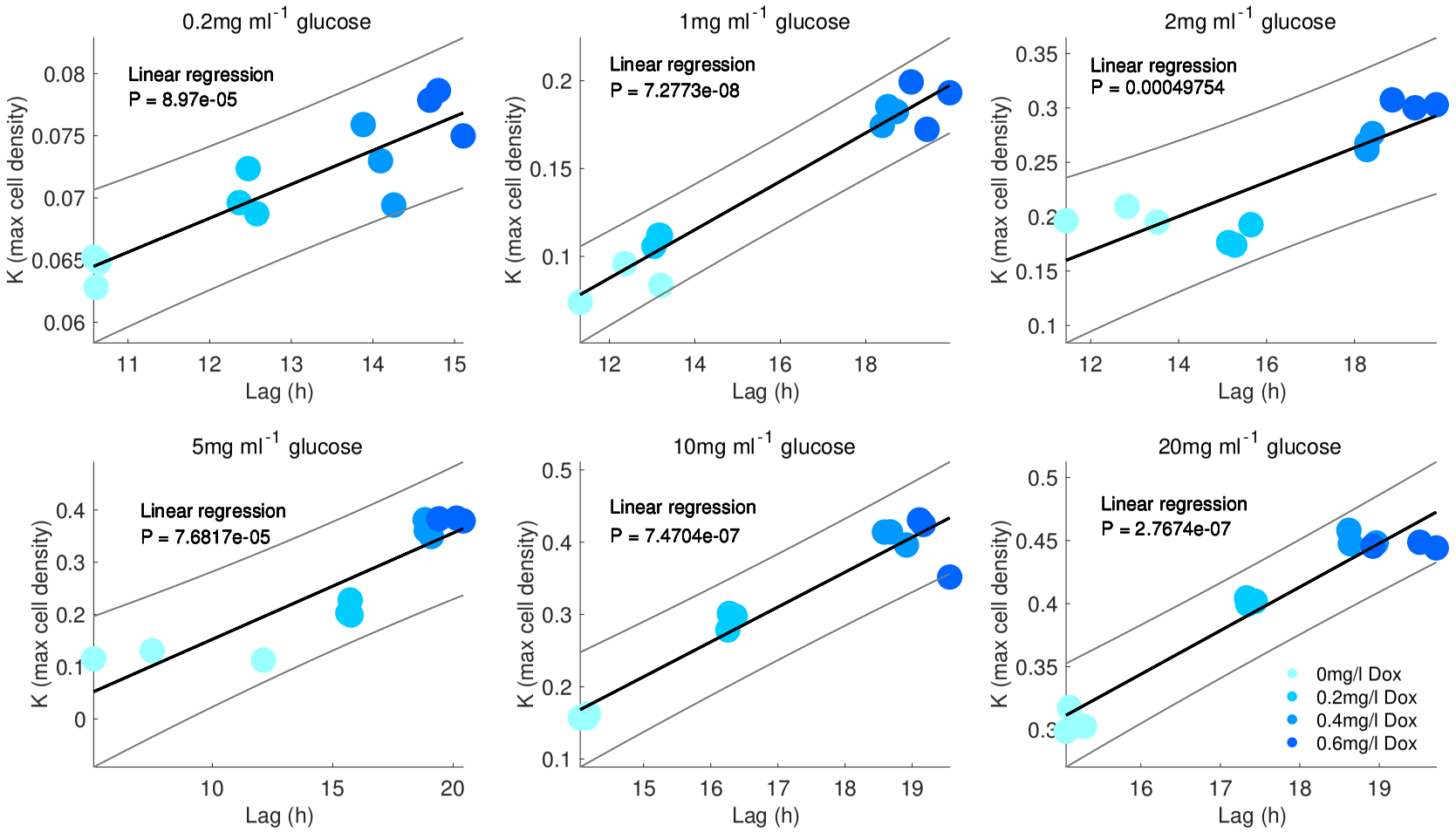

Figure 7: The relationship between K (defined as the maximum cell density) on the y axis, against lag time shown on the x axis. Linear regressions are shown as solid lines, with ± estimated 95% confidence intervals (CI, 3 replicates) shown as dashed lines.

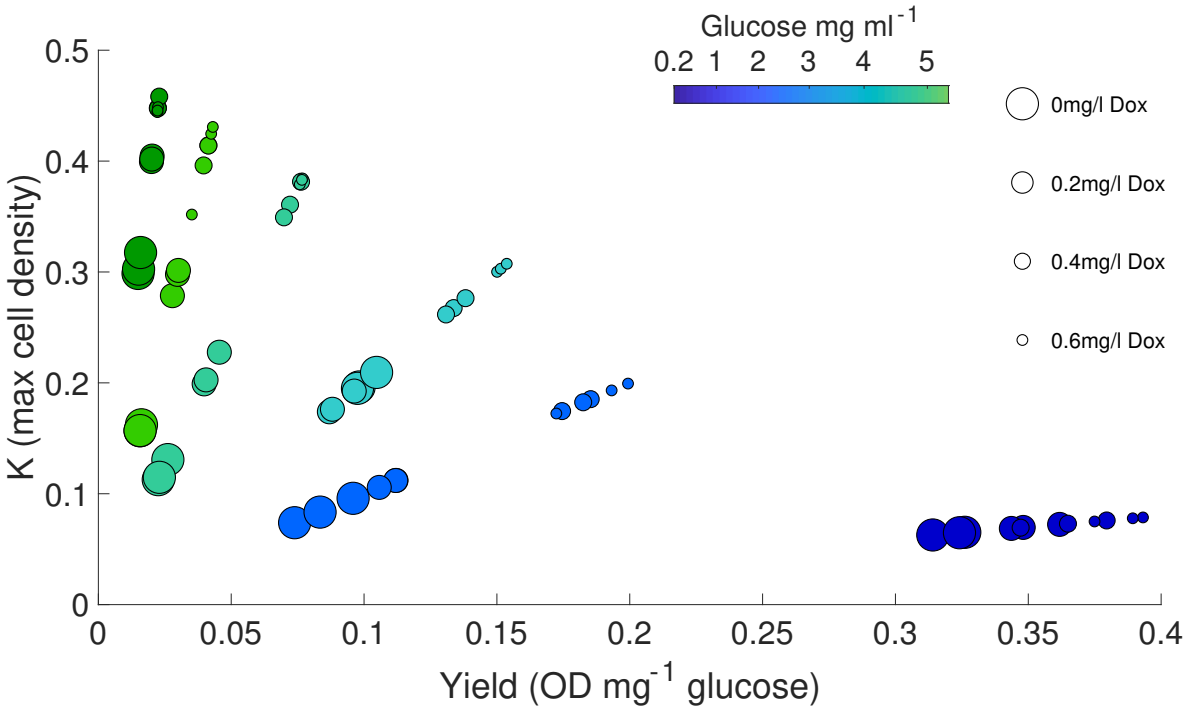

Figure 8: The variation in K (y axis) as a function of yield (x axis) across populations exposed to varying glucose and doxycycline concentrations. Different colour intensities represent varying glucose supply and circle size represents varying doxycycline concentration. K is found to be maximised when the supply of glucose is greatest, and with large doses of doxycycline (smaller circles).

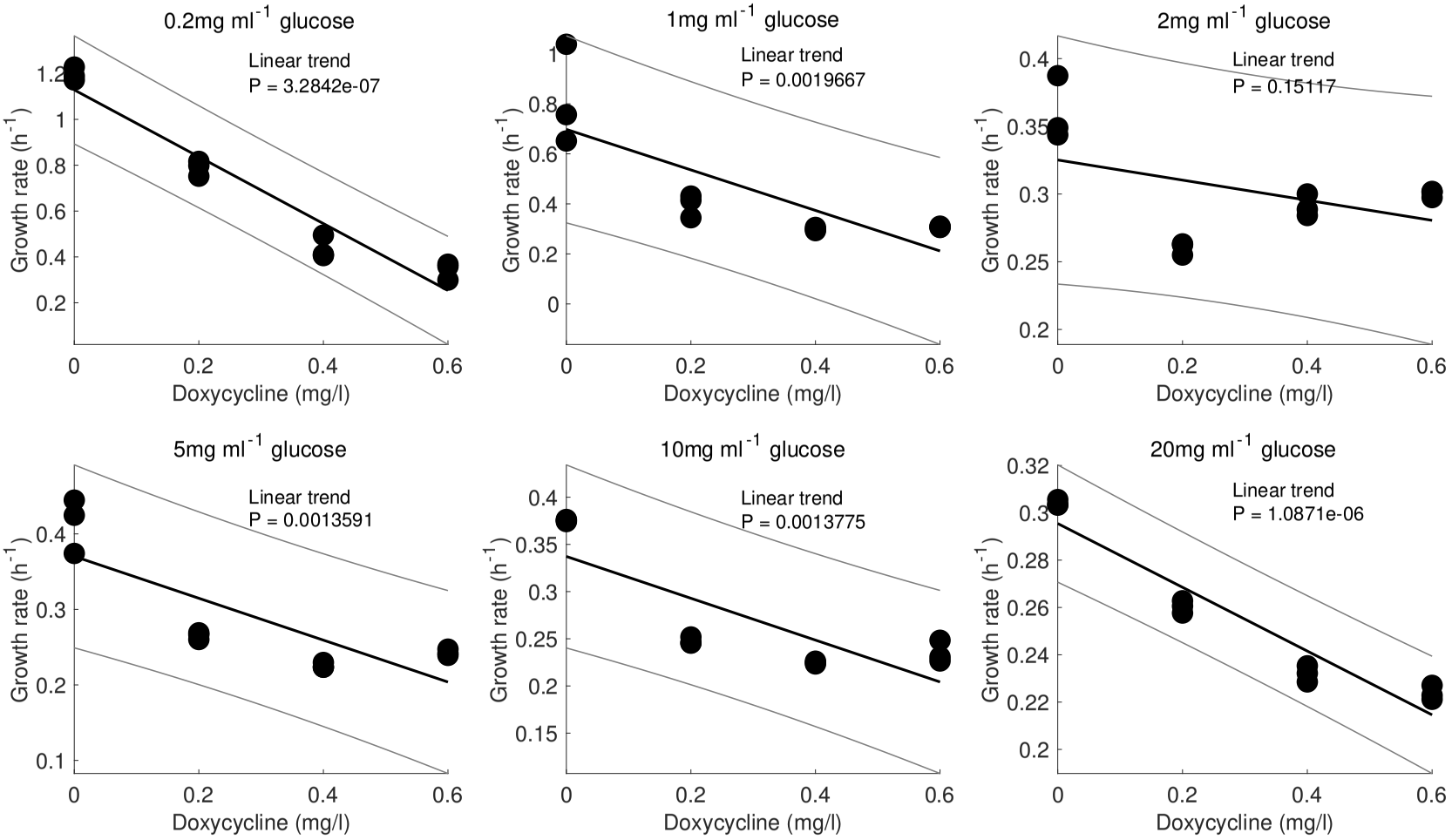

Figure 9: The relationship between doxycycline (x axis) and growth rate (y axis) is dependent on the concentration of glucose available within the media. Doxycycline does not appear to result in a dose-dependent decrease in growth rate with 2mg ml^{-1}, however it does with different glucose supplies. Linear regressions are shown as solid lines, with ± estimated 95% confidence intervals (CI, 3 replicates) shown as dashed lines.

2.4.1 Doxycycline-induced benefits are lost in complex media

Having identified that doxycycline improves resource efficiency when grown in M9CAA, and that K is optimised by intermediate concentrations of glucose, we next sought to identify if this benefit is observed in other types of media. Lysogeny broth (LB) is a rich media containing the majority of precursors needed for optimal growth (e.g. amino acids), allowing cells to grow more rapidly than they otherwise would in a nutrient limited media. Populations of *E.coli* MG1655 were grown in LB media for 72 hours in the presence and absence of doxycycline (0.2, 0.8, 1, 2 and 3mg/l) and growth was measured as OD every 20 minutes. Note that the concentrations of doxycycline used here are greater than that used in M9CAA media due to the higher MIC measured in LB.

The growth of doxycycline-exposed cultures is initially inhibited at 24 hours, and the cell density is found to recover to levels similar to that found in the drug-free populations by 72 hours (figure 10). As such, by 72 hours doxycycline does not appear to have a negative impact on cell density relative to the control. However, unlike in M9CAA (figure 2), the doxycycline-exposed populations in LB show no stimulation of growth above that seen in the drug-free control at any time point. This is further evident when we quantify the growth of doxycycline-exposed cultures relative to drug-free (figure 11) as we find that none of the doxycycline-exposed cultures exceed the cell density of the drug-free populations at any of the three time points shown (24, 48 and 72 hours). The raw growth curves for this data set are shown in supplementary figure S4.

The metabolic capacity of *E.coli* varies depending on the type of resource available, and richness of that resource in the environment. In this case, growth in LB media eradicates the benefits to cell density induced by doxycycline observed in M9CAA and this is likely due to the changes in metabolism on different media types (for example, the increased production of fermentative by-products in LB media due to inefficient metabolism) [118, 119]. The finding that rich media eradicates doxycycline-

induced benefits to growth leads us to hypothesise that this phenotype could be influenced by metabolic processes. Specifically, the stimulation of growth in M9CAA but not in LB suggests that this phenotype is dependent on the presence of glucose in the media, and the resulting metabolic pathways involved in the utilisation of glucose.

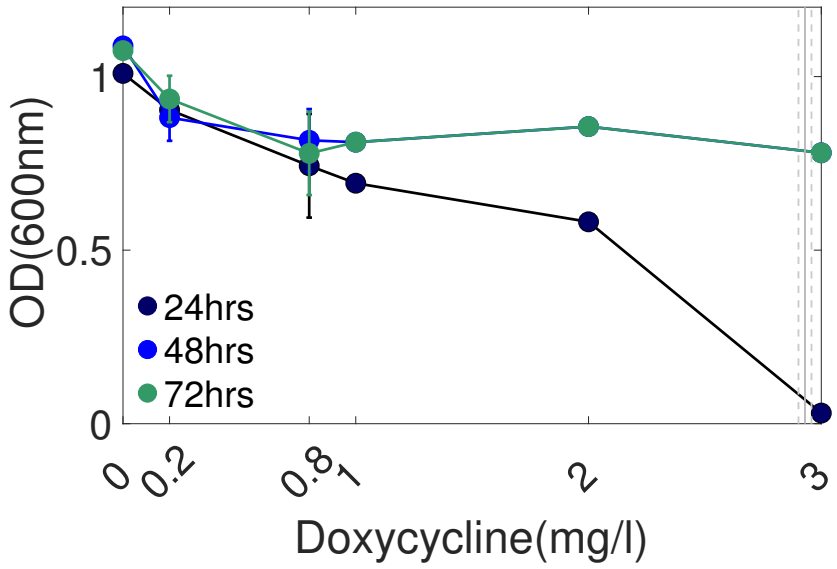

Figure 10: Experimental data on the growth of *E.coli* in LB media, shown as OD(600nm) on the y axis, as a function of doxycycline concentration shown on the x axis. The different coloured lines represent measurements at different times points, with the dark blue line representing 24 hours, light blue 48 hours and finally green for 72 hours. The vertical grey line represents the IC99, and the vertical dashed lines represent the 95% confidence intervals. Caution should however be taken when estimating the IC99 from this dataset due to the limited number of doxycycline concentrations used. Doxycycline is not found to result in any benefit to *E.coli* in terms of cell density when grown in LB. *(*n=3).

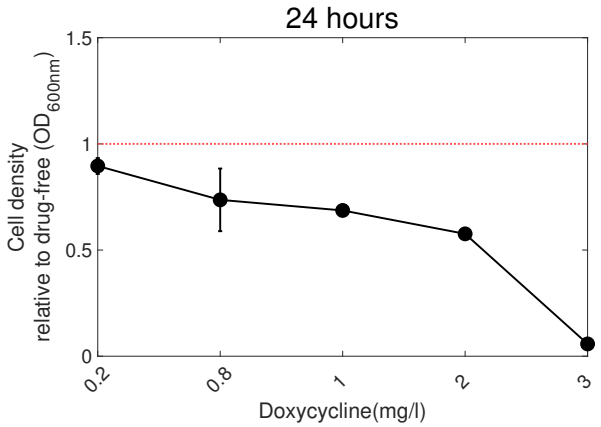

(a)

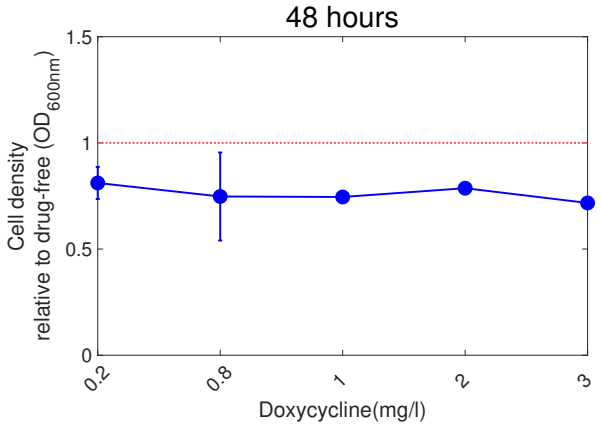

(b)

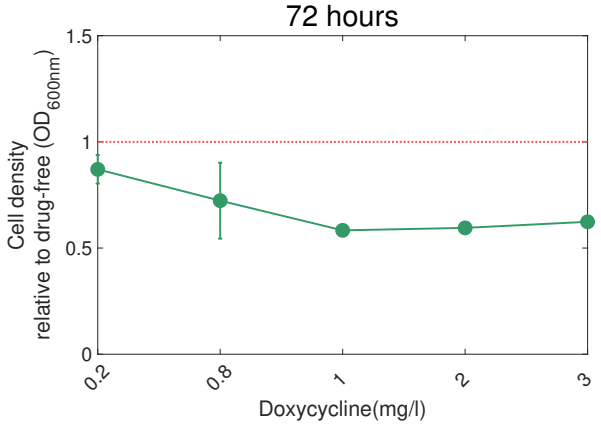

(c)

Figure 11: The cell density at 24 (a), 48 (b) and 72 (c) hours as a function of doxycycline dose, relative to the growth of drug-free populations (red dotted line) for populations of *E.coli* grown in LB media. *n=3*.

2.5 The impact of antibiotics on the long-term viability of *E.coli* populations

Given that doxycycline drastically impacts the initial stages of growth, and indeed the efficiency of resource use, it would be logical that there would also be drug-induced impacts on the long-term viability of a bacterial population. For the purpose of this work, we define bacterial death as the loss of cell viability, as determined by a drop in CFU/ml over time. Microbial birth i.e. growth rate, and death are known to be interlinked, for example slower growth rates result in delayed entry into death phase [9]. Here, doxycycline has been found to reduce growth rate relative to a drug-free culture, as shown in figure 9, as well as impacting on other key factors in the onset of growth such as lag phase (figure 4c). Moreover, the main cellular target of doxycycline, the ribosome, is also directly related to growth rate [120] and the response to nutrient fluctuations [121, 122]. Ribosome degradation, for example plays a key role in starvation survival [100, 123]. We therefore sought to understand the impact that ribosome-binding antibiotics such as doxycycline have on microbial death and long-term population viability.

For this, we measured *E.coli* population dynamics over an extended period of time in the presence of the ribosome-binding antibiotics doxycycline and erythromycin. Erythromycin was used here to allow a comparison to be made against two ribosome-binding antibiotics from different antibiotic classes (doxycycline being a tetracycline and erythromycin a macrolide antibiotic). As such, any impact of long-term cell viability could be established as a doxycycline-specific effect, or a general effect of ribosome-targeting antibiotics. Although both antibiotics have a similar mode of action, they are structurally different and have different ribosomal binding sites - doxycycline binds to the 30s subunit whilst erythromycin binds to the 50s subunit. It was hypothesised that given the similar mode of action, both antibiotics would have a similar effect on long-term viability.

In addition, we measured the growth of *E.coli* in antibiotics with alternative cellular

targets as a control. The antibiotics penicillin and rifampicin were selected as they represent antibiotics from different classes, with different modes of action. Penicillin is a β-lactam antibiotic that inhibits cell wall formation in gram negative bacteria through the inactivation of penicillin binding proteins [124]. Rifampicin, on the other hand, is part of the rifamycin class of antibiotics. It carries out its inhibitory action by binding to and inhibiting DNA-dependent RNA polymerase [125]. Both rifampicin and penicillin are generally considered to be bactericidal in nature, whilst doxycycline and erythromycin are generally considered as bacteriostatic antibiotics.

E.coli populations were exposed to these antibiotics at concentrations that inhibit 20% or 50% of growth for 28 days without the addition of fresh glucose. Dose responses for each antibiotic are displayed in supplementary figure S1. In the absence of antibiotic (Fig 12a-d, black line), cell numbers increase to $\sim$8x10^8 cells/ml in the first 24hrs, but rapidly decline to $\sim$4.7x10^8 cells/ml by day 3, and finally $\sim$9x10^7 cells/ml by day 28. This represents approximately a 90-fold reduction in viability, indicating that the populations are likely to be in rapid death phase from day 3 onwards. This is supported by glucose measurements, revealing a steep decrease in availability between 24-48 hours in drug-free conditions (figure 14), therefore glucose exhaustion is the probable cause of cell death. The standard curve used with the glucose assay is displayed in supplementary figure S5

We observe a surprising, novel phenotype upon exposure to doxycycline and erythromycin - an improvement in growth and long-term viability (figure 12a-b). The data shows that, although the number of viable cells decreases initially on days 6-8 in cultures exposed to doxycycline and erythromycin respectively, this is followed by further phases of population growth. This increased growth results in overall improvements to the long-term viability of the populations relative to the drug-free control. In contrast, the drug-free populations rapidly collapse in cell number from day three onwards, with no evidence of similar resurgences in growth.

This data is reflected in area under the time curve (AUC) measurements, showing a significant increase in overall cell density over the 28 days relative to the drug-

free control with both doxycycline ($p < 1.5 \times 10^{-5}$) and erythromycin ($p < 1.6 \times 10^{-6}$), as shown in figure 13a-b. This would suggest that exposure to doxycycline or erythromycin results in a greater number of cells over the 28 day time period, in other words increased growth.

Whilst we see improved viability and growth with the use of ribosome-binding antibiotics, exposure to neither the beta-lactam antibiotic penicillin (Fig 12c) or the RNA polymerase inhibitor rifampicin (Fig 12d) results in growth profiles similar to the drug-free control, with no overall benefit to long-term viability or indeed growth. We observe a decrease in AUC with penicillin ($p < 0.002$) and no significant change with rifampicin, as shown in figure 13c-d. Taken together these results suggest that ribosome-binding antibiotics, whilst inhibitory on day 1 of exposure, eventually lead to stimulation of growth and a delay in population collapse as culture times are extended, thereby supporting our hypothesis that antibiotics which impact bacterial growth will also impact on long-term viability during starvation. We next sought to further confirm that this improved viability is due to antibiotic-ribosome binding. For the sake of simplicity, future experiments were carried out only with doxycycline.

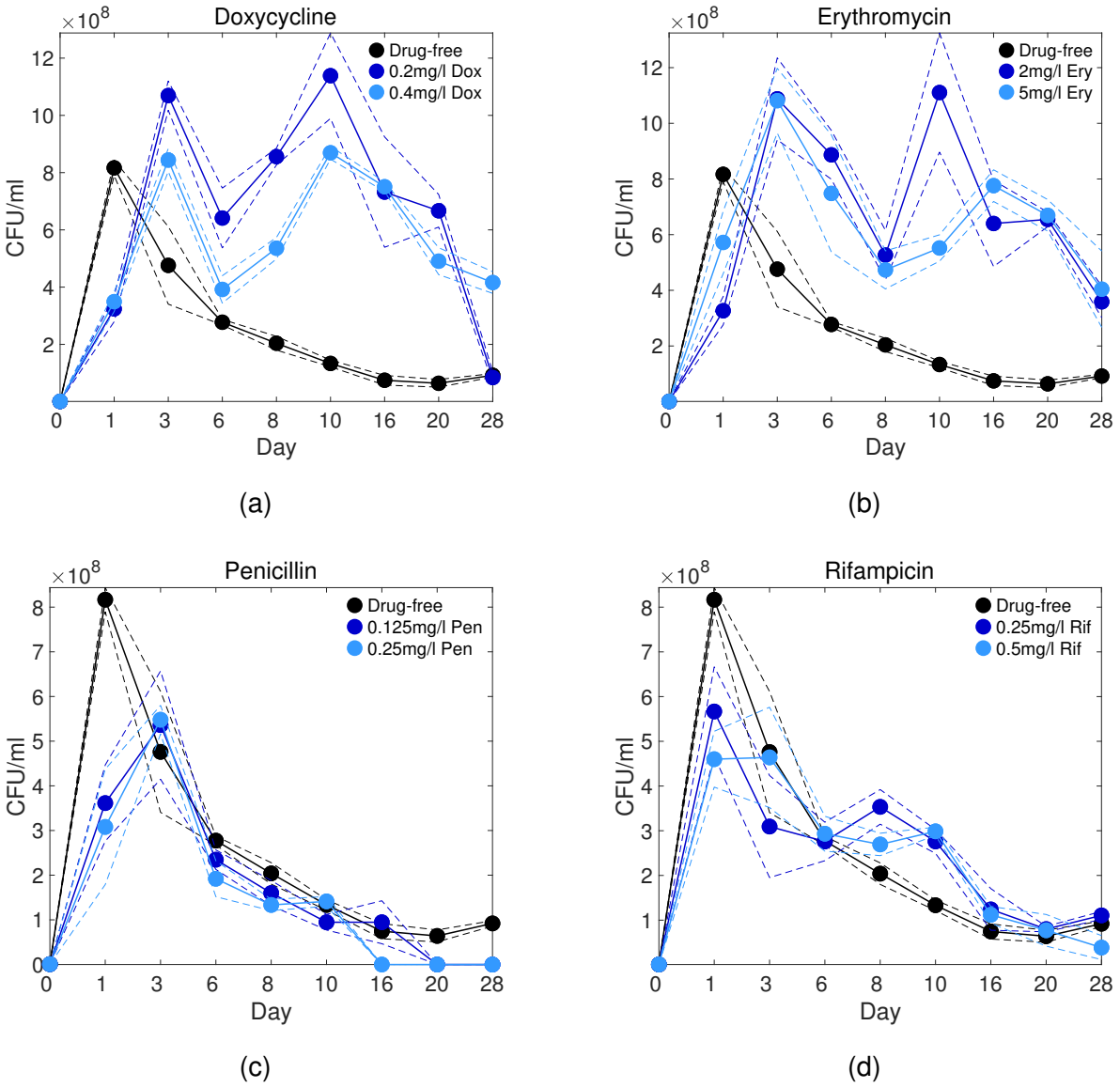

Figure 12: Changes in cell viability over 28 days in populations of E.coli exposed to antibiotic. In the absence of antibiotic (a, black line), cell number rapidly declines after day 3. However, exposure to the ribosome-binding antibiotics doxycycline (a) or erythromycin (b) results in multiple phases of growth and decline, with overall benefits to long-term viability. The initial exposure of *E.coli* to doxycycline and erythromycin leads to further growth of the populations over the extended time period. Exposure to the antibiotics penicillin (c) or rifampicin (d) fails to confer an advantage to long-term viability relative to the drug-free control. The mean data is displayed as a solid line, with $\pm$ estimated 95% confidence intervals (CI) shown as dashed lines. n=3.

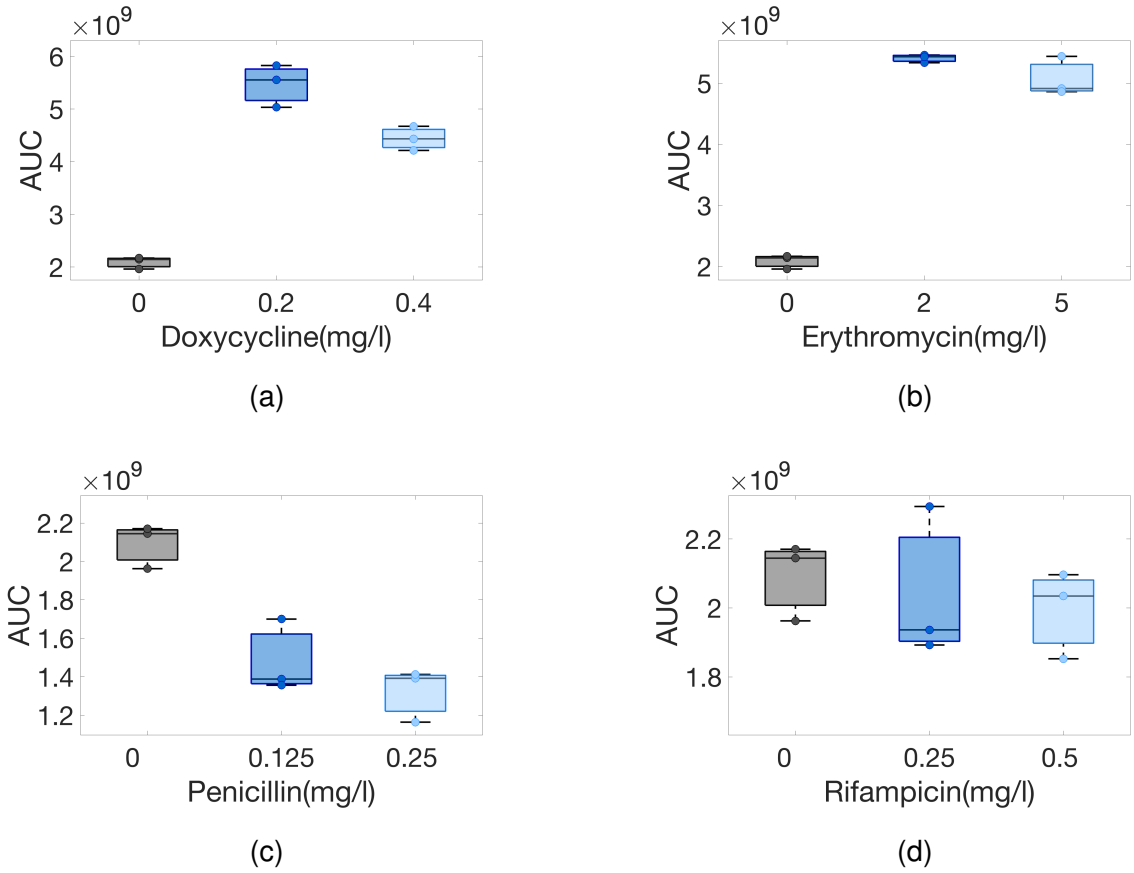

Figure 13: Area under the time curve (AUC) was calculated. Treatment with doxycycline significantly increases AUC (one way ANOVA: F(2,8) = 118.3, p <1.5 x 10-5)(Post hoc Tukey: Drug-free vs 0.2mg/l (p <1.37 x 10-5), Drug-free vs 0.4mg/l (p <1.2 x 10-4)), as does erythromycin (one way ANOVA: F(2,8) = 251.5, p <1.6 x 10-6)(Post hoc Tukey: Drug-free vs 2mg/l (p <2.3 x 10-5), Drug-free vs 5mg/l (p <4.3 x 10-6)). Penicillin leads to a decrease in AUC (one way ANOVA: F(2,8) = 21.8, p <0.0018)(Post hoc Tukey: Drug-free vs 0.125mg/l (p <0.006), Drug-free vs 0.25mg/l (p <0.002)), whereas there is no significant difference in AUC with rifampicin (one way ANOVA: F(2,8) = 0.28 p = 0.76). The medians and first and third quartiles are shown in the overlaid boxplots.

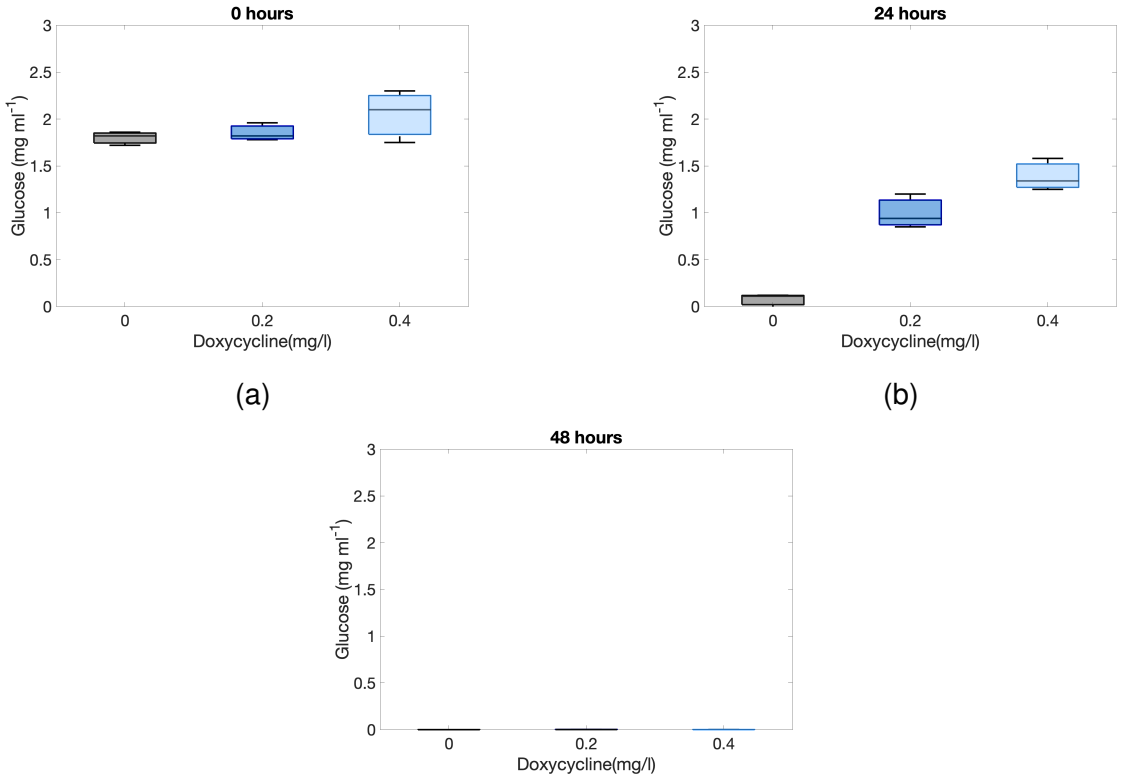

Figure 14: The glucose concentration in cultures exposed to 0, 0.2 and 0.4 mg/l of doxycycline for 72 hours was measured using a colorimetric glucose assay. The glucose concentration was determined using a standard curve of known glucose concentrations. (a) At 0 hours, glucose concentrations are high due to a lack of growth, however by (b) 24 hours glucose is almost completely exhausted in drug-free cultures. After 48 hours, (c) the remaining glucose in doxycycline-treated cultures has also been exhausted. The delay in glucose depletion within doxycycline-treated cultures is due to initial growth inhibition. n = 3

2.6 Doxycycline-induced benefits are lost in a resistant strain

If the physical binding of the antibiotic to the ribosome is key to the observed benefits in K and long-term viability, then hindering this binding should reduce or eradicate any benefits. In order to confirm this hypothesis, we explored the response of a tetracycline-resistant strain of *E.coli* to doxycycline exposure. There are multiple cellular mechanisms that interfere with doxycycline-ribosome interactions, thereby conferring resistance towards doxycycline. Examples include efflux [126], alterations to the antibiotic structure [127] and finally ribosome protection [128]. We utilised a tetracycline-resistant strain of *E.coli* (GBc) [129] that is resistant to doxycycline via the latter mechanism, ribosome protection (tet36) [130]. Ribosome protection proteins work by dislodging tetracycline molecules and their derivatives from their binding site on the ribosome, thereby freeing the ribosome for tRNA binding and allowing protein synthesis to continue, even in the presence of otherwise inhibitory concentrations of antibiotic [128].

In order to establish the effect of antibiotic treatment on the growth of the resistant strain, *E.coli* GBc was initially grown in drug-free conditions and two concentrations of doxycycline (0.6 and 0.8mg/l) for 72 hours. This allowed for all glucose in the media to be exhausted. The doxycycline-sensitive strain, *E.coli* MG1655 was grown in identical conditions for the purposes of comparison. As shown in figure 15a, whilst doxycycline-resistance provides benefits to the initial stages of growth, by 72 hours there is no significant difference in K in the doxycycline-exposed populations relative to drug-free (figure 16a). This is in contrast to the doxycycline-sensitive *E.coli* strain that has a stimulation in growth upon exposure to doxycycline (figure 15b), resulting in a significantly higher K in doxycycline relative to drug-free conditions by 72 hours (figure 16b).

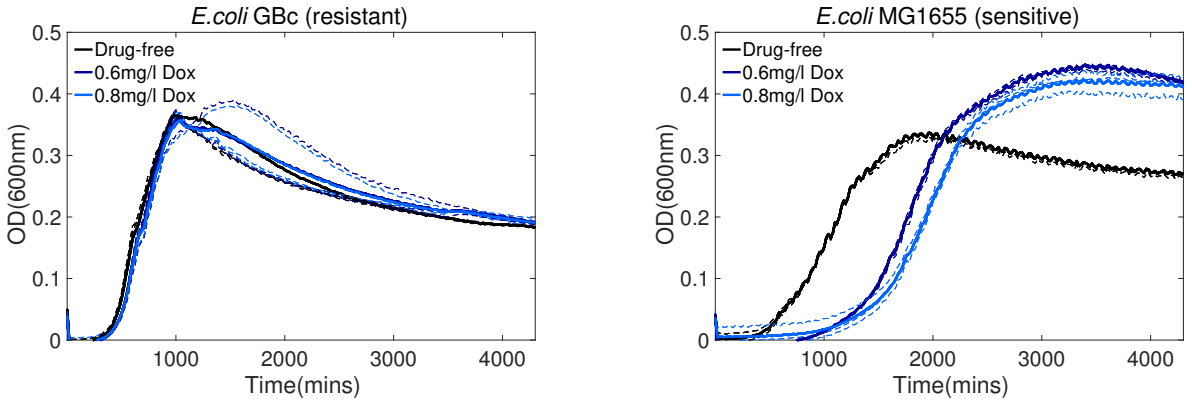

(a) (b)

Figure 15: The growth dynamics of doxycycline-resistant (*E.coli* GBc) and doxycycline-sensitive (*E.coli* MG1655) strains of *E.coli* in the presence and absence of doxycycline. Doxycycline does not result in a stimulation of growth above that of the drug-free control in *E.coli* GBc, unlike that seen in *E.coli* MG1655. However, resistance does appear to confer an initial benefit to the growth of drug-free *E.coli* GBc in comparison to drug-free *E.coli* MG1655. The solid line represents the mean, and dashed lines represent individual replicates. *n=4*.

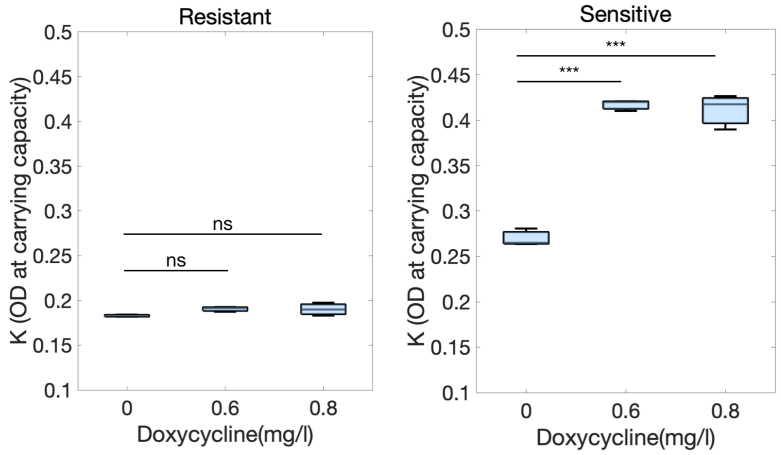

Figure 16: There is no significant difference in K at 72 hours between doxycycline-treated and drug-free cultures of the doxycycline-resistant strain *E.coli* GBc. In comparison, with the doxycycline-sensitive *E.coli* MG1655 a significant difference is found in K at 72 hours between populations in drug-free conditions and those exposed to either 0.6 or 0.8mg/l doxycycline (one way ANOVA: $F(2,8) = 127.6$, $p < 0.001$)(Post hoc Tukey: Drug-free vs 0.6mg/l doxycycline ($p < 0.001$), Drug-free vs 0.8mg/l doxycycline ($p < 0.001$)).

To assess any changes to growth and viability during nutrient exhaustion, we conducted long term batch cultures for 28 days with *E.coli* GBc (Figure 17a) alongside *E.coli* MG1655, as shown previously (Fig 2a-d, black line). During this 28 day period, no resources were added and no waste was removed, thereby allowing the population to move through all stages of growth and eventually enter death phase. We observe no benefit to long-term viability in doxycycline-treated *E.coli* GBc populations, relative to drug-free (Fig 17b). Furthermore, pre-treatment with doxycycline actually leads to a reduction in cell density at some stages of starvation in the resistant strain. For example, populations treated with either 0.2 or 0.4mg/l doxycycline have an average $\sim$8.5 and $\sim$99 fold reduction in cells/ml by day 10, compared to a $\sim$1.8 fold reduction in drug-free populations. Figure 17 shows that, relative to the doxycycline-sensitive strain MG1655, resistance provides no benefit to growth during starvation or long-term viability in the presence of doxycycline. This data therefore suggests that it is indeed the physical binding of doxycycline to the ribosome, and its associated downstream effects, that result in benefits to long-term viability in *E.coli* MG1655.

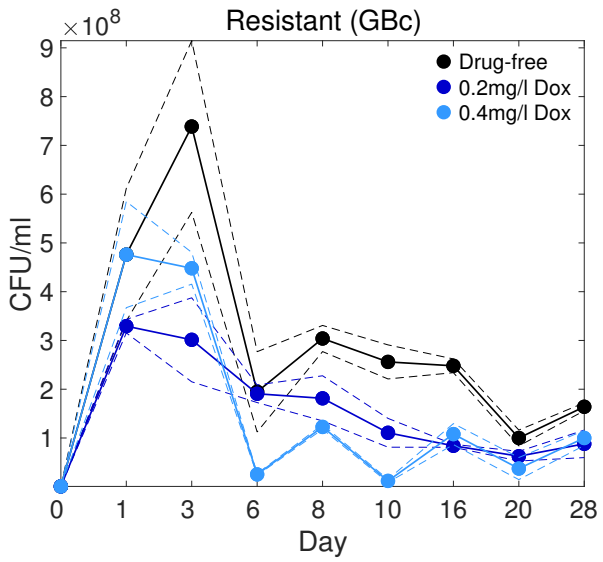

(a)

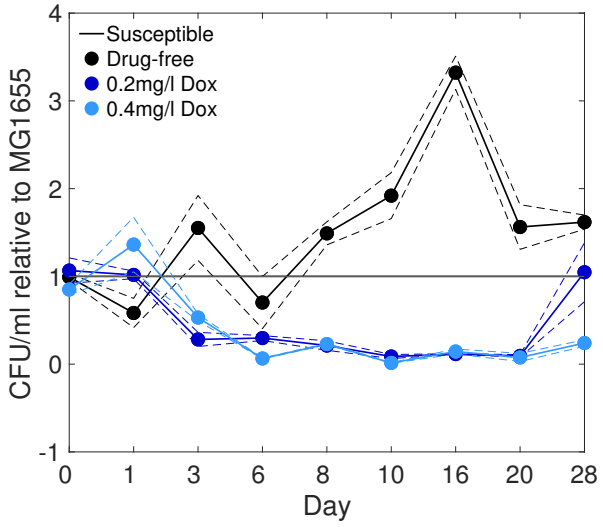

(b)

Figure 17: Exposure to doxycycline in the doxycycline-resistant strain GBc (a) does not result in any benefit to population long-term viability. Relative to doxycycline-sensitive strain MG1655 (b), in the presence of doxycycline, the resistant strain has fewer cells/ml as carbon is exhausted. The mean data is displayed as a solid line, with $\pm$ estimated 95% confidence intervals (CI) shown as dashed lines. n=3.

2.7 Improved growth on doxycycline-treated cell debris

In both doxycycline and erythromycin treated cultures, we observed a resurgence in growth at $\sim$10 days following an initial decline in population density (Fig 12a-b). By this time point, all available glucose is exhausted, which led us to question how this resurgence in growth occurred. Under starvation conditions when the main carbon source has been exhausted, bacteria are known to recycle the debris of lysed cells [107, 131]. Moreover, GASP mutants can arise, allowing them to more effectively use cell debris as a source of carbon [109, 132, 133]. It is therefore plausible that the antibiotics used here improve *E.coli's* ability to use cell debris as a carbon source, thus causing the observed resurgence in growth.

To investigate this, we propagated *E.coli* in M9CAA for 48 hours, allowing for complete glucose exhaustion (Fig 18a). The supernatant was then isolated and filter sterilised to remove any remaining live cells. Following this, fresh *E.coli* was used to re-inoculate the supernatant, with some cultures additionally supplemented with either subinhibitory concentrations of doxycycline (0.2mg/l), 2mg ml^{-1} of glucose, or both. If *E.coli* is able to utilise the cell debris and dissolved organic compounds within the supernatant, we would anticipate measurable levels of growth in the presence of supernatant.

We find no significant difference in growth rates (Fig 18b) between cultures inoculated into supernatant, however we do find a significant increase in the maximum population density (Fig 18c) in drug-treated populations relative to the drug-free control ($p \approx 0.012$). When cultures are supplemented with fresh glucose, no significant difference is found in growth rate or maximal population density between drug-free and doxycycline-treated populations (Fig 18d-e), as glucose is now the preferred carbon source. This data suggests that treatment with doxycycline does improve the ability of *E.coli* to use the debris found in spent supernatant as a carbon source. Moreover, this could account for the resurgence in growth seen previously.

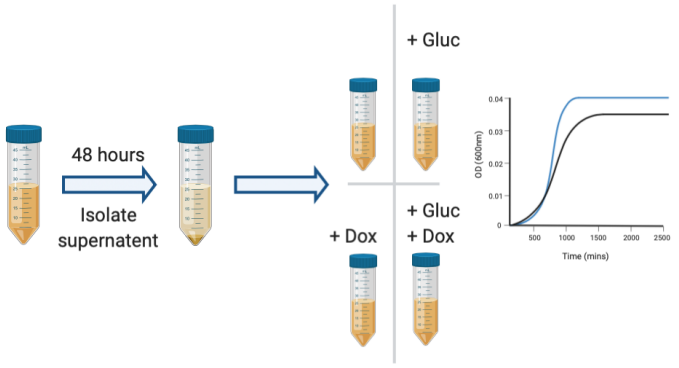

(a)

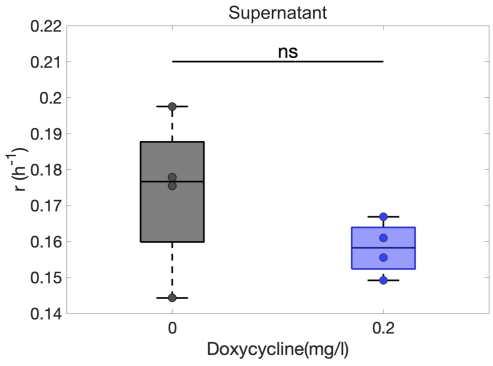

(b)

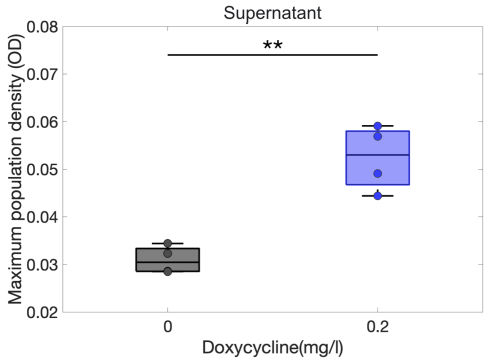

(c)

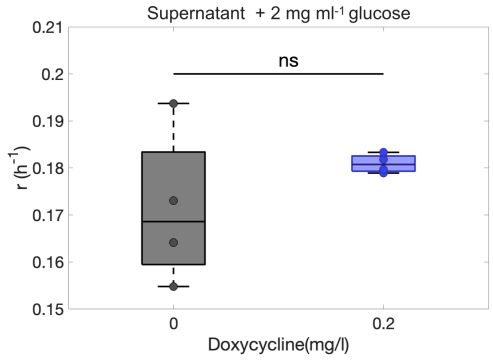

(d)

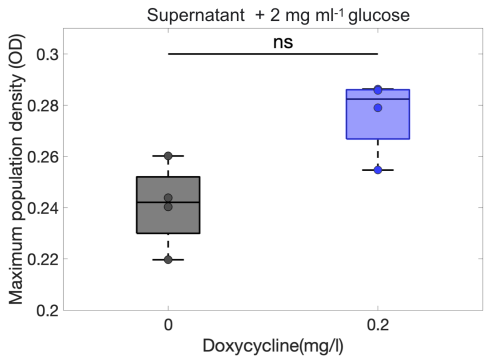

(e)

Figure 18: *Caption continued on the next page*

Figure 18: (a) Graphic of the protocol used. Briefly, populations of *E.coli* were grown for 48 hours in the absence of drug. The supernatant was then isolated and split into cultures that were inoculated with 10^6 cfu/ml *E.coli*. These cultures were then either left to grow with no alterations to the media, or supplemented with fresh glucose, doxycycline, or both. Optical density readings were then taken over 48 hours. The protocol graphic was created using BioRender. (b&d) Growth rate wasn't significantly altered by the addition of doxycycline in either glucose-free or glucose-supplemented supernatant. Likewise, K did not vary between doxycycline-treated and drug-free cultures in glucose-supplemented media (e). However, in glucose-free media (c), K was significantly higher in doxycycline-treated cultures (t-test, $p \approx 0.012$). The medians and first and third quartiles are shown in overlaid boxplots.

In addition, we observe what appears to be diauxic growth in the cultures that have been grown in supernatant with additional glucose, as shown in figure 19. Diauxic growth is a phenomenon first described by Monod in 1949 [134] and is often observed when microbes are grown on two different sugars, for example glucose and lactose [135]. The growth is characterised by a period of growth, followed by a lag phase after the exhaustion of the preferable sugar, and then a further growth stage as the second sugar is utilised. The reason for these two phases of growth is primarily due to carbon catabolite repression, as the the uptake and use of the secondary nutrient is repressed until the first is exhausted [136]. The observation of diauxic growth here in glucose supplemented supernatant suggests that there is indeed some useable resource present in the supernatant which is utilised once glucose is exhausted. Acetate is excreted during growth in excess glucose and then consumed when glucose is exhausted. It is therefore possible that acetate, as well as other organic compounds produced in the initial phase of growth are the alternative resources present in the supernatant and result in this diauxic behaviour [137].

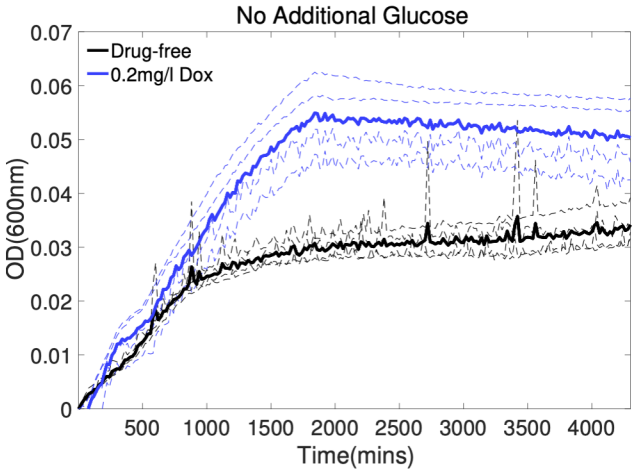

(a)

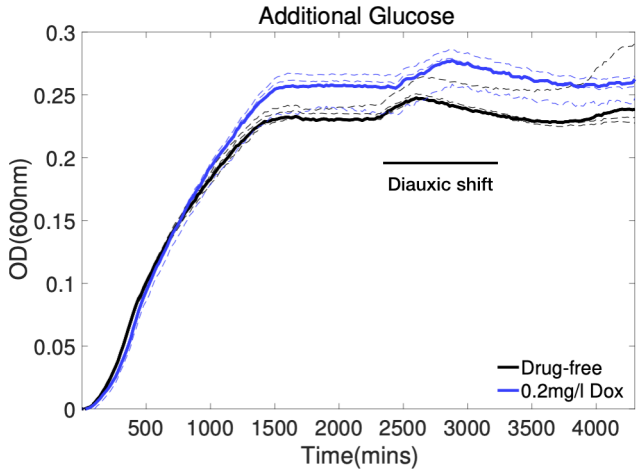

(b)

Figure 19: (a) Exposure to doxycycline provides a benefit to growth in supernatant. (b) With the addition of fresh glucose, we observe no significant benefit to growth in doxycycline-exposed cultures. Both doxycycline and drug-free cultures go through a diauxic shift at $\approx$ 2600 minutes. The mean data is displayed as a solid line, with individual replicates shown as dashed lines. n=4.

2.8 Quantifying the expression of metabolic genes during glucose exhaustion

To gain insight into the doxycycline-induced changes in gene expression, we utilised a library of fluorescent *E.coli* reporter strains that have GFP-tagged promoters [138]. Each strain possesses a low copy plasmid containing the gene of interest upstream of gene for GFP (figure 20).

Using this library, we are able to observe the temporal dynamics of promoter expression over a period of starvation by measuring GFP expression as a proxy for promoter activity. This is unlike the use of transcriptomics that would only offer snapshots of gene expression at defined times. We measured the activity of various gene promoters involved in carbon metabolism and glucose uptake over 72 hours in the presence and absence of 0.4mg/l doxycycline, and without the addition of fresh media. The strains used in this work, and gene functions are detailed in table 1.

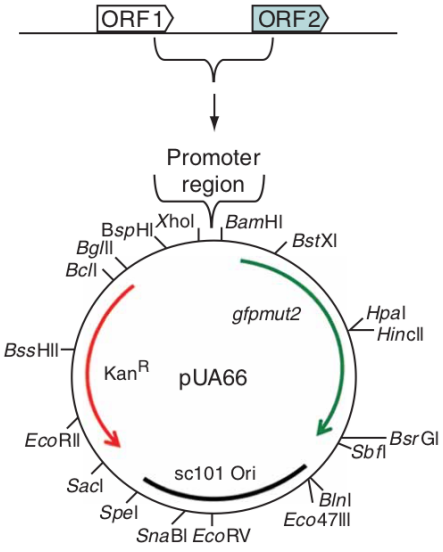

Figure 20: A map of the low-copy plasmid used to produce the gfp-tagged *E.coli* promoter strains, taken from reference [138]

GFP tagged promoter	Product	Function
glpX	Fructose-1,6-bisphosphate	Gluconeogensis
pyk	Pyruvate kinase	Glycolysis
pgi	Glucose-6-phosphate isomerase	Glycolysis/gluconeogensis
pfkA	6-phosphofructokinase	Glycolysis
pfkB	6-phosphofructokinase	Glycolysis
lpd	Dihydrolipoyl dehydrogenase	Multiple including glycolysis and TCA
icd	Isocitrate dehydrogenase	TCA cycle
sdhc	Succinate dehydrogenase subunit	TCA cycle
gltA	Citrate synthase	TCA cycle
fumB	Fumarate hydratase	TCA cycle
aceB	Malate synthase A	Glyoxylate cycle
ackA	Acetate kinase	Acetate biosynthesis/catabolism
poxB	Pyruvate dehydrogenase	Acetate biosynthesis
ompC	Outer membrane porin	Porin activity
ptsA	Phosphoenolpyruvate--protein phosphotransferase	Glucose transport
ptsG	PTS system glucose-specific EIICB component	Glucose transport

Table 1: The GFP-reporter strains used in this study.

2.8.1 Central carbon metabolism

Doxycycline targets a key, energy-intensive cellular system. After all, it is estimated that ribosome biogenesis alone accounts for $\approx$ 60% of energy expenditure within the cell [139]. As such, antibiotic treatment not only impacts on ribosome functioning, but also a wide range of downstream metabolic processes. There is extensive literature demonstrating the changes in metabolism and gene expression induced by antibiotics, with bacteriostatic antibiotics largely resulting in reduced rates of cellular metabolism whilst bactericidal antibiotics are reported to increase metabolic rates [33, 91, 8, 5]. For example, chlortetracycline has been shown to result in the up-regulation of ribosomal subunits and the down-regulation of major carbon metabolic pathways [8]. Tigecycline, a semisynthetic derivative of minocycline, results in a reduction in the transcription of genes involved in the TCA cycle and cellular respiration in *Acinetobacter baumannii* [140]. Furthermore, through utilising the same GFP reporter library used here, tetracycline has previously been shown to

induce large genome-wide alterations in expression, including the up regulation of genes involved in the early oxidative stress response [141].

We therefore sought to understand if doxycycline (0.4mg/l) results in differential expression of central carbon metabolism genes under the conditions used here, and if this expression is altered as nutrients are depleted. Indeed, we find differential expression of genes involved in all of the key metabolic pathways studied, (glycolysis/gluconeogenesis, TCA cycle, glyoxylate cycle and acetate metabolism), confirming that aside from interactions with the ribosome, doxycycline also induces downstream metabolic changes (figure 21).

As doxycycline-induced benefits to K were only observed in glucose media (such as the M9CAA used in section 2.3), key genes involved in the metabolism of glucose were selected. Specifically, the expression of four genes involved in glycolysis and gluconeogenesis (*pyk, pgi, pfkA* and *pfkB*) were studied and none were found to have substantial changes in expression with exposure to 0.4mg/l doxycycline, as shown in figure 22a. Previous studies have found significant down regulation of genes involved in the TCA cycle with tetracycline treatment [91], however, surprisingly in the conditions used here we find $\sim$2.5x higher maximum expression of both *lpd* and *icd* in doxycycline-exposed culture relative to the drug-free control, and $\sim$1.5x higher maximum expression of *sdhC* (figure 22b). Both *fumB* and *gltA* were found to have lower expression in doxycycline-exposed populations.

Acetate is produced and excreted into the external environment by cells during exponential growth on fermentable sugars such as glucose, in a process known as 'overflow metabolism'. Here, we have measured the expression of *ackA* and *poxB*, genes involved in the biosynthesis of acetate. In addition, we also measure the expression of a gene involved in the glyoxylate cycle, *aceB*. The glyoxylate cycle, involving isocitrate lyase (encoded by *aceA*) and malate synthase (encoded by *aceB*, studied here) allows bacteria to bypass the TCA cycle and utilise acetate alongside other alternative carbon sources [142, 143]. We find that whilst there is little evidence of change in maximum expression level *poxB* within doxycycline-exposed

cultures, we do find higher expression of *ackA* and *aceB* (figure 22c). Furthermore, as the glyoxylate cycle allows cells to utilise fatty acids and acetate [144, 145], both of which are likely present in the supernatant of a starving culture, it is possible that the up regulation of the glyoxylate cycle gene *aceB* contributes to the increases in population density measured in doxycycline-treated supernatant (Fig 18d).

We next aimed to identify if the observed increases in expression are dose-dependent. The *aceB* and *icd* reporter strains were grown in similar conditions as previously described, but with a range of doxycycline concentrations (0, 0.4, 0.6 and 0.8mg/l). In addition, we examined the variations in expression over a range of doxycycline concentrations in a gene that previously showed no measurable change in expression - *poxB*. Figure 23 shows that the expression of these genes increases in a dose dependant manner. Moreover, we find that the expression of *poxB* is also upregulated in larger concentrations of drug. Indeed, with all three genes we measure significantly higher maximal expression levels in increasing concentrations of doxycycline, as shown in figure 24. This demonstrates that doxycycline does indeed induce changes in the expression of key metabolic genes. The raw growth curves are displayed in supplementary figures S6-S8.

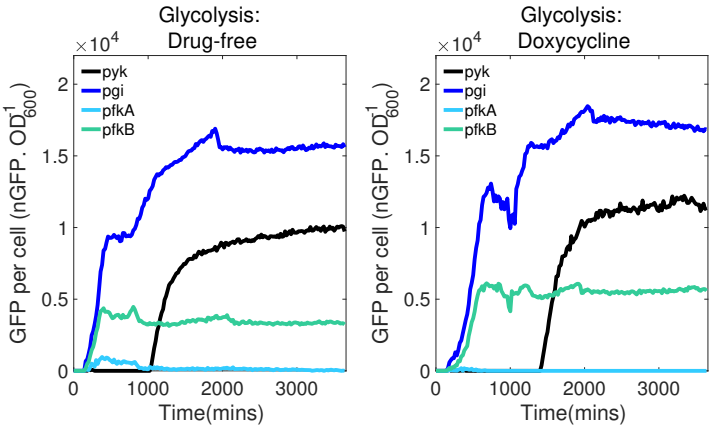

(a)

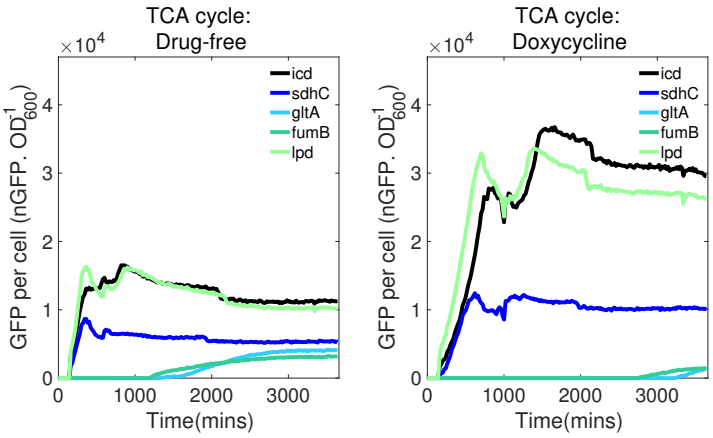

(b)

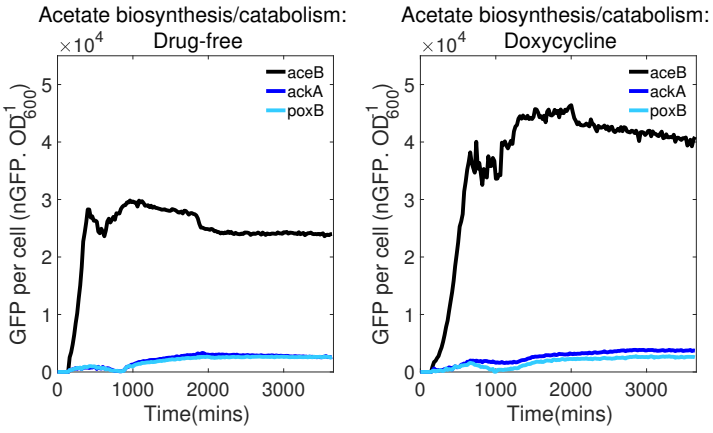

(c)

Figure 21: The levels of GFP expression normalised to OD(600nm) for promoters of genes involved in (a) Glycolysis, (b) the TCA cycle and (c) acetate biosynthesis and catabolism, exposed to 0.4mg/l doxycycline or left drug-free. Note that only the mean of three replicates is shown for simplicity, however the data for all three replicates can be found in supplementary figures S6-S8.

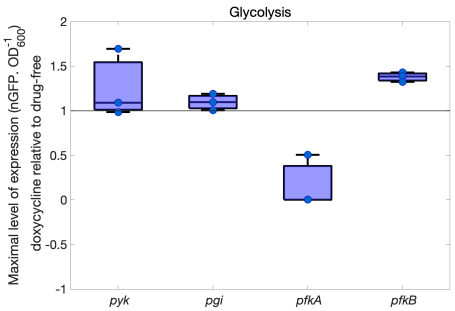

(a)

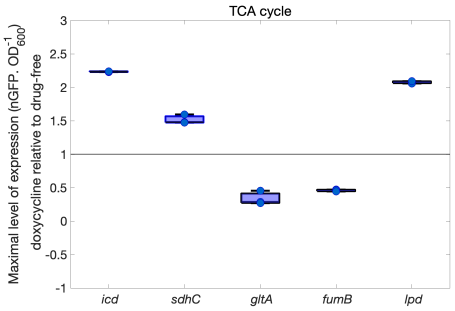

(b)

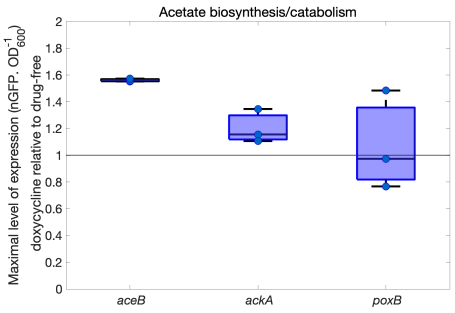

(c)

Figure 22: The maximal level of expression for doxycycline-exposed *E.coli* with tagged promoters for genes involved in (a) glycolysis, (b) the TCA cycle and (c) acetate biosynthesis and catabolism, relative to the drug-free control.

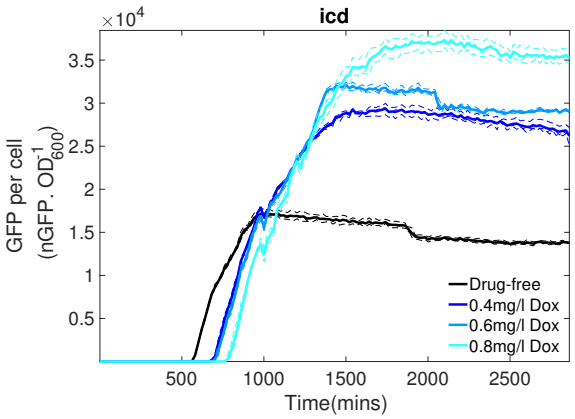

(a)

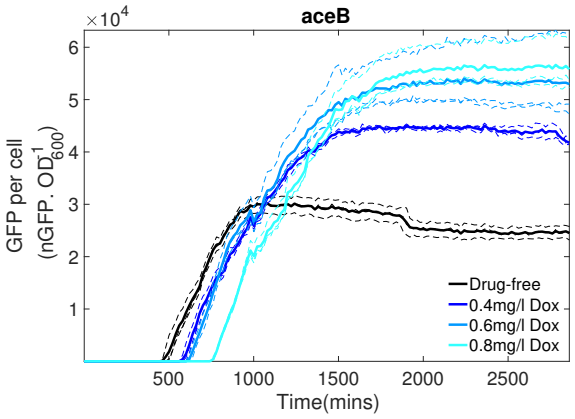

(b)

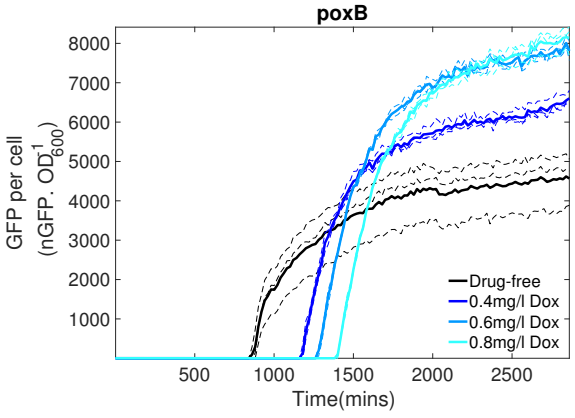

(c)

Figure 23: The normalised, dose-dependent levels of expression (GFP/OD) for selected promoters (*icd, aceB* and *poxB*) over 48 hours. The mean is displayed as a solid line and individual replicates as dashed lines.*n = 4*.

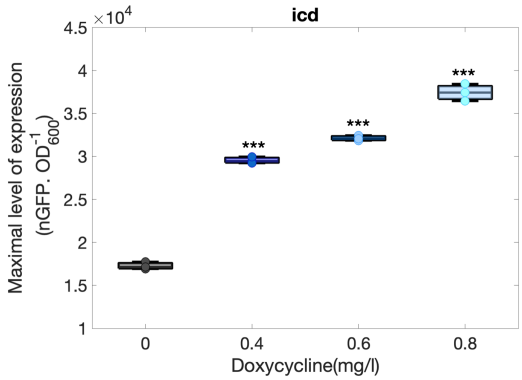

(a)

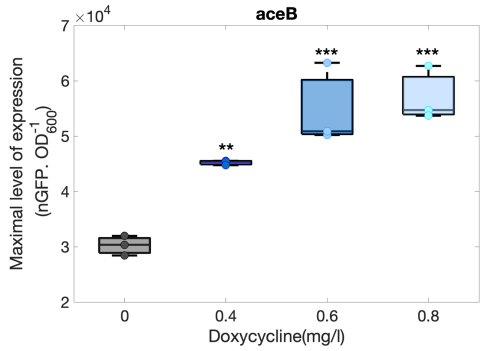

(b)

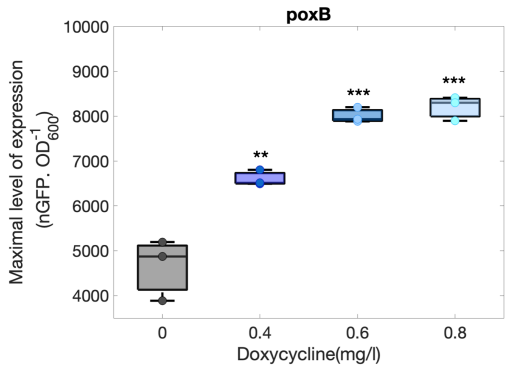

(c)

Figure 24: The maximal level of expression for *E.coli* with tagged promoters for *icd, aceB* and *poxB* as a function of doxycycline concentration. One way ANOVA with post-hoc tukey, ns = not significant, * = p <0.05, ** = p <0.01, *** = p <0.001.*n=4*.

2.8.2 Glucose uptake

E.coli is required to uptake nutrients from the environment, such as glucose in order to survive. Given that metabolism and resource uptake are interconnected processes [146], and we have measured variations in metabolic gene expression with doxycycline exposure, we next sought to identify changes in the expression of genes involved in glucose uptake.

Glucose uptake is generally facilitated by outer membrane porins, primarily OmpC and OmpF. Furthermore, the proportion of these two porins in the cell membrane will vary depending on the environmental conditions, for example in response to nutrient availability and the presence of toxins such as antibiotics. Under conditions of nutrient deprivation, OmpF will be favoured as it is the larger of the two porins, and therefore facilitates rapid uptake of resources versus the smaller OmpC porin [147]. Unfortunately, a GFP-reporter strain for OmpF is not available within the GFP library, however we did measure the expression of the OmpC promoter upon exposure to doxycycline over 60 hours. Given that doxycycline is present in the media, being the smaller of the two porins, we would anticipate increased expression of OmpC.

We find that after an initial dip in the expression between 8-16 hours, the *E.coli* population exposed to 0.4mg/l doxycycline has higher expression of the OmpC promoter (figure 25a). This is logical when we consider the trade-off between permeability and resource uptake during antibiotic exposure. As OmpC is the smaller pore, it is favoured over OmpF when an antibiotic is present as this reduces the uptake of antibiotic into the cell. However there is a trade-off with nutrient uptake, as fewer resources can be transported through a smaller pore [148] and this represents a trade-off between 'self-preservation and nutritional competence' (SPANC) [149]. In other words, there is a balance between protection against stress (such as antibiotics) and the uptake of nutrients.

In *E.coli*, the phosphoenolpyruvate-carbohydrate phosphotransferase system (PTS) is one of the primary systems responsible for the transport of sugars such as

glucose into the cells cytoplasm. As such, when glucose is present the PTS system is highly active and prevents the expression of non-PTS sugar transport systems via carbon catabolite repression [150].

The *ptsG* gene encodes the membrane receptor $IICB^{Glc}$ for the glucose-specific E11 transporter, and thus plays a key role in the PTS system. We find that whilst doxycycline-exposed cultures initially have lower expression of *ptsG*, by the end of the measurement period the level of expression is higher relative to the drug-free population (figure 25b). It has been reported that interference with the process of glycolysis results in lower expression of *ptsG* [151], however we did not find any substantial changes in the expression of glycolytic genes in the presence of doxycycline in this study. It is possible that initially *ptsG* expression is down regulated in order to reduce uptake of doxycycline. However, as the drug is degraded over time, expression may be upregulated.

The *ptsA* gene is also part of the PTS system and shows lower expression levels in doxycycline-exposed cultures versus drug-free, as shown in figure 25c. Together this suggests that genes for glucose uptake are initially not as highly expressed in the presence of doxycycline, and this could be due to the trade-off between reduction in drug uptake into the cell versus the uptake of resources. The raw growth curves and GFP expression over time are displayed in supplementary figure S9.

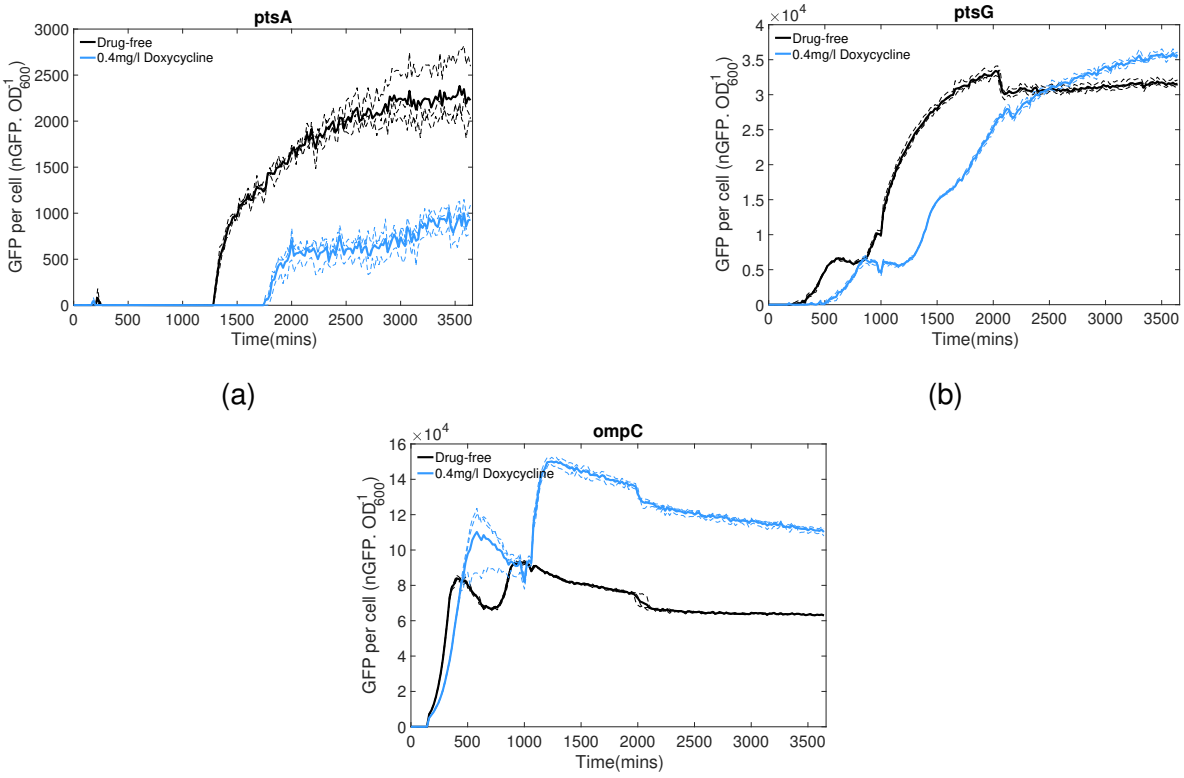

Figure 25: The levels of GFP expression normalised to OD(600nm) for promoters of genes involved in glucose uptake. The solid line represents the mean, whilst the dashed lines represent individual replicates *n=4*.

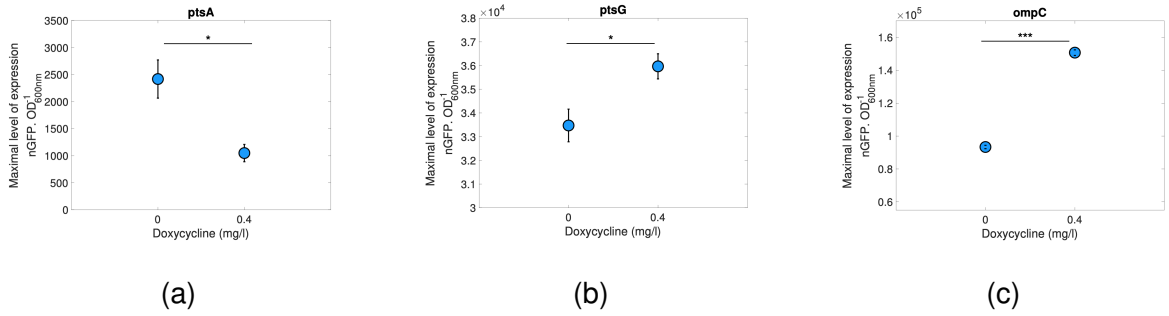

Figure 26: The maximal levels of GFP expression normalised to OD(600nm) for promoters of genes involved in glucose uptake. Two sample t-test, ns = not significant, * = p <0.05, ** = p <0.01, *** = p <0.001.*n=4*

2.9 Whole-genome resequencing of doxycycline-exposed, starved *E.coli*

Through growing cultures exposed to the antibiotic doxycycline for an extended period of time, we have demonstrated that exposure to this ribosome-binding antibiotic can have surprising benefits towards the growth of *E.coli*. Antibiotic-induced benefits on bacterial cells have been demonstrated in the past, for example antibiotics can result in increases in yield [7] and hormesis [20]. However, to the best of our knowledge, this is the first time that an antibiotic has been shown to result in improvements to both growth during starvation and long-term viability. When considered alongside the observation that doxycycline can increase a bacterial populations density in the short term, our understanding of doxycycline as a growth-inhibiting antibiotic is challenged.

Next, whole genome resequencing was carried out on starved *E.coli* cultures treated with doxycycline in order to elucidate mutations that contribute towards the long-lived phenotype observed previously in this chapter. Indeed, WGS has been used previously to identify mutants present in starved cultures and it has been found that the selection pressure of nutrient deprivation results in the rapid accumulation of mutations within a bacterial population [152]. It has been reported that 93.5% of cells surviving till day 11 of starvation carried a mutation, and primarily in the genes effecting the RNA-polymerase core enzyme. Other previous studies have identified that the media composition and type of vessel can impact on both the rate of death and mutation frequency [104, 153].

WGS was performed on *E.coli* cultures that were starved of nutrients for 21 days without the addition of fresh media. Doxycycline was added to a subset of the cultures at two different subinhibitory concentrations (0.2 and 0.4mg/l) and four cultures were left drug-free as a control. The *E.coli* populations were sampled on days 1, 3, 7, 10, 14 and 21 at which point 10 μl of culture was removed and serially diluted before being spread on agar plates for CFU counts - this allowed us to track

changes in cell viability over time. Additionally, at these time points 5ml of culture was removed in order to sequence whole population samples. This is preferable in our case to the sequencing of clones as we anticipated that the low levels of growth in a starving culture would result in low frequency mutations throughout the population. Three identical, drug-free cultures underwent CFU counts on the same sampling days, but without the removal of 5ml in order to ensure that the removal of media for sequencing did not significantly influence the growth and death of the populations. In addition, four populations of the ancestral strain were sequenced to ensure continuity between the *E.coli* MG1655 strain used here and that used to generate the reference sequence. The samples were centrifuged on the day of collection and immediately frozen to ensure that further changes in CFU number did not occur. DNA extraction was performed using the GeneJet kit and sequencing was performed by Hinrich Schulenburg at The University of Kiel (Evolutionary Ecology and Genetics). The CFU over time for these cultures is displayed in figure 27.

2.9.1 Ancestral polymorphisms

A number of polymorphisms were identified in the ancestral *E.coli*, suggesting that these are mutations that have accumulated during multiple passages through media, or through repeated freezing and thawing. These mutations include a 776bp deletion in *crl* that was present at a frequency of 100% in both the ancestral and experimental populations. *crl* is a gene for a sigma factor-binding protein. Both insertion mutations [154] and deletion mutations [155] in *crl* have been identified within *E.coli* MG1655 and it is thought that inactivation of this gene is beneficial under starvation conditions, such as during growth on a stab culture. We also identified a 1bp insertion in *glpR* - various polymorphisms in this gene have been observed previously and are thought to be due to the use of glycerol in media [154, 156]. The same study identified an single bp insertion in *gatC* - thought to

abolish the ability to use galactitol as a resource, whilst here we observed a 2bp deletion. Additional polymorphisms identified in the ancestral strain include a single bp substitution in *ybiY*, a 1bp deletion in *yeaR* and finally a 6bp deletion in *yfgI*. All of these mutations were excluded from further analysis.

2.9.2 Polymorphisms across all starved populations

Many polymorphisms were found to be shared amongst both drug-free and drug-exposed conditions, and thus are likely adaptations to starvation. For example, multiple SNPs were detected in the oxidoreductase complex, *rsxC* - this gene is involved in maintaining the reduced state of *soxR*, a gene involved in the protection of cells against superoxide [157], a common stress in starving cultures [158].

In total, over 432 individual polymorphisms were found across all conditions and time points, with the majority present at low frequency (below 10%). It should be noted that for the purpose of this study, mutations occurring on day one of the experiment have been excluded from further analysis as these are likely to be the result of adaptation to the media. Figure 27 shows the time points at which mutations reaching frequencies over 10% appear in each antibiotic condition. We find that in all conditions, high frequency mutations are found in *ftsE*, this is a gene involved in cell division and mutations within it have previously been associated with acid stress [159]. In addition, high frequency mutations were also identified in *cyoB* across all conditions. *cyoB* is involved in the production of a Cytochrome bo(3) ubiquinol oxidase subunit, a component of the aerobic respiratory chain.

Only six mutations were found to reach a frequency of 10% or above in the drug-free conditions. Yet cultures exposed to 0.2mg/l doxycycline had 23 mutations above 10% frequency, and cultures exposed to 0.4mg/l doxycycline had 13. It is possible that the increased cell densities, alongside any metabolic changes induced by doxycycline, resulted in the greater number of high frequency mutations measured in doxycycline-

exposed populations. Furthermore, we observe fluctuations in the appearance and disappearance of mutations, even in those that reach the highest frequencies. This could be due to their extinction within the population, or alternatively the frequencies could drop below the detectable limit.

We calculated the dN/dS ratio to establish if there is selection pressure on mutations within protein-coding regions in either drug-free or drug-exposed conditions. This compares the ratio of synonymous to non-synonymous mutations within the population over time, with a value above one indicating an excess of non-synonymous versus synonymous mutations [160]. There is a visible change in the trend between conditions, in that the dN/dS ratio appears to decrease over time in drug-free conditions, whilst it increases over time in both 0.2 and 0.4mg/l doxycycline (figure 28). It is therefore possible that there is a larger selection pressure on protein coding regions within doxycycline-treated populations relative to a drug-free control.

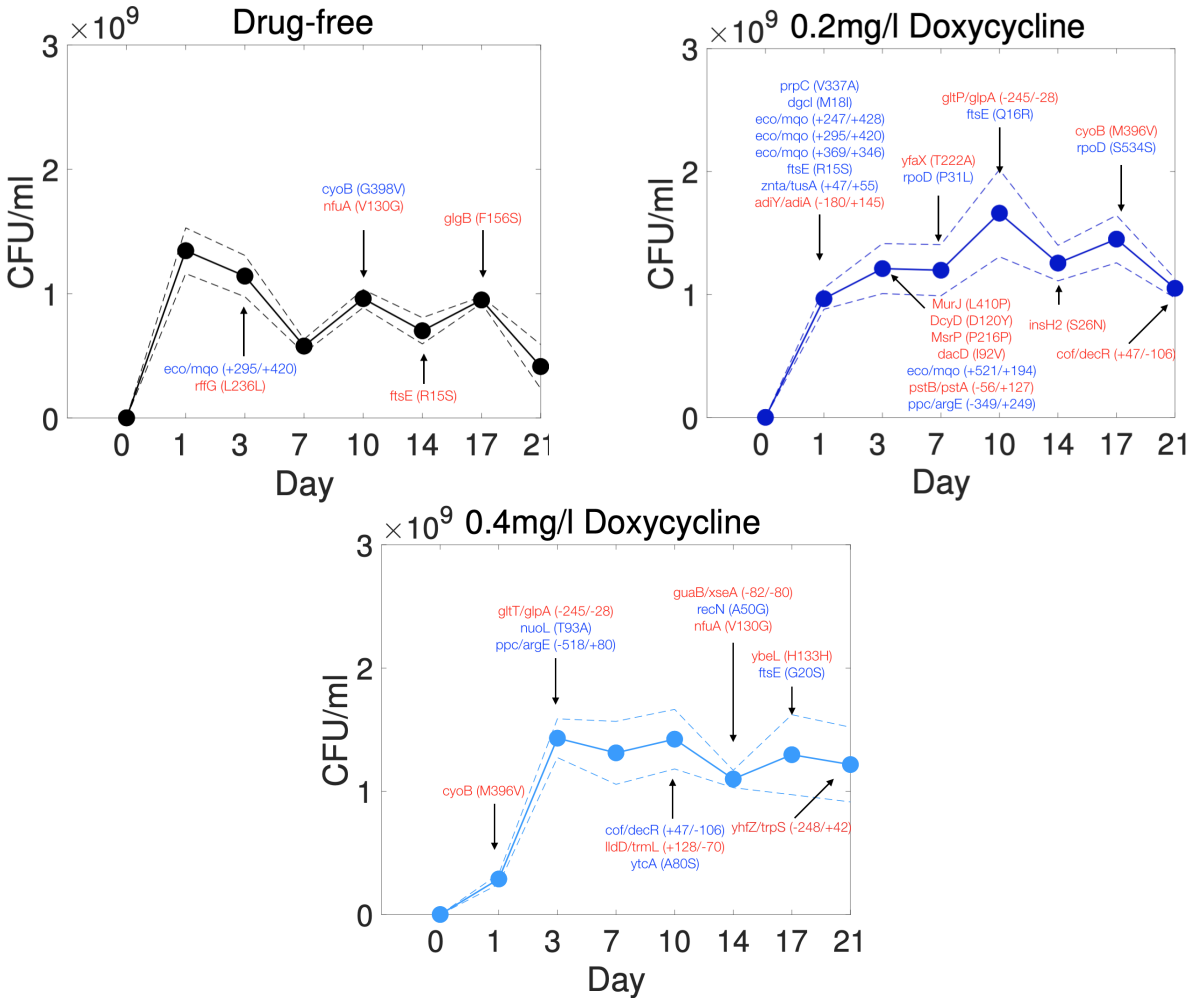

Figure 27: The growth curves obtained from large volume batch culture of *E.coli* pre-exposed either to 0, 0.2mg/l and 0.4mg/l doxycycline and grown for 21 days without the addition of fresh media. Mutations appearing at a frequency above 10% are shown for each antibiotic condition at the time point in which they first occur. Genes shown in red represent mutations that do not occur at any other time point, whilst blue genes represent mutations that are also present at future time points.

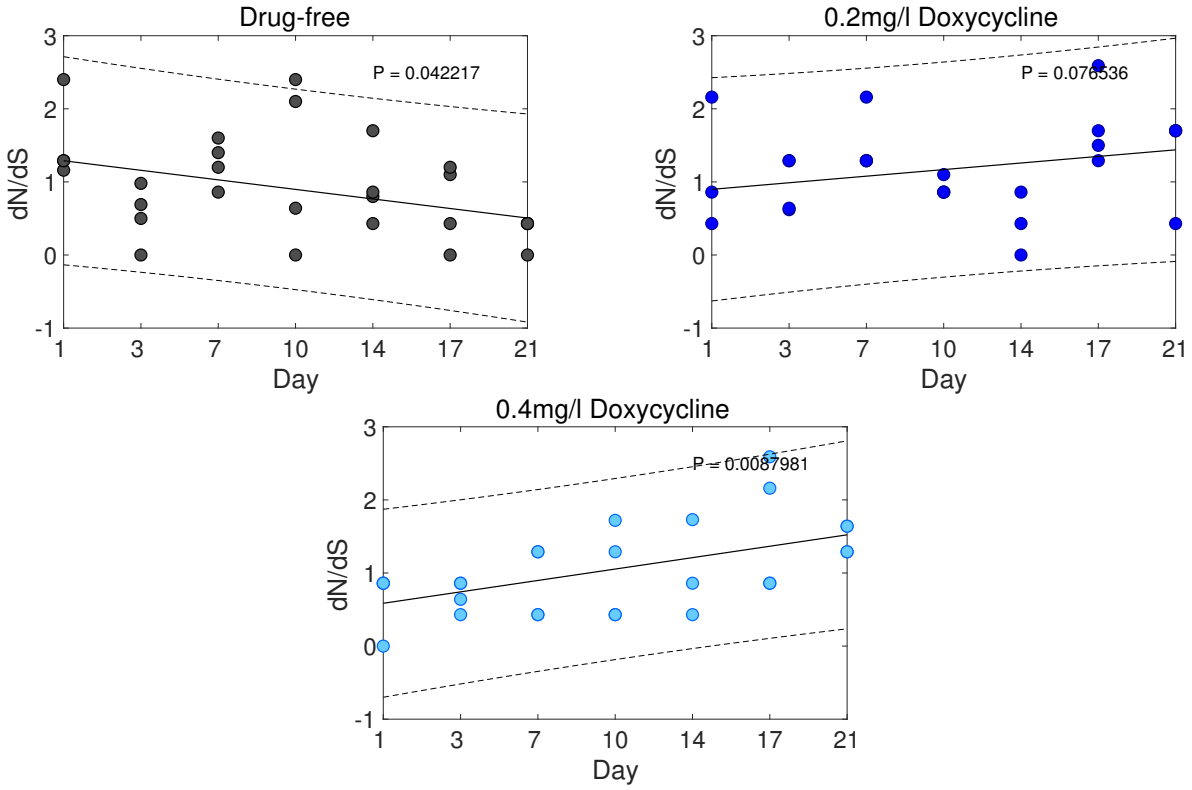

Figure 28: The trajectory of dN/dS ratio was found to decrease in drug-free condition over 21 days, whilst it increased with both 0.2 and 0.4mg/l doxycycline. A dN/dS value above 1 indicates that there is an excess of nonsynonymous to synonymous mutations, and therefore the mutations are likely to be adaptive. The linear regressions are shown as a solid line, with $\pm$ estimated 95% confidence intervals (CI, 4 replicates) shown as dashed lines.

2.9.3 Polymorphisms unique to doxycycline-exposed cultures

Certain SNPs were found to be unique to doxycycline-treated cultures, for example SNPs in the sigma factor *rpoD* were identified in populations exposed to 0.2mg/l doxycycline, and in the DNA repair protein recN with 0.4mg/l doxycycline. Mutations in genes that encode RNA polymerase (such as rpoD) have wide ranging impacts on adaptation, including improved growth on minimal media [161]. In addition, mutations in RNA polymerase genes have previously been shown to arise during prolonged periods of starvation [152]. This suggests that they play an adaptive role in the response to starvation.

Certain mutations were found to be present in both of the antibiotic-treated conditions, but not in drug-free populations, as illustrated in table 2. Cultures exposed to doxycycline were found to have a 134bp deletion in *argV* encoding tRNA(argV), one of the seven arginine tRNAs. A possible consequence is a reduction in protein synthesis, compounding the effect of doxycycline. Further mutations common to doxycycline-treated cultures include a substitution in *ybbL*, a putative aldolase involved in the regulation of sugar metabolism. It is likely that the rate of cell turnover in these populations is relatively low, and consequently it is difficult to establish the role of mutations in the starvation response as they are unlikely to reach fixation within a population.

Gene	Function	Position (bp)	Status
cof/decR	HMP-PP phosphatase/DNA-binding transcriptional activator	468,277	Intergenic
dgcI	Probable diguanylate cyclase	875,404	Nonsynonymous
yneE	Uncharacterised	1,608,166	Nonsynonymous
dgcF	Probable diguanylate cyclase	1,611,549	Synonymous
glpT/glpA	Proton/glutamate-aspartate symporter/ Anaerobic glycerol-3-phosphate dehydrogenase subunit A	2,352,619	Intergenic
ygbL	Aldolase	2,863,903	Nonsynonymous
yhcD	Uncharacterised	3,363,010	Synonymous
lldD/trmL	L-lactate dehydrogenase/tRNA (cytidine(34)-2-O)-methyltransferase	3,781,108	Intergenic
ytiD	Uncharacterised	4,556,770	Nonsynonymous
argV	tRNA(argV)	2,818,358	Δ 134bp

Table 2: SNPs and indels unique to doxycycline-treated populations over the course of starvation. These polymorphisms were identified in both 0.2 and 0.4mg/l doxycycline.

2.10 Summary

Here, through measuring the dynamics of *E.coli* populations exposed to various different antibiotics over a prolonged period of starvation, we were able to identify a novel microbial benefit conferred specifically by ribosome-targeting drugs - improvements to growth and long-term viability. Indeed, whilst doxycycline is detrimental to initial growth through the extension of lag phase, populations ultimately have a higher population density and improved population viability over an extended time period. We established that this phenotype is due to the binding of the antibiotic to the ribosome, as there was an absence of any benefit to long-term viability in a doxycycline-resistant strain of *E.coli*. It is possible that this phenotype is conferred partly by the increased use of cell debris as a nutrient source, as we observed in doxycycline-exposed *E.coli* cultures.

Furthermore, through the use of a GFP reporter library and whole genome sequencing we were able to track the metabolic and genotypic changes induced by doxycycline during the early stages of nutrient deprivation, through to long-term starvation. Tetracycline antibiotics have been found to alter the expression of metabolic genes [91, 8], and here doxycycline was indeed found to induce metabolic changes in *E.coli*. It is possible that these metabolic changes improve bacterial growth on the cellular debris and organic compounds present in a starved culture, thereby improving long-term viability. However, further work would be needed to confirm this such as monitoring metabolic gene expression during growth on spent supernatant.

This data ultimately highlights a novel property of ribosome-binding antibiotics, the ability to improve bacterial growth and viability during starvation. This has broader implications on infection medicine and our understanding of antibiotic function, as antibiotic doses which initially appear effective in preventing bacterial growth in the short-term can inadvertently benefit the growth of a microbial population over long time periods. Moreover, antibiotic resistance can be costly to bacterial growth in

the absence of antibiotics [162], however this data reveals an additional cost of resistance - reduced long-term viability.

CHAPTER THREE

RIBOSOME PRODUCTION CAPACITY AND STARVATION SURVIVAL

3.1 Overview

Following on from the results in Chapter 2, we next aimed to investigate the impact that interference with ribosome production would have on the ability of an *E.coli* population to survive starvation. We achieve this through the use of an rRNA knockout strain set. The key findings were as followed:

1. K is increased with decreasing rRNA operon copy number
2. Intermediate numbers of rRNA operons optimise an *E.coli* population for starvation survival.
3. There is no apparent cost to growth upon nutrient upshift in rRNA knockout strains.

Given that we have shown ribosome-binding antibiotics impact the process of cell death, and any benefit to long-term viability is lost in an antibiotic-resistant strain, we next sought to understand how other perturbations to ribosome functioning impact on death. For this, we utilise an *E.coli* strain set with reduced numbers of rRNA (*rrn*) operons [163]. The strains used here are shown in table 3. Whilst the wild type (WT) has seven almost identical *rrn* operons, the knockout strains have between 1-6 *rrn*

operons removed. It should be noted that the seven rRNA promoters have different activity (*rrnE* >*rrnG* >*rrnC* > *rrnD* >*rrnB* >*rrnA* >*rrnH*) [164].

Ribosome production is a costly process, so much so that during periods of rapid growth the transcription of the *rrn* promoters can be responsible for approximately 60% of cellular transcription [139]. Ribosome synthesis is therefore a highly regulated cellular process in order to prevent excessive costs to the cell. Under-production of ribosomes can result in inefficient use of the available resources, as they cannot be utilised in a time effective manner. Conversely, ribosome over-production will be energetically costly and wasteful for the cell [120, 165, 166].

Ribosome biogenesis is therefore carefully balanced with the influx of nutrients from the environment and the cells own maintenance cost in order to maximise the metabolism of nutrients whilst reducing cost to the cell. Furthermore, as growth rate is highly dependent on the availability of nutrients within the environment, there is also a strong correlation between growth rate and cellular ribosome content. This allows the cell to keep up with protein synthesis demands [120]. The optimal ribosome production rate is maintained via a negative feedback loop between the cellular ribosome pool and availability of resources. As such, when resources are depleted, the overproduction of proteins will result in further exhaustion of nutrients and consequently a reduction in ribosome production [167].

In most environments, a number of these seven *rrn* operons will be redundant as *E.coli* will still be able to maintain growth with fewer than seven operons. However, this redundancy exists to allow rapid growth upon exposure to very high resource concentrations [168]. Furthermore, it has been shown that all seven *rrn* operons *are* required for optimal growth in fluctuating environments [169] and the optimal *rrn* copy number is highly dependent on resource availability [7].

Here, we ask if there is an optimal number of ribosomes for long-term starvation. As ribosome production is such a tightly regulated cellular process, the introduction of a ribosome-binding antibiotic is likely to disrupt the balance. This is likely to have consequences on growth, and it would also impact on death.

We utilised the *rrn* strain set to artificially reduce the number of functional ribosomes in the cell, and thus measure the impact of perturbations to ribosome functioning on longevity. As ribosome production is known to confer a metabolic burden [170, 171], we hypothesised that strains with fewer *rrn* operons, and thus less capacity for ribosome production [163, 170] would have prolonged viability in nutrient limiting conditions compared to the WT. Additionally, we hypothesised that the growth and long-term viability of these *rrn* deletion mutants would closely mirror that of *E.coli* exposed to doxycycline, as both the deletion of *rrn* operons and doxycycline treatment impair protein translation. However, we did anticipate that there would be some variation in phenotype between the *E.coli rrn* knockout strains and doxycycline-exposed *E.coli* due to the effect of doxycycline on ribosome production. Tetracycline antibiotics have been shown to initially up-regulate a number of genes involved in ribosome production, presumably to counteract the effect of the antibiotic [172, 91]. Consequently, ribosome quantities in doxycycline-exposed cells may initially be greater than drug-free cells, and this could result in differences between the growth of doxycycline exposed *E.coli* and *rrn* knockout mutants that possess fewer ribosomes.

3.2 Contributions

The experimental design, implementation of protocols, and data analysis were carried out by Emily Wood. Prof Ivana Gudelj and Prof Robert Beardmore assisted with experimental design and data analysis. The *E.coli rrn* knockout strains were gifted by Prof Tobias Bollenbach.

1571

Strain	Type	Source
WT	MG1655	-
Δ 1	MG1655 Δ *rrnE*	[163]
Δ 2	MG1655 Δ *rrnGB*	[163]
Δ 3	MG1655 Δ *rrnGBA*	[163]
Δ 4	MG1655 Δ *rrnGBAD*	[163]
Δ 5	MG1655 Δ *rrnGBADH/ptRNA67*	[163]
Δ 6	MG1655 Δ *rrnGBADHB/ptRNA67*	[163]

Table 3: The *E.coli rrn* knockout strains used in this chapter. All strains are from reference [163]

3.3 Fewer *rrn* operons are optimal for growth in defined minimal media

Fewer *rrn* operons, and therefore a smaller ribosomal pool has been shown to optimise yield previously [7]. We first sought to identify the optimal number of *rrn* operons for growth under the conditions used here, and identify if a reduction in *rrn* operons mirrors the dose-dependent increase in population density observed with doxycycline (fig 2). The *E.coli rrn* strains were grown in 2mg/ml glucose and OD measurements were taken every 20 minutes over a period of 48 hours. During this time period no additional resources were introduced into the culture, allowing for the populations to go through all growth stages and glucose to be completely exhausted. Indeed, we find that by the end of the measurement period it is the strains with fewer *rrn* operons that have reached the highest population densities, as shown by figure 29.

This is reflected in a significant linear increase in K with decreasing numbers of *rrn* operons (figure 30a). As we observed with doxycycline-exposed cultures, we also find that fewer *rrn* operons results in a longer lag phase (figure 30b). However, in contrast to the data collected on growth in doxycycline, we do find a significant linear increase in growth rate with decreasing *rrn* copy number (figure 30c). The data therefore indicates that reductions in *rrn* copy number come at the cost of a longer lag period, but simultaneously benefits both K and growth rate. Note that the *E.coli* strain possessing 1 *rrn* operon failed to grow under the conditions used, presumably due to insufficient ribosome production for growth.

1594

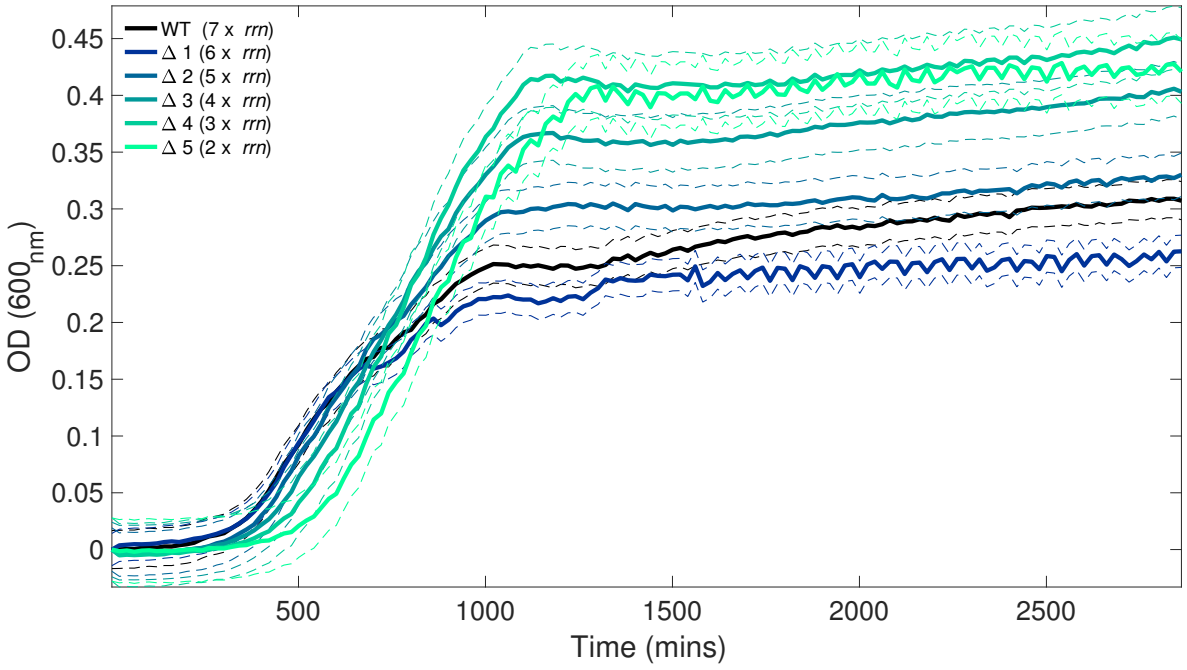

Figure 29: The blank-corrected growth of the seven *E.coli rrn* strains over 48 hours without the addition of fresh media. The mean growth is shown as solid lines and the individual replicates are displayed as dashed lines. *n=3*.

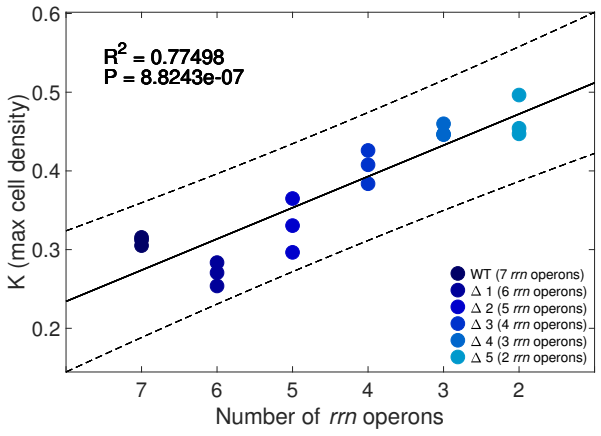

(a)

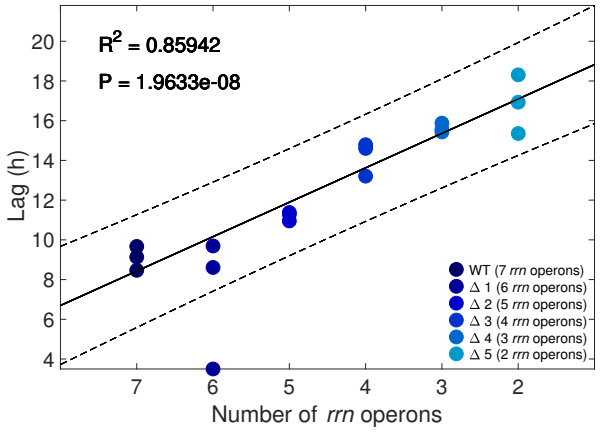

(b)

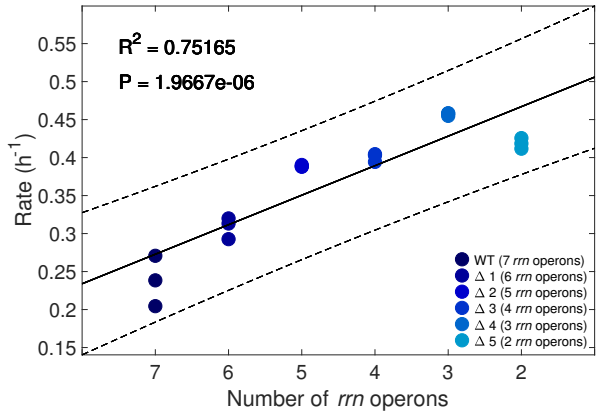

(c)

Figure 30: The relationship between *rrn* operon number and a) K (defined as the OD at stationary phase), b) lag time and c) growth rate. A significant linear relationship is found between *rrn* operon number and K, lag time and growth rate. Linear regressions are shown as a solid line, with $\pm$ estimated 95% confidence intervals (CI, 3 replicates) shown as dashed lines.

3.4 The WT *rrn* copy number is suboptimal for longevity

In order to study the effects of *rrn* operon copy number on longevity, we propagated WT *E.coli* alongside the knockout strains for 14 days without the addition of fresh media, thereby allowing all glucose to be exhausted and the populations to enter a starved state. In our case long term batch culture is optimal for the study of starvation as, unlike alternative systems such as serial transfer which introduce frequent bottlenecks, or continuous culture (chemostat) involving the removal of spent medium, we are able to measure the natural progression of a culture as nutrients are exhausted [104]. Figure 31 shows that cell viability declines rapidly after day 2 in the WT (black line), however in strains with fewer operons (blue lines), the drop in viability is either delayed or not observed within the measured time frame. The strain with 1 *rrn* operon grows poorly, presumably due to insufficient ribosome production rates (grey line). The figure insert displays an example of cell viability over time in both the WT (7 x *rrn*) and the *E.coli* strain with 5x*rrn* operons. The CFU dynamics for each individual *rrn* strain are displayed in supplementary figure S10.

We find that the optimal number of *rrn* operons for maximal cell viability is highly time-dependent (Fig 32), with the maximum cell density shifting from those strains with a greater *rrn* copy number on day 1 to those with an intermediate operon number by day 14. Whilst there is little variation in cell number between the knockout strains relative to the WT on day 1 (Fig 33c), by days 5 and 14 (Fig 33d-e) it is clear that the WT strain no longer possess the optimal number of *rrn* operons for maximising cell viability. This data suggests that whilst a higher *rrn* copy number may maximise growth rate under certain conditions [173, 7], an intermediate number of *rrn* operons is optimal for long term survival. This supports the hypothesis that it is the interference with ribosome activity that improves viability, both through the artificial reduction in *rrn* copy number as shown here, as well as through the addition of a ribosome-targeting antibiotic.

1623

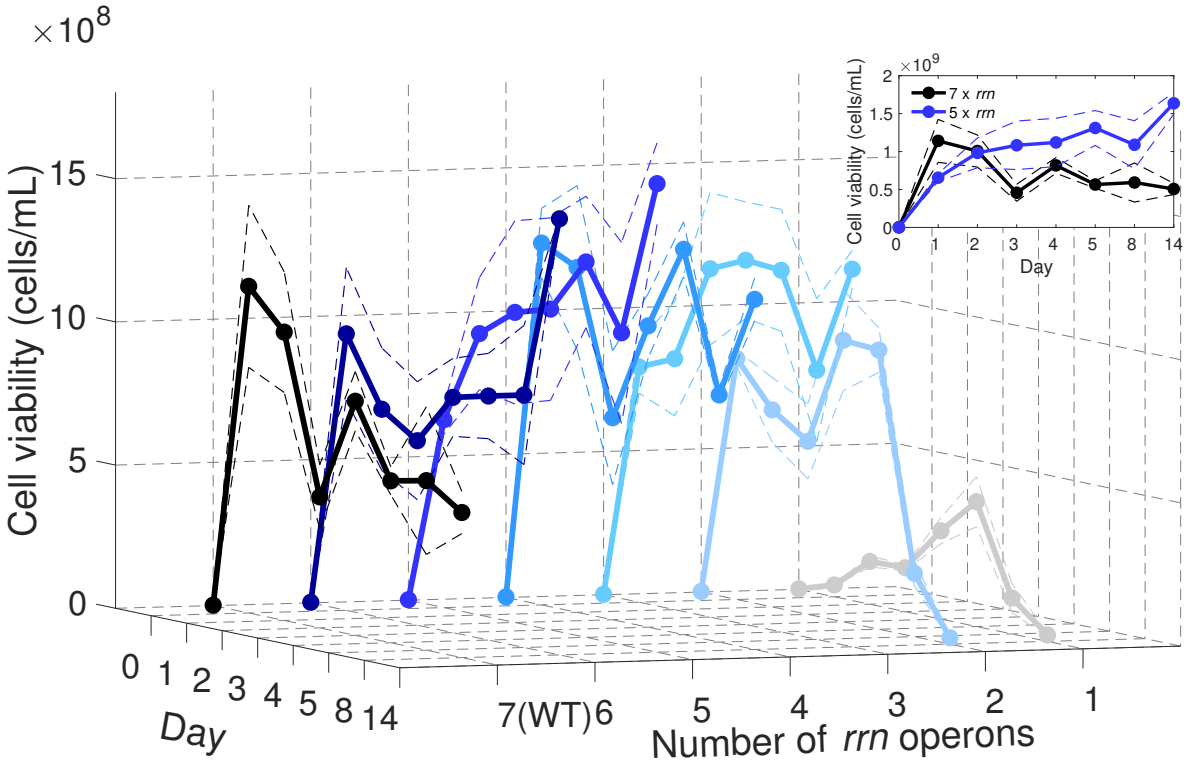

Figure 31: Collated CFU data from different *rrn* knockout strains over 14 days of starvation. The mean is shown as a solid line, with ± estimated 95% confidence intervals (CI, 3 replicates) shown as dashed lines.

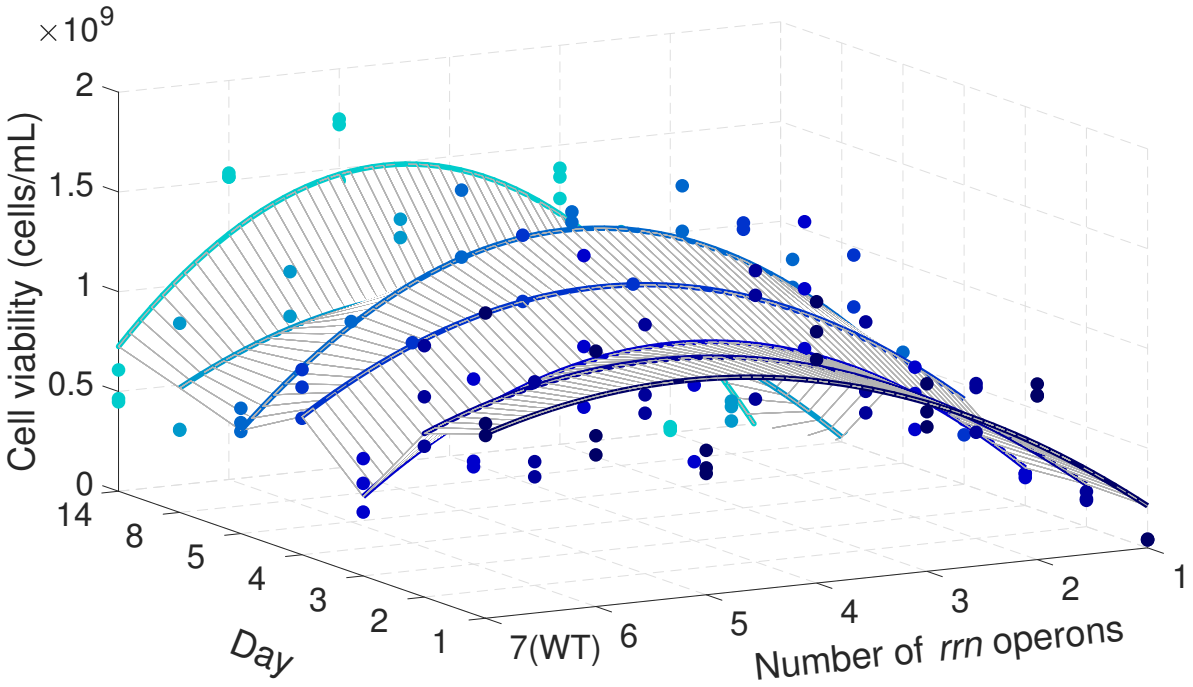

Figure 32: Cell viability (z axis) is shown as a function of both time (y axis) and *rrn* operon number (x axis). We observe a shift in the optimal *rrn* copy number to strains with fewer *rrn* operons as time progresses. Both linear and quadratic regressions were calculated, with the best fit according to the adjusted R^2 value shown. Regressions are shown as solid lines.

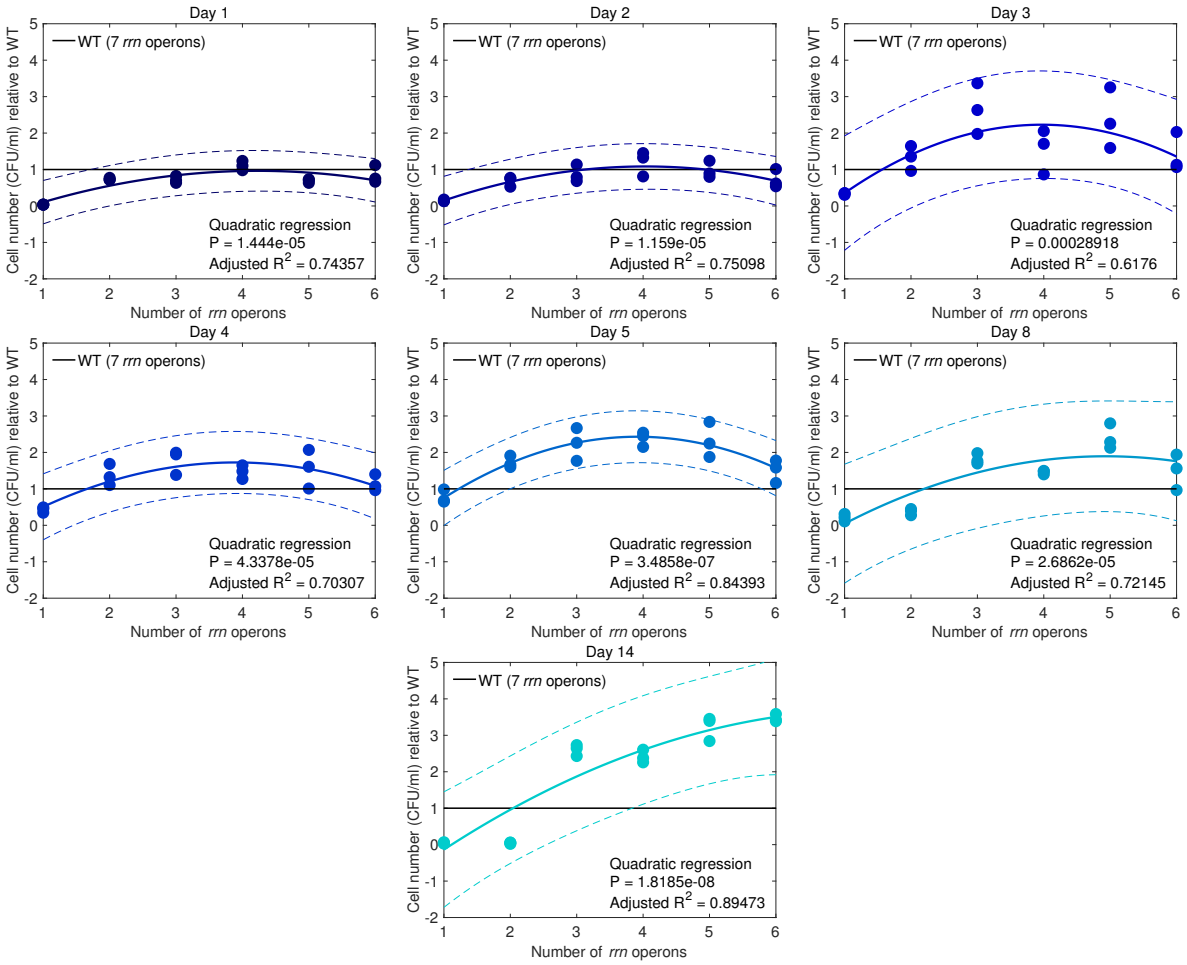

Figure 33: The optimality of *rrn* operon copy number changes over time, relative to the WT. Cell viability (y axis) relative to the WT is shown as a function of *rrn* operon number (x axis), with different subplots showing different time points. Both linear and quadratic regressions were calculated, with the best fit according to the adjusted R^2 value shown. Regressions are shown as solid lines, with $\pm$ estimated 95% confidence intervals (CI, 3 replicates) shown as dashed lines.

It has previously been reported that upon nutrient upshift [169], strains with fewer *rrn* operons are at a disadvantage relative to the wild-type and grow poorly. This is due to the reduced capacity for ribosome production, and hence decreased utilisation of new nutrients. To test the ability of these strains to grow upon nutrient upshift, we transferred 1x10^6 cells from each of the cultures that had been starved of nutrients for 14 days into M9CAA media supplemented with 0.2mg/ml of glucose. The growth of these cultures was measured 24 hours after nutrient upshift by counting CFU's. Surprisingly, here we find that strains with fewer *rrn* operons have greater cell density upon nutrient upshift in comparison to the wild-type with 7 *rrn* operons, as shown in figure 34. This can not be accounted for by the higher cell density at the end of the 14 day period with these strains, as the starting cell density was normalised before nutrient upshift. It is possible that the inconsistencies between previous data and our own is due to extended starvation period used here.

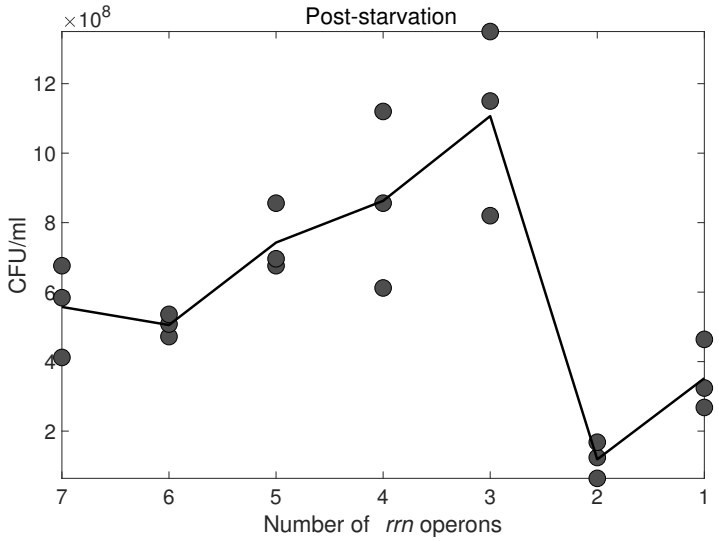

Figure 34: *E.coli* strains with fewer *rrn* operons have greater population density than the WT 24 hours after nutrient upshift, following 14 days of nutrient starvation. Each circle represents an individual replicate and the solid line represents the mean. *n = 3*

3.5 Summary

The data presented here suggests that the benefits to long-term viability measured in Chapter 2 are not unique to antibiotics, but rather a consequence of interfering with ribosome biogenesis. We found that the outcome of starvation is strongly influenced by the *E.coli's rrn* operon copy number, with the WT becoming suboptimal in comparison to those strains with fewer operons as the duration of nutrient deprivation increases (figure 31).

Ribosome production capacity, and consequently *rrn* operon copy number are key microbial traits, strongly influenced by bacterial lifestyle and the environment. In microbes such as *E.coli*, ribosome biogenesis must be kept under tight control in order to keep up with the cells' ever changing protein production needs, as the number of ribosome determines the rate of protein synthesis.

Wild-type *E.coli* possess 7 *rrn* operons, though not all are needed for optimal steady-state growth, and optimality alters depending on nutrient state [7]. However, possessing a greater number of *rrn* operons is beneficial upon entering a new environment as it allows for rapid production of new ribosomes [174, 168]. This is reflected in the ecological strategies of environmental microbes, as resource availability selects for different growth parameters, for example the reduction in lag time conferred by a larger number of *rrn* operons is crucial to bacteria in fluctuating environments. In contrast, aquatic microbes in stable, nutrient deficient environments are likely to have fewer *rrn* operons [174]. Less clear, however, is the impact that *rrn* copy number, and consequently ribosome biogenesis, has on microbial longevity.

Altogether, this data suggests that interference with cellular ribosome functioning influences population dynamics during starvation, and that this could lead to unforeseen benefits to microbial populations during treatment with ribosome-targeting antibiotics such as doxycycline. Furthermore, if improvements to viability are primarily due to interference with ribosome functioning, then other ribosome-targeting

antibiotics aside from doxycycline and erythromycin should also display this phenotype. Further work could therefore seek to identify how widespread this viability benefit is amongst ribosome-targeting drugs.

CHAPTER FOUR

THE GENOMIC BACKGROUND OF DOXYCYCLINE-INDUCED BENEFITS TO GROWTH IN *E.COLI*

4.1 Overview

In Chapter 2, we showed the benefits to both population density and longevity conferred by doxycycline treatment. We next sought to understand how variations in genomic background alter these antibiotic-induced benefits, in addition to gaining a better understanding of the genomic basis for antibiotic susceptibility. To this end, the keio collection, compromising of 4,000 *E.coli* single gene knockouts was utilised. The key findings were as followed:

1. Doxycycline induces large phenotypic variations across single gene knockout strains.
2. Through a combination of principle component analysis and K-means clustering we can uncover groups of genes conferring particular phenotypes.
3. Metabolic gene knockouts are overrepresented in low-K clusters.
4. Certain groups of strains confer unusual phenotypes, such as the inability to grow in media in the absence of doxycycline where, conversely, growth is observed in the presence of doxycycline.

In Chapter two we showed the lag-yield trade-off induced by doxycycline treatment in *E.coli* MG1655, and next we sought to understand the genetic basis for this phenotype. In order to establish if any particular groups of genes or indeed cellular pathways are key to doxycycline-dependent improvements in growth, we utilised the keio collection. This is a library of *E.coli* strains comprising of single gene knockout strains for every non-essential gene, 3,985 in total [175]. Reverse genetics approaches such as this have become a powerful tool to explore the phenotypic response to mutations in the context of different environmental pertubations [176]. Through measuring the phenotypic response to doxycycline across thousands of genes, we can assess the impact of each mutation on the fitness of *E.coli* in response to antibiotic treatment, and how this changes over time as nutrients are exhausted.

Previous studies have utilised the keio collection to deduce the phenotypic response to drug challenge in various genetic backgrounds. For example, Liu et al. [177] generated an 'antibiotic barcode' for 22 antibiotics, identifying a set of genes that can be used for rapid typing of different antibiotics. Furthermore, by measuring the growth response of all keio knockout strains in response to various stressors, Nichols et al. generated 10,000 phenotypes, exploring not only the response to stress but also gene essentiality [178]. Whilst the authors utilised colony size as a measure of population growth, here we sought to understand the impact of antibiotic exposure on all aspects of the bacterial growth curve.

Through the use of an extensive gene knockout library such as the keio collection, it is possible to not only develop a better understanding of the relationship between genotype and phenotype, but also begin to deduce the function of previously uncharacterised genes [179, 178]. Mutations are a source of great phenotypic variation within bacterial populations, and the effect of mutations on growth is heavily context dependent. In other words, the size of a beneficial or detrimental impact on growth as a result of a mutation is dependent on the environmental conditions. Moreover, functionally associated genes are likely to result in similar phenotypes over varying environments. Therefore, by exploring the phenotypes of gene knockout strains in

response to perturbations we can begin to link those genes into likely functionally-related groups.

Here, we utilised a doxycycline concentration found to inhibit 50% of growth in the keio WT strain *E.coli* BW25113, allowing us to measure the phenotypic response to doxycycline against a background of individual gene knockouts. This allowed us to assess which strains retain the doxycycline-induced improvements to growth measured in the WT, and which strains lose any benefit. Furthermore, by measuring the phenotypic response over 48 hours we were able to assess the response to doxycycline over various stages of growth, and by doing so uncovered surprising phenotypes. For example, strains in which doxycycline both shortens lag time and increases final population density relative to the Keio WT, and indeed strains that only grow in the presence of doxycycline.

It was hypothesised that through the use of the keio collection, the genetic basis for the different phenotypic outcomes induced by doxycycline could be elucidated. For example, if doxycycline doesn't stimulate the growth of a particular strain, it is likely that the knocked out gene is relevant to this phenotype.

The original aim of this work was to screen the response to doxycycline in all 3,985 keio strains. However, due to the ongoing COVID-19 pandemic, this work could not be fully completed and as such the data in this chapter is presented as a preliminary study. At the time of thesis submission, the growth profiles of 1,266 strains in the presence and absence of doxycycline had been completed, resulting in 2,532 growth curves. Initially, strains with gene knockouts involved in metabolic processes were screened, followed by an arbitrary selection of the remaining keio library.

4.2 Contributions

The experimental design, implementation of protocols, and data analysis were carried out by Emily Wood. Prof Ivana Gudelj assisted with experimental design and data analysis. Prof Robert Beardmore provided funding (EPSRC), as well as assisting with experimental design and data analysis.

4.3 Doxycycline-induced benefits to K in *E.coli* BW25113

Exposure to doxycycline over a prolonged period of time results in a lag-K trade-off in *E.coli* MG1655, with higher doses of doxycycline prolonging lag phase but resulting in a higher cell density relative to a drug-free population (as shown in figure 2). To explore this phenotype in the genetic background of the keio collection, we first need to establish if a similar trade-off is present in the keio WT strain, *E.coli* BW25113. This WT strain is derived from *E.coli* MG1655 and as such we anticipated a similar phenotypic response towards doxycycline, including the dose-dependent benefits to population density.

Separate populations of *E.coli* BW25113 were grown in the presence of a various concentrations of doxycycline (0.2, 0.4 and 0.8mg/l), or left drug-free. These cultures were grown in M9CAA for 72 hours without the addition of any fresh media, and growth was monitored every 20 minutes as OD measurements. A dose response for *E.coli* BW25113 in doxycycline is displayed in supplementary figure S12.

We find that the growth of *E.coli* BW25113 in doxycycline closely mirrors that of *E.coli* MG1655, with increasing doses of doxycycline resulting in improvements to the final population density (as shown in figure 35). The advantages offered through carrying out an extended antibiotic susceptibly test such as this are clear. The drug-free population reaches stationary phase by $\sim$12 hours, after which point no further growth is observed - had the growth measurements been stopped at this point, the highest concentration of doxycycline used here (0.8mg/l) would appear

to be effective in inhibiting bacterial growth due to the prolonged lag phase. And yet, when measurements are extended up to 72 hours, as they have been here, we observe a stimulatory effect from doxycycline with increases in cell number beyond that seen in the drug-free control.

We confirm that there is a linear, dose dependent increase in K (max population density) with increasing doses of doxycycline, as shown in figure 36a. The highest dose of doxycycline (0.8mg/l) was found to result in $\sim$2.6x higher final population density relative to the drug-free population. Furthermore, as with *E.coli* MG1655, we measure a dose-dependent increase in lag time (figure 36b). However, unlike *E.coli* MG1655 we observe a significant linear decrease in growth rate with increasing concentrations of doxycycline (Fig 36c). This suggests that although the two strains of *E.coli* are genetically very similar, they do have slightly different phenotypic responses to doxycycline.

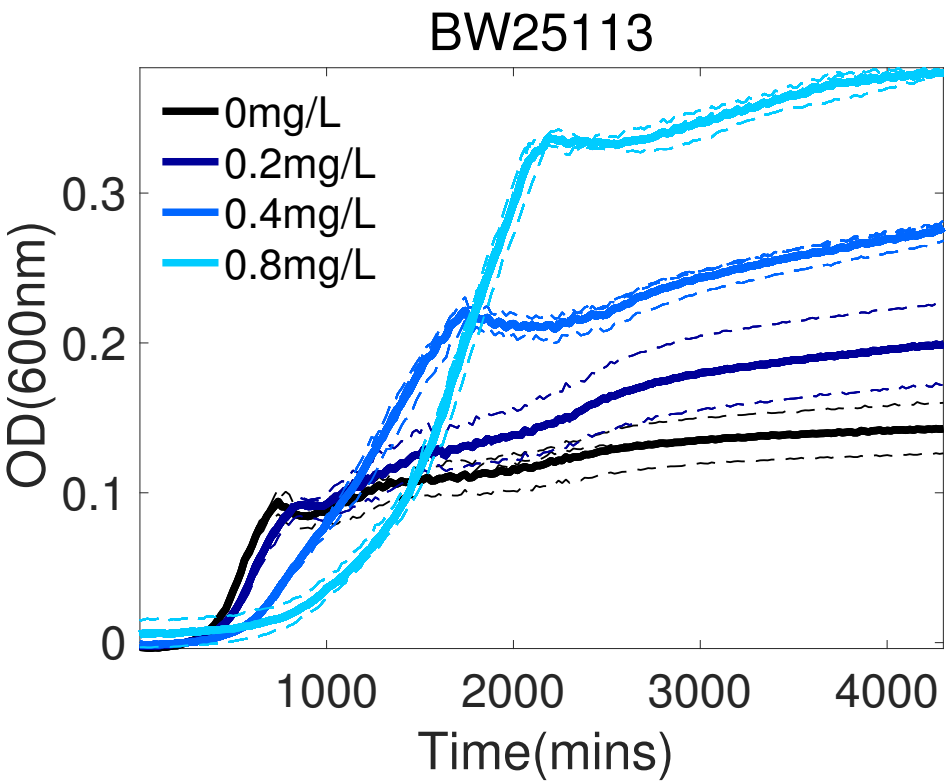

Figure 35: The raw growth curves for *E.coli* BW25113, the ancestral keio strain, exposed to various doses of doxycycline. Growth is measured as OD_{600nm}. The OD of populations exposed to doxycycline exceeds that in the drug-free control populations by the end of the growth period (72 hours). The mean is displayed as a solid line and individual replicates as dashed lines. *n=3*

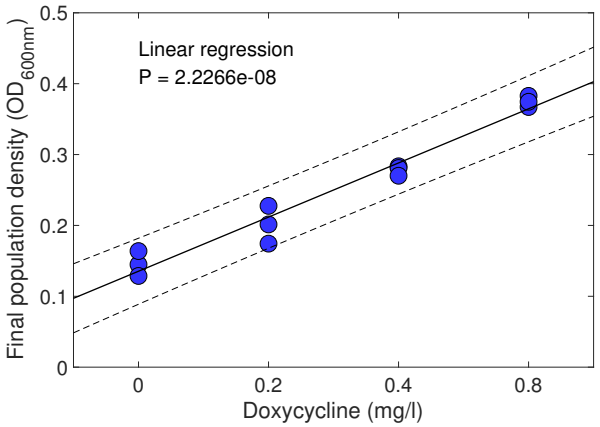

(a)

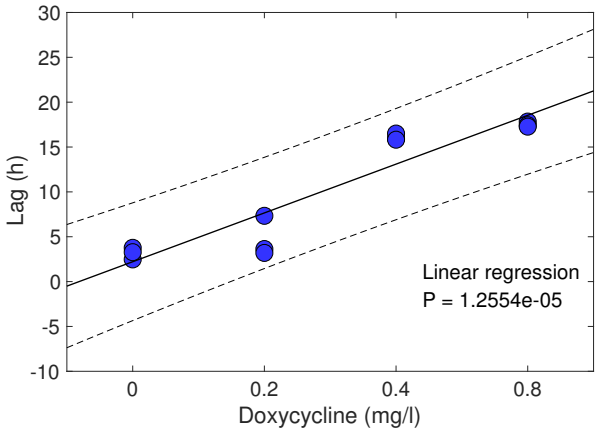

(b)

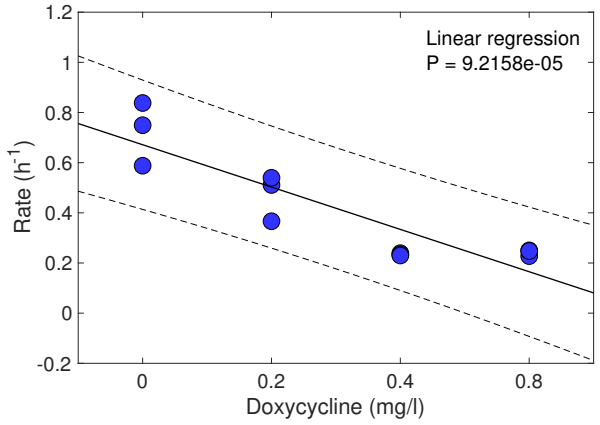

(c)

Figure 36: The final population density (a), lag time (b) and growth rate (c) are shown on the y axis as a function of increasing doxycycline concentration (x axis). We observe a positive linear relationship between population density and lag time with increasing doses of doxycycline, however there is a decrease in growth rate. Linear regressions are displayed as solid lines, with 95% CI shown as dashed lines.

4.4 The phenotypic response to doxycycline across all 1,266 single gene knockout strains

The phenotypic response to doxycycline across all of the keio library strains tested was examined in M9CAA supplemented with 2mg/ml glucose, with or without the addition of 0.4mg/l doxycycline (the concentration deemed to be the WT IC^{50}, that is the concentration of doxycycline that inhibits 50% of growth). The strains were transferred via pin replicator into microplates with an agar-filled reservoir surrounding the wells to prevent evaporation during the extended incubation period. Cultures were then left to grow for 48 hours without the addition of fresh nutrients, with growth measured as OD every 20 minutes. A 48 hour growth period was selected as both drug-free and doxycycline exposed cultures of the WT *E.coli* BW25113 strain were found to have reached stationary phase by this time point. This resulted in a total of 2,532 growth curves. Although only the growth of single replicates has been measured for each strain, we did additionally measure the growth of 96 of these strains in triplicate to check reproducibility. The blank corrected growth curves for all of the tested strains, in both drug-free and doxycycline-exposed conditions are displayed in supplementary figures (Fig S15-S28).

First, the difference in growth parameters for each strain in 0.4mg/l doxycycline relative to drug-free conditions was broadly assessed. Across all of the strains, doxycycline was generally found to result in decreased K, as shown in figure 37a. This would therefore suggest that in the majority of strains, the benefits to K that were found in the WT are lost. However, the lag time is generally extended in doxycycline conditions relative to drug-free (figure 37b) and growth rates were generally found to decrease (figure 37c), as found in the WT.

Nichols et al. [178] obtained 'fitness scores' based on the presence or absence of colony growth in different conditions, including doxycycline treatment (0.25, 0.5, 0.75 and 1mg/l doxycycline). We therefore sought to validate our results against those obtained by Nichols et al. by measuring the correlation between K in the strains

measured here, and the fitness scores in four different concentrations of doxycycline. The fitness scores were based on the size of the bacterial colony, hence K was used as a comparison as this is also a measure of final population density after a defined period of time. As shown in supplementary figure S13, there is poor correlation between K in 0.4mg/l doxycycline relative to drug-free, and the fitness scores obtained in different concentrations of doxycycline. However, the methods used by Nichols et al. (colony size measurements) differ from those used here (measurement of growth as OD). Moreover, M9CAA media was used in this study rather than LB and this too could result in the deviation in phenotypic response to doxycycline.

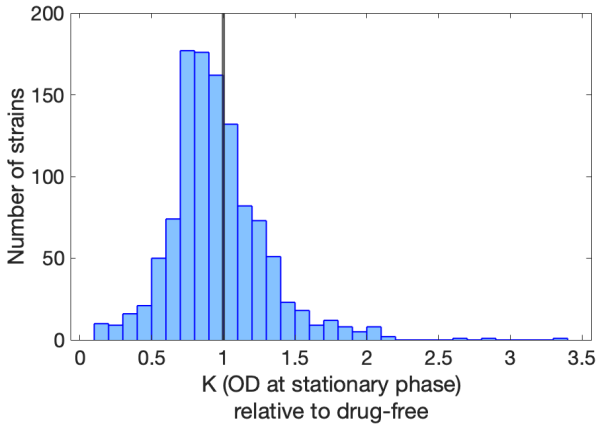

(a)

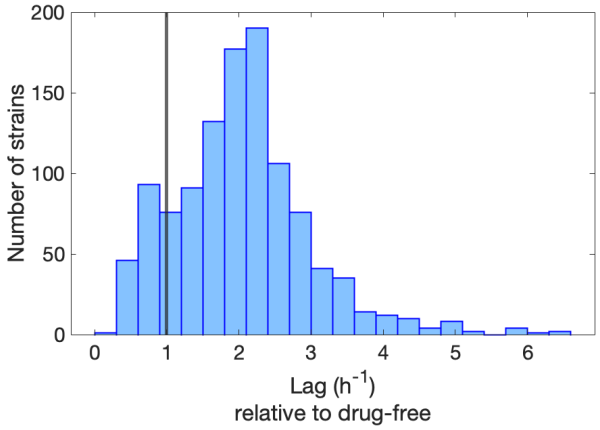

(b)

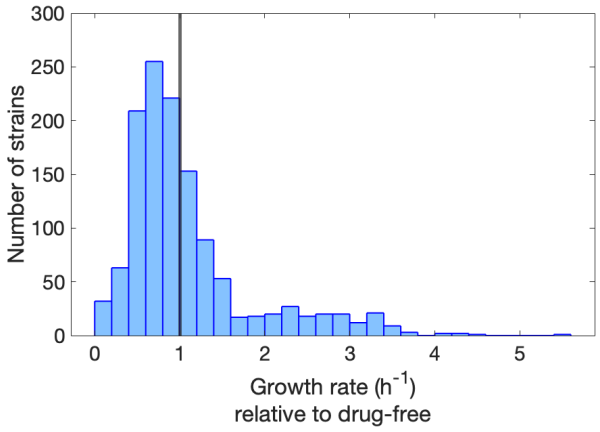

(c)

Figure 37: The distribution of K, rate and lag are shown in 0.4mg/l doxycycline normalised to the drug-free control for each strain. There is a significant difference in the K (Wilcoxon signed rank test, $p < 0.0001$), rate (Wilcoxon signed rank test, $p < 0.0001$) and lag (Wilcoxon signed rank test, $p < 0.0001$) in doxycycline conditions relative to drug-free.

4.5 Clustering the keio strains by growth over 48 hours.

The growth data obtained in doxycycline-exposed cultures was normalised to the growth of the identical strain in drug-free conditions and subjected to hierarchal clustering. From the clustergram displayed in figure 38a, we find that in the majority of strains, doxycycline is detrimental to at least one aspect of growth, versus growth in drug-free conditions. And yet, in some mutants the exposure to doxycycline confers a benefit over growth in drug-free media, as we find in the WT strain. Note that in figure 38, green indicates that the OD is greater in 0.4mg/l doxycycline relative to drug-free conditions, whilst red indicates that OD has decreased in doxycycline relative to drug-free conditions.

Strains displaying similar growth profiles in doxycycline were found to cluster together. For example, figure 38b displays strains that are characterised by a shorter lag phase but lower population density in doxycycline cluster together. These strains are of interest to us as they deviate from the lag-K trade-off observed in the WT *E.coli* strain.

In addition, we find that functionally-associated genes cluster together, with similar phenotypic response towards doxycycline. For example, the genes *sdhA*, *sdhC* and *sdhD* all encode succinate dehydrogenase, an enzyme that catalyses the oxidation of succinate into fumarate as part of the TCA cycle. These three genes were all found to cluster together in a phenotype characterised by a long lag phase and smaller population density relative to drug-free conditions, as shown in figure 38(c). This is therefore consistent with our expectation that genes encoding proteins with similar, or indeed the same function will result in similar phenotypic responses towards antibiotic exposure.

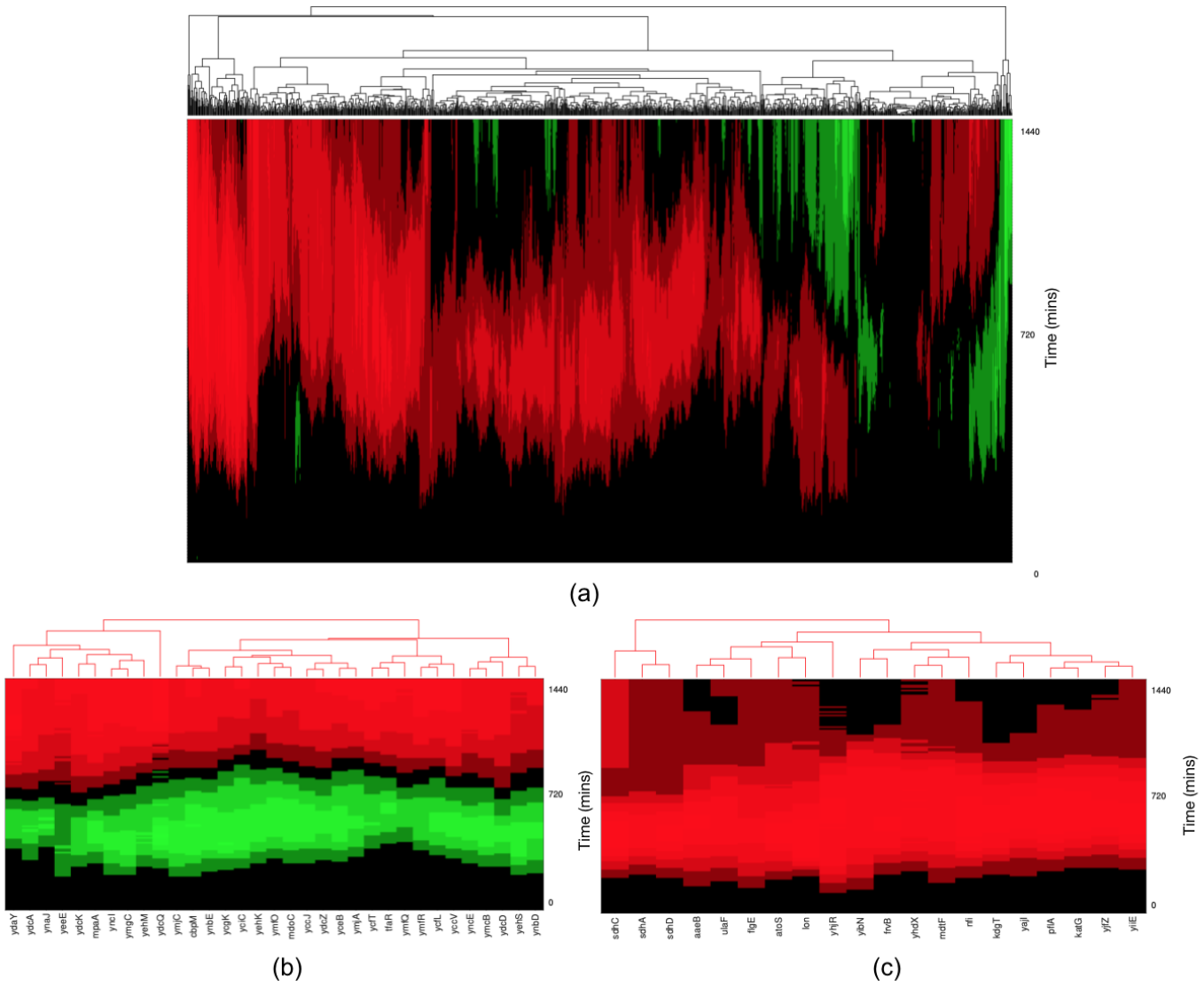

Figure 38: (a) A clustergram showing the clustering of genes by their growth in doxycycline relative to growth in drug-free media. The mutant strains are shown on the x axis and time (0-1400 mins) is displayed on the y axis. Green indicates that the OD is greater in doxycycline conditions relative to drug-free, whilst red indicates that is lower. (b) A subset of the clustergram contains genes that cluster together based on a shorter lag phase and lower population density in doxycycline relative to drug-free conditions. (c) The genes encoding Succinate dehydrogenase (*sdhA, sdhC* and *sdhD*) are found to cluster. *n=1*.

4.6 Principle component analysis of the growth curves in drug-free and doxycycline-treated cultures

To gain more insight into the association between genomic background and growth response to doxycycline, we next carried out principle component analysis (pca) on the 2,532 growth curves obtained in the presence and absence of doxycycline. This allowed us to cluster the data and identify the aspects of growth that best describe drug-free and doxycycline-exposed cultures.

The first three principle components were found to account for 94.7% of the variance within the data, with principle component one (PC1) alone explaining 80.7% of the variance, as shown by figure 39a. The temporal dependence of PC1 closely resembles the 'typical' growth of an *E.coli* population, with a relatively short period of lag followed by exponential growth and finally reaching stationary phase by the end of the measurement period. PC2 on the other hand more closely resembles an *E.coli* population that has a longer lag phase, but also lower final population density. Finally, PC3 is similar to PC2 but with a slightly higher final population density. PC2 and PC3 appear to show a rate-K trade-off, as they represent growth curves with a larger growth rate than that of PC1, but at the cost of a smaller K.

Figure (fig 39b) shows a scatter plot for the first two principle components, with drug-free growth shown as blue circles, and growth in doxycycline shown as red circles. We find that there is poor separation of doxycycline- and drug-free cultures based on PC1 and PC2, with data points clustering tightly together. It is likely that this is due to the the high percentage of variance explained by PC1.

However, when we project the data onto the PC2-PC3 space (fig 39c), we find a wave of phenotypic diversity in doxycycline-treated cultures, and better separation of the two conditions. This would suggest that doxycycline-treated cultures have a prolonged period of lag and fits in with the diversity in lag time identified in doxycycline-treated cultures previously (figure 37b).

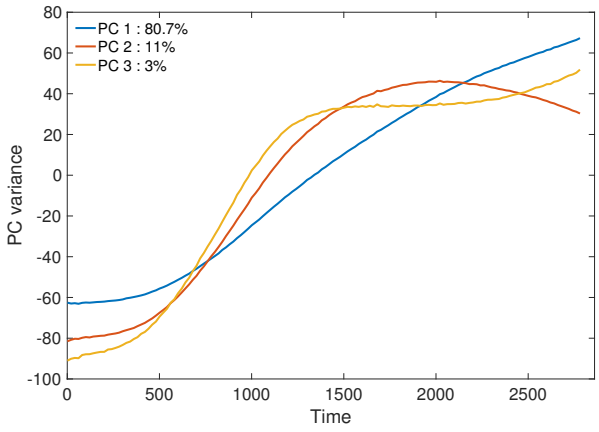

(a)

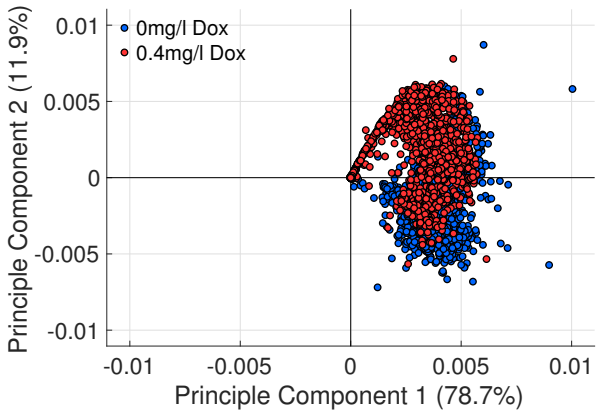

(b)

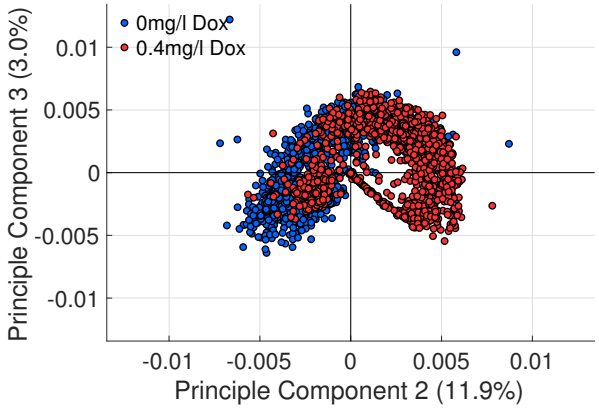

(c)

Figure 39: a) The temporal depedence of each PC1, PC2 and PC3 over 48 hours. PCA of the 1,266 keio knockout strains in the presence (red circles) and absence (blue circles) of doxycycline. Growth curves for all knockout strains are shown projected onto the a) PC1-PC2 and b) PC2-PC3 space.

4.7 Principle component analysis of doxycycline-exposed cultures relative to the drug-free control

We next aimed to identify clusters of strains with similar growth responses to doxycycline, relative to the drug-free control. For this, we normalised the growth data of doxycycline-exposed cultures against drug-free cultures and projected it onto the PC1-PC2-PC3 space. In this case, the first three principle components were found to account for 86.5% of the variance within the data, with PC1 explaining 58.5% of the variance, PC2 19.3% and finally PC3 8.4%. When we plot the temporal dependence of the first three principle components, as shown in figure 40a, we find that PC1 resembles strains with poor growth in doxycycline relative to drug-free conditions. PC2 on the other hand best resemble strains with elevated population density in doxycycline, and PC3 represents strains with further improvements to population density and a shortened period of lag.

Figure 40b shows the distribution of strains across the PC1-PC2-PC3 space, and we further elucidated clusters of strains with similar phenotypic responses to doxycycline through the use of K-means clustering. The growth curves were isolated from each cluster and are displayed in figure 41. We will now describe these clusters in turn, from the one representing the most strains to the least. The majority of strains (805, 63%) were located in cluster 8 and these have what we might refer to as a 'typical' response to doxycycline, largely mirroring that of the WT. From figure 41, we find that the strains located in cluster 8 generally have elevated population density relative to the drug-free control at the end of the measurement period.

The second largest cluster is number 6, containing 157 strains (12.4%), and these strains generally had little variation in growth between doxycycline and drug-free conditions, although some were found to have a shorter lag time. Cluster 2 was found to contain 95 strains (7.5%), and these strains had poor growth in doxycycline, in that the final population density was low in comparison to the drug-free culture or no growth was observed at all. The next largest was cluster 5 with 86 genes (7%),

and similar to cluster 2 it contained genes with a lag time extension and low final cell density in response to doxycycline. Cluster 7 contains 58 (4.7%) strains, largely comprised of those that were unable to grow in doxycycline or had very poor growth towards the end of the measurement period.

The next largest cluster (26 strains - 2.1%) was cluster 10 and represents a very surprising phenotype - those strains that only grow in doxycycline, alongside strains with substantially higher population density by 48 hours relative to drug-free. Cluster 1 was also found to contain strains with an usual phenotype in response to doxycycline - these 22 strains (1.7%) had a lower cell density, but also a shortened lag period. The remaining clusters contain very few strains - cluster 9 was only found to contain 13 (1%), cluster 4 contained 5 (0.4%) and finally cluster 3 only contained one strain. The growth of strains in these final clusters closely resemble that found in cluster 1.

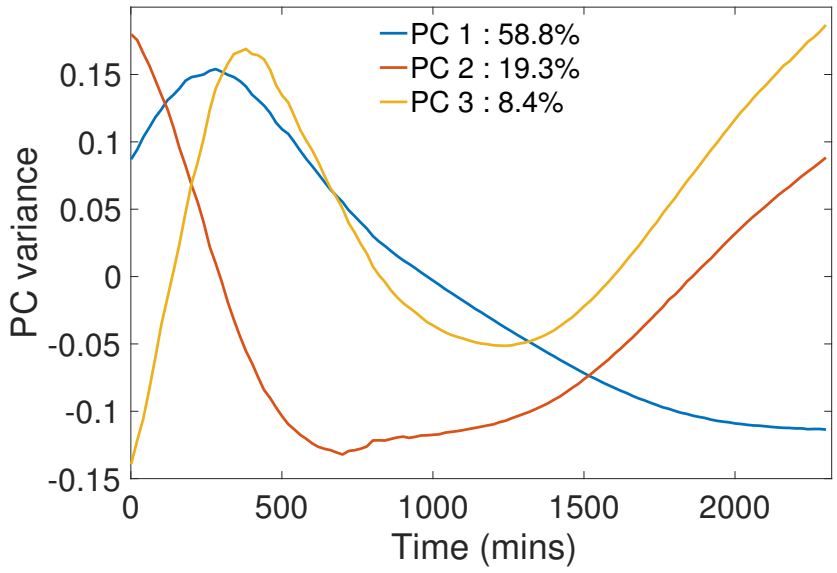

(a)

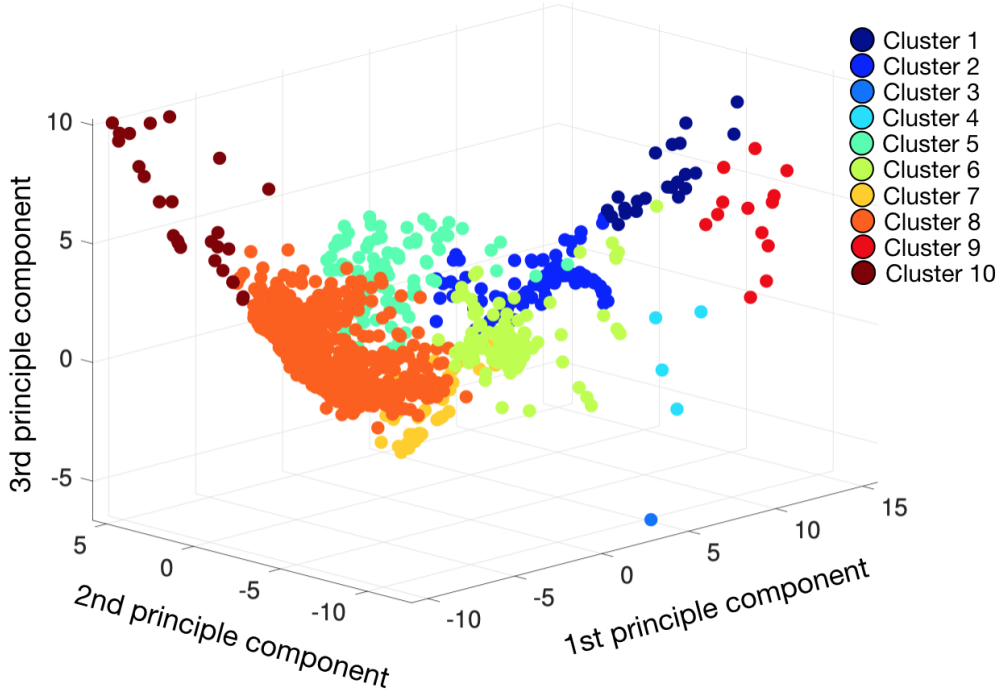

(b)

Figure 40: a) The temporal depedence of PC1, PC2 and PC3 over 48 hours for doxycycline-exposed cultures relative to drug-free. b) PCA of 1,266 keio knockout strains in the presence of doxycycline, relative to drug-free. Growth curves for all knockout strains are shown projected onto the PC1-PC2-PC3 space. The different colours represent different clusters of strains, as identified by k-means clustering.

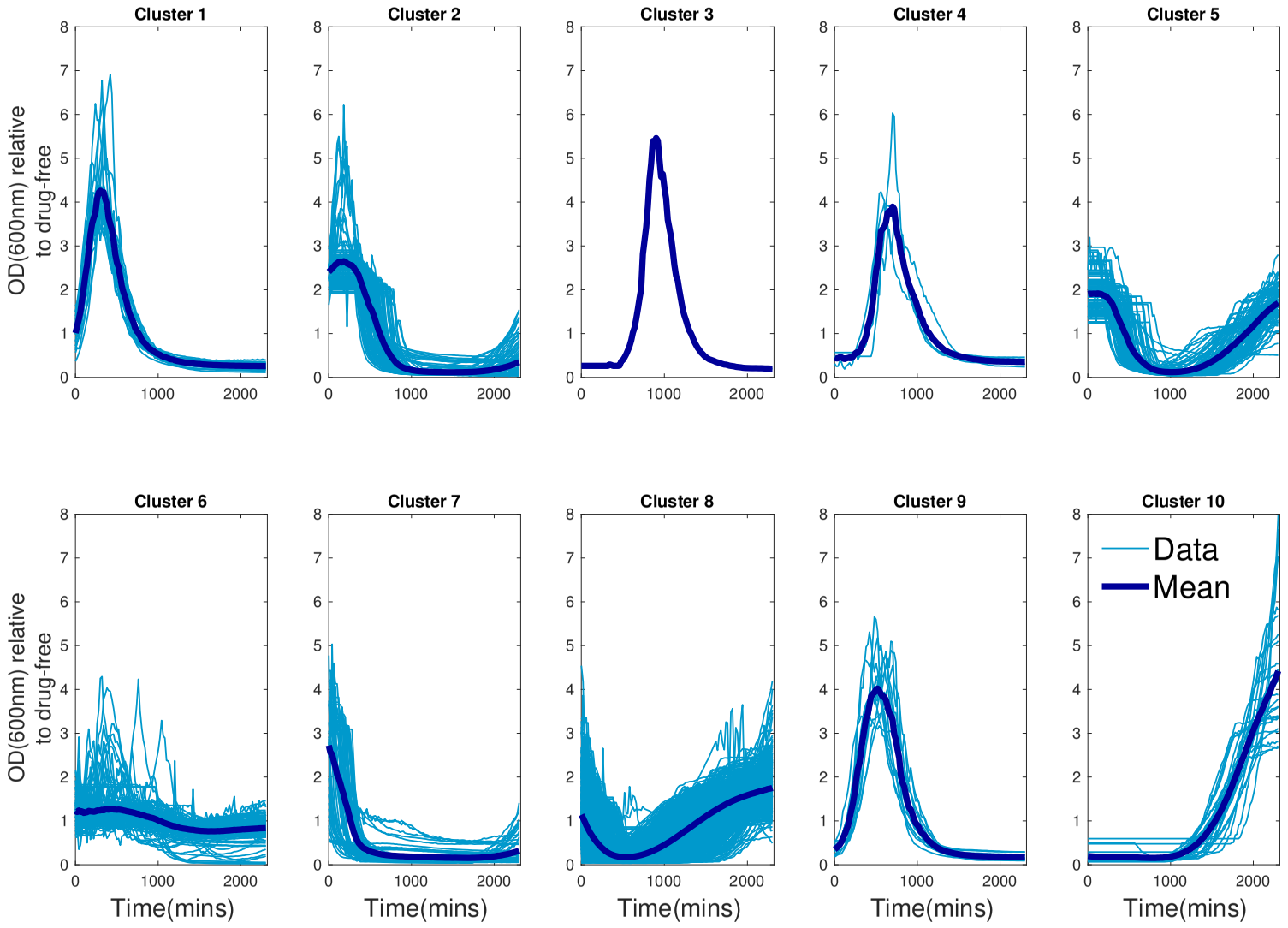

Figure 41: The growth curves of the strains from each cluster, as determined by k-means clustering, were extracted and plotted. These growth curves represent the growth of cutures exposed to doxycycline, relative to the drug-free control. The light blue lines represent the growth of individual strains, and the dark blue lines represent the mean of all growth curves found within that cluster.

Next, we assessed the relationship between gene function and the phenotypic response to doxycycline. To achieve this, the gene knockout strains were assigned to different groups of functional class based on the 'Clusters of Orthologous Groups of proteins' (COGs) [180], as shown in table 4. This approach allows us to assign each gene to one of 23 different functional categories, although many genes will be assigned to the 'general function prediction only (R)' or 'unknown (S)' categories due to lack of evidence regarding their function. For simplicity, all genes were assigned to one category only. The distribution of COG terms assigned to all of the keio strains tested is displayed in supplementary figure S14.

The COG terms assigned to each cluster are displayed in figure 42. Among the COG categories assigned within each cluster, certain ones were found to be enriched (COG enrichment was studied through the use of Fisher's exact test). For example, cluster 1 was enriched for genes in COG family S, that is genes with an unknown function. Both cluster 2 and 5 were found to be enriched for COG term L (replication and repair). Additionally, cluster 2 was enriched for term I (lipid metabolism). As cluster 2 largely represents strains with poor growth in doxycycline, this would imply that the genes involved in replication and repair, and those involved in lipid metabolism are important to the doxycycline-induced benefits observed in the WT.

Cluster 6 was found to be enriched for terms F (Nucleotide metabolism and transport), R and S. Cluster 7 was enriched for terms M (cell wall/membrane/envelope biogenesis) and T (signal transduction) - these strains grew extremely poorly in doxycycline, or indeed not at all. It is logical that disruptions to the cell membrane could impact the permeability of the cell, and therefore influence the uptake of doxycycline and consequently reduce growth.

The largest cluster, number 8, was found to be enriched for a broad range of terms including C (energy production and conservation), H (coenzyme metabolism) and K (transcription), this is to be expected given the large number of strains contained within this cluster. The remaining clusters (3,4,9 and 10) were not found to be enriched for any particular COG term.

In summary, whilst clusters containing the majority of strains with a 'typical' response towards doxycycline were found to be enriched for a variety of different COG terms, the clusters with poor growth in doxycycline were found to be enriched for COG terms primarily associated with metabolism and cell wall biogenesis and repair. This would suggest that impairment of these key cellular processes eradicates the benefits to K found upon doxycycline exposure in the WT. In chapter two, doxycycline exposure was found to alter the expression of metabolic genes, and it is therefore logical that metabolic gene knockout strains would also have a response to doxycycline that deviates from the WT. Furthermore, interference with the cell membrane could effect the uptake of doxycycline into the cell, resulting in the poor growth measured here.

COG term	Functional annotation
A	RNA processing
B	Chromatin structure
C	Energy production
D	Cell cycle control
E	Amino acid metabolism and transport
F	Nucleotide metabolism and transport
G	Carbohydrate metabolism and transport
H	Coenzyme metabolism
I	Lipid metabolism
J	Translation
K	Transcription
L	Replication and repair
M	Cell wall/membrane biogenesis
N	Cell motility
O	Post translational modification
P	Inorganic ion transport
Q	Secondary structure
T	Signal transduction
U	Intracellular trafficking
Y	Nuclear structure
Z	Cytoskeleton
R	General function prediction
S	Unknown

Table 4: COG terms and associated functional annotation.

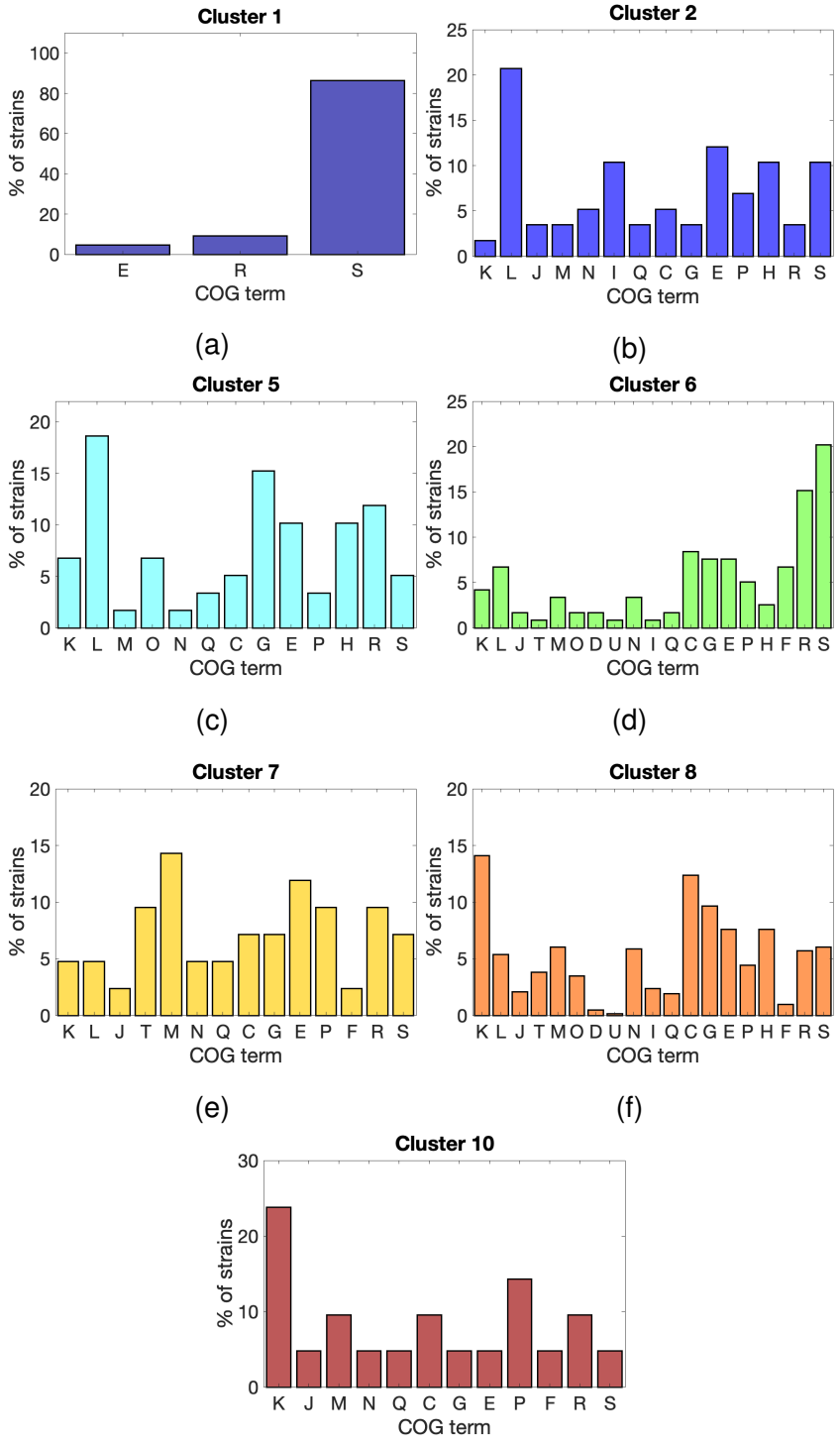

Figure 42: Single COG terms were associated with the genes from each cluster. The different colours correspond to the colours of the clusters shown in the previous PCA plot. Clusters 3,4 and 9 have been excluded as they contain few genes. COG term enrichment measurement were carried out using a Fishers exact test.

4.8 Keio knockout strains that lose doxycycline-induced benefits to growth

A key motivation of this work was to identify strains that deviate from the doxycycline-induced benefits to growth outlined in chapter two. More specifically, the extension of lag time and increase in population density observed after an extended growth period in doxycycline, identified with both *E.coli* MG1655 and the keio WT strain *E.coli* BW25113. By identifying single gene knockout strains in which this phenotype is absent, we can better understand its genetic basis.

To quantify this, we isolated the growth data of 510 strains found to have a lower final population density (K) in doxycycline relative to drug-free cultures. Note that strains that failed to grow in either both or just one of the conditions were excluded from further analysis. Furthermore, as the WT experienced a lag time extension in media containing doxycycline we also sought to identify which strains retain an extension in lag but lose the benefit to cell density, and indeed which strains actually experience a shorter lag with doxycycline. Figure 43a shows a scatterplot of the K against lag time in these low-K strains (in doxycycline normalised to the growth of same strain in drug-free conditions).

We find that there is a large distribution of lag time for these strains, and so k-means clustering was used to separate these strains into five separate clusters based on lag, as represented by the different colour data points in figure 43a. The growth curves of the strains within each cluster were then isolated and are displayed in figure 43b. Both clusters 1 and 2 are small, containing only 4 and 5 strains respectively and represent strains with an extremely extended lag time relative to drug-free. Cluster 3 was found to encompass the majority of low-K keio strains (407), and largely contained strains with an slightly extended lag time relative to the drug-free control.

Cluster 4 contained 98 strains with an intermediate lag time, 3-4x longer than the drug-free control. Finally, cluster 5 was found to contain 181 strains with a partic-

ularly unusual phenotype - although the final population density was small relative to the drug-free, the lag was either similar to, or actually shorter than the drug-free population. This is surprising given that with the concentration of doxycycline used here (0.4mg/l) and indeed with most ribosome-targeting antibiotics [181], we would anticipate a substantial increase in lag time as we observed in the WT (figure 35). In this cluster however, doxycycline is actually beneficial to *E.coli* in terms of lag time.

COG categories (table 4) were assigned to the strains in the three largest clusters (3,4 and 5), as shown in figure 44. COG enrichment was studied through the use of Fisher's exact test. We find that cluster 3 is enriched for genes in categories C (Energy metabolism) and H (coenzyme metabolism) - both of which are considered to be under the broad category of metabolism. In chapter 2 we demonstrated that doxycycline exposure results in changes to the expression of multiple key metabolic genes, and here we find that removal of genes involved in carbon metabolism also results in drastic changes to phenotype in doxycycline. All of the TCA cycle gene knockout strains tested here (barring $\triangle$ sucA) were found to lose the doxycycline-induced benefit to cell density (as shown in figure 45a), and all were therefore located in cluster 3. Moreover, all four glycolysis gene studied (figure 45b) and two key glyoxylate cycle gene knockout strains (figure 45c) used here were also found to be in cluster three and had therefore also lost the benefit to K but retained extension to lag time. This would suggest that these carbon metabolism genes are indeed key to the improved resource efficiency observed in the WT *E.coli* strain.

Cluster 4 is not enriched for any particular COG term, indicating that that no particular functional group results in the phenotype observed within this cluster. Finally, cluster 5 was found to have strains enriched in COG terms R (general function prediction only) and S (unknown function). A large proportion of *E.coli* genes have functions that have yet to be deduced, with approximately one third of all protein-coding genes from bacterial genomes still having unknown functions [182]. By linking these genes to particular phenotypes we can begin to associate them with particular phenotypes and genes of known function [178]. The fact that

the removal of these poorly characterised genes from the genome results in such an unusual response to doxycycline (shortened lag phase) indicates that they do indeed play a role in the antibiotic response.

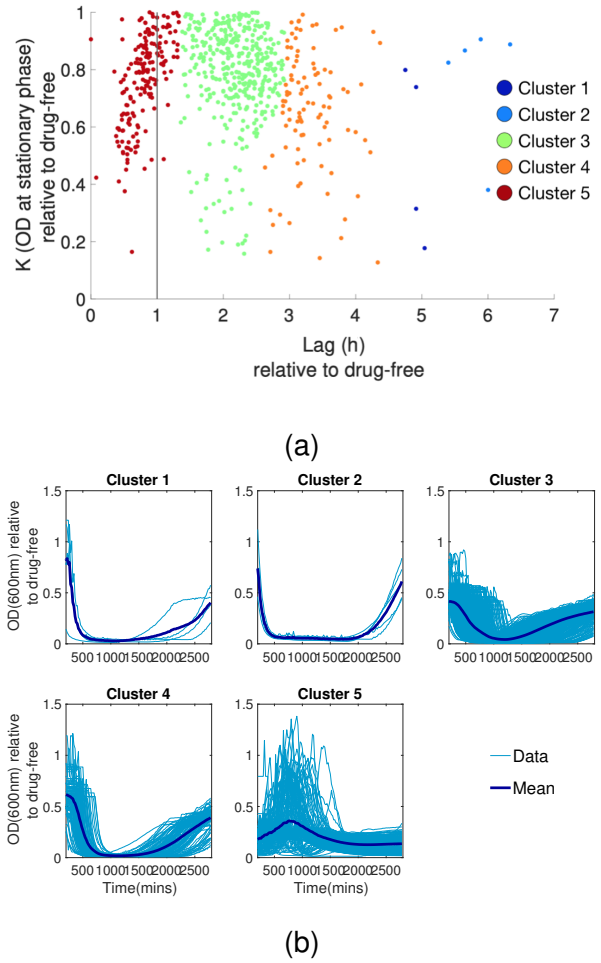

Figure 43: (a) The relationship between the lag time shown on the x axis and and K shown on the y axis. Data is shown for strains with a low K relative to the drug-free control, that is a relative K lower than one. K-means clustering was carried out and the resulting 5 clusters are shown as different colours. (b) The growth curves of the strains within the five clusters are shown (light blue lines), alongside the mean (dark blue line).

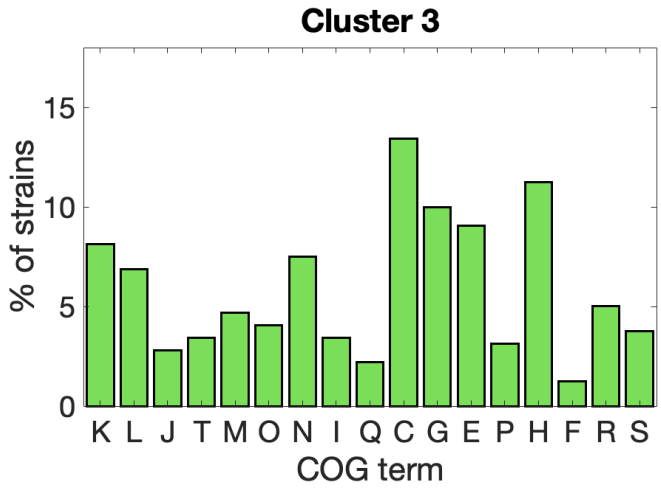

(a)

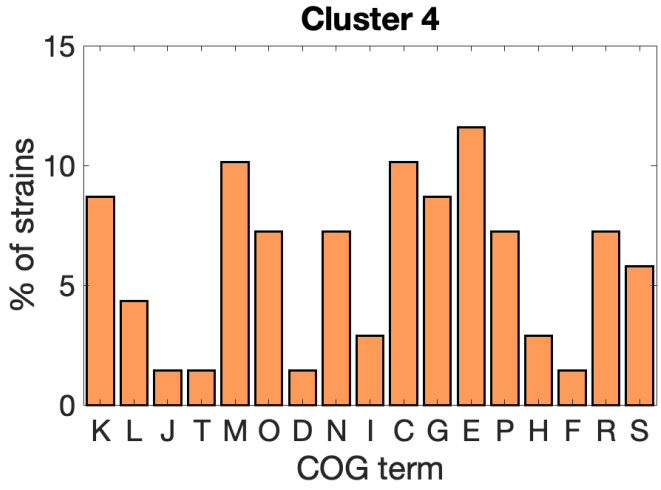

(b)

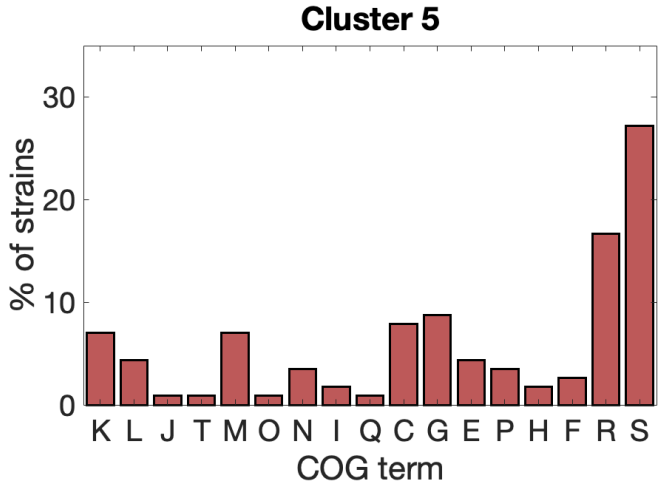

(c)

Figure 44: The genes from each cluster were assigned to COG terms. Note that each gene was only associated with a single COG term and clusters 1 and 2 have not been shown due to small numbers of genes located within these clusters. COG term enrichment measurement were carried out using a Fishers exact test - cluster 3 was found to be enriched for COG terms C ($p < 0.05$) and H ($p < 0.01$) whilst cluster 5 was found to be enriched for COG terms R ($p < 0.01$) and S ($p < 0.01$).

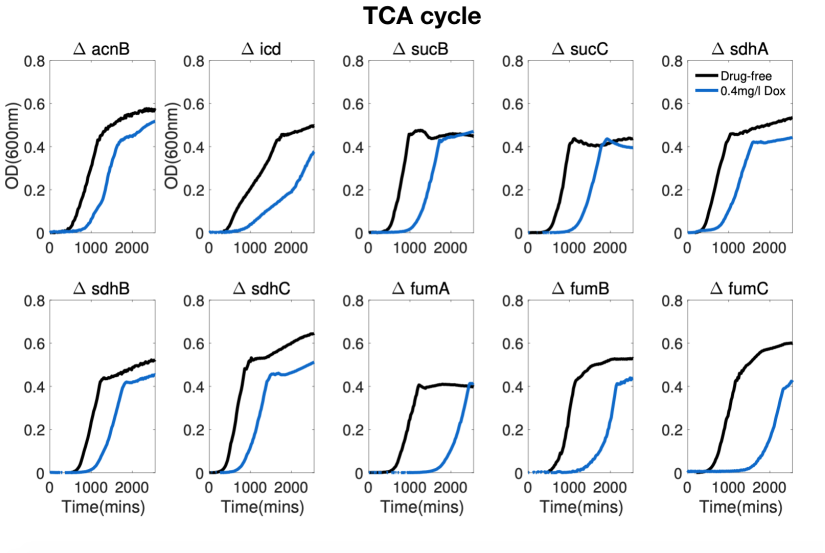

(a)

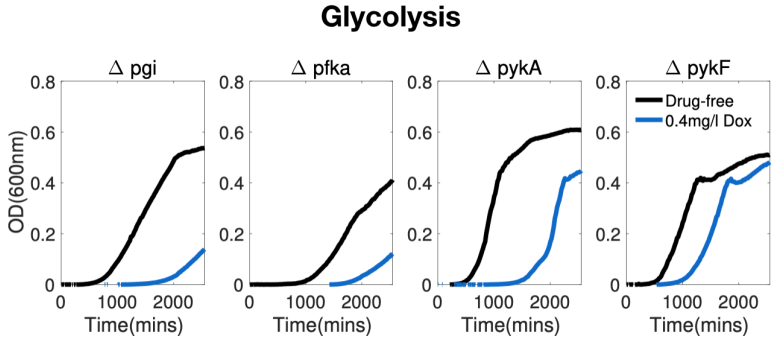

(b)

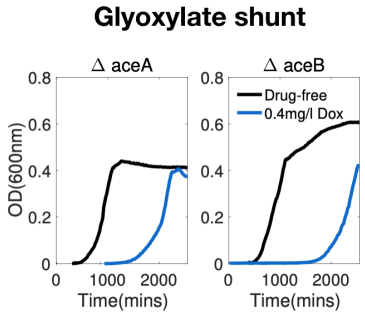

(c)

Figure 45: The growth curves of key carbon metabolism gene knockout strains identified in cluster 3. Knockout strains involved in the TCA cycle (a), glycolysis (b) and the glyoxylate shunt (c).

4.9 Conditionally essential genes

Conditionally essential genes are defined as genes that are required for the growth and proliferation of an organism within a particular environment. Thus, by identifying genes that are essential within various different environmental conditions, we can develop a better understanding of gene function. For example, auxotrophs that are unable to synthesise an essential compound will therefore be unable to grow unless that compound is available in the external environment.

During the development of the keio collection, only 8% of genes could not be disrupted and were therefore deemed essential to growth [175] and this included a number of genes that were uncharacterised at the time. Conditionally essential genes have been further explored using the keio collection, revealing a number of genes that are fundamental to cell growth in both nutrient rich [178] and nutrient poor conditions [183]. Within poor media, 196 genes were previously reported to be conditionally essential, with approximately half of those genes being identified as essential due to auxotrophy [178] and this overlapped significantly with other studies [183]. Figure 46 shows this overlap between the conditionally essential genes identified previously.

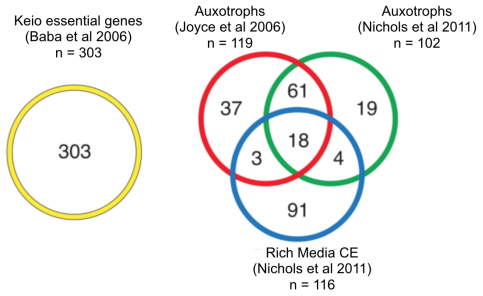

Figure 46: The number of genes previoulsy found to be essential and therefore unable to be removed as part of the keio library construction, auxotrophs in two different studies and finally conditionally essential (CE) under nutrient rich conditions. Figure adapted from reference [178]

Here, we identified a total of 21 strains (1.7%) that failed to grow in M9CAA, both with and without doxycycline (Table S1). However this is not an extensive list of all the conditionally essential genes due to the incomplete dataset used. It is of course also possible that the strains had lag times that extended past our 48 hour measurement period, for example some keio strains have been reported to have a lag time exceeding 7 days [184]. We do however find some overlap between the conditionally essential genes identified here and those identified in previous studies. For example, the $\triangle$*guaB* strain failed to grow in glycerol minimal media [183] and in rich media [178], as *guaB* mutants are guanine auxotrophs. We too identified the *guaB* gene to be conditionally essential in the conditions used here. The $\triangle$*iscC* gene was previously identified as conditionally essential in glycerol minimal media [183], and we also found it to be essential. Finally, the $\triangle$*cysG* strain also failed to grow in this study, and has previously been identified as an auxotroph [178]. The COG terms assigned to each gene are shown in figure 47a, and this group of genes was found to be enriched in COG term 'S' , that is genes with unknown function.

4.10 Hypersensitivity to doxycycline

Through this dataset we can identify gene knockout strains that result in 'hypersensitivity' to doxycycline. For the purpose of this analysis we define hypersensitive strains as those that grow to measurable levels in drug-free media, but are unable to grow in the concentration of doxycycline used (0.4mg/l, a concentration deemed to inhibit 50% of growth in the WT strain *E.coli* BW25113). In total, we identified 114 strains that fail to grow in doxycycline, and these are displayed alongside the gene function in supplementary table (Table S2).

Unsurprisingly, amongst the strains that are 'hypersensitive' towards doxycycline are $\triangle$*acrA* encoding a multi-drug efflux pump subunit and $\triangle$*mdlB* encoding a putative multi-drug resistance-like ABC exporter. We know that deletions of genes involved

in the AcrAB-TolC efflux pump can result in increased sensitivity to many antibiotics [177], and so it is logical that here the removal of *acrA* resulted in increased sensitivity towards doxycycline. Likewise, we find that the Δ*ompA* strain has increased sensitivity towards doxycycline. OmpA is a non-specific outer membrane porin, and *ompA* mutations have been reported to increase sensitivity towards a variety of antibiotics from different classes including β-lactams, glycopeptides, amphenicols, licosamides and tetracyclines [57]. Additional growth curves of the *ompA* and *acrA* knockout strains are displayed in supplementary figure S29.

We found that the majority of genes linked with this hypersensitivity phenotype either have an unknown function, or general function prediction only when assigned to COG functional groups, as shown in figure 47b.

Three of the strains found to only grow in drug-free media (*tolB, paL* and *acrA*) were also classified as 'multi-stress responsive' (MSR) strains by Nichols et al. - defined as strains displaying 30 phenotypes or more across the various stressors tested [178]. The removal of these genes results in a diverse range of phenotypes depending on the environment, and so it is logical that the removal of these genes also results in a severe phenotype with doxycycline (hypersensitivity).

4.11 'Super strains'

In the majority of Keio strains tested here, doxycycline treatment was detrimental to at least one aspect of bacterial growth. For example, in some cases K may be large relative to the drug-free control, but lag time would be extended. However, in 20 strains, we find that both lag and K benefit from doxycycline treatment, and we refer to these as 'super strains'. Now, 50% of these strains have uncharacterised functions and this is unsurprising given the large number of uncharacterised genes in the 1,266 strains tested here. Out of the genes that are characterised however, we find two that are involved in the processing of amino acids (*lrp* and *ygjG*) and

two involved in DNA damage/repair (*ung* and *mutH*). Although uncovering the true biological reason behind this phenotype would require further investigation, we can speculate based on our existing knowledge of these genes.

Although the primary role of Lrp is the synthesis and uptake of amino acids, it is also a global regulator of multiple cellular pathways, including metabolism, virulence and motility [185]. Moreover, it has a key role in stationary phase processes, particularly in nutrient forging as resources become depleted. In chapter 2 we demonstrated the benefits that doxycycline can confer in starving populations of *E.coli* through improved growth on cell debris - it is possible that doxycycline mitigates against the loss of Lrp, thus improving cell growth relative to drug-free populations. Of course we must also consider that the removal of a global regulator such as Lrp may have unforeseen, downstream effects on the regulation of other genes.

DNA repair genes such as *mutH* are repressed during stationary phase by RpoS due to decreased rates of DNA synthesis. However they are important for the modulation of mutation rate in response to stress [186]. The mechanism behind lag time shortening and increased cell density in response to doxycycline in these mutants is unclear. Additional growth curves for the *lrp* and *mutH* knockout strains are displayed in supplementary figure S30.

4.12 Keio strains found only to grow in doxycycline

We uncovered a further unexpected phenotype in this dataset - strains that failed to grow in drug-free conditions but were able to grow in doxycycline. Considering that doxycycline is traditionally thought of as a drug that has purely detrimental effects on bacterial cells, it is surprising to find knockout strains that are *only* able to grow in its presence.

In total 19 strains were found to only grow in media containing 0.4mg/l doxycycline, as shown in supplementary table S3. Only four of the deleted genes in these strains

had uncharacterised functions, in contrast to the high numbers of uncharacterised genes observed overall in the keio strains tested. Moreover, five of the characterised genes were involved in transcriptional regulation (*adiY, xapR, perR, purR* and *soxS*). In figure 47c we show the COG terms assigned to each gene, and we find that this group of strains is enriched both for genes of unknown function (S), but also genes involved in transcription (K). One of these gene (*soxS*) has previously been reported as a conditionally essential gene in rich media [178]. SoxS is a global regulatory protein that plays a key role in the cells oxidative response system, and its deletion is therefore likely to have wide ranging consequences on the cells response to stress. Moreover, SoxS is heavily involved in the response to doxycycline, given that SoxS expression results in up regulation of *acrAB* [187]. The transcriptional regulator PerR is also involved in the response to oxidative stress, more specifically it response to peroxide stress [188].

In addition, we find that the *sodB* deleted strain only grows in doxycycline. SodB (superoxide dismutase) is involved in the cells antioxidant response, is found to be elevated during periods of starvation [189]. It would therefore appear that doxycycline allows growth in these strains that have a reduced response to oxidative stress. Additional replicate growth curves of the *nagC*, *soxS* and *sodB* knockout strains are displayed in supplementary figure S31.

Now, it should be noted that whilst SodB, SoxS and PerR play a role in the cells oxidative stress response, tetracycline antibiotics have also been shown to mediate the cells response to oxidative stress through the scavenging of ROS such as superoxide [29, 30]. It is therefore possible that whilst the *sodB*, *soxS* and *perR* knockout strains are unable to grow in drug-free conditions due an insufficient oxidative stress response, the addition of doxycycline alleviates this and allows growth to occur.

In contrast, the growth of these strains was not found to be doxycycline-dependent in the study by Nichols et al. [178]. Only one strain (*soxS*) was identified as conditionally essential, however it was also unable to grow in doxycycline. Furthermore, none of these genes were identified as 'multi-stress' responsive genes. It is possible

that the different media conditions used here (M9CAA versus LB agar), as well as the difference in growth quantification (OD versus colonies) resulted in this disparity between phenotypes.

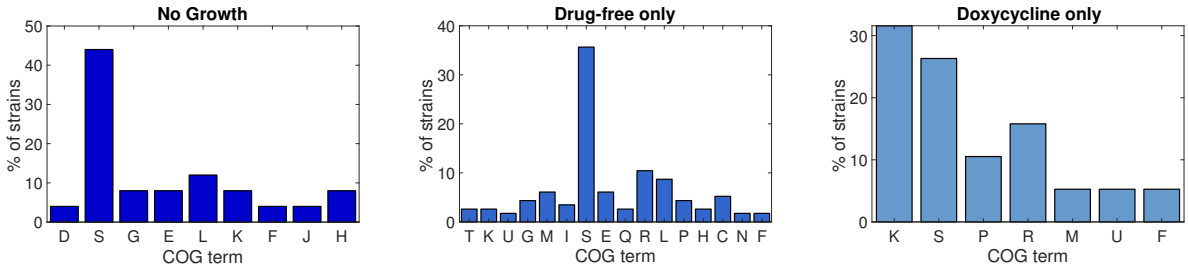

(a) (b) (c)

Figure 47: The knockout strains found to be a) conditionally essential in the media used, b) grow only in drug-free media and c) grow only in doxycycline were assigned to single COG functional groups. Enrichment analysis was then carried out via a Fisher's exact test. We find that all of these strain groups are enriched for unknown genes (S), however the group of strains only able to grow in doxycycline (c) is also enriched for COG term 'K', that is genes involved in transcription ($p < 0.0001$).

4.13 Summary

The keio library of single gene knockouts has been used here to demonstrate the phenotypic variability induced by doxycycline. The original hypothesis was that by clustering strains with similar phenotypic responses to doxycycline, the genomic basis for these phenotypes could be elucidated. Indeed, through PCA analysis and K-means clustering, strains with similar phenotypes were clustered and the key functional groups were extracted from each cluster by linking genes to COG terms. Interestingly, strains were identified that experienced no benefit to growth with the addition of doxycycline (unlike the WT strain *E.coli* BW25113), and this group of strains was found to be over-represented for genes involved in core metabolic processes, including those part of central carbon metabolism. This supports data obtained in previous chapters demonstrating the effects that doxycycline can have on metabolic pathways.

Furthermore, a previous study by Nichols et al. found that keio strains with similar

functions cluster together in their phenotypic response to various perturbations [178], and this is also found here with doxycycline. This clustering indicates that the method used here is valid, as it is logical that genes with similar functions form part of the same phenotypic cluster.

A number of unusual phenotypes were identified, for example strains that have benefits to both lag time and cell density in doxycycline. Surprisingly, certain strains failed to grow in drug-free media, but were able to grow with doxycycline. A number of these strains had gene knockouts involved in the oxidative stress response, and given that tetracyclines are known antioxidants it is possible that doxycycline protects against ROS in these strains, thereby allowing growth to occur. Further work would be needed to confirm this, such as an ROS assay to deduce if doxycycline is indeed reducing the levels of ROS produced by these strains.

Despite the limitations in this data set due to coronavirus-related interruptions, we have identified a number of strains that have interesting growth dynamics in the presence of doxycycline and therefore warrant further study.

CHAPTER FIVE

TRACKING THE EVOLUTION OF CARBAPENEM RESISTANT *KLEBSIELLA PNEUMONIAE* WITHIN A SINGLE PATIENT

5.1 Overview

The data presented in previous chapters originated from well-established laboratory strains of bacteria. Now, we will explore the adaptation of *Klebsiella pneumoniae* to repeated antibiotic exposure within a patient over the course of 18 months. In doing so, we identify the phenotypic and genotypic changes over time, in addition to testing the robustness of genotypic data as a diagnostic tool to predict antimicrobial resistance in clinical samples. The key findings were as followed:

1. Inconsistencies exist between the antimicrobial resistance profile predicted by phenotypic and genotypic data.
2. Through nanopore sequencing we resolved whole chromosome and plasmid structures.
3. Long-read sequencing gives us insight into the structural genomic changes

occurring within *K. pneumoniae* over the course of an infection.

Klebsiella pneumoniae is a gram-negative bacteria found ubiquitously in nature, including in the human body as an intestinal commensal bacteria. However, they are also the causative agent of serious, life-threatening human infections such as pneumonia [190] and bloodstream infections [191]. The threat posed by these infections is only amplified by their frequent occurrence in immunocompromised individuals and neonates. The prevalence of *K.pneumoniae* is reflected in data indicating that as of 2018, *K.pneumoniae* accounted for 9,617 cases of bacteraemia's in the UK annually [192]. Moreover, the increasing incidence of extended-spectrum β-lactamase (ESBL) and carbapenemase-producing *K.pneumoniae* are of particular concern due to the difficulties associated with effective antibiotic treatment.

Carbapenem antibiotics are a group of broad spectrum β-lactams, often used as an antibiotic of last resort in the treatment of infections caused by multi drug resistant pathogens. In particular, carbapenems are one of the few groups of antimicrobials remaining for the treatment of extended-spectrum β-lactamase (ESBL)-producing pathogens, and thus it is crucial that outbreaks of carbapenem-resistant bacteria are carefully tracked. However, in recent years there has been increasing incidence of carbapenemase-producing *Enterobacteriaceae*, with the world health organisation deeming carbapenem-resistant *Acinetobacter baumannii, Pseudomonas aeruginosa* and *Enterobacteriaceae* as large threats to human health [193].

Carbapenem-resistant *K.pneumoniae* in particular are a group of rapidly spreading, multi-drug resistant pathogen that not only result in prolonged hospital stays, but also increased rates of mortality [69]. By far the most prevalent mechanism of carbapenem resistance is the production of carbapenemases, including bla_{KPC}, bla_{NDM}, bla_{VIM}, bla_{IMP} and $\text{bla}_{\text{OXA-48}}$ [194] that inactivate carbapenems by hydrolysis. These genes are often carried on plasmids, allowing rapid dissemination throughout microbial populations. Carbapenem-resistant *K.pneumoniae* are particularly hard to treat as they are commonly reported to be resistant towards a broad range of

clinically relevant antibiotics, and often harbour additional antimicrobial resistance and virulence genes on large plasmids alongside carbapenemase genes [195, 69].

An alternative mechanism conferring carbapenem resistance is alterations in porin production, and these variations can also further amplify the resistance conferred by the presence of a β-lactamase. More specifically, the loss or modification of the non-specific porins OmpK35 and OmpK36 can reduce susceptibility towards carbapenems through impaired uptake of antibiotic into the cell. The majority of ESBL-producing *K.pneumoniae* only express OmpK36, or are found to lack both OmpK36 and OmpK35, resulting in lower drug susceptibility [196]. Further modifications have been reported in the minor porin OmpK37, however the role of this porin in resistance is less clear, despite its loss having been implicated in reduced susceptibility towards carbapenems [197].

The first reports of *Klebsiella pneumoniae* carbapenemase (KPC)-producing *K.pneumoniae* originated from the USA in 2001 [67], but the KPC gene has since spread worldwide and now represents one of the most common mechanisms of carbapenem resistance in *K.pneumoniae*. Moreover, the incidence of carbapenemase-producing *Enterobacteriaceae* has been shown to have increased markedly in the UK in recent years, with the metallo-β-lactamase NMD-1 found to be the most common amongst clinical isolates [195].

The severity of these infections is further compounded by the regular failure in clinical detection of carbapenemases through routine screening, resulting in ineffective treatment and wider dissemination [198]. There are multiple examples of automated antimicrobial susceptibility testing systems producing false predictions of susceptibility towards carbapenem antibiotics in KPC-producing *K.pneumoniae* [199, 200, 201]. If, however, an isolate is found to be resistant to carbapenems, clinical PCR tests will typically be carried out to identify the presence of the 'big four' carbapenemase genes (bla_{KPC} non-metallo carbapenemase, $bla_{OXA\text{-}48\ like}$ non-metallo carbapenemase, bla_{NDM} metallo carbapenemase and finally bla_{VIM} metallo carbapenemase). Nevertheless, this is a relatively time-consuming process

and consequently phenotypic tests are frequently used in isolation to determine a pathogens AMR profile.

Due to the severity of carbapenem resistant *K.pneumoniae*, hospital outbreaks are extensively tracked and studied to reveal the pathogen origin and track genotypic changes over time [79, 202, 203]. Although these types of studies are crucial in the assessment of infection spread through a community, they tell us little about the adaptation of the pathogen within the human body as an infection progresses. For this, we need to perform studies of pathogen adaptation within a patient over the course of the infection.

Pathogen transmission from the external environment also contributes significantly towards the spread of antibiotic resistance. Indeed, community and hospital acquired infections are prevalent, with serious concerns over the spread of pathogens such as vancomycin-resistant enterococci (VRE) and methicillin-resistant *Staphylococcus aureus* [204]. Swabs taken from the surfaces of hospital rooms can reveal the presence of multidrug-resistant pathogens that consequently infect patients [205, 206]. However, adaptation to antibiotics within the host can also result in the development of antibiotic resistance [83], and so it is also key to understand the within-host evolution of pathogens.

Examples of within-host adaptation include point mutations that develop during antibiotic treatment, resulting in a previously susceptible infection becoming antibiotic resistant. For example, Blair et al. [83] found that a single base pair substitution within the AcrB protein (a component of the AcrAB-TolC efflux pump) that arose during antibiotic treatment resulted in treatment failure. Larger genomic modifications, such as large deletions and amplifications can also arise during treatment and alter antibiotic susceptibility [207, 208]. Furthermore, the instability of structural variations such as amplifications can result in heteroresistance [209, 210] and an 'accordion effect' whereby the genomic regions expand and contract in response to stressors such as antibiotics [211, 210, 212]. It is therefore key that we understand how the selective pressures imposed by long-term antibiotic treatment

alters pathogens genomes over time, both in terms of small polymorphisms and larger genomic modifications.

We hypothesised that over the course of long-term chronic infection, the *K.pneumonia* isolates studied here would accumulate not only SNPs, but also larger structural variations in the genome. Indeed, experimentally evolved bacteria can acquire large genomic modifications such as amplifications [213, 7] and deletions [214, 215] in response to antibiotic exposure. And yet, these types of large genomic modifications are rarely identified directly within clinical isolates [208]. It is possible that these types of genomic modification fail to be identified due to the use of short read sequencing, or are simply not present due to sampling over relatively short time periods [84]. We postulated that repeated antibiotic treatment over the span of many years would result in large genomic modifications. Alternatively, it is plausible that the isolates represent different clonal types that have been acquired over the course of the infection period. Although infections can be dominated by one clonal type [84, 216], it is also possible for multiple clonal types to be acquired over time, with sporadic colonisation from the environment [217, 218].

In addition, we sought to assess the use of nanopore sequencing to elucidate the resistomes of complex clinical pathogens. Unlike short-read sequencing, nanopore sequencing is able to reliably re-construct plasmid structures that are often found to harbour key AMR genes [219], and thus we anticipated that both the presence and location of AMR genes could be accurately detected. Plasmids play a central role in the dissemination of AMR genes, and so it is important to understand the genetic context of these genes, as well as plasmid dynamics within the cell (for example the mobilisation of plasmid genes into the chromosome).

Here, we perform a retrospective study of a particularly complex, multi-drug-resistant *K.pneumoniae* infection within a single patient. The *K.pneumoniae* isolates acquired span 18 months of infection and have been repeatedly exposed to antibiotic treatment. Furthermore, these isolates were found to be consistently carbapenem-resistant. Through whole genome sequencing using the Oxford Nanopore GridION

platform, we were able to fully reconstruct the isolates chromosomes and plasmids, detect the presence of antibiotic resistance genes and identify large genomic structural variations.

5.2 Contributions

The bacterial isolates and clinical data presented in this chapter were acquired by Dr Fergus Hamilton (NHS North Bristol Trust). Prof Robert Beardmore contributed towards the study design and acquisition of clinical isolates. The computing facilities required for analysis of genomic data resulting from sequencing were provided by Prof Ivana Gudelj. The costs of library preparation and sequencing were provided by a mini-grant from The University of Exeter Sequencing Service, funded by the UK Medical Research Council (MRC) Clinical Research Infrastructure Initiative (award number MR/M008924/1). The implementation of protocols and analysis of data were carried out by Emily Wood.

5.3 Clinical data

All of the isolates used in this chapter were acquired from a single patient over the course of an 18 month period. The patient presented with a multi-drug resistant *K.pneumoniae* infection following a hip fracture that required surgery in India. Upon return to the UK, the hip was replaced for a second time, however the patient was frequently readmitted to hospital suffering from bacteraemia. The infection of prosthetic joints such as the hip represent a challenging problem to infection medicine and can result in poor clinical outcome. Difficulties in treatment are only compounded by the development of multi-drug resistance [220].

As this is a retrospective study certain isolates were unavailable for further characterisation, however the clinical data (antibiotic resistant profile, antibiotic exposure etc.) was available and is presented below.

Figure 48 displays the patients clinical course, that is the antibiotic treatments administered over the course of the infection. Samples collected in December 2017 were identified as containing both *E.coli* and *K.pneumoniae*, with the following isolates through to May 2019 consisting of only *K.pneumoniae*. The majority of the treatment consisted of Ceftazidime/avibactam and meropenem, however these antibiotic treatments proved to be ineffective as the patient frequently presented with recurrent bacteraemia.

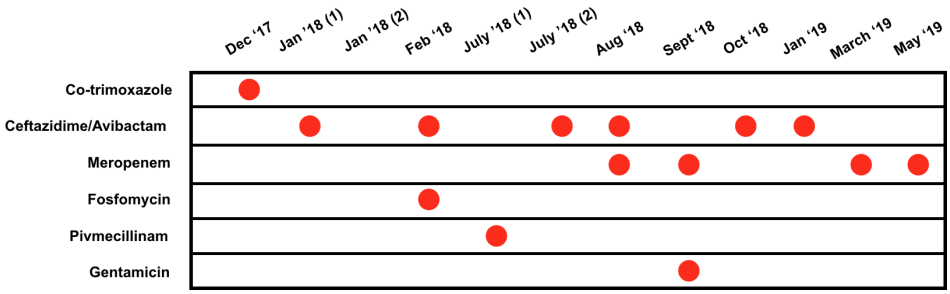

Figure 48: Patient carriage of *E.coli* (Dec 2017) and *K.pneumoniae* (Jan 2018 - May2019). Red circles indicate the antibiotic treatment used. Note that in the second return to hospital in January 2018, no treatment was given

.

The antibiotic susceptibility profiles for each isolate were determined within the hospitals clinical laboratory using a combination of disk diffusion assays and the Vitek 2 (bioMérieux, Marcy-l'Étoile, France). The Vitek 2 is an automated antimicrobial susceptibility testing system, allowing high throughput analysis of patient samples. It determines the MIC of clinical isolates by comparing their growth in antibiotic against a database of known MIC values [221]. Furthermore, bioMérieux claims that MIC can be determined based on only 3 concentrations of antibiotic and in as little as 4 hours [222].

Figure 53 shows an extensive list of all the antibiotics that these isolates were tested against, as well as the detection of ESBL production. Empty squares indicate that data was not collected for that antibiotic at that particular time point. Although the isolates are resistant to a broad range of antibiotics across all time points,

there are antibiotics for which this susceptibility fluctuates. For example, six of the isolates tested are susceptible to fosfomycin whilst three are resistant at clinically relevant concentrations. Likewise, variations were identified in the detection of ESBL production - the isolates obtained in January and early July 2018 were found to be ESBL negative whilst all other isolates were classified as positive.

Figure 49 displays the clinical antibiotic susceptibility data obtained from the Vitek only, as the disk diffusion assays only give an indication of resistance or susceptibility, not a MIC value. Again, it is clear that the isolates are resistant to the majority of antibiotics, although there were fluctuations in the susceptibility towards Ertapenem, Gentamicin, Meropenem and Tigecycline.

	Dec '17 (1)	Dec '17 (2)	Jan '18 (1)	Jan '18 (2)	Feb '18	July '18 (1)	July '18 (2)	Aug '18	Sept '18	Oct '18	Jan '19	March '19	May '19
Co-amoxiclav	R	R	R	R	R	R	R	R	R	R	R	R	R
Ciprofloxacin	R	R	R	R	R	R	R		R	R	R	R	R
Cefpodoxime	R	R	R	R	R	R	R		R	R	R	R	R
Gentamicin	R	R	R	R	R	S	S	R	R	S	R	S	S
Co-trimoxazole	R	R	R				R	R	R	R	R	R	R
Pip/tazobactam	R	R	R	R	R	R	R	R	R	R	R	R	R
Amikacin		R	R			R	R	R	R	R	R	R	R
Aztreonam	R		R		R		R	R	R	R	R	R	R
Chloramphenicol	R		R					R					
Ceftazidime	R		R				R	R	R	R	R	R	R
Colistin	S		R					S	S	S	S	S	
Ceftriaxone	R		R				R	R	R	R	R	R	R
Cefotaxime	R		R				R	R	R	R	R	R	R
Ertapenem	R		R		R	R	R	R	R	R	I	I	I
Cefepime			R				R	R	R	R	R	R	R
Fosfomycin	R	S	R		S	R	S	R		S	S		
Meropenem	R	R	R		R	S	R	S	S	R	S	S	S
Tigecycline	R		R				R	R	R	I	R	R	R
Tobramycin		R	R				R	R	R	R	R	R	R
Amoxicillin	R	R	R				R	R	R	R	R	R	R
Cefalexin		R		R	R	R							
Trimethiprim		R		R	R	R							
Ampicillin			R				R	R	R	R	R	R	R
Pivmecillinam			R	R	R	S	R	R					
Ceftaz/avibactam							S	S	S	S		S	S
ESBL	P	P	N		P	N	P	P	P	P	P	P	

Table 5: The antibiotic resistance profile of each isolate, as determined by automatic antibiotic susceptibility testing (Vitek) and disk diffusion at the clinical laboratory. Red cells represent resistance, green cells sensitive and blue cells intermediate. The numbers underneath the data on which the isolates were collected accounts for multiple isolates taken within a single month.

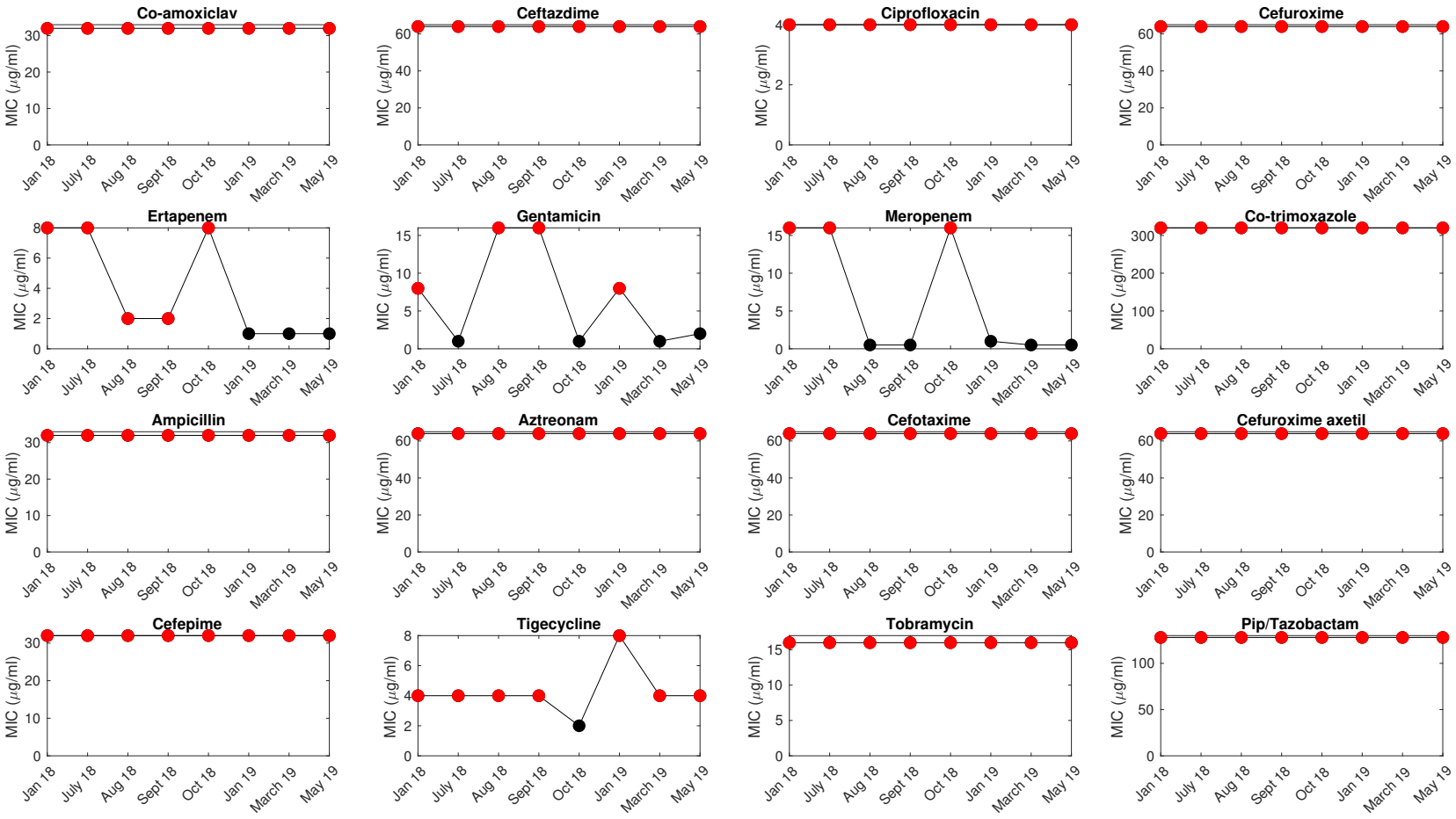

Figure 49: The minimal inhibitory concentrations of various antibiotics across all patient samples, obtained through clinical data. Red circles signify that the pathogen is 'clinically resistant' to that antibiotic at that concentration. Black circles signify that the pathogen is 'clinically susceptible' to that antibiotic at that concentration.

5.4 Characterisation of *K.pneumoniae* isolates

Although clinical data was available for 12 isolates obtained between December 2017-May 2019, only six isolates were available for further characterisation due to issues with sample storage (August '18, September '18, October '18, January '19, March '19 and finally May '19). The growth dynamics of bacteria can provide us with a plethora of information on its fitness, for example the acquisition of antibiotic resistance genes are often associated with fitness costs, and growth may therefore be impaired [162, 41]. In order to assess the phenotypic variation between the different isolates, we first grew them in M9CAA with 2mg/ml glucose and without the use of any antibiotic. Figure 50a shows the raw growth curves for the six isolates over 48 hours and we find that the growth profiles for each isolate are very similar. However, the isolate from May 2019 was found to have significantly lower K than the initial isolate from August 2018 (figure 50b). The similarities found in the growth dynamics between different isolates leads us to postulate that these isolates may originate from the same initial population.

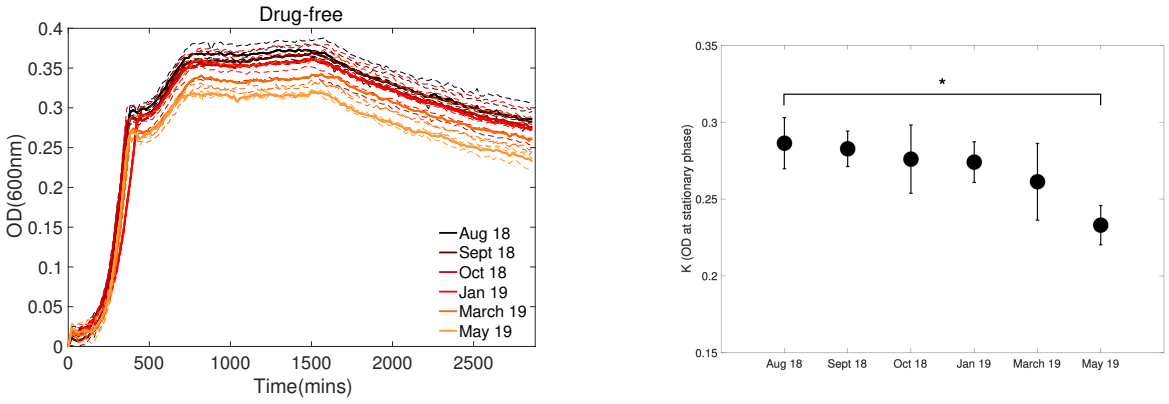

(a) (b)

Figure 50: a) The growth profiles of all six *K.pneumoniae* isolates in the absence of antibiotics. Growth was measured as optical density (OD_{600nm}). Although there is little variation in growth between strains, it is the most recent isolate from May 2019 that reaches the lowest population density. b) K for the different isolates in drug-free media. There was a significant difference in K between the isolate obtained in August 2018 and in May 2019 (One way ANOVA with post hoc Tukey $p < 0.05$). *n=3*.

5.4.1 Phenotypic response to antibiotics : Antibiotics mechanism of action

As seen in Figure 49, the response to certain antibiotics was found to fluctuate substantially over time, therefore we next wanted to better characterise the response towards a selection of these antibiotics. In particular, antibiotics that had been used in the treatment of this infection. Through doing so, we aimed to identify if these are true fluctuations in antibiotic susceptibility, as this could indicate adaptation over time. Based on these criteria, the phenotypic response to both gentamicin and meropenem was investigated in greater detail.

Gentamicin is an aminoglycoside antibiotic that inhibits bacterial translation by binding irreversibly to the 30S ribosome, promoting mistranslation and thereby resulting in error-prone protein synthesis. It is generally thought to have both bacteriostatic and bactericidal action [223].

Meropenem is a carbapenem antibiotic - a member of the β-lactam class of antibiotics. It is widely reported as being bactericidal in nature and like other β-lactam's binds to penicillin-binding proteins that catalyse the formation of peptidoglycan, thereby inhibiting bacterial cell wall synthesis [224].

5.4.2 Phenotypic response to gentamicin

The clinical data indicated that the majority of isolates were resistant to gentamicin at clinically relevant concentrations, aside from the isolates obtained in July '18, October '18, March '19 and May '19 that were deemed susceptible. We grew all six available *K.pneumoniae* isolates in three different concentrations of gentamicin (0.5, 8 and 16mg/l), and in drug-free media for 24 hours with OD measurements taken every 20 minutes. These drug concentrations were selected based on the clinical breakpoint of 8mg/l for gentamicin.

Surprisingly, we find that all of the isolates tested were able to grow in all of the gentamicin concentrations used, up to 16mg/l (Fig 51a). Therefore, according to this data, all of the strains are resistant to gentamicin at clinically relevant doses. This is in disagreement with the data obtained by automated testing, as out of the isolates available to us, only the August, September and January isolates were identified as resistant to gentamicin (Fig 49). The raw growth curves are displayed in supplementary figure S32.

This is not the first example of a discrepancy between susceptibility data produced by the automated systems such as the Vitek and alternative methods. For example, across 46 clinical isolates of *K.pneumoniae*, a mere 30.4% agreement in MIC between Vitek and broth microdilution was found, with a 23.9% major error rate and a 39.1% minor error rate [201]. Other studies have also identified large discrepancies between data produced by the Vitek and alternative antimicrobial susceptibility tests [225, 226], whilst some find it to be fairly reliable [227, 228].

When we further examine the phenotypic response to gentamicin, we find that lag time increases as a function of gentamicin concentration, as shown in figure 51b. This could account for the discrepancies found between our data and that obtained from the Vitek, as Vitek relies on relatively short time spans to measure antibiotic susceptibility. Little variation is found in growth rate (fig 51c), aside from the final isolate that has a reduced growth rate with increasing concentration of gentamicin.

2427

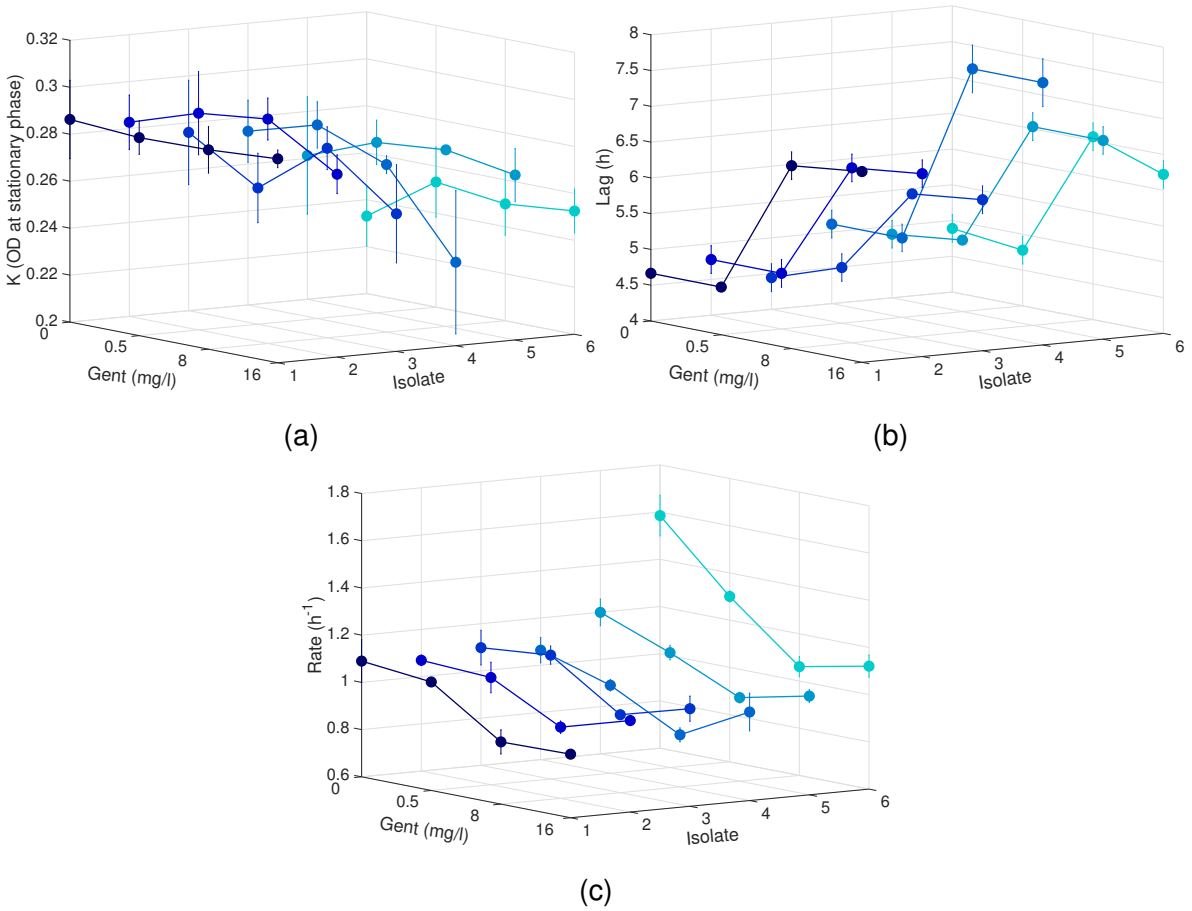

Figure 51: The a) K (maximum cell density) values, b) Lag time and c) Growth rate for each isolate in varying doses of gentamicin. Isolates 1-6 refer to the isolates obtained in August 2018, September 2018, October 2018, January 2019, March 2019 and May 2019 respectively. All isolates were able to grow in the highest dose of gentamicin used (16mg/l). however the lag time increased in the two largest concentrations of gentamicin across all isolates. Growth rate was found to be elevated in the final isolate within drug-free conditions. *n=3*.

5.4.3 Phenotypic response to meropenem

The clinical data obtained by the Vitek indicated that the response to Meropenem was highly variable over time. The isolates obtained in July ’18, August ’18, Sept ’18, Jan ’19, March ’19 and May ’19 were susceptible to meropenem whilst the other six isolates were classified as resistant at clinically relevant concentrations. Now, meropenem was used frequently during the treatment of this patient (figure 48) and the reliability of these phenotypic results will have been vital to guide treatment regimes. Despite six of the isolates being classified as clinically susceptible to meropenem, this antibiotic was still ineffective in the management of the infection, and so we sought to identify if discrepancies exist between the Vitek data and that obtained by the methods used here. We grew all six available *K.pneumoniae* isolates in three different concentrations of meropenem (0.5, 1 and 16mg/l), and in drug-free media for 24 hours with OD measurements taken every 20 minutes. The clinical breakpoint for resistance towards meropenem is 4mg/l.

Whilst the isolates obtained in August ’18, January ’19 and May ’19 all grow up to 1mg/l meropenem, the September ’18, October ’19 and March ’19 isolates do not grow in any of the concentrations used (figure 52a). This is in contrast the clinical data that classified the October ’18 isolate as resistant to meropenem at clinically relevant doses, as shown in figure 49. With the isolates that were found to grow in meropenem, we find a dose-dependent increase in lag time (figure 52b), and little change in growth rate (figure 52c). The raw growth curves are displayed in supplementary figure S33.

The discrepancies between the Vitek data and phenotypic data presented here could be due to a multitude of factors, including differences in media and variations in the measurement period. However, given the inaccuracies identified in Vitek data [225, 226], it is possible that the misclassification of the October 2018 isolate as resistant to meropenem is a true error. Carbapenem resistance is a growing threat to global heath and as such it is crucial that accurate data is obtained on the

prevalence of carbapenem resistant organisms to not only aid surveillance but also improve patient outcome.

It should be noted that further characterisation of growth in a greater number of doses would better elucidate the MIC of meropenem for each isolate. However, this was not possible within the timeframe of this work due to the pandemic-related lab closure.

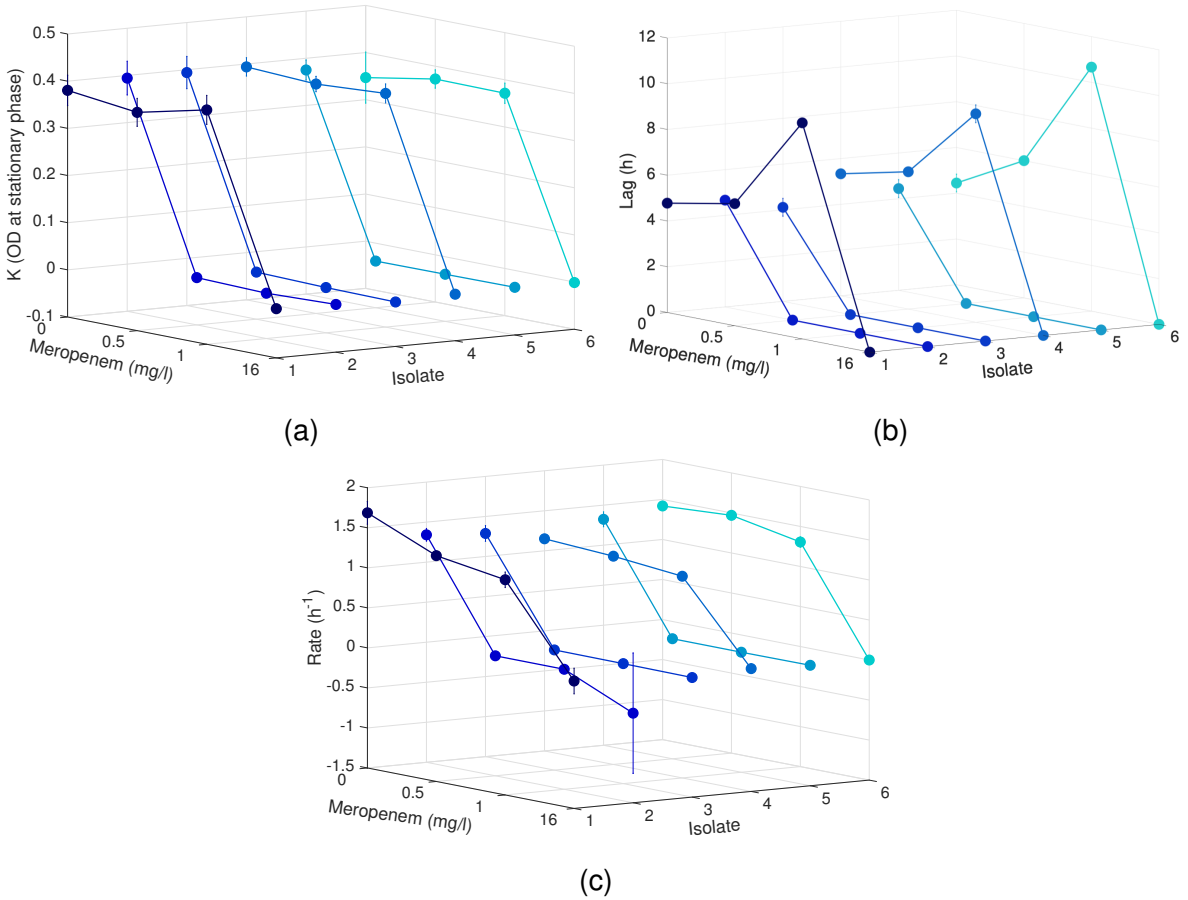

Figure 52: The a) K (maximum cell density) values, b) Lag time and c) Growth rate for each isolate in varying doses of meropenem. Isolates 1-6 refer to the isolates obtained in August 2018, September 2018, October 2018, January 2019, March 2019 and May 2019 respectively. Only isolates 1,4 and 6 were able to grow in any dosage of meropenem, with all growing up to 1mg/l, and for isolates able to grow in meropenem, a longer lag period is measured in 1mg/l. Little difference is found in growth rate when isolates are able to grow in meropenem. *n=3*.

5.5 Nanopore sequencing of clinical *K.pneumoniae* isolates

Whole genome sequencing can provide us with a plethora of information on the AMR profile of a pathogen, alongside other important information such as the virulence factors and sequence type. Antibiotic resistance genes are, however, often carried on plasmids that disseminate through bacterial populations and this poses a problem when using short read sequencing. Plasmids often contain many repeat sequences that are incredibly difficult to resolve with short reads alone [219], thus the result can be incomplete assemblies and uncertainties about the separation of chromosomal and plasmid DNA. Long read sequencing, on the other hand, affords us a solution to this problem as the long reads can span the whole length of these repeat regions. As a result, whole plasmid and chromosome sequences can be assembled, often into single contigs [229].

For the purpose of characterising the genomes of the *K.pneumoniae* isolates, long-read Nanopore GridION sequencing was chosen. Although nanopore sequencing has the disadvantage of a higher error rate than alternative sequencing platforms (making it challenging to elucidate point mutations), the resolution of the genome structure is far superior to short-read sequencing.

Moreover, due to the low cost and relative ease of nanopore sequencing there is increasing interest in its use within infection medicine as a diagnostic tool [230]. Unlike phenotypic antimicrobial susceptibility tests that have a relatively long turnover time ($\sim$ 48-72 hours), nanopore sequencing can provide data on AMR genes in real time. This is particularly relevant to time-sensitive infections such as sepsis that require rapid decisions to be made in order to optimise treatment options.

Here, we use nanopore sequencing to characterise the genomes of clinical *K.pneumoniae* isolates in order to track genomic changes over time and we evaluate the use of this sequencing platform as a stand alone tool to assess antimicrobial resistance. The accuracy could be improved through the use of short read sequencing alongside nanopore, thus producing a hybrid assembly. However, this was outside

the scope of this work.

5.5.1 Sequencing run

The Nanopore GridION platform was used to generate complete genomic sequences for the *K.pneumoniae* isolates obtained in August 2018, October 2018, January 2019 and May 2019. These are hereafter referred to as 'KP1', 'KP2', 'KP3' and 'KP4' respectively. The isolates were grown in M9CAA for 24 hours without the addition of any antibiotic. M9CAA was used to allow control over the growth conditions and avoid excessive genomic changes accumulating during growth.
DNA was the extracted using the Ambion GeneJET genomic DNA purification kit with an additional elution step. Three replicates were prepared for each of the four isolates, and each sample was barcoded using the Rapid Barcoding Kit (Oxford Nanopore), thus allowing all 12 samples to be multiplexed onto a single flow cell. The GridION library was prepared with a FLO-PRO002 flow cell and run for 72 hours using MinKNOW with high accuracy basecalling. The resulting FAST5 files were base called using Guppy v3.3.0, resulting in 22.97Gb of data, equating to a total of 3.85 million reads. The sequenced isolates are summarised in Table 6. Further information on the sequencing, such as the distribution of read length is displayed in supplementary figures S34-S36.

Isolate	Time point	Replicates	Average reads generated	Mapped reads	Error rate
KP1	August 2018	3	341847	99.87%	9.09%
KP2	October 2018	3	343606	99.92%	9.15%
KP3	March 2019	3	291078	99.91%	9.08%
KP4	May 2019	3	231394	99.9%	9.14%

Table 6: The *K.pneumoniae* isolates sequenced.

5.6 Multi-locus sequence typing

The multilocus sequence typing (MLST) scheme was first developed in 2005 [231] and has since been used worldwide to aid the characterisation of clinical isolates. Through the use of MLST we can better understand the genetic diversity between the *K.pneumoniae* isolates. Moreover, we can establish if these isolates belong to a common sequence type (ST) such as ST258, a particularly high-risk carbapenem-resistant lineage of *K.pneumoniae* [232].

To investigate the relatedness of the isolates across different time points, the core genome MLST for each isolate was determined using the *Klebsiella* Sequence Typing tool (`http://bigsdb.pasteur.fr/klebsiella/klebsiella.html`), against the nanopore sequence data. This is based on a seven marker gene set (*gapA, infB, mdh, pgi, phoE, rpoB, tonB*).

All isolates were determined to be closest to ST427, also previously identified in a Spanish hospital from 2007-2008 [233]. It should be noted however that the relatively low accuracy of nanopore sequencing can make MLST analysis difficult as it relies on single nucleotide differences within these housekeeping genes. It should also be noted that although all of the isolates were of the same sequence type, multiple different microbial species and strains can be present within a single infection site at any one time [218], and therefore through the sequencing of a clonal population here alternative populations may have been missed. However, the identification of similar growth phenotypes alongside the presence of the same ST's does suggest that all of these isolates are part of the same lineage.

5.7 Chromosome and plasmid elucidation

The genomes were assembled using the de novo assembler Flye (V2.8.3) [234], resulting in whole chromosome and plasmid contigs. These contigs were then identified as either chromosomal or plasmid in origin through the use of 'mlplasmids' [235]. We identified that each of the four isolates harboured two plasmids and this included so called 'mega plasmids', defined as plasmids greater than 100Kb in size. BLAST analysis was carried out to reveal if the plasmids found here closely match against any previously reported:

- Plasmid pKP1-1 had closest identity to *K.pneumoniae* strain U25 plasmid PU25001 (Accession number : KT203286.1, 211813bp, >99% identity).
- Plasmid pKP1-2 had closest identity to *K.pneumoniae* strain KP33 plasmid pkp3302 (Accession number : AP018749.1, 102910bp, >99% identity).
- For isolate KP2, the plasmid pKP2-1 had closest identity to *K.pneumoniae* strain KP33 plasmid pkp3301 (Accession number : AP019748.1, 296750bp, >99% identity).
- Plasmid pKP2-2 had closest identity to *K.pneumoniae* strain U25 PU25001 (Accession number : KT203286.1, 211813bp, >99% identity).
- The pKP3-1 plasmid from isolate KP3 has closest identity to *K.pneumoniae* strain KP33 plasmid pkp3302 (Accession number : AP018749.1, 102910bp, >99% identity).
- Plasmid pKP3-2 was found to closely identify with *K.pneumoniae* strain KP33 plasmid pkp3301 (Accession number : AP019748.1, 296750bp, >99% identity).
- The plasmid pKP4-1 plasmid had closest identity to *K.pneumoniae* strain KP33 plasmid pkp3302 (Accession number : AP018749.1, 102910bp, >99% identity).

- The final plasmid pKP4-2 had closest identity to *K.pneumoniae* strain KP33 plasmid pkp3301 (Accession number : AP019748.1, 296750bp, >99% identity).

Using the PlasmidFinder web server [236], the replicon type of each plasmid was identified and these are displayed in table 9. IncFIB(K) and IncFII(K) plasmids were identified in all of the sequenced isolates, both of which are associated with the dissemination of antibiotic resistance within clinical isolates. The IncFII(K) plasmid in particular is frequently found to carry the ESBL genes $bla_{CTX\text{-}M\text{-}15}$ and the carbapenemase bla_{KPC} [237]. In this case the IncFII(K) plasmids were not found to posses either of these resistance genes, however ESBL genes were identified on other plasmids and within the chromosome.

Multireplicon plasmids were identified, that is plasmids containing multiple replication initiation points. For example, K2-P2 harboured both IncFIB and IncFII replicons. This is fairly common in clinical isolates, with multireplicon plasmids representing a fusion between different plasmid types [238].

Isolates KP2, KP3 and KP4 were all found to harbour a large IncFIB(pNDM-Mar)-IncHI1B(pNDM-MAR) plasmid. IncFIB(pNDM-Mar) and IncHI1B(pNDM-MAR) plasmids have been found to carry both $bla_{CTX\text{-}M\text{-}15}$ and bla_{NDM} [239]. In this case the plasmids were not found to harbour bla_{NDM}, however they were all found to possess the $bla_{CTX\text{-}M\text{-}15}$ gene, as will be discussed later. Overall, the similarity in the plasmids identified for each isolate further supports our hypothesis that these isolates are of the same clonal type and have adapted over time, or alternatively belong to separate subpopulations.

A summary of the chromosome and plasmid lengths, as well as the replicon types is displayed in table 7. There are variations in the lengths of the chromosomes and common plasmids between the isolates, for example a 178,777bp difference in length between the chromosomes of isolates KP1 and KP2 which could indicate genomic variation such as large indels.

2586

Isolate	Identity	Length (bp)
KP1	Chromosome	5,513,781
	pKP1-1 : IncFIB(K)	108,693
	pKP1-2 : IncFII(K)	102,718
KP2	Chromosome	5,335,004
	pKP2-1 : IncFIB-IncHI1B	260,582
	pKP2-1 : IncFIB(K)-IncFII(K)	211,466
KP3	Chromosome	5,276,817
	pKP3-1 : IncFIB(K)	102,472
	pKP3-2 : IncFIB-IncHI1B	317,179
KP4	Chromosome	5,274,125
	pKP4-1 : IncFIB(K)	94,939
	pKP4-2 : IncFIB-IncHI1B	317,183

Table 7: A summary of the plasmid and chromosome lengths for each isolate (KP1-KP4).

5.8 Genome content - CRISPR-Cas system

Next, we examined the content of the *K.pneumoniae* genomes with the use of qualimap (v2.2.1) [240]. The genome of isolate KP1 was found to have 9,344 CDS, 84 tRNA's, 25 rRNA's (5S, 16S, 23S) and 3 cluster regular interspaced short palindromic repeats (CRISPR) arrays. Isolate KP2 was identified as having 9,496 CDS, 84t tRNA's, 25 rRNA's and 4 CRISPR arrays. Next, isolate KP3 was found to possess 9,308 CDS, 85 tRNA's, 25 rRNA's and 3 CRISPR arrays. Finally, isolate KP4 was found to have 9,301 CDS, 87 tRNA's, 25 rRNA's and 3 CRISPRs.

CRISPR-Cas is a microbial adaptive immune system that limits the acquisition of new genetic material, often acquired through horizontal gene transfer or via bacteriophage. Often these systems are found to be located on the chromosome, however they have also been identified within plasmids [241], albeit rarely. In addition, chromosomal CRISPR systems are more frequently identified in plasmid-free strains of *K.pneumoniae* than those harbouring plasmids.

CRISPR systems are relatively uncommon in *K.pneumoniae*, with a recent study identifying CRISPR-Cas systems in only 37% of 217 studied *K.pneumoniae* chromosomal sequences, and only 5% of 699 studied plasmid sequences [241]. Here, with find both chromosomal and plasmid encoded CRISPR-Cas systems within all of the isolates studied, as shown in table 8. Three CRISPR arrays were identified in the chromosomes of isolates KP1 and KP2. Isolates KP3 and KP4 were found to possess two chromosomal CRISPR arrays and one plasmid CRISPR array each (pKP2-1 and pKP3-2).

A large study of plasmid-associated CRISPR systems found that 45/47 of plasmids harbouring the system had an IncFIB replicon, and a further 36 of them had an additional IncHI1B replicon [241]. Moreover, the CRISPR system was often found associated with plasmids that also carried $bla_{CTX\text{-}M}$, bla_{NDM} and bla_{OXA}. Here, we also find a CRISPR system carried on an IncFIB-IncHI1B mega-plasmid in isolates KP3 and KP4.

Relatively little is known about CRISPR-Cas systems within plasmids. However, the acquisition of plasmid mediated CRISPR-Cas systems is thought to play a role in the competition between different plasmid types. As plasmids are often associated with a fitness burden to the cell [242], plasmid-mediated CRISPR may reduce the costs associated with plasmid carriage.

Isolate	Location	Length (bp)	Position(bp)	Number of spacers	DR length	Identity
KP1	Chromosome	766	2,941,682 - 2,942,448	12	29	CRISPR-associated Cas3 family helicase
	Chromosome	577	2,951,180 - 2,951,757	9	29	CRISPR-associated Cas3 family helicase
	Chromosome	747	3,910,289 - 3,911,036	12	28	CRISPR-associated protein
KP2	Chromosome	578	323,541 - 324,119	9	29	CRISPR-associated Cas3 family helicase
	Chromosome	765	332,851 - 333,616	12	28	CRISPR-associated Cas3 family helicase
	Chromosome	744	4,699,272 - 4,700,016	12	28	CRISPR-associated protein
KP3	Chromosome	765	2,839,309 - 2,840,074	12	28	CRISPR-associated Cas3 family helicase
	Chromosome	578	2,848,804 - 2,849,382	9	29	CRISPR-associated Cas3 family helicase
	Plasmid (pKP3-1)	746	283,541 - 284,287	12	28	CRISPR-associated protein
KP4	Chromosome	764	4,234,801 - 4,235,565	12	28	CRISPR-associated Cas3 family helicase
	Chromosome	576	4,244,300 - 4,244,876	9	29	CRISPR-associated Cas3 family helicase
	Plasmid (pKP3-2)	749	239,119 - 239,868	12	28	CRISPR-associated protein

Table 8: The locations and identities of CRISPR systems within the genomes of the six *K.pneumoniae* isolates.

5.9 Antimicrobial resistance

The antibiotic resistance genes present within each assembled genome were determined using ResFinder [243] - this is a webservice that uses BLAST to rapidly identify both chromosomal point mutations and acquired antimicrobial resistance genes in whole-genome data and then predicts the resulting phenotype. A summary of the AMR genes identified are shown in table 9, and a summary of the changes in AMR profile over time is displayed in figure 53. The isolates were found to have complex resistomes, with various chromosomal and plasmid encoded antimicrobial resistance genes present in the genome. Despite this, there was little change in the AMR profile over time. The phenotypic predictions made by ResFinder (based on the WGS data) are displayed in supplementary tables S4-S7. Now we will discuss the AMR genes identified in the context of the different antibiotic classes.

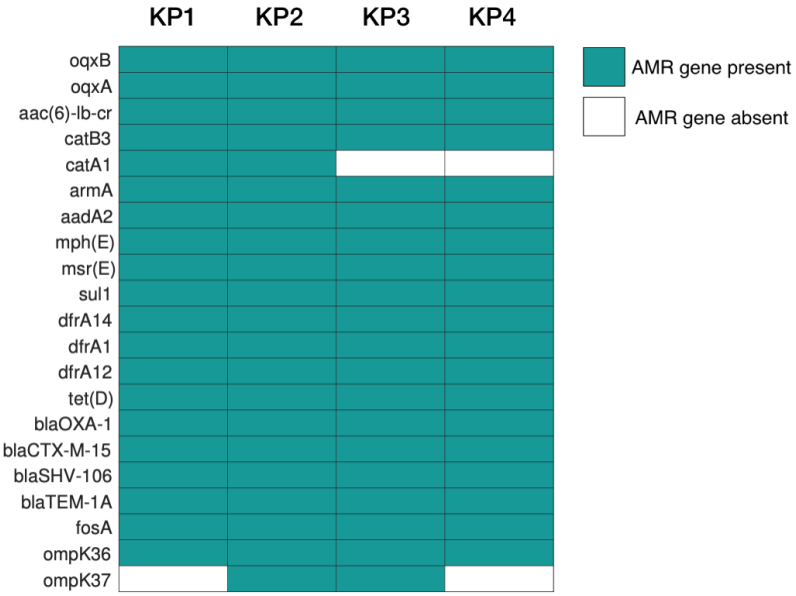

Figure 53: The presence and absence of various antibiotic resistance genes and mutations over the four sequenced isolates. Green represents genes that are present and white represents the absence of the gene or mutation.

Isolate	ST	Length (bp)	ID	AMR genes	Virulence genes
KP1	427	5,513,781	Chromosome	*aac(6')-Ib-cr, oqxA, oqxB, fosA, dfrA12, sul1, dfrA, dfrA14, tet(D),mph(E), msr(E), aaAD2, armA, catB3, blaOXA-1 blaTEM-1A , blaCTX-M-15, blaSHV-16 blaSHV-28*	*iutA*
		108,693	pKP1-1 - IncFIB(K)		*traT*
		102,718	pKP1-2 - IncFII(K)	*catA1*	
KP2	427	5,335,004	Chromosome	*aac(6')-Ib-cr, oqxA, oqxB, blaSHV-28, catB3 blaOXA-1, blaSHV-16, dfrA1, fosA*	*iutA*
		260,582	pKP2-1 - IncFIB(pNDM-Mar) IncHI1B(pNDM-MAR)	*armA, aadA2, tet(D), mph(E), msr(E), dfrA14, dfrA12, sul1, blaCTX-M-15, blaTEM-1A*	*iucC, iutA, terC*
		211,466	pKP2-2 - IncFIB(K) IncFII(K)	*catA1*	*traT*
KP3	427	5,276,817	Chromosome	*aac(6')-Ib-cr, blaOXA-1, blaSHV-106 blaSHV-28, dfrA1, catB3, oqxA, oqxB, fosA*	*iutA*
		102,472	pKP3-1 - IncFIB(K)		*traT*
		317,179	pKP3-2 -IncFIB(pNDM-Mar) IncHI1B(pNDM-MAR)	*armA, aadA2, tet(D), mph(E), msr(E), dfrA14, dfrA12, sul1, catB3, aac(6')-Ib-cr, blaCTX-M-15, blaTEM-1A, blaOXA-1*	*iucC, terC*
KP4	427	5,274,125	Chromosome	*fosA, aac(6')-Ib-cr, dfrA1, catB3, blaOXA-1 blaSHV-16, blaTEM-1A, oqxA, oqxB*	*iutA*
		94,939	pKP4-1 - IncFIB(K)		*traT*
		317,183	pKP4-2 - IncFIB(pNDM-Mar) IncHI1B(pNDM-MAR)	*armA, aadA2, tet(D), mph(E), msr(E), dfrA14, dfrA12, sul1, catB3, aac(6')-Ib-cr, blaCTX-M-15, blaTEM-1A, blaOXA-1*	*iucC, iutA, terC*

Table 9: The AMR and virulence genes identified on the final *K.pneumoniae* assemblies.

5.9.1 Carbapenem and cephalosporin resistance

Clinical PCR tests had sought out the presence of the 'big 4' carbapenamase resistance genes within the isolate from January 2018 (bla_{KPC} non-metallo-carbapenamase, $bla_{OXA\text{-}48\text{-}like}$ non-metallo-carbapenamase, bla_{NDM} metallo-carbapenamase and finally bla_{VIM} metallo-carbapenamase). This isolate was found to possess the $bla_{OXA\text{-}48\text{-}like}$ carbapenemase gene, known to produce a relatively weak carbapenemase that can also hydrolyse narrow spectrum cephalosporins [244].

The low level carbapenemases activity results in difficulties when it comes to detection via phenotypic tests, as the presence of a carbapenemase does not always result in a resistant phenotype. And yet, it is important to detect the presence of these genes in order to avoid complications in treatment, in part due to the reduced susceptibility towards beta-lactamase inhibitors such as tazobactam [75]. The isolate from January was unavailable to study here, however through WGS we identified that all of the four isolates sequenced possessed $bla_{OXA\text{-}1}$, otherwise known as $bla_{OXA\text{-}30}$. OXA-1 is a beta-lactamase that significantly hydrolyses ureudopenicllins such as piperacillin but only weakly hydrolyses narrow-spectrum cephalosporins. Often it is associated with $bla_{CTX\text{-}M}$ [245], as we find here, and this results in the added complication of resistance towards β-lactam-β-lactamase inhibitor combinations such as piperacillin/tazobactam [246]. The misidentification of $bla_{OXA\text{-}1}$ as $bla_{OXA\text{-}48}$ by the clinical PCR test has the potential to result in treatment complications, primarily due to the weak carbapenemase activity of $bla_{OXA\text{-}1}$, as alone it is unlikely to account for the observed resistance towards the carbapenem antibiotic meropenem. It is possible that the isolate obtained in January and utilised for the PCR test possessed different AMR genes to the later isolates, however it was not possible to test this as the January isolate could not be obtained.

We next sought to identity if the $bla_{OXA\text{-}1}$ gene changed over the course of the infection. No polymorphisms were identified in the gene between the isolates,

however the copy number and location of the gene was found to vary. Isolates KP1 and KP2 possessed two copies of the gene located in the chromosome, yet the later isolates KP3 and KP4 only possessed one chromosomal copy of the gene each. However, both KP3 and KP4 were found to carry one copy of the gene within the large IncFIB-IncHI1B plasmid (pKP3-2 and pKP4-2). Fluctuations in selection pressure are thought to favour genes harboured on plasmids, as the cell can rapidly increase the copies of the gene in response to stress e.g. antibiotic treatment [247, 248]. It is possible that the variable use of antibiotics such as meropenem and ceftaz/avibactam resulted in the switch from a chromosome to plasmid-carried $bla_{OXA\text{-}1}$ gene. The population could of course be heterogenous for both plasmid and chromosomal $bla_{OXA\text{-}1}$, however whole population samples would need to be sequenced to determine this.

All isolates were found to have SNPs in the *ompK36* porin gene known to result in resistance towards cephalosporins. Moreover, isolates KP1, KP2 and KP3 have mutations in *ompK36* known to confer resistance specifically towards carbapenems. Isolates KP2 and KP3 have additional mutations in the *ompK37* minor porin gene. The SNPs identified in the *ompK36* and *ompK37* porin genes are displayed in table 10, although some caution has to be taken when considering SNPs identified through nanopore sequencing due to the higher error rate. Loss or alterations in OmpK36 have been shown to result in increased resistance towards carbapenems, particularly when a carbapenemase gene is also present [249, 77]. However, the role of OmpK37 mutations in antibiotic resistance is however less clear.

We hypothesise that the presence of genetic modifications in the *ompK36* and *ompK37* genes, alongside two chromosomal copies of the OXA-1 gene in the October isolate resulted in the resistant phenotype observed within this isolate in the clinical data (figure 53). However, we were not able to replicate this resistant phenotype in the laboratory, as shown in figure 52. It is of course possible that through multiple passages through media (once for subculturing in the clinical lab, second for storage in our own lab and third for antibiotic susceptibility testing),

resistance towards meropenem was lost in this isolate.

The variability in *ompK* mutations, alongside variations in the position of $bla_{OXA\text{-}1}$ on the chromosome and plasmid could account for fluctuations in the response to carbapenem antibiotics such as meropenem. However, functional studies would be required to fully confirm the impact of these genomic changes on the phenotypic response to antibiotic.

Although all of the isolates possessed OXA-1 alongside porin mutations associated with resistance towards cephalosporin antibiotics [250], all were found to be susceptible to ceftazidime/avibactam (a combination of a cephalosporin and β-lactamase inhibitor). Ceftaz/avibactam is reported to be an effective treatment for carbapenem-resistant *Enterobacteriaceae*, as avibactam has strong activity against carbapenemases, as well as ESBLs [251]. Although resistance towards ceftaz/avibactam has been identified in strains with mutations in OmpK36 [252], in this case all isolates with known *ompK36* mutations retain susceptibility.

Gene	Nucleotide change	Amino acid change	Phenotype	KP1	KP2	KP3	KP4
ompK36	ctg → agc	L191S	cephalosporins	○	○	○	
ompK36	aac → gag	N305E	cephalosporins	○			
ompK36	gaa → cgt	E232R	cephalosporins	○	○	○	
ompK36	ctg → gtt	L228V	cephalosporins	○	○	○	
ompK36	ttc → tgg	F207W	cephalosporins	○	○	○	
ompK36	gat → gag	D224E	cephalosporins	○	○	○	
ompK36	ctt → gta	L59V	cephalosporins	○	○	○	○
ompK36	aac → agc	N49S	cephalosporins	○	○		○
ompK36	gct → tct	A217S	carbapenem	○	○	○	
ompK36	aac → cac	N218H	carbapenem	○	○	○	
ompK37	att → atg	I70M	carbapenem		○	○	

Table 10: Mutations in ompK36 and ompK37, with predicted phenotype within the sequenced isolates KP1, KP2, KP3 and KP4.

5.9.2 ESBLs

ESBLs represent a serious risk to successful clinical outcome as they confer resistance towards both β-lactam antibiotics and extended-spectrum cephalosporins. As such, ESBL-producing *Enterobacteriaceae* were declared as pathogens of 'critical priority' by the world health organisation (WHO) in 2017 [193]. Aside from bla_{OXA-1}, the ESBLs SHV and TEM were also identified across all of the isolates. The presence of these genes is reflected in the clinical antimicrobial susceptibly data (table 53), as there was extensive resistance towards β-lactam antibiotics including amoxicillin.

All of the isolates were found to harbour chromosomal bla_{SHV-28} but this is to be expected as *K.pneumoniae* is intrinsically resistant to ampicillin through chromosomally-encoded SHV β-lactamase [253]. The bla_{SHV-28} gene was first

identified in South Korea in 2004, and found to differ from $bla_{SHV\text{-}1}$ by only a single amino acid substitution [254].

All isolates are found to possess $bla_{CTX\text{-}M\text{-}15}$, with isolates KP2, KP3 and KP4 all harbouring one copy of the gene on the large IncFIB-IncHI1B plasmid, whilst KP1 harbours one copy on its chromosome. CTX-M ESBLs, and particularly CTX-M-15 are the dominant ESBL worldwide, with a greater prevalence than TEM and SHV [63]. CTX-M β-lactamases readily hydrolyse β-lactam antibiotics including third and fourth generation cephalosporins, however they have no action against carbapenems such as imipenem and meropenem.

Finally, all of the isolates were found to harbour the ESBL gene $bla_{TEM\text{-}1A}$, however once again isolates KP2, KP3 and KP4 all harbour one copy of the gene on the large IncFIB-IncHI1B plasmid, whilst KP1 harbours one copy on its chromosome. Consistent with the genotypic antibiotic resistance profile, we find that all of the isolates are classified towards a broad range of β-lactam antibiotics as determined by the Vitek and summarised in figure 53. This includes aztreonam, amoxicillin, ampicillin and pivmecillinam.

In addition, the isolates were classified as resistant towards the β-lactam-β-lactamase inhibitor combinations co-amoxiclav and pip/tazobactam. Co-amoxiclav is a combination of amoxicillin and the β-lactamase inhibitor clavulanic acid, whilst pip/tazobactam is a combination of piperacillin and the β-lactamase inhibitor tazobactam. These drug combinations effectively inhibit TEM, SHV and CTX-M, and consequently are utilised when ESBLs are detected [255]. However, OXA-1 has been shown to reduce susceptibility towards β-lactam-β-lactamase inhibitor combinations [255, 246], and as such we hypothesise the presence of $bla_{OXA\text{-}1}$ in the genome of all sequenced isolates contributes towards this resistance phenotype. The isolates were found to retain susceptibility towards the β-lactam-β-lactamase inhibitor combination ceftaz/avibactam (a combination of the cephalosporin antibiotic ceftazidime and the β-lactamase inhibitor avibactam), and indeed this was used frequently in treatment. Avibactam is widely reported to be effective against

carbapenem-resistant *Enterobacteriaceae*, as we find here [256, 257].

5.10 AMR profile

Alongside carbapenemase and ESBL genes, the isolates were found to possess additional genes conferring resistance to a broad range of other antimicrobials. For example, all isolates were found to possess *aac(6')-Ib-cr*, *armA* and *aadA2* genes conferring resistance to aminoglycosides - however the location of these genes on either the chromosome or the large IncFIB-IncHI1B plasmid varied, as shown in table 9. Both the phenotypic and genotypic data presented here suggest that every isolate is resistant to the aminoglycoside gentamicin at clinically relevant concentrations, however this is in disagreement with the data obtained from the Vitek as only the initial isolate KP1 was classified as resistant.

All isolates were found to harbour genes encoding chloramphenicol acetlytransferase enzymes (CATs) conferring resistance towards chloramphenicol. Namely, all isolates harboured the *catB3* and *catA1* genes. The *oqxA* and *oqxB* genes encoding the OqxAB efflux pump were also identified across all isolates - this efflux pump has been implicated in resistance towards fluoroquinolones, and the Vitek data indeed classified all isolates as resistant to the fluoroquinolone antibiotic ciprofloxacin.

However, discrepancies were identified between the Vitek and genomic data in regards to fosfomycin resistance. All of the isolates were found to possess a chromosomal gene encoding fosfomycin-inactivating enzyme (*fosA*), however the Vitek classified KP1 as resistant and KP2 as susceptible at clinically relevant concentrations (KP3 and KP4 were not tested for fosfomycin resistance). This further demonstrates the issues surrounding the use of genotypic data alone to determine AMR profiles. Genes conferring resistance to folate pathway antagonists such as trimethoprim and sulfonamides were found across all isolates. This included *dfrA1, dfrA12* and *dfrA14* which once again varied in location across the different

isolates. In addition, all were found to possess the *sul1, sul2* genes conferring resistance towards sulfonamides. Although phenotypic data was not available for the susceptibility of the four sequenced isolates towards trimethoprim, the earlier isolates obtained in Dec '17, Jan '18, Feb '18 and July '18 were classified as resistant. Indeed, all of the sequenced isolates were classified as phenotypically resistant toward co-trimoxazole, a combination of sulfamethoxazole and trimethoprim (figure 53).

5.11 Virluence factors

K.pneumoniae are known to produce a plethora of virulence factors that contribute towards colonisation of the host, pathogencitiy and invasion of host tissues. Among the key virulence factors commonly identified are polysaccharide capsules, adhesins and aerobactin siderophores [258]. The virulence factors present in the *K.pneumoniae* isolates were determined using a combination of VirluenceFinder [259] and the Pasteur *K.pneumoniae* database.

All isolates were identified as having a chromosome-located *iutA* gene encoding an aerobactin siderophore receptor. In addition, the isolates KP2, KP3 and KP4 were found to have *iucC* (siderophore aerobactin) and *terC* (tellurite resistance) carried on the large IncFIB-IncHI1B replicon plasmid. Siderophore production is key to both bacterial growth and virulence as it enhances iron uptake, and the production of aerobactin in particular has been linked to 'hypervirluent' strains of K.pneumoniae [260]. Finally, all of the sequenced isolates harboured a *traT* gene on the IncFIB(K) plasmid that encodes the TraT complement resistance protein associated with enhanced serum resistance [261].

5.12 Structural variations in the genome

In bacterial genomics, much attention is given to the detection of SNP's, for example single base deletions or substitutions. However, large structural changes can also significantly impact the genome, for example by resulting in a change to gene copy number or position. Consequently, structural variations (SVs) can impact on gene functioning [262, 263]. We therefore sought to identify large SVs in both the chromosomes and plasmids of the sequenced *K.pneumoniae* isolates. The use of nanopore sequencing is useful here as the long reads are likely to span the whole length of a variation, including repeat regions. As a result, SVs can be reliably detected.

Changes in the genome coverage can be indicative of SVs such as amplifications, as this would result in a higher read depth in the amplified region. To this end, we aligned the genomes of all isolates against the earliest available isolate (KP1) and quantified genome coverage, as shown in figures 57-60. A small amplification was identified in plasmid pKP4-1 (Fig 60). The amplification was estimated to be 713bp and spanned the choline transporter gene *betU*.

Sniffles was used to identify structural variations in the chromosome of isolates KP2-KP4 when aligned against the assembly of the initial isolate, KP1. As shown in table 11, no significant SVs were identified in KP2, however three were found in KP3 and KP4. Both isolates KP3 and KP4 have a 9,853bp deletion spanning genes encoding hypothetical proteins. In addition, both isolates were found to have a 55,518bp deletion spanning key antibiotic resistance genes (*catB3, blaOXA* and *aac(6')-Ib-cr*), leaving only single copies of these genes in the chromosome in comparison to KP1 and KP2 that were found to have two copies. The later isolates did however carry copies of these genes on the large IncFIB-IncHI1B plasmid, as shown in table 9.

KP3			
Start position (bp)	**End position (bp)**	**Status**	**Genes**
2,219,022	2,228,875	DEL	Hypothetical
3,909,962	3,965,480	DEL	*dinG, catB3, blaOXA, aac(6')-Ib-cr*
5,464,477	5,469,671	INV	Hypothetical
KP4			
Start position (bp)	**End position (bp)**	**Status**	**Genes**
2,219,022	2,228,875	DEL	Hypothetical
3,909,961	3,965,479	DEL	*dinG, catB3, blaOXA, aac(6')-Ib-cr*
5,471,581	5,474,111	INV	Hypothetical

Table 11: Structural variations identified in the chromosome of KP2-KP4 when aligned to KP1.

In addition, variations were found in the structure of the large IncFIB-IncHI1B plasmid found in isolates KP2-KP4 - namely pKP2-1 was $\sim$57Kbp smaller than the equivalent plasmids in later isolates (pKP3-2 and pKP4-2), despite high levels of similarity in the rest of the plasmid sequences (figure 54). This variation in plasmid structure accounts for the absence of the aac(6')-Ib-cr, bla_{OXA-1} and catB3 genes in pKP2-1 that are identified in the IncFIB-IncHI1B plasmid of later isolates.

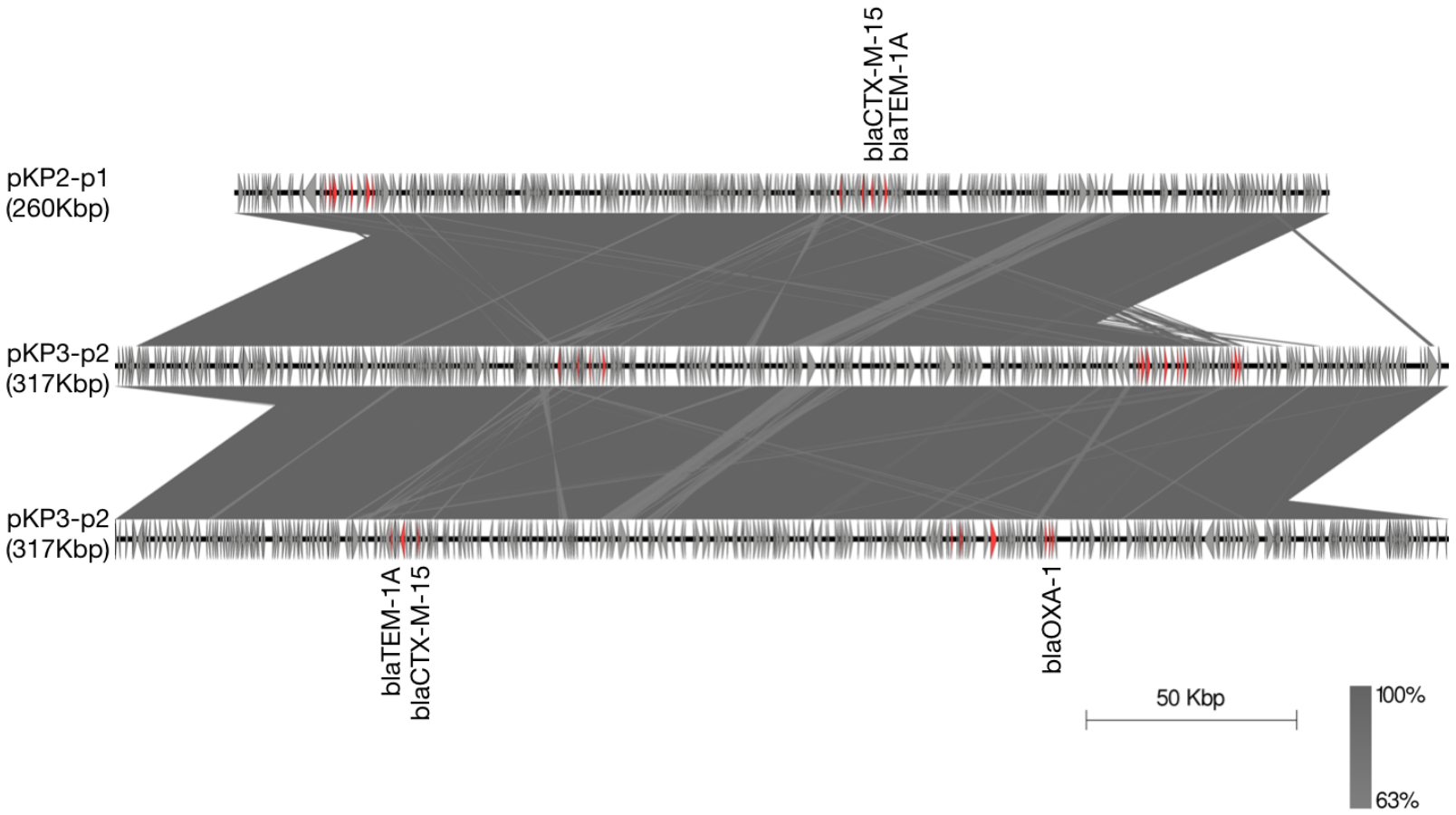

Figure 54: Linear comparison of the IncFIB-IncHI1B plasmids in KP2-KP4. The grey shaded regions represent the sequence identify (63-100%). AMR genes are represents as red arrows, and the positions of bla_{OXA-1}, $bla_{CTX-M-15}$ and bla_{TEM-1A} are indicated. Visualisation was performed using EasyFig.

5.12.1 Chromosomal integration of a large plasmid fragment containing $bla_{CTX\text{-}M\text{-}15}$ in KP1

Isolate KP1 was found to have a large chromosomal region (176,800bp) with approximately 1.4x higher read depth than the rest of the genome (fig 55), and this is clearly displayed on the coverage plot for the KP1 chromosome shown in figure 57. Furthermore, this region was found to span multiple antibiotic resistance genes (Table 13) including $bla_{CTX\text{-}M\text{-}1}$, *tetA* and *ant1* in addition to the multidrug transport gene *emrE*. Within this region we also find the genes *repB* (RepFIB replication protein B) and *repA* (RepFIB replication protein A) that are found in plasmids belong to the IncFIB family [264]. Moreover PlasmidFinder confirmed the presence of an IncFIB integron at position 4,081,710-4,082,146bp on the chromosome and a IncHI1B integron at position 4,004,716-4,005,284bp on the chromosome. This is indicative of a plasmid fragment that has integrated into the chromosome. We next aligned the genomes of KP2-KP4 against KP1, and determined SVs using the Sniffles structural variant caller (v1.0.12a) [265]. This revealed that isolates K2-K4 did indeed have a 176,857-176,859bp deletion in this location on the chromosome, and the plasmid fragment was therefore absent in these isolates.

Isolate	Start position	End position	Length(bp)	Indel type
KP2	4001548	4178405	176857	Deletion
KP3	4001547	4178406	176859	Deletion
KP4	4001548	4178405	176857	Deletion

Table 12: The deletion of the plasmid fragment in isolates KP2-KP4.

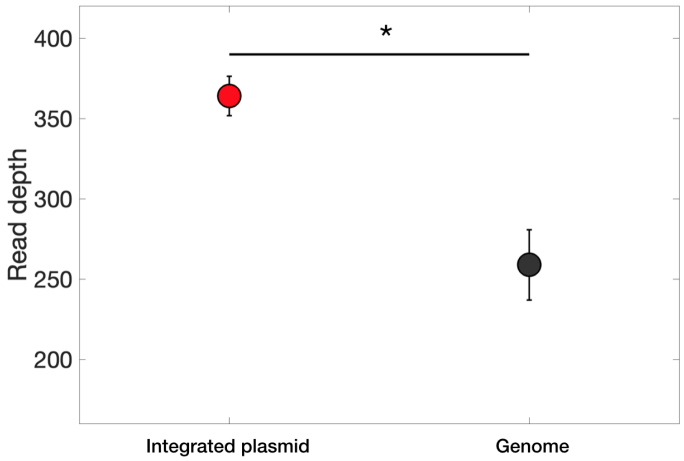

Figure 55: The read depth (coverage) of the region found to contain an integrated plasmid fragment (3,996,200bp - 4,176,000bp) found in KP1 versus the rest of the genome with the region removed. We find that there is a significant increase in the read depth of this region in KP1 versus the rest of the genome. (t-test, $p < 0.05$). *n=3*.

Mobile elements such as IncFIB plasmids are a primary source of AMR genes, and we hypothesise in this case that the IncFIB-IncHI1B plasmid found in KP3 and KP4 has integrated into the chromosome within KP1. As we have only sequenced a clonal population, it is of course possible that the actual population is heterogeneous with a mixture of free and integrated plasmids. Alternatively, cells with the integrated plasmid may have been outcompeted by those with the free plasmid early on in the infection.

The integration of plasmids into the chromosome of clinical isolates has been observed elsewhere. For example, Turon et al. identified a large plasmid fragment containing the bla_{OXA-48} gene that had integrated into the genomes of clinical *E.coli* isolates [266] and Gorrie et al. found entire plasmid sequences containing multiple AMR genes had integrated into the chromosome of clinical *K.pneumoniae* isolates [80]. These plasmid integration events are thought to be beneficial to the cell as it minimises the risk of plasmid loss during replication, thus preserving beneficial

genes such as AMR genes [267]. In some cases, only single plasmid genes will become integrated into the genome. This is frequently observed with AMR genes - for example the chromosomal integration of the *K.pneumoniae* carbapenemase gene bla_{KPC} has reported many times [268, 269]. In this case it appears that a large fragment of the IncFIB-IncHI1B plasmid has become integrated rather than a single gene.

Figure 56 shows the comparative analysis between the region of the KP1 genome containing the integrated plasmid fragment (3,996,200-4,176,000bp) and pKP2-1. We found that there is high sequence identity between KP1 and two separate sections of pKP2-1 harbouring multiple AMR genes (*aadA2, sul1, armA, msr(E), mph(E), dfrA14, tet(D),* bla_{TEM-1A} *and* $bla_{CTX-M-1}$).

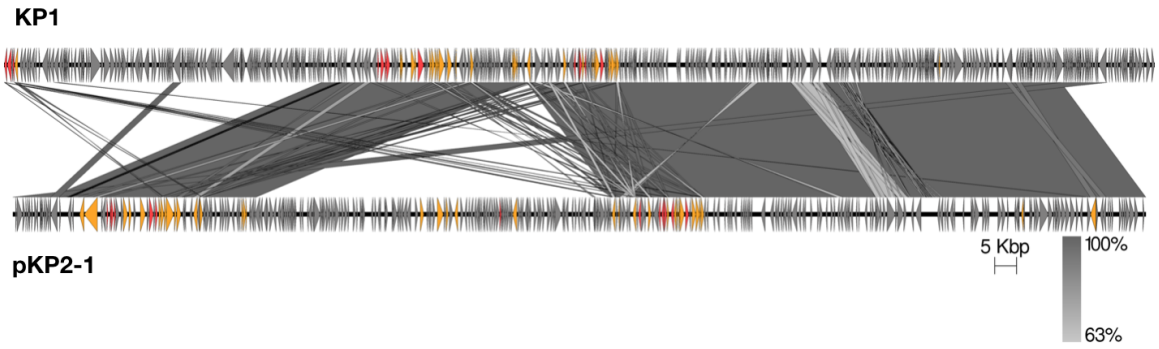

Figure 56: Linear comparison of the integrated plasmid fragment in KP1 (3,996,200-4,176,000bp) and the IncFIB-IncHI1B plasmid from KP2 (pKP2-1). The grey shaded regions represent the sequence identify (63-100%). Mobile elements are represented as yellow arrows, and AMR genes by red arrows. All other genes are shown as grey arrows. Visualisation was performed using EasyFig.

Start position (bp)	End position (bp)	Gene	Product	Start position (bp)	End position (bp)	Gene	Product
4,004,585	4,004,863	*repB*	RepFIB replication protein A	4,058,952	4,059,572	*tetR*	Tetracycline repressor protein class H
4,004,872	4,005,369	*repB*	RepFIB replication protein A	4,060140	4,060,998	*blaTEM-1A*	Beta-lactamase TEM-1A
4,011,221	4,0122,34	*xerD*	Tyrosine recombinase XerD	4,061,181	4,061,738	*tnpR*	Transposon Tn3 resolvase
4,012,519	4,012,875	*dfrA*	Dihydrofolate reductase	4,063,818	4,064,597	*blaCTX-M-1*	Beta-lactamase CTX-M-1
4,013,294	4,014,073	*aadA2*	Streptomycin 3-adenylyltransferase	4,081,266	4,081,748	*repB*	RepFIB replication protein A
4,014,237	4,014,584	*emrE*	Multidrug transporter EmrE	4,081,745	4,082,140	*repA*	Replication protein RepA
4,014,578	4,015,417	*sul1*	Dihydropteroate synthase	4,088,273	4,089,481	*pvuIIM*	Modification methylase PvuII
4,018,911	4,019,531	*armA*	16S rRNA (guanine(1405)-N(7))-methyltransferase	4,097,291	4,097,941	*ecoRIIR*	Type-2 restriction enzyme EcoRII
4,021,829	4,023,151	*msr(E)*	ABC-F type ribosomal protection protein	4,097,995	4,098,291	*ecoRIIR*	Type-2 restriction enzyme EcoRII
4,023,358	4,024,241	*mph(E)*	Macrolide 2'-phosphotransferase	4,098,243	4,098,551	*ecoRIIR*	Type-2 restriction enzyme EcoRII
4,028,105	4,028,539	*merR*	Mercuric resistance operon regulatory protein	4,098,761	4,099,243	*dcm*	DNA-cytosine methyltransferase
4,033,315	4,033,875	*hin*	DNA-invertase hin	4,099,343	4,099,990	*dcm*	DNA-cytosine methyltransferase
4,035,437	4,036,165	*dsbC*	Thiol:disulfide interchange protein DsbC precursor	4,100,117	4,100,860	*dnaC*	DNA replication protein DnaC
4,045,568	4,046,335	*hemB*	Delta-aminolevulinic acid dehydratase	4,115,762	4,116,772	*virB*	Virulence regulon transcriptional activator VirB
4,046,399	4,046,710	*allB*	Allantoinase	4,116,772	4,117,788	*parA*	Plasmid partition protein A
4,048,767	4,050,200	*dcm*	DNA-cytosine methyltransferase	4,160,627	4,160,869	*relE*	mRNA interferase RelE
4,050,234	4,050,491	*ecoRIIR*	Type-2 restriction enzyme EcoRII	4,161,438	4,161,710	*addA*	ATP-dependent helicase/nuclease subunit A
4,050,514	4,051,071	*ecoRIIR*	Type-2 restriction enzyme EcoRII	4,165,960	4,166,691	*nirQ*	Denitrification regulatory protein NirQ
4,050,514	4,051,071	*ecoRIIR*	Type-2 restriction enzyme EcoRII	4,178,428	4,179,783	*ltrA*	Group II intron-encoded protein LtrA
4,053,976	4,054,734	*xerD*	Tyrosine recombinase XerD	4,183,439	4,184,188	*dnaC*	DNA replication protein DnaC
4,056,016	4,056,228	*frmB*	S-formylglutathione hydrolase	4,189,413	4,190,285	*recE*	Exodeoxyribonuclease 8
4,056,472	4,057,581	*frmA*	S-(hydroxymethyl)glutathione dehydrogenase	4,190,609	4,191,178	*recE*	Exodeoxyribonuclease 8
4,057,676	4,058,101	*tetD*	Tetracycline resistance protein	4,191,223	4,192,809	*recE*	Exodeoxyribonuclease 8
4,058,506	4,058,856	*tetD*	Tetracycline resistance protein				

Table 13: The genes present in the 179,700bp integrated plasmid in the chromosome of isolate KP1.

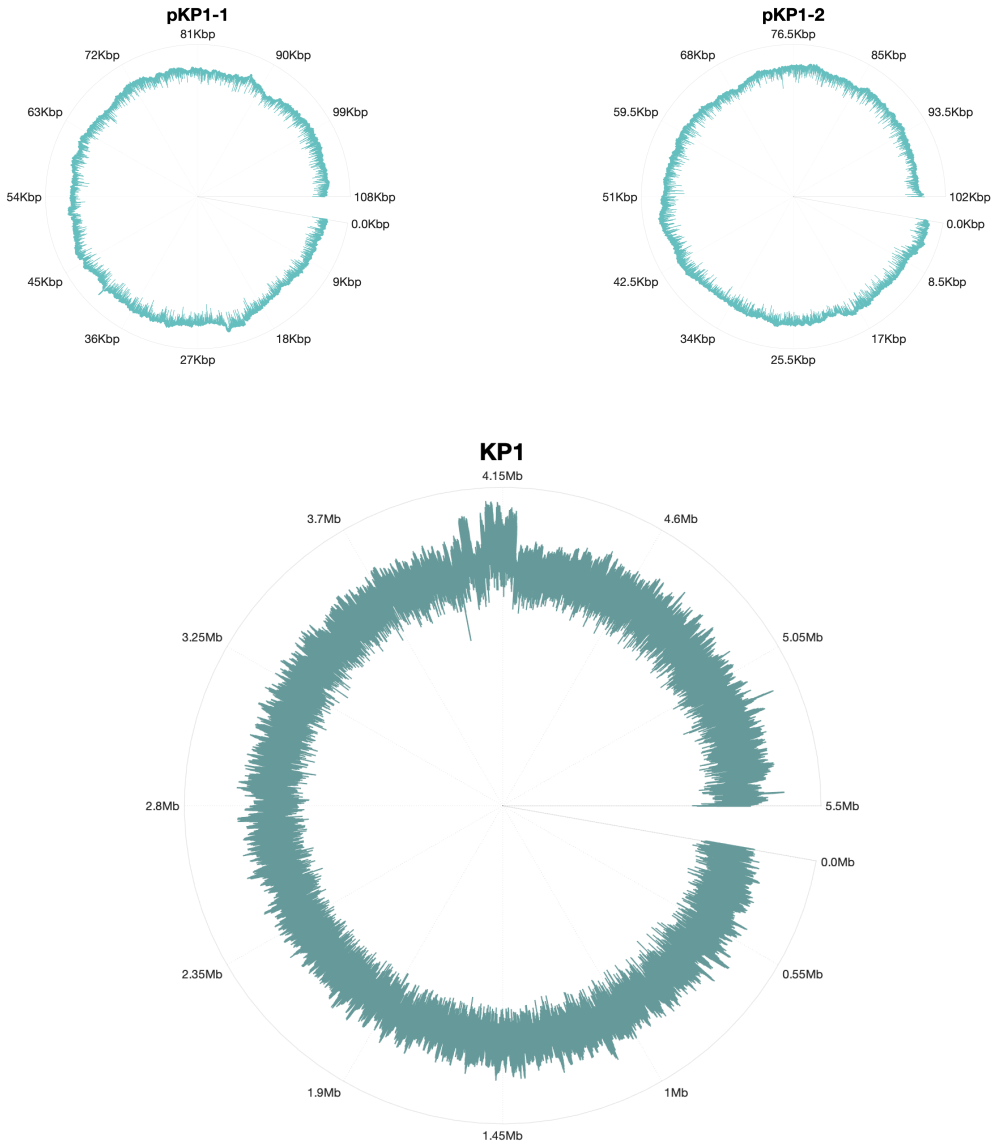

Figure 57: The genome coverage of isolate KP1 (August 2018). The whole 5.3Mb chromosome was assembled into a single contig with mean coverage of 278, with two plasmids assembled as seperate contigs. Plasmid one (pKP1-1) was 108Kbp in length and mean coverage of 133.5, and plasmid two (pKP1-2) was 102Kbp in length and mean coverage of 138.6.

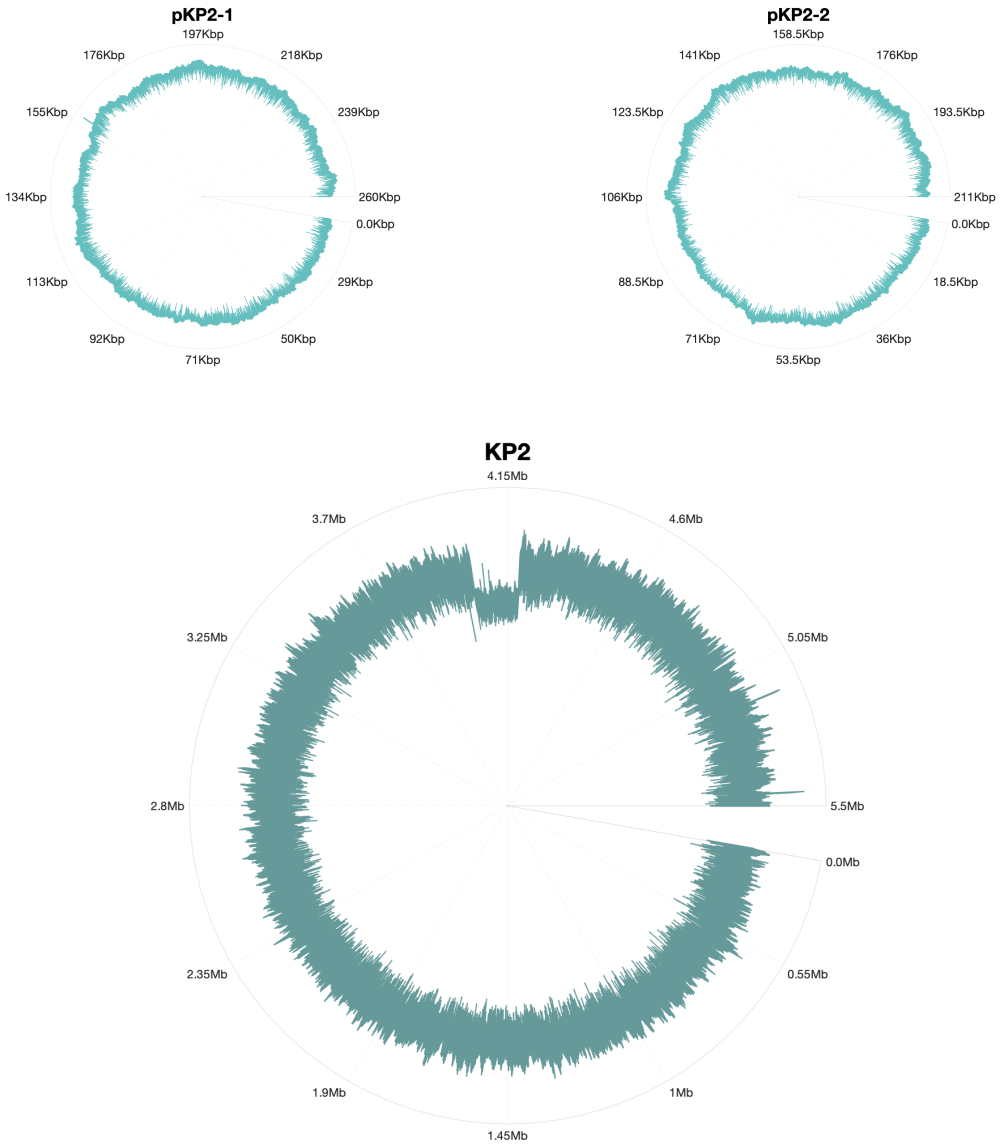

Figure 58: The genome coverage of isolate KP2 (October 2018). The whole 5.3Mb chromosome was assembled into a single contig with a mean coverage of 301.6, with two plasmids assembled as seperate contigs. Plasmid one (pKP2-1) was 260Kbp in length and mean coverage of 173.1, and plasmid two (pKP2-2) was 211Kbp in length and mean coverage of 146.7.

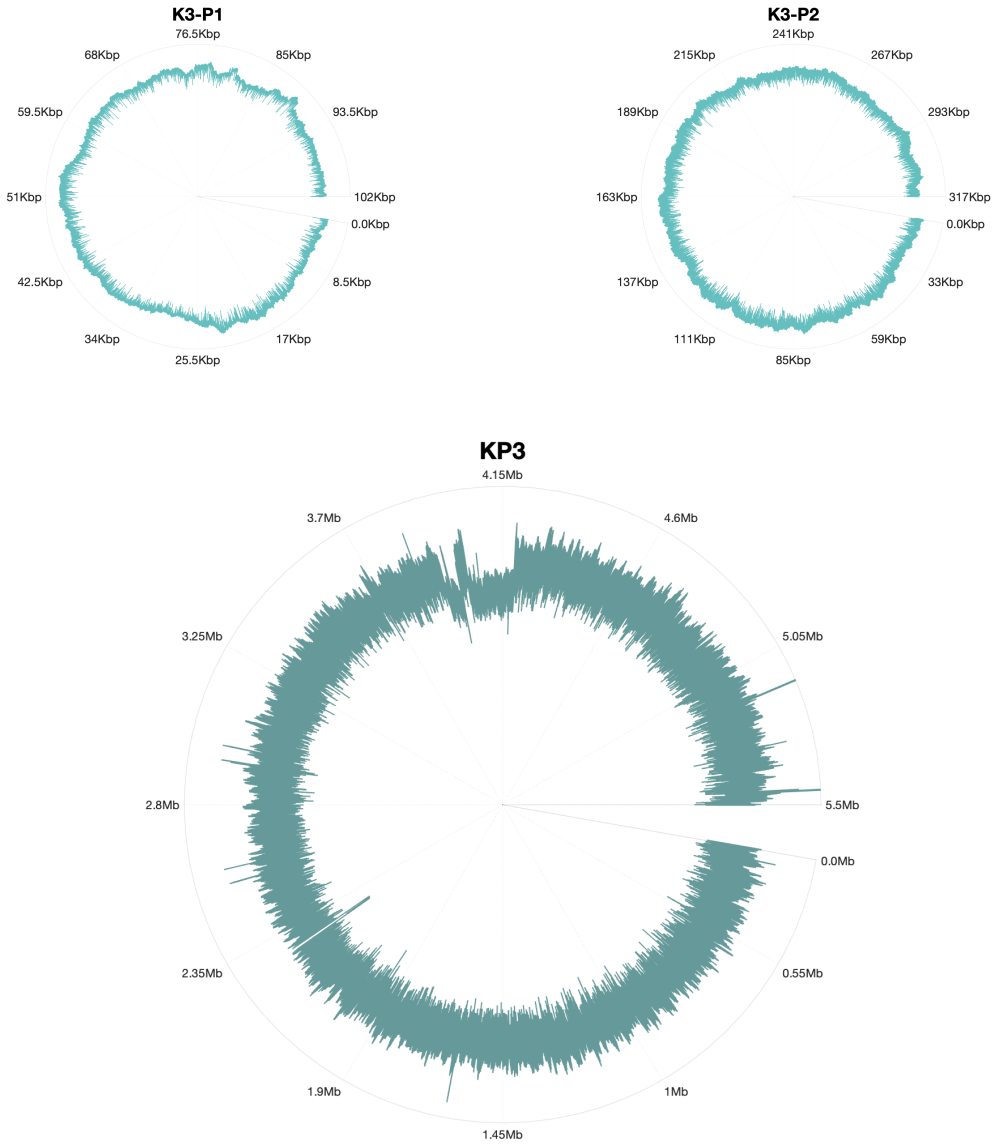

Figure 59: The genome coverage of isolate KP3 (Janurary 2019). The whole 5.3Mb chromosome was assembled into a single contig with mean coverage of 263, with two plasmids assembled as seperate contigs. Plasmid one (pKP3-1) was 102Kbp in length and mean coverage of 67.1, and plasmid two (pKP3-2) was 317Kbp in length and mean coverage of 176.2.

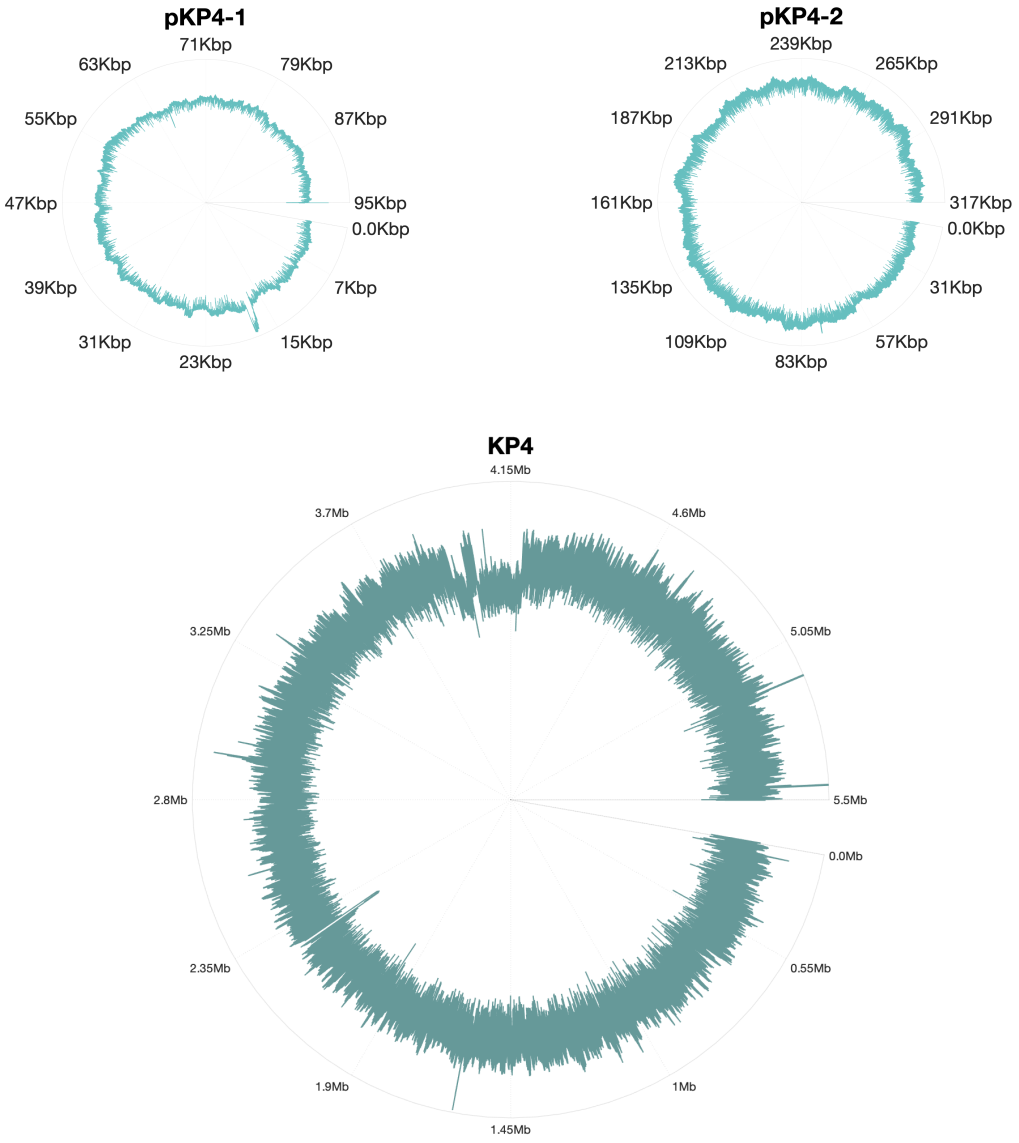

Figure 60: The genome coverage of isolate K4 (May 2019). The whole 5.3Mb chromosome was assembled into a single contig with a mean coverage of 191.8, with two plasmids assembled as seperate contigs. Plasmid one (pKP4-1) was 94Kbp in length with mean coverage of 50.3 and plasmid two (pKP4-2) was 317Kbp in length with mean coverage of 126.6.

5.13 Summary

In this chapter we aimed to track the adaptation of *K. pneumoniae* during a long-term infection. Through nanopore sequencing we were able to identify that the isolates sequenced were all of the same sequence type and possessed similar AMR profiles, thereby suggesting that the isolates originated from the same lineage. We found that for a number of antibiotics, the AMR data generated by the Vitek correlated well with that predicted through the genotypic data. For example, both predicted resistance across all isolates to ceftazidime, ciprofloxacin, ampicillin, aztreonam, ceftaxime, cefuroxime axeil, cefepime, tobramycin and pip/tazobactam. However, there were a number of discrepancies; for example from the genotype we predicted resistance towards fosfomycin across all of the sequenced isolates, but this was not replicated in the Vitek data. More crucially, discrepancies were identified in the AMR profile for antibiotics that were used in treatment. The data obtained from the Vitek predicted fluctuating susceptibility towards gentamicin whilst both the genotypic and phenotypic data obtained in this study would classify all of these isolates as resistant. This points towards potential errors in the Vitek predictions of susceptibility.

This set of isolates was of particular interest due to their resistance towards carbapenem antibiotics. Carbapenem resistance is a growing problem for infection medicine as it puts serious limitations on treatment options, consequently leading to poor treatment outcomes [195, 69]. Through WGS we were able to identify the presence of mutations in OmpK porin genes that have previously been associated with resistance towards carbapenems [77]. Alongside this we also identified the weak carbapenemase OXA-1 and various ESBL genes such as CTX-M-15 which could further contribute towards carbapenem resistance [78].

Furthermore, the long reads produced by nanopore sequencing allowed us to resolve variations in the genome structure, and of particular interest was the integration of a large plasmid fragment into the chromosome of the pKP1-1 initial

isolate obtained in August 2018 (KP1). This integrated plasmid contained multiple antibiotic resistance genes, including the ESBL gene $bla_{CTX\text{-}M}$. Further investigation would be required to identify if the *K. pneumoniae* population was heterogenous for integrated and free plasmids, or if this integration event was unique to that one particular time point.

Although in this case there are clear discrepancies between phenotypic and genotypic data, we have to be cautious in our association of genotypic resistance determinants with phenotypic resistance at clinically relevant doses of antibiotic [270]. As interest in WGS as a diagnostic tool in clinical practice grows, we must consider the pitfalls when compared to the exclusive use of phenotypic data. One of the primary drawbacks is that genotypic data can not accurately determine susceptibility when resistance is conferred by an unknown mechanism, as sequence data is often compared against databases of previously described resistance mechanisms to predict phenotype.

Moreover, the presence of a gene known to confer antibiotic resistance does not necessarily translate into phenotypic resistance at clinically relevant levels [83], meaning that antibiotics may be incorrectly discounted as a treatment option. Although detecting the presence of antibiotic resistance genes can be carried out with relative ease, challenges may also arise when antibiotic resistance is conferred by large structural variations in the genome. Here, we find that the primary structural variant is the integration of a mobile genetic element, however other studies have also highlighted the importance of alternative SVs such as genome duplications within clinical isolates, and their consequent role in the development of antibiotic resistance [210, 262]. These structural variations will only further complicate the use of WGS as a diagnostic tool.

5.13.1 Temporal changes in the AMR profile and genomes of the *K.pneumoniae* isolates

We hypothesised that prolonged antibiotic treatment would result in genomic changes in antibiotic resistance genes, as well as larger genomic modifications. Indeed, we find that substantial genomic changes occur between the *K.pneumoniae* isolates, namely a reduction in the number of SNP's within the ompK36 gene, the insertion and eventual deletion of a inserted plasmid fragment within the chromosome, the deletion of a large chromosomal region carrying AMR genes in KP3 and KP4, as well as the loss of a plasmid harbouring the *cat1* gene. In addition, fluctuations were found in the phenotypic AMR profile of these isolates, particularly in the response to meropenem and gentamicin, both of which were used in the treatment of this infection.

Although all of these isolates were identified as likely belonging to the same clonal group, it is possible that different subpopulations were present within the same infection site. This would mean that any genomic changes simply represent a genetically diverse infection, rather than temporal adaptive changes. In order to clarify this, whole population samples would need to be taken, or alternatively multiple bacterial colonies from the samples collected at each time point. Both the key phenotypic and genotypic changes occurring between the isolates are summarised in figure 61.

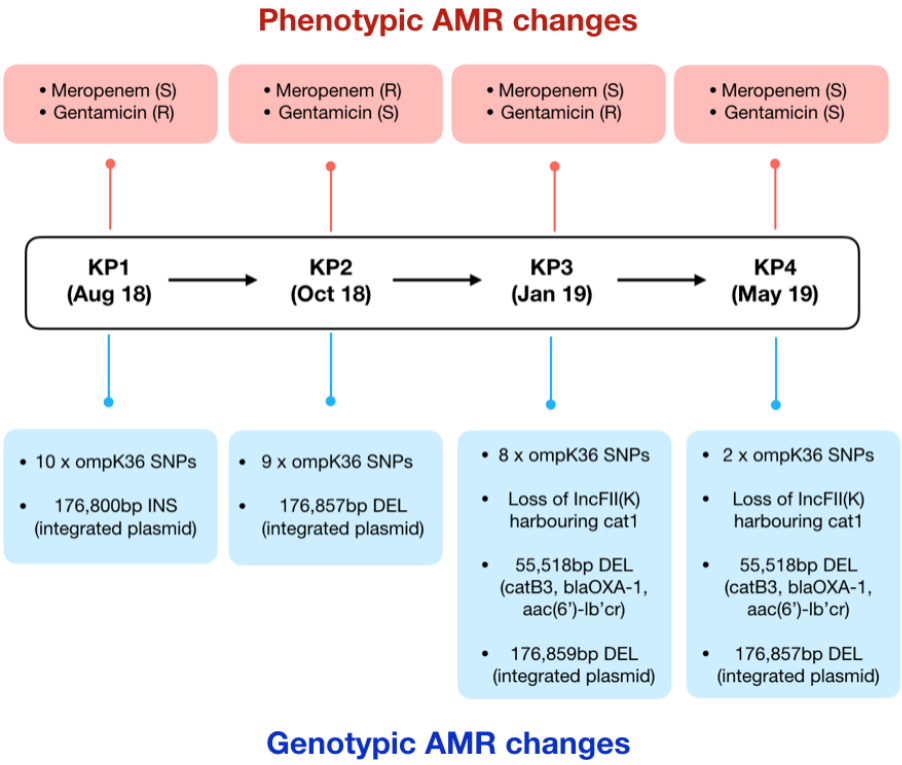

Figure 61: A summary of the key phenotypic and genotypic changes occurring within the *K.pneumoniae* isolates over time, relative to the initial isolate. Note that the phenotypic changes refer to those identified in the data obtained from the Vitek 2. R = resistant, S = susceptible, DEL = deletion, INS = insertion.

CHAPTER SIX

COMPARATIVE GENOMICS OF *ESCHERICHIA COLI* ISOLATES FROM A SINGLE PATIENT OVER 26 MONTHS

6.1 Overview

In the previous chapter we described the within-host adaptation of clonal *K.pneumoniae* isolates over the course of an extended infection period. Next, we sought to understand the genomic adaptations occurring in clinical isolates of *E.coli*, sampled from a patient over the course of 26 months. Through doing so, we aimed to identify if the isolates were clonal, the AMR determinants present and any changes in genome structure over time. The key findings were as followed:

1. Through nanopore sequencing we identified that the sequence type of isolates varied over different sampling points.
2. The isolates harboured a diverse range of AMR and virulence plasmids.
3. The AMR profile was highly variable, with certain isolates harbouring plasmids with ESBL genes.

Whilst *Escherichia coli* often resides in the human gut as a commensal for years, posing no harm to the health of its host [271], when located in other areas of the human body it can become one of the most prevalent gram-negative pathogens colonising humans. The result is a wide-range of diseases, such as urinary tract and bloodstream infections. Extraintestinal *E.coli* (ExPEC) infections in particular are rapidly on the rise, resulting in widespread global dissemination [272]. ExPEC *E.coli* are broadly split into three groups, uropathogenic *E.coli* (UPEC) that are the causative agent of infections such as urinary tract infections, neonatal meningitis *E.coli* (NMEC) and finally sepsis-associated *E.coli* (SEPEC) [273].

Of notable concern is the spread of ESBL-producing *E.coli* due to their ability to resist commonly used antibiotics such as extended-spectrum cephalosporins, resulting in severely limited treatment options [274, 275]. Since the 1980's multiple different ESBLs have been identified, with the four main groups being bla_{TEM}, bla_{CTX}, bla_{SHV} and finally bla_{OXA}. Moreover, mutations in these ESBL genes have been reported to facilitate adaptation and enhanced resistance towards antimicrobials [276]. ESBL enzymes act through the hydrolysis of the β-lactam ring, however they can be effectively inhibited by β-lactamase inhibitors such as clavulanic acid and tazobactam [277]. As a result, infections predicted to be caused by an ESBL producing pathogen will likely be treated with a β-lactam-β-lactamase inhibitor combination.

As with other AMR genes, ESBL genes are often harboured on plasmids, allowing rapid dissemination throughout bacterial populations via horizontal gene transfer [278]. Moreover, these plasmids are often found to carry multiple other antibiotic resistance and virulence genes [53, 62], resulting in further complications to treatment. However, chromosomal ESBL genes have been identified, both in clinical [266, 279, 280] and non-clinical settings [281].

Aside from the production of β-lactamase enzymes, many other antimicrobial resistance mechanisms exist in *E.coli*. For example, through the production of efflux pumps which actively pump drug out of the cell [282], or alterations to the drug

target [283]. However, multi-drug-resistance is often conferred by a combination of these mechanisms.

There is a plethora of data on the spread of multidrug-resistant *E.coli* within hospital environments [284, 285], however little is known about pathogen dynamics and genomic variation within individual long-term infections. By exploring pathogens genomes over an extended period of antibiotic use in a single patient, we not only improve our understanding of the genomic diversity within infection sites, but also the relationship between genomic changes and fluctuations in AMR profile. For example, it is generally considered that extraintestinal infections with *E.coli* are caused by isolates originating from a single clone, and as such diagnosis is based on the characterisation of single clones. However, extraintestinal infections can be both polyclonal and monoclonal, and isolates from single patients can have a high level of genetic diversity [286]. Yet, despite advances in WGS, there are still limited examples of studies on pathogen genomes within single patients over time [84, 83].

The aim of the work within this chapter was to characterise *E.coli* isolates originating from a single patient treated for cholangitis over the course of 26 months. Through a combination of phenotypic and genotypic work, we sought to elucidate the resistomes of these isolates, identify if they were clonal, and identify any genomic variation between the different isolates. Furthermore, we sought to further validate the use of nanopore sequencing to characterise the genomes of complex clinical pathogens.

6.2 Contributions

The bacterial isolates and clinical data presented in this chapter were acquired by Dr Fergus Hamilton (NHS North Bristol Trust). Prof Robert Beardmore contributed towards the study design and acquisition of clinical isolates. The computing facilities required for the analysis of the genomic data were provided by Prof Ivana Gudelj.

The purchase of the minION and flow cells were covered by a 'Showering fund' grant (Metagenomics and evolution of microbes in response to antibiotic treatment), a fund supporting research in the department of pathology within the North Bristol NHS trust.

6.3 Clinical data

All of the isolates utilised in this chapter were acquired from an elderly male patient suffering from recurrent cholangitis. Cholangitis is an infection of the bile and biliary tract, often caused by a physical obstruction such as a gallstone [287]. Although cholangitis often presents as a short-term infection that is rapidly resolved with the use of antibiotics, it can develop into a chronic infection and pose a serious risk to health with a 5-13% mortality rate [288]. The most common pathogen associated with cholangitis is *E.coli* [289, 290], followed by *Klebsiella*, *Enterococcus* and finally *Enterobacter* [291].

A variety of antibiotics are used in the treatment of cholangitis, including cefriaxone and metronidazole alongside β-lactam-β-lactamase inhibitor combinations such as piperacillin-tazobactam, ticarcillin-clavulanate and ampicillin-sulbactam. These combination treatments aid the clearance of ESBL-producing bacteria as they often retain susceptibility towards β-lactamase inhibitors. Usage generally spans 7-10 days depending on infection severity [291]. The speed and accuracy of initial diagnosis and treatment are crucial to patient outcome, with misuse resulting in severe consequences to patient health, raising the risk of complications such as septic shock [292]. A key aspect of diagnosis is the accurate detection of ESBL's, particularly those that can result in reduced susceptibility towards β-lactamase inhibitors [293].

Figure 62 displays the patients clinical course, that is the antibiotic treatments administered over the course of the infection. All samples were identified as *E.coli* by the automated testing system (Vitek 2) within the clinical laboratory. The

majority of treatment consisted of ciprofloxacin, gentamicin and pip/tazobactam, with co-amoxiclav additionally administered 24 months into the infection. However, the patient frequently presented with recurrent bacteraemia.

In total, the clinical data for seven isolates was acquired retrospectively and six of these isolates were available for further characterisation and sequencing. We were unable to grow the isolate obtained at 20 months from the sample provided.

Figure 62: Patient carriage of *E.coli* over 26 months. Red circles indicate the antibiotic treatment used at each time point.

The antibiotic susceptibility profiles for each isolate were determined within the hospitals clinical laboratory using a combination of disk diffusion assays and the Vitek 2 (bioMerieux). Figure 14 displays a list of all the antibiotics that the isolates were tested against, as well as the detection of ESBL production. Empty squares indicate that data was not collected for that particular antibiotic at that timepoint. The AMR profile was found to vary substantially between different isolates, although all isolates were consistently classified as resistant towards ampicillin, a β-lactam antibiotic. All but one isolate (sampled at 23 months) were also consistently classified as resistant towards co-amoxiclav. Given that co-amoxiclav is a combination of amoxicillin and the β-lactamase inhibitor clavulanic acid, this suggests that the

isolates possess a mechanism for β-lactamase inhibitor resistance. The final two isolates are found to have identical AMR profiles, and this is to be expected given the short time span between sampling.

Figure 63 displays the AMR data obtained from the Vitek alone, as this gives an indication of MIC value and it was found to mirror the data in table 14, with fluctuating susceptibility towards most of the antibiotics tested against. Overall, the variability in the AMR data is suggestive of either a polyclonal infection, colonisation by different clonal types over time, or alternatively the adaptation of a single dominant clonal type.

	Day 1	11 months	20 months	23 months	24 months	26 months (1)	26 months (2)
Co-amoxiclav	R	R	R	S	R	R	R
Ceftazidime	R	S	S	S	S	S	S
Ciprofloxacin	I	S	I	S	S	R	R
Cefpodoxime	R	S	S	R	S	S	S
Cefuroxime	R	S	S	R	S	S	S
Ertapenem	S	S	S	S	S	S	S
Gentamicin	S	S	S	S	S	R	R
Meropenem	S	S	S	S	S	S	S
Co-trimoxazole	S	R	R	S	S	R	R
Pip/tazobactam	R	S	S	S	S	S	S
Amikacin	S	S	S	S	S	S	S
Amoxicillin	R	R					
Ampicillin	R	R	R	R	R	R	R
Aztreonam	R	S	S	I	S	S	S
Cefotaxime	R	S	S	R	S	S	S
Cefuroxime axetil	R	S	S	R	S	S	S
Cefepime	I	S	S	I	S	S	S
Cefoxitin	R						
Tigecycline	S	S	S	S	S	S	S
Trimethoprim	S						
Tobramycin	S	S	S	S	S	R	R
ESBL				P			

Table 14: The antibiotic resistance profile of each isolate, as determined by automatic antibiotic susceptibility testing (Vitek) and disk diffusion at the clinical laboratory. Red cells represent resistance, green cells sensitive and blue cells intermediate.

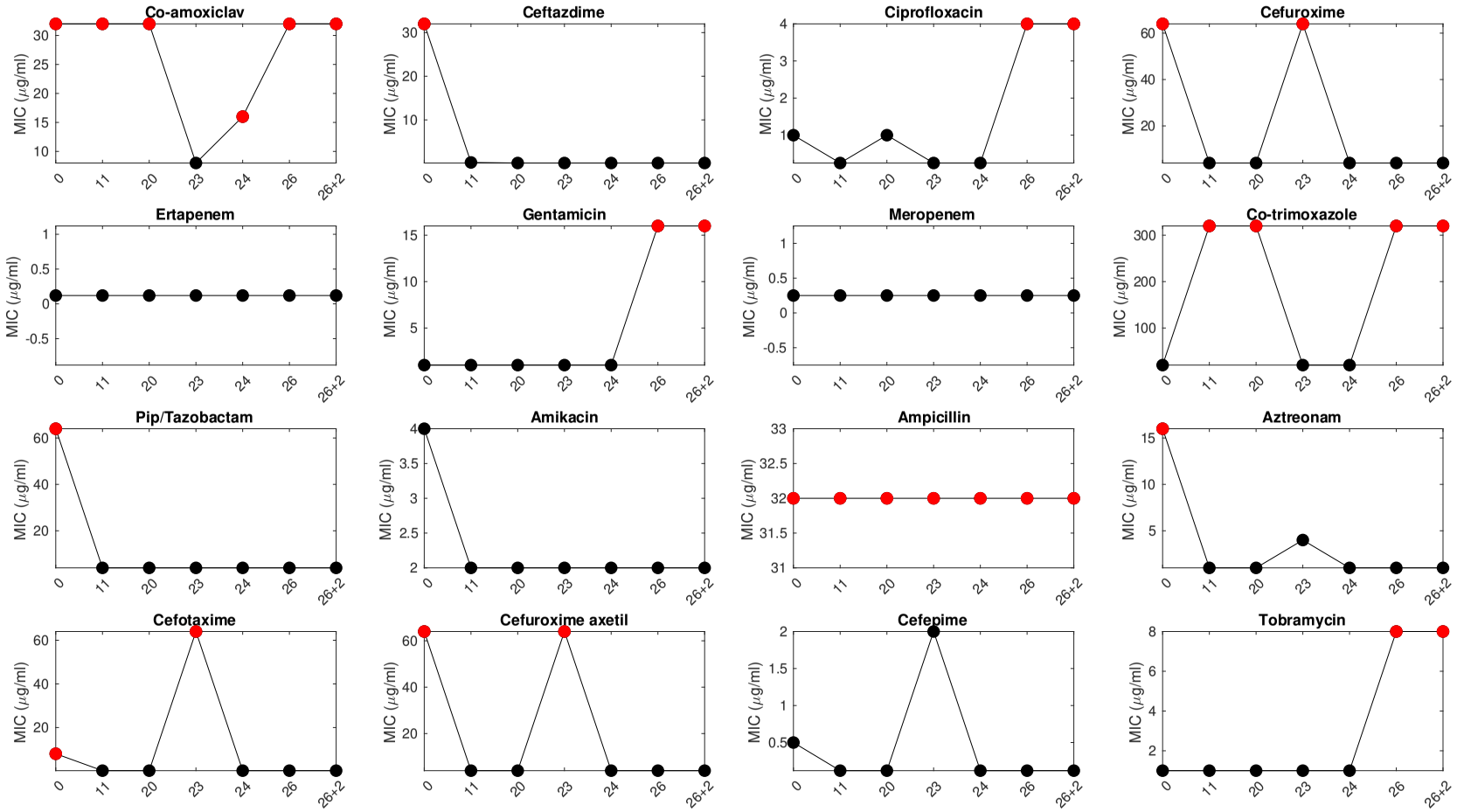

Figure 63: The minimal inhibitory concentrations of various antibiotics across all patient samples, obtained through clinical data. Red circles signify that the pathogen is 'clinically resistant' to that antibiotic at that concentration. Black circles signify that *E.coli* is 'clinically susceptible' to that antibiotic at that concentration.

6.4 Bacterial isolates characterisation

The isolates obtained at the following six time points were available for further characterisation: Day one, 11 months, 23 months, 24 months, 26 months and finally an isolate obtained at 26 months and 2 days that we hereafter refer to as 26 months(2). As the isolates were all obtained over the course of the same infection over a long time scale, we first sought to identify if these isolates are isogenic or if they are genetically diverse.

In order to measure variations in the growth between different isolates, they were initially grown in M9CAA for 24 hours, in the absence of any antibiotic. Figure 64a shows the raw growth curves obtained for all of these isolates and there are clear differences in the growth between the isolates obtained at different time points. The main source of variation is in the OD at stationary phase (K), which we quantify in figure 64b. We find the initial isolate from day one has significantly lower K than the isolates from other time points. Moreover, the isolates from months 23 and 24 have the greatest K. This would either suggest that the isolates have adapted to become more fit over the course of the infection, resulting in this increase in K relative to day one, or alternatively these isolates could be part of a polyclonal *E.coli* infection.

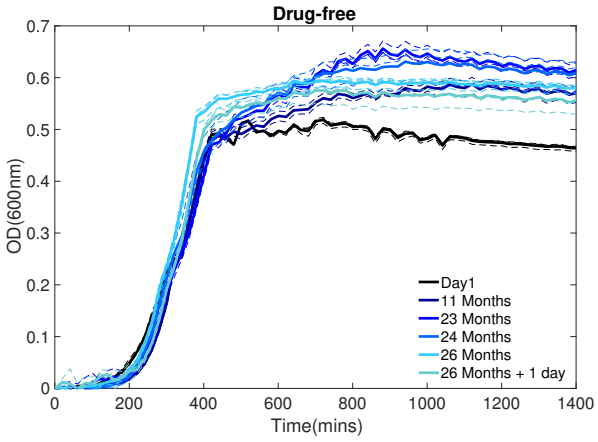

(a)

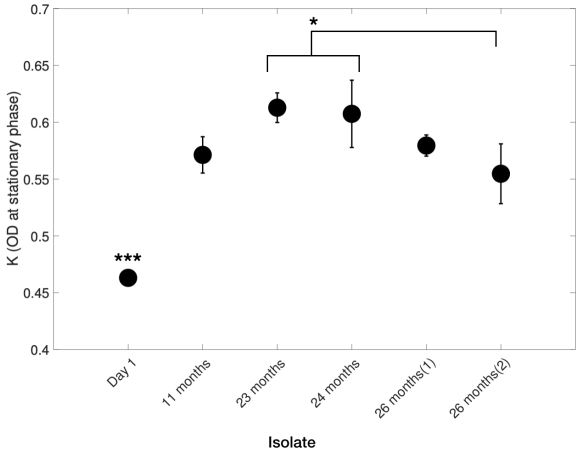

(b)

Figure 64: a) The growth profiles of the six *E.coli* isolates grown in the absence of antibiotics. Growth was measured as optical density (OD_{600nm}). b) We find that all isolates have significantly higher K than the initial isolate after 24 hours of growth. In addition, the isolates obtained after 23 and 24 months have significantly higher k than the isolate obtained at 26 months(2). (One way ANOVA with post hoc Tukey * = p <0.05, ** = p <0.01, *** = p <0.001) *n=3*

6.4.1 Phenotypic response to antibiotics : Antibiotics mechanism of action

Previous studies [225, 226], as well as work presented within this thesis (sections 5.4.2 and 5.4.3) indicate that the Vitek can be prone to misclassifying pathogens as resistant or susceptible to antibiotics. Consequently, the phenotypic response towards antibiotics was measured here in order to identify any discrepancies in the Vitek data. For this, we selected two antibiotics that had been repeatedly used in treatment, gentamicin and ciprofloxacin. Ciprofloxacin is generally considered to be a 'bactericidal antibiotic' and is part of the fluoroquinolone class of antibiotics. It kills bacteria through the inhibition of DNA topoisomerase and DNA gyrase, thereby preventing cell division [294]. Gentamicin's mechanism of action has been described in the previous chapter.

6.4.2 Phenotypic response to ciprofloxacin

The clinical data obtained from the Vitek (figure 14) indicated that the majority of isolates were susceptible, or had intermediate susceptibility towards ciprofloxacin. However, the final two isolates (26 months) were classified as resistant to ciprofloxacin at clinically relevant concentrations. We grew the six available *E.coli* isolates in two different concentrations of ciprofloxacin (0.1 and 4mg/l), and in drug-free media for 24 hours, measuring growth every 20 minutes as OD(600nm). We find that our data is largely in agreement with the results obtained from the Vitek, as shown in figure 65a. The final two isolates obtained 26 months into the infection were both able to grow in 4mg/l ciprofloxacin, and would therefore be classified as resistant. The isolates obtained on month 23 were not found to grow in any dose of ciprofloxacin, whilst the isolates from 11 and 24 months were able to grow up to 0.1mg/l. However, we do observe a small amount of growth in the 11 month isolate at the end of the measurement period in 4mg/l ciprofloxacin. It is possible that, had the measurement period been extended, this isolate would have been found to grow to a higher cell density in this dose. When the isolate was able to

grow in cipro, we found that increasing doses of ciprofloxacin generally result in an increase in lag time (figure 65b) and a decrease in growth rate (figure 65c). Overall, this data indicates that the Vitek was accurate in determining the AMR profile for ciprofloxacin. The raw growth data is displayed in supplementary figure S37.

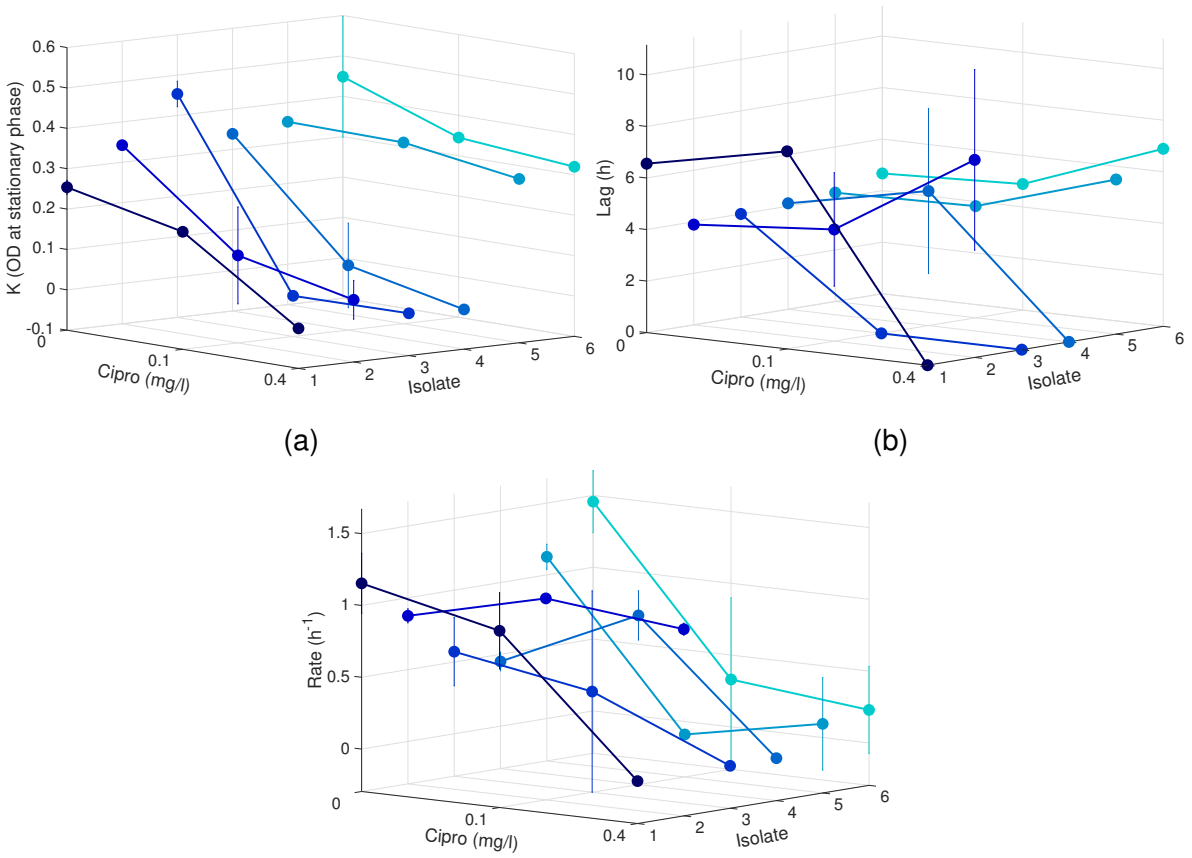

Figure 65: The a) K (population density at stationary phase) values, b) Lag time and c) Growth rate for each isolate in varying doses of ciprofloxacin. Isolates 1-6 refer to the isolates obtained on Day one, 11 months, 23 months, 24 months, 26 months(1) and 26 months(2) respectively. The final 2 isolates were able to grow in the highest dose of ciprofloxacin (4mg/l) whereas isolates 2-4 grow poorly in any dose of ciprofloxacin. Lag was found to increase with increasing dose of ciprofloxacin when that isolate is able to grow in cipro. It should be noted that isolate 2 (11 months) is able to grow in 4mg/l ciprofloxacin, but with a very long period of lag. Growth rate is found to increase with ciprofloxacin - this is particulary evident in the final two isolate that grew to large cell densities in 4mg/l cipro, but lower growth rates. *n=3*

6.4.3 Phenotypic response to gentamicin

The data from the Vitek indicated that all of the isolates were susceptible to gentamicin up until 26 months, at which point they are classified as resistant to gentamicin at clinically relevant concentrations. We grew the six available *E.coli* isolates in three different concentrations of gentamicin (1, 16 and 32mg/l), and in drug-free defined minimal media for 24 hours.

We find that the isolates obtained between day one and 24 months were only able to grow up to 1mg/l gentamicin, and would therefore be classified as clinically susceptible. However, the final two isolates from 26 months were both able to grow up to 32mg/l gentamicin, and would be classified as clinically resistant (fig 66a). This is in agreement with the data obtained from the Vitek.

A prolonged lag phase is measured in the presence of gentamicin in the isolates obtained at 11, 23 and 24 months. However, gentamicin was not found to result in an extended lag phase in the final two isolates, even in the highest concentration used (fig 66b). Likewise, no measurable difference is found in the growth rate between gentamicin doses in the final two isolates, whilst increasing concentration results in a lower growth rate in the isolates obtained between day one and 24 months (fig 66c). For the two antibiotics tested here, we find that the susceptibility data generated in this study is largely in agreement with that obtained from the Vitek. This is in contrast to the discrepancies identified between our own phenotypic data and that obtained by the Vitek in the previous chapter with *K.pneumonia*. The raw growth data is displayed in supplementary figure S38.

3149

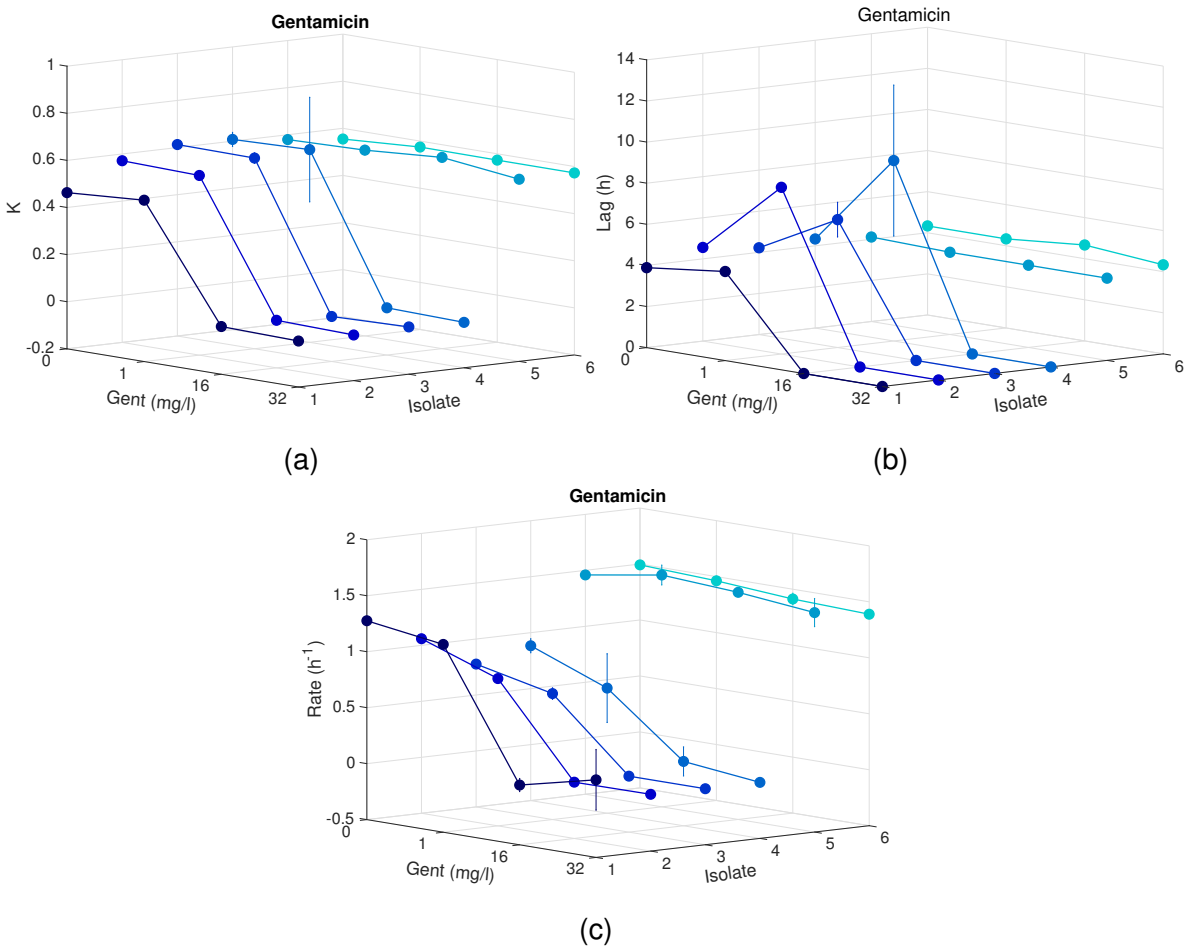

Figure 66: The a) K (population density at stationary phase), b) Lag time and c) Growth rate for each isolate in varying doses of gentamicin. Isolates 1-6 refer to the isolates obtained on Day one, 11 months, 23 months, 24 months, 26 months(1) and 26 months(2) respectively. *n=3*

6.5 Nanopore sequencing of the *E.coli* isolates

Next, whole genome sequencing was performed in order to elucidate the genomic basis for antibiotic resistance within these isolates, as well as identify their clonal type and any genetic modifications in either the chromosome or plasmids between isolates. Nanopore sequencing has successfully been utilised both on its own and in conjunction with short read sequencing to elucidate the genomes of clinical *E.coli* isolates. For example, nanopore sequencing was used to generate a complete genome assembly of *E.coli* isolates belonging to the common sequence type 131, a major intestinal pathogen that has disseminated worldwide [274]. A combination of Oxford Nanopore, PacBio and short read sequencing was used by Gonzalez-Escalona et al. to characterise shinga-toxin producing *E.coli* [229]. Furthermore, nanopore sequencing has been used to aid infection control during outbreaks of pathogenic *E.coli* in hospital settings, with the rapid sequencing provided by nanopore allowing for the real time tracking of pathogen spread [295].

In this case, an additional benefit of nanopore sequencing is the improved reconstruction of plasmid sequences, as plasmid sequences possess many repeat regions which are difficult to elucidate through short read sequencing alone. Clinical isolates of *E.coli* are often reported to possess key AMR and virulence genes on plasmids, and so accurate reconstruction of plasmid structure is key to fully understanding the *E.coli* resistome. Here, we sequenced four *E.coli* isolates obtained from a single patient over the course of 26 months on the Oxford Nanopore MinION platform. The resulting long reads allowed accurate reconstruction of plasmids and chromosomes, alongside elucidation of AMR and virulence genes.

6.5.1 Sequencing run

The Nanopore MinION platform was used to generate complete genomic sequences for the *E.coli* isolates obtained at the following points during the course of infection :

Day 1, 11 months, 23 months and 26 months (as shown in table 15). These isolates will herein be referred to as EC1, EC2, EC3 and EC4 respectively. The isolates were grown in M9CAA for 24 hours without the addition of any antibiotic.

DNA was then extracted using the Ambion GeneJET genomic DNA purification kit with an additional elution step. Three replicates were prepared for each of the four isolates, and each sample was barcoded using the Rapid Barcoding Kit (Oxford Nanopore), thus allowing all 12 samples to be multiplexed onto a single flow cell. The MinION library was prepared with a FLO-PRO002 flow cell and run for 36 hours using MinKNOW with high accuracy basecalling. The resulting FAST5 files were base called using Guppy v3.3.0, resulting in 8.17Gb of data, equating to a total of 1.24 million reads. The sequenced isolates are summarised in Table 15. Further information on the sequencing, such as the distribution of read length is displayed in supplementary figures S39-S41.

Isolate	Time point	Replicates	Average reads generated	Mapped reads	Error rate
EC1	Day 1	4	84676	98.28%	10.07%
EC2	11 Months	4	50836	97.85%	10.04%
EC3	23 Months	4	88920	97.28%	9.8%
EC4	26 Months	4	97508	99.31%	9.85%

Table 15: The *E.coli* isolates sequenced.

6.6 Serotypes

Serotyping is a method of *E.coli* classification essential for the surveillance of infectious disease. Currently, over 160 different serological types of *E.coli* have been identified, and these are based on the lipopolysaccharide (O antigen) and H-flagellar antigens. Traditional methods for identifying these antigens are incredibly time consuming, whereas WGS allows us to rapidly determine the serotype of *E.coli* strains by comparing against databases of known O and H-antigen genes. For

the purpose of this study, SeroType finder was used for serotyping [296] with the standard threshold of 85% ID and minimum length of 60%. This tool performs a BLAST search of serotype database genes against the provided genome assembly and outputs predicted O and H types. All of the isolates were found to be different serotypes - isolate EC1 was H17:08, EC2 was H23, EC3 was H42:O83 and EC4 was H25:O84. This suggests that either the patient has a polyclonal infection, or that different clonal types of *E.coli* have been acquired over time. However, to establish this whole population samples would need to be collected, but as this was a retrospective study this was not possible.

6.7 Multi-locus sequence type

To further investigate the relatedness of these clinical isolates, the core MLST profile for each isolate was determined from the nanopore sequence data using the web based platform MLST [297] and the seven marker gene set : *adk, fumC, gyrB, icd, mdh, purA and recA*.

The majority of serious, multi-drug-resistant ExPEC *E.coli* are sequence type 131 (ST131) [298], however we did not find this ST among the isolates sequenced. All six isolates were found to belong to different ST's - EC1 matched closely to ST88, EC2 to ST2792, EC3 to ST1485 and finally EC4 to ST57.

E.coli ST88 has previously been associated with ESBL-producing *E.coli* [299] and it is reported to be globally distributed within both humans and animals [300, 301]. Recently, *E.coli* ST1485 has been associated with multi-drug resistant infections in animals [302]. *E.coli* ST2792 was first identified in 2013 within broilers in southern Japan, however it was not found to be ESBL-producing [303]. Finally, *E.coli* ST57 has been isolated from both animals and humans and is reported to be ESBL-producing [304].

Given that each isolate matches to both a different serotype and different ST, we can

state with relative certainty that these isolates are different clonal types of *E.coli*. A limitation of this study, as with the *K.pneumonia* isolates in the previous chapter is that only a small subset of the microbial population has been characterised and sequenced, limiting our understanding of the microbial community as a whole. Furthermore, some caution has to be taken as MLST determination is reliant on the detection of single nucleotide changes in these housekeeping genes and this could be impacted by the relatively high error rate associated with nanopore sequencing.

6.8 Chromosome and plasmid elucidation

The genomes were assembled using the de novo assembler Flye (V2.8.3) [234], resulting in whole chromosome and plasmid contigs. These contigs were then identified as either chromosomal or plasmid through the use of 'mlplasmids' [235]. Whilst the chromosomes and plasmids of isolates EC2 and EC3 assembled into single contigs, isolate EC1 possessed an additional chromosomal contig (48,070bp) and isolate EC4 possessed two additional small chromosomal contigs (2,864bp and 2,857bp).

Next, BLAST analysis was carried out to reveal if the plasmids identified in these isolates closely matched any previously reported:

- Plasmid pEC1 was found to match closely to the *E.coli* O1:H42 strain CLSC36 plasmid pcys-1 (Accession number : CP041299.1, >99% identity). Similarly to pEC1, this plasmid was also found to harbour the *ompT* virulence gene.
- pEC2 matched closely to *E.coli* strain EC008 plasmid pEC008 (Accession number KY748190.1, >99% identity).
- The first plasmid of isolate EC3, pEC3-1, closely matched to *E.coli* strain EC28 plasmid P2 (Accession number CP049102.1, >99% identity), a plasmid found in a uropathogenic ,ESBL-producing strain of *E.coli*.

- pEC3-2 matched closest to *E.coli* plasmid PC59-112 (Accession number : KJ484637.1, >99% identity).
- The final plasmid of isolate EC3 (pEC3-3) had closest identity to *E.coli* strain SMS-3-5 plasmid PSM35-8 (Accession number : CP0009721.1, >99% identity).
- The final isolate possessed two plasmids. The first plasmid, pEC4-1 had closest identity to *E.coli* strain RHBSTW-00152 plasmid pRHBSTW-00152-3 (Accession number CP056812.1, >99% identity).
- The final plasmid (pEC4-2) matched with *E.coli* plasmid pCOV33 (Accession number : MG649046.1, >99% identity).

Using the PlasmidFinder web server [236], the replicon type of each plasmid was identified, and these are displayed in table 17. The only plasmid found to be common to 3/4 isolates (EC2,EC3 and EC4) was the IncI1-I(Gamma) replicon plasmid, ranging from 121-37 kb and reported to be widespread in both humans and animals [305]. This could suggest that a IncI1-I(Gamma) backbone plasmid is in circulation within this infection site. All of the remaining plasmids identified in the isolates were unique to each isolate - EC1 was found to harbour a single plasmid type with a IncFIB(AP001918)-IncFII(pSE11) replicon, and IncFIB(AP001918) plasmids have been reported in a wide range of pathogenic *E.coli* carrying a diverse set of AMR and virulence genes [306, 307, 269]. EC3 possessed a IncFIA-IncFIB multi-replicon plasmid and a p0111 plasmid (first identified in an enterohemorrhagic strain of *E.coli* in 2009 [308], and since identified across multiple different multi drug resistant strains of bacteria [309, 310]). Finally, EC4 was found to have a large psL483 replicon plasmid. A summary of the chromosome and plasmid lengths, as well as the replicon types is shown in table 16.

The diversity of plasmids identified between isolates supports our hypothesis that these are indeed different clonal types of *E.coli* that have either been acquired over

time, or form part of a polyclonal infection.

Isolate	Identity	Length (bp)
EC1	Chromosome	4,957,273
	pEC1-1 : IncFIB-IncFII	145,898
EC2	Chromosome	5,351,716
	pEC2-1 : IncI1-I(Gamma)	121,012
EC3	Chromosome	5,148,955
	pEC3-1 : IncFIA-IncFIB	167,831
	pEC3-2 : IncI1-I(Gamma)	110,452
	pEC3-4 : p0111	94,641
EC4	Chromosome	5,178,012
	pEC4-1 : IncI1-I(Gamma)	37,823
	pEC4-2 : psL483	107,188

Table 16: A summary of the plasmid and chromosome lengths for each isolate (EC1-EC4).

6.9 Genome content

Next, we examined the content of the *E.coli* genomes with the use of qualimap (v2.2.1) [240]. The genome of isolate EC1 was found to have 8,420 CDS, 92 tRNA's, 22 rRNA's and 2 CRISPRs. Isolate EC2 had 8,532 CDS, 83 tRNAs, 22 rRNAs and 2 CRISPRs. Next, isolate EC3 was found to possess 8,959 CDS, 92 tRNAs, 22 rRNAs and 1 CRISPR. Finally, isolate EC4 had 7,958 CDS, 87 tRNAs, 22 rRNAs and 2 CRISPRs.

6.10 Antimicrobial resistance

The clinical data indicates a diverse AMR profile between these different isolates, with fluctuating susceptibility towards different antibiotics over time. Given the serotype and MLST data, it is likely that these fluctuating AMR profiles are as a result of different clonal types of *E.coli* being sampled, rather than a single clonal type adapting to antibiotic treatment over the course of treatment.

To identify the genomic basis for this resistance, we used ResFinder [243] against the assembled genomes. A summary of the antibiotic resistance genes detected at each time point is presented in figure 67 and the locations of the AMR genes (e.g. whether they are found on the chromosome or a plasmid) is displayed in table 17. From this genomic data we can attempt to predict the phenotypic response towards antibiotics of different classes, as shown in tables S8-S11. However, it should be noted that the presence of an AMR gene does not always result in detectable levels of phenotypic response in clinically relevant concentrations of drug.

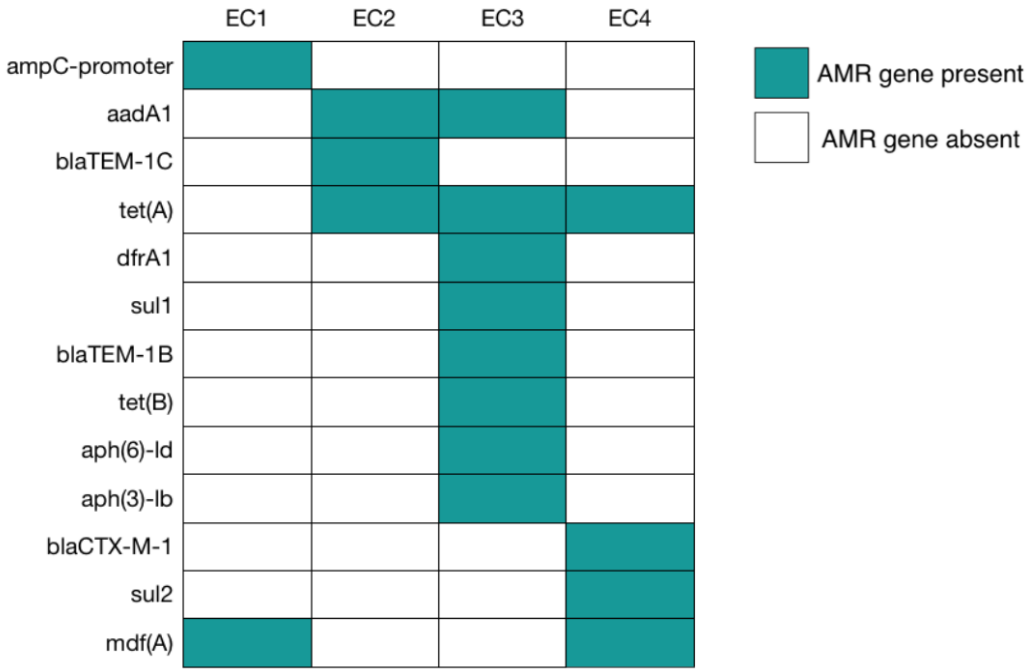

Figure 67: A summary of the presence and absence of various antibiotic resistance genes and mutations over the four sequenced isolates. Green represents genes that are present and white represents the absence of the gene or mutation.

Isolate	Serotype	MLST	Length (bp)	ID	AMR genes	Virluence genes
EC1	H17:O8	ST88	4,957,273	Chromosome	*mdf(A)*, *ampC*-promoter (g.-42C>T)	*focC, fyuA , gad, hra, iha , irp2 lpfA, mchB, mchC, papC, sfaD terC*
			145,898	pEC1-1 IncFIB(AP001918)-IncFII(pSE11)		*cvaC, hlyF, iroN, iss, iucC, iutA mchF, ompT, sitA, traT*
EC2	H23	ST2792	5,351,716	Chromosome		*air, astA, chuA, eilA, gad, hra, iss lpfA, ompT, terC, traT*
			121,012	pEC2-1 IncI1-I(Gamma)	*aadA1, dfrA1, sul1, tet(A), blaTEM-1C*	
EC3	H42:O83	ST1485	5,148,955	Chromosome	*sul2, tet(B)*	*air, chuA, eilA, gad, hra, iha, ireA iucC, iutA, kpsE, kpsMII_K5, lpfA mchF, mcmA, ompT, papA_F20 papC, sitA, terC, yfcV*
			167,831	pEC3-1 IncFIA - IncFIB(AP001918)	*aph(3')-Ib, aph(6')-Id, sul2 tet(A), blaTEM-1B*	*cvaC, etsC, hlyF, iroN, iss, iucC iutA, mchF, ompT, sitA, traT, tsh*
			110,452	pEC3-2 IncI1-I(Gamma)	*aadA1, sul2, dfrA1, blaTEM-1B*	*cib*
			94,641	pEC3-3 p0111		
EC4	H25:O84	ST57	5,178,012	Chromosome	*mdf(A)*	*chuA, fyuA, gad, hra, irp2, iss mchB, mchC, mchF, ompT, sitA terC*
			37,823	pEC4-1 IncI1-I(Gamma)		
			107,188	pEC4-1 psL483	*sul2, blaCTX-M-1, tet(A)*	*cib*

Table 17: The AMR and virulence genes identified within each of the sequenced isolates.

The *E.coli* isolates were found to have diverse resistomes, with different AMR genes present in both the chromosome and plasmids. None of the AMR genes were found to be shared between all four isolates, and this fits in with the evidence suggesting that there isolates are different clonal types. In the initial isolate (EC1), only one gene conferring antibiotic resistance was identified - *mdf(A)* encoding the membrane protein MdfA which confers resistance to a range of toxic compounds, including antibiotics [311]. The *mdf(A)* gene was also identified on the later isolate EC4. In addition to this AMR gene, EC1 was found to have a mutation in the *ampC* promoter that is reported to result in elevated resistance to multiple β-lactam antibiotics such as piperacillin and amoxicillin, as well as β-lactam-β-lactamase inhibitor combinations like co-amoxiclav [312, 313]. The mutations detected in this gene could therefore explain the extensive resistance towards β-lactam antibiotics and β-lactam-β-lactamase inhibitor combinations in this isolate, as shown in figure 67. Furthermore, AmpC enzymes are known to hydrolyse cephalosporins [313, 314] and this could contribute towards resistance to cephalosporin antibiotics found within the clinical data (figure 67).

Isolate EC2 was found to possess the plasmid-encoded AMR genes *aadA1*, *tet(A)* and $\text{bla}_{\text{TEM-1C}}$. The gene *aadA1* is known to confer resistance to the certain amino-glycoside antibiotics, but not the ones tested by the Vitek (gentamicin, amikacin and tobramycin), and so the phenotypic outcome of this gene is uncertain. The *tet(A)* and $\text{bla}_{\text{TEM-1C}}$ genes confer resistance to beta-lactam antibiotics, indeed we find that this isolate is classified as clinically resistant towards the β-lactam antibiotics amoxicillin and ampicillin (figure 67). Isolate EC3 harboured a wide range of both chromosomal and plasmid encoded antibiotic resistance genes - *aadA1, tet(A), tet(B), dfrA1, sul1*, $\text{bla}_{\text{TEM-1B}}$, *aph(3')-Ib* and *aph(6')-Ib*, associated with resistance towards beta-lactams, sulfonamides, aminoglycosides and trimetho-prim. This isolate was classified as ESBL positive and also resistant towards two cephalosporin antibiotics (cefpodoxime and cefuroxime), however it was susceptible to sulfonamides and aminoglycosides. This further demonstrates the disconnect

that can be present between the detection of AMR genes and actual phenotypic resistance.

The final isolate, EC4, was found to posses three AMR genes on its largest plasmid (pEC4-2) - *tet(A), sul2* and $bla_{CTX\text{-}M\text{-}1}$. From the clinical data, the final isolate was predicted to be resistant towards the aminoglycoside antibiotics gentamicin and tobramycin. Although the AMR genes detected do not confer resistance towards aminoglycosides, this isolate was also found to harbour the gene *mdfA* that has been associated with resistance towards aminoglycosides [311]. The presence of this *mdfA* gene could also explain the resistance towards ciprofloxacin identified by the Vitek. However, further investigation would be needed to confirm this hypothesis, such as the removal of the *mdfA* gene followed by repeated antibiotic susceptibility tests. This was the only sequenced isolate found to possess $bla_{CTX\text{-}M\text{-}1}$, an ESBL gene mediating resistance towards a range of β-lactam antibiotics, including extended-spectrum cephalosporins such as cefepime. Finally, *sul2* is know to confer resistance towards sulphonamide antibiotics [315], and indeed the isolate was reported as being resistant towards co-trimoxazole.

In summary, the isolates were found to have diverse resistomes, with AMR genes harboured both on the chromosome and within plasmids. The variation in AMR genes between the isolates fits in with data suggesting that these are different clonal types, and the fluctuating AMR profiles measured in the Vitek. Moreover, the genetic determinants for resistance were identified in some isolates, but the genomic data failed to explain the phenotypic response in some cases. For example, *sul1* was not found to result in phenotypic resistance towards sulfonamides in EC3. Predicting the AMR phenotype from genomic data is challenging for many reasons, for example an AMR gene may not be expressed, or a mutation never previously associated with AMR could be conferring the phenotype [270]. WGS is a promising tool for assessing the AMR profiles of clinical pathogens, however caution must be taken when drawing conclusions about the phenotypic response to antibiotics.

6.11 Virulence

Virulence factors are key to the success of pathogenic ExPEC *E.coli* as they allow effective colonisation of extraintestinal tissues within the host. Furthermore, these virulence factors are often found on mobile genetic elements, such as plasmids, allowing effective transmission [316]. There are five main groups of virulence factors expressed by pathogenic *E.coli* and these are adhesins, toxins, iron acquisition factors, lipopolysaccharides and invasins. Moreover, these can either be located on the bacterial cell surface, or excreted into the external environment [273].

In order to elucidate the virulence factors present in the *E.coli* isolates, the online database 'VirulenceFinder' [259] was used. This tool compares the assembled genomes against known virulence factors to identify those present in the *E.coli* isolates. A variety of virulence factors were identified, as shown in table 17 and summarised in table 18 alongside their functions.

Multiple virulence factors were found to be common to all isolates (*gad, hra, lpfA, terC, iss* and *ompT*), however many others were not. Bacterial virulence factors are essential to many aspects of infection, from protection against the human immune system to adhering to surfaces within the body. For example, serum resistance proteins are key to the survival of *E.coli* in the bloodstream, allowing dissemination throughout the body [317]. Indeed, all of these isolates harbour virulence genes involved in serum survival, such as *iss*. The acquisition of iron is another key requirement for ExPEC *E.coli*, allowing the uptake of iron from the bloodstream. All isolates were found to carry siderophore genes involved in iron uptake, with some carrying multiple genes (e.g. *sitA, fyuA, iroN, irp2* and *ireA*.)

Virulence genes are not routinely detected in clinical pathogens, and yet they can inform us on the presence of different clonal groups and aid our understanding of disease severity. By increasing our understanding on the association between infection severity and patterns of virulence factors, we can explore the effect that they have on patient outcome alongside other host determinants [318, 319].

Gene	Function	EC1	EC2	EC3	EC4
gad	Acid resistance	■	■	■	■
hra	Heat resistance	■	■	■	■
lpfA	Fimbrial protein	■	■	■	■
terC	Tellurite resistance	■	■	■	■
iss	Serum survival	■	■	■	■
ompT	Outer membrane protease	■	■	■	■
mchF	Microcin transporter protein	■		■	■
traT	Serum resistance	■	■	■	
sitA	Siderophore production	■		■	■
chuA	Outer membrane hemin receptor		■	■	■
fyuA	Siderophore receptor	■			■
iha	Adhesin	■		■	
irp2	Yersiniobactin	■			■
mchB	Microcin H47 precursor	■			■
mchC	MccH47 system	■			■
papC	P fimbriae	■		■	
cvaC	Colicin V precursor	■		■	
hlyF	Hemolysin F	■		■	
iroN	Enterobactin siderophore receptor	■		■	
iucC	Aerobactin synthase	■		■	
iutA	Ferric aerobactin receptor	■		■	
air	Enteroaggregative immunoglobulin repeat protein		■	■	
eilA	Enteroaggregative protein		■	■	
cib	Colicin ib production			■	■
focC	F1C fimbriae biogenesis	■			
sfaD	F1C fimbriae biogenesis	■			
astA	Enteroaggregative E.coli heat-stable enterotoxin (EAST1)		■		
ireA	Siderophore receptor			■	
KpsE	Capsule polysaccharide export protein			■	
KPsII-k5	Polysialic acid transport protein			■	
mcmA	Microcin M			■	
ycfV	Fimbrial protein			■	
etsC	Putative type I secretion outer membrane protein			■	
tsh	Temp-senstive hemagglutinin			■	

■ **Gene present**

□ **Gene absent**

Table 18: A summary of the presence and absence of various virluence genes in all four sequenced isolates. Green represents genes that are present and white represents the absence of the gene.

6.12 Chromosome and plasmid structure

In order to elucidate any structural variations in the genome, we first examined the read depth across all chromosomes and plasmids. The coverage for each isolate, normalised to mean coverage, is shown in figures 69-72. Although for the majority of isolates the read depth is fairly evenly distributed across the genome, we do find areas with large variations in read depth.

In partcular, plasmid pEC2-1 has areas with substantially higher read coverage than the rest of the genome, as shown in figure 70 and this is suggestive of an amplification. However, when we examine the genes present in these regions, we find that the majority of genes are hypothetical and it is therefore difficult to hypothesise a reason for this increase in read depth. The high coverage region ranging 57,804-60,524bp on this plasmid was found to harbour the *pilV* gene that is reported to play a role in the transmissibility and survival of *Enterobacteriaceae* [54].

6.13 Summary

In this chapter, the assembled genomes of four *E.coli* isolates acquired from a single patient diagnosed with chronic cholangitis over the course of 26 months have been presented, and the key genotypic and phenotypic features of all four sequenced *E.coli* isolates are presented in figure 68. The AMR profile varied substantially between the isolates, with the initial isolate classified as resistant towards the most antibiotics (x11), from a wide range of classes. All future isolates were resistant toward ampicillin, however resistance towards other antibiotics fluctuated with time. For example, only the final sequence isolate EC4 was found to be resistant towards gentamicin, ciprofloxacin and tobramycin. Given that ciprofloxacin and gentamicin were used frequently in treatment, it is perhaps not surprising that resistance towards these antibiotics was detected in the final isolate.

Through nanopore sequencing, all of the isolates were identified as different clonal

groups and the resistomes were elucidated. The AMR genes identified included key ESBL genes such as CTX-M-1 and TEM-1C that not only pose a challenge to successful treatment, but are also difficult to deduce from phenotypic data. Despite the genomic differences between isolates, similarities were found, for example all were found to harbour genes conferring resistant towards β-lactam antibiotics. Furthermore, all isolates possessed an IncI1-I replicon plasmid, although the plasmid size and gene content varied.

WGS is a promising tool to diagnose clinical antimicrobial resistance, and so the AMR profiles generated by the Vitek and nanopore sequencing were compared here. In contrast to the previous chapter, the phenotypic data generated by the Vitek was found to be an accurate assessment of the susceptibility towards two different antibiotics that were used frequently in treatment, as well as aligning relatively well with the AMR genes detected through sequencing.

One of the initial aims of this work was to identify structural variants present in the genomes of clinical pathogens. Despite two amplifications being identified on plasmid pEC2-1, they were largely found to span hypothetical genes and thus any phenotypic outcome is hard to predict. Nevertheless, it is possible that the subculturing steps used here have resulted in the loss of larger genomic modifications and future work could involve sequencing samples obtained directly from a patient without the use of culturing. Indeed, nanopore sequencing has been been used successfully by others to sequence metagenomic samples directly from patients [269, 320].

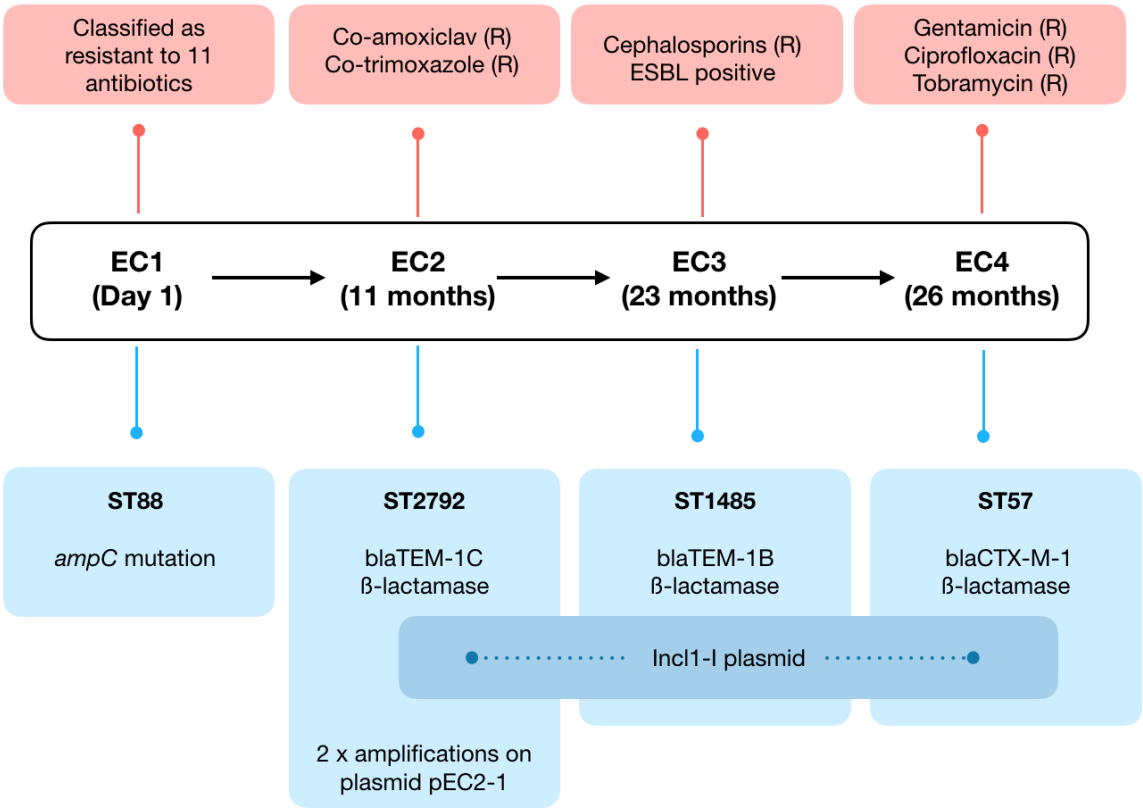

Figure 68: A summary of the key phenotypic and genotypic features of the four sequenced *E.coli* isolates. The key ESBL's identified in each isolate are displayed. Note that the phenotypic changes refer to those identified in the data obtained from the Vitek 2. R = resistant, S = susceptible, ST = sequence type.

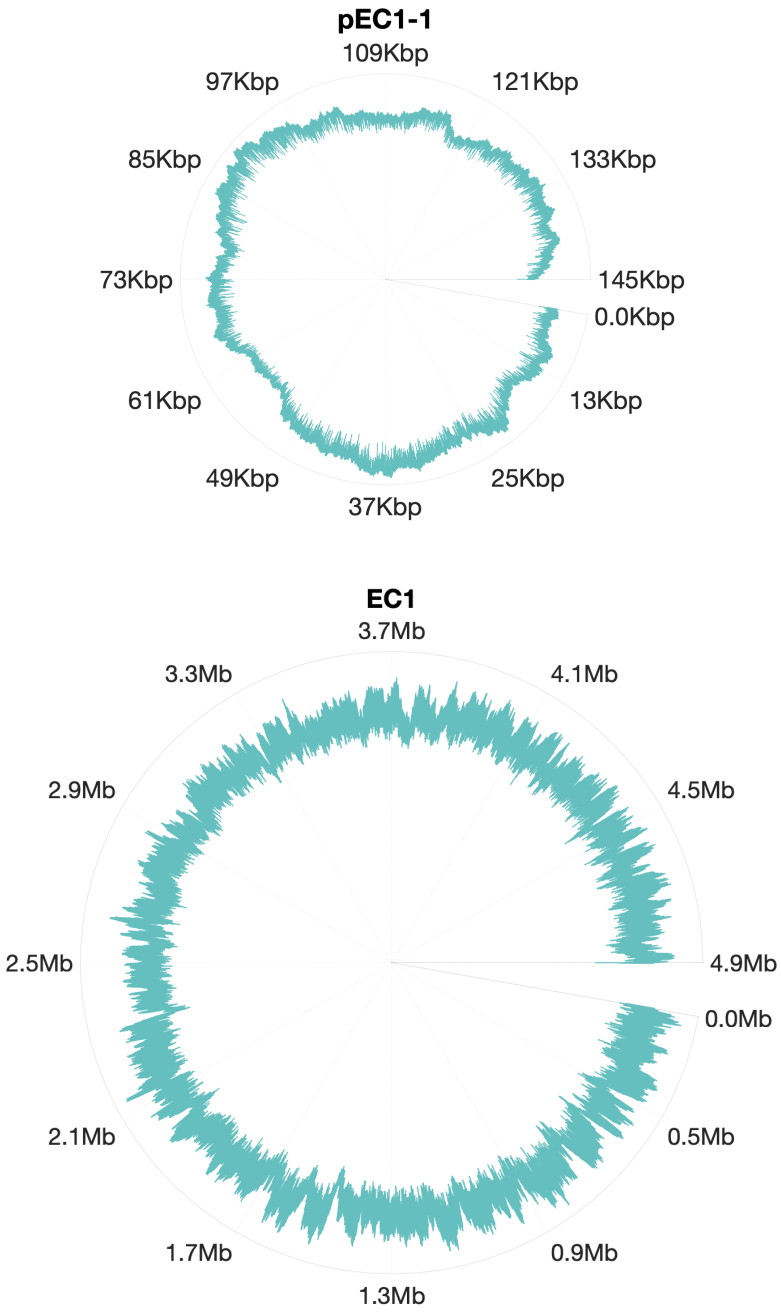

Figure 69: The genome coverage of isolate EC1 (Day one). The whole 4.9Mb chromosome was assembled into a single contig with mean coverage of 98.5, and one plasmid assembled as a seperate contig (145Kbp) with a mean coverage of 40.7.

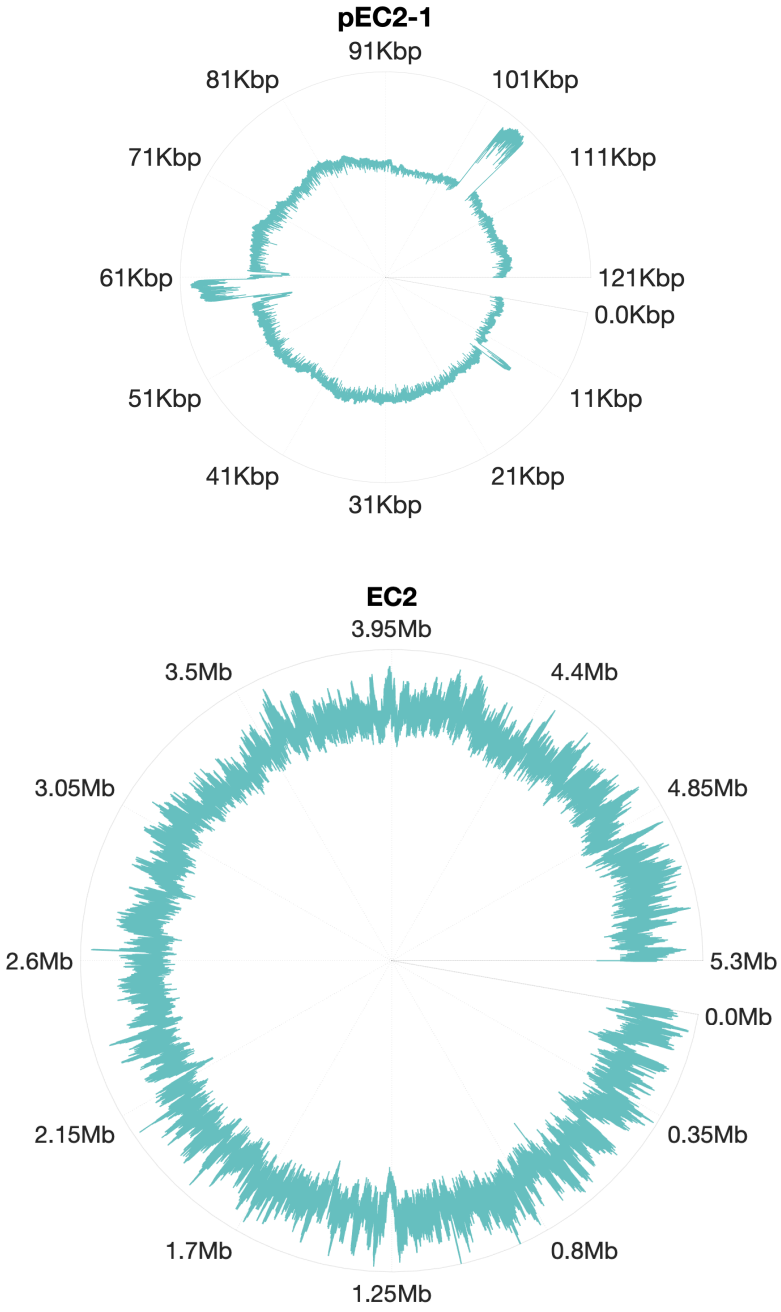

Figure 70: The genome coverage of isolate EC2 (11 months). The whole 5.3Mb chromosome was assembled into a single contig with a mean coverage of 46.1, and one plasmid assembled as a seperate contig (121Kbp) with a mean coverage of 33.2.

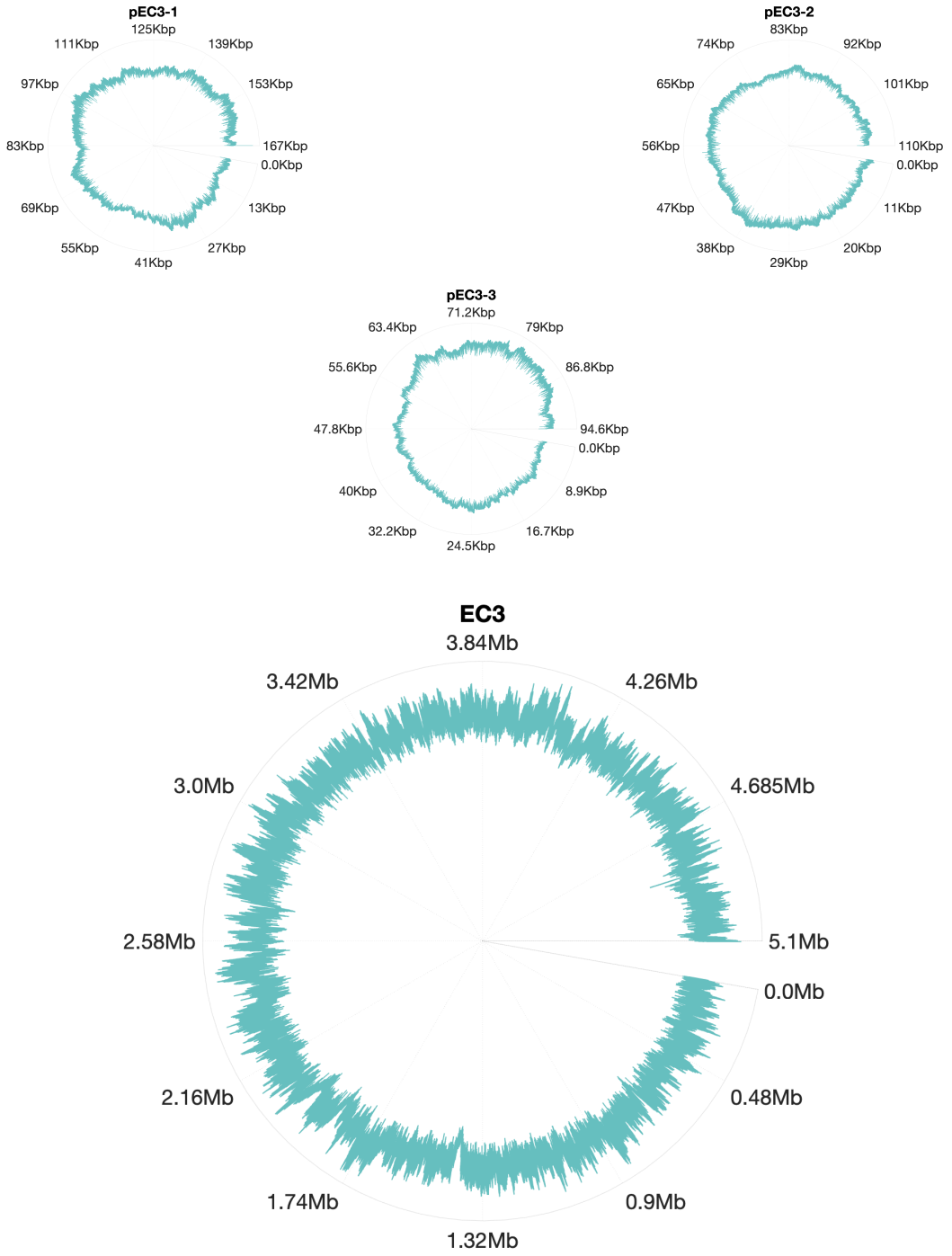

Figure 71: The genome coverage of isolate EC3 (23 months). The whole 5.1Mb chromosome was assembled into a single contig with a mean coverage of 75.7. Three plasmids assembled as seperate contigs. Plasmid one was 167Kbp in length with a mean coverage of 25.7, plasmid two was 110Kbp with a mean coverage of 38.1 and finally plasmid three was 94Kbp in length with a mean coverage of 19.

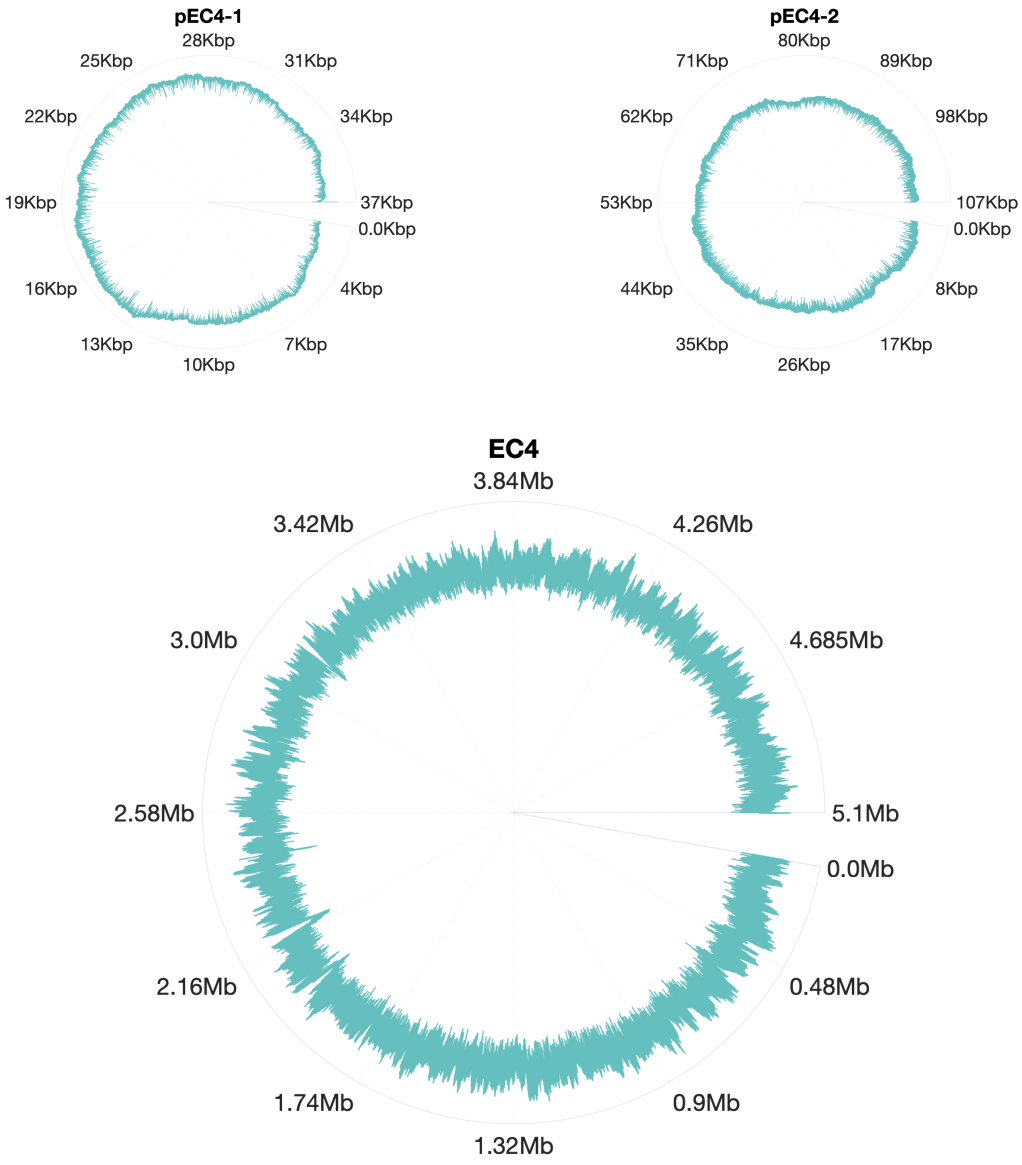

Figure 72: The genome coverage of isolate EC4 (26 months).The whole 5.1Mb chromosome was assembled into a single contig with a mean coverage of 105.6 Two plasmids assembled as seperate contigs. Plasmid one was 38Kbp with a mean coverage of 62.5 and plasmid two was 107Kbp in length with mean coverage of 89.9.

CHAPTER SEVEN - CONCLUSIONS

7.1 Ribosome-binding antibiotics can result in improved growth and long-term viability in *E.coli*

Antibiotics have been pivotal in our fight against microbial infections, and are generally considered to be molecules that have substantial negative impacts on the bacteria that they target. However, this work demonstrates quite the opposite, antibiotics can in fact provide microbial benefits. The efficacy of bacteriostatic antibiotics is often based on the extent of inhibition in the early stages of microbial growth [16, 87], and yet until now the outcome on microbial growth and survival over long time periods has been unknown. Through the long-term culturing of *E.coli* populations exposed to antibiotics from various different classes, we have demonstrated that exposure to ribosome-binding antibiotics such as doxycycline and erythromycin does indeed impede initial growth, but eventually results in growth stimulation and improvements to long-term viability during nutrient starvation, delaying population collapse. Moreover, resistance towards doxycycline through a ribosome-protection mechanism eradicates these benefits, indicating that antibiotic-ribosome binding is indeed key to the these improvements in growth.

Whilst drug-free populations experienced exponential death as nutrients are exhausted, those treated with ribosome-binding drugs go through multiple stages of death and growth resurgence (figure 12). We offer an explanation for this phenotype by demonstrating that doxycycline improves the ability of *E.coli* to scavenge carbon from the debris of lysed cells (figure 18).

In order to explore the influence of doxycycline on *E.coli* metabolic pathways, a GFP promoter library was utilised, with GFP expression used as a proxy for promoter expression. Doxycycline was indeed found to induce differential expression of

genes involved in central carbon metabolism over a 72 hour period, as well as genes involved in glucose transport. These findings are summarised in figure 73, showing the up-regulation of genes involved in both the TCA cycle and glyoxylate cycle. This up-regulation of the glyoxylate cycle could provide an explanation for the doxycycline-induced improvements to growth in spent supernantant as well as improvements to long-term viability, as the glyoxylate cycle allows the cell to utilise alternative carbon sources such as acetate and fatty acids. This could be further investigated by measuring the expression of glyoxylate cycle genes during growth on spent supernatant in the presence and absence of doxycycline.

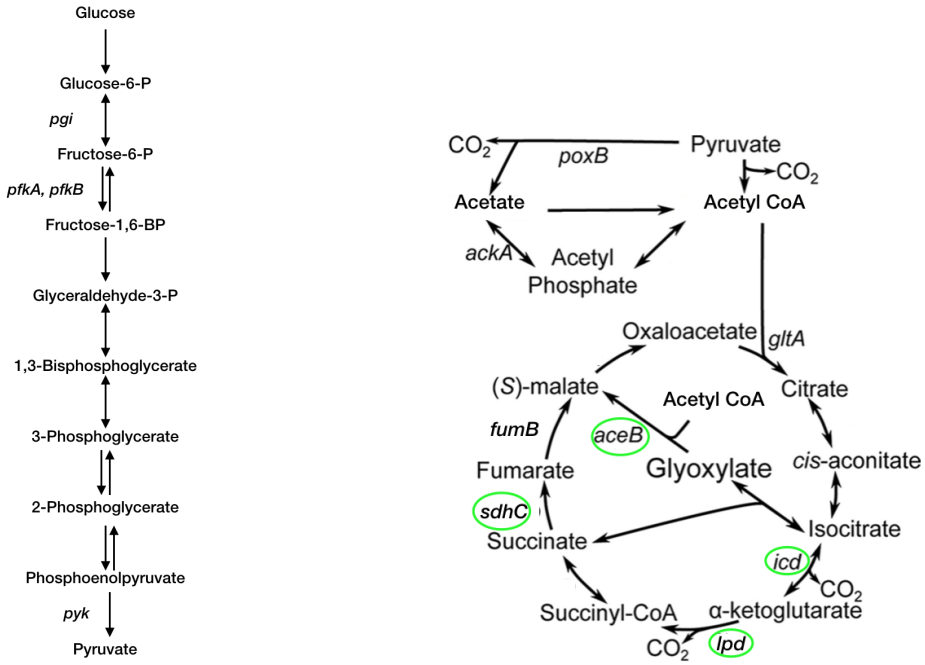

(a) (b)

Figure 73: A summary of the significant changes in maximal expression of the GFP-tagged promoters involved in a) glycolysis and b) the TCA cycle. Only the genes studied are displayed here. The genes circled in green had higher maximal expression in 0.4mg/l doxycycline when compared to a drug-free control. Genes that are not circled did not experience a substantial change in promoter expression in 0.4mg/l doxycycline. The schematic of the TCA cycle shown in (b) was adapted from reference [321].

This data raises the question, if an antibiotic initially reduces microbial growth but simultaneously improves long-term viability, can it still be considered an antimicrobial? It is possible that the phenotypes found here also arise within the human body during treatment, however future work would be needed to confirm this, such as repeating these experiments using clinical bacterial isolates. If ribosome-binding antibiotics do inadvertently benefit bacterial growth during treatment, this could have detrimental effects on patient outcome.

The data presented here also allows us to question the natural role of antibiotic production in the environment. Traditionally, antibiotics were thought to be produced exclusively as 'war-fare' molecules, with the sole function of inhibiting the growth of competitors [322, 323]. However, alternative theories suggest that they may play a more passive role as signalling molecules [13]. It is possible that antibiotics could be produced as a type of 'public good' to prolong the life of kin in the surrounding environment, however this was outside of the scope of this study. Additionally, studies have sought to understand how antibiotic-resistant and antibiotic-susceptible bacteria co-exist [324, 325], and the data presented here could provide one mechanism by which this occurs - although antibiotic resistance is beneficial during exponential growth, it can be detrimental to long term-viability. Conversely, susceptibility towards certain antibiotics is beneficial during nutrient starvation and this could result in coexistence.

Future work could seek to explore the impact that doxycycline exposure at various stages of starvation has on the long-term viability of bacterial populations. If this phenotype is indeed mediated by alterations to metabolism in the early stages of growth, then the addition of doxycycline at later time points may fail to confer any benefit to growth or long-term viability. In addition, a limitation of this work was the number of antibiotics used to investigate this phenotype. Future work could therefore seek to identify this phenotype in a broader range of antibiotics from a range of classes to further verify if it is indeed unique to ribosome-binding antibiotics.

7.2 Optimising ribosome production capacity for starvation survival

Thus far we have only observed benefits to growth and viability in antibiotics that target the ribosome and we therefore hypothesised that a reduction in the number of functional ribosomes would also result in this benefit. To this end, in chapter three we explored the relationship between *rrn* operon copy number and long-term viability. Indeed, we found that population density increased with a reduction in *rrn* copy number, mirroring that seen with doxycycline. Moreover, we identified that an intermediate number of *rrn* operons optimised the bacterial population for survival in nutrient-depleted conditions. This not only supports our previous hypothesis, but also provides information on the fundamental role of ribosome functioning during starvation.

7.3 Doxycycline induces a diverse phenotypic response in single gene knockout strains

We next sought to further our understanding on the mechanistic basis of doxycycline-induced benefits to growth, and indeed the general phenotypic response to doxycycline through the use of a reverse genetics approach. For this, we utilised the keio collection, a library of *E.coli* strains in which single non-essential genes have been knocked out. Through clustering these strains based on their growth dynamics in doxycycline over 48 hours, we were able to identify those strains that lost the doxycycline-induced benefits to K and the functional groups enriched in these clusters. Furthermore, we identified a number of unusual phenotypes, such as strains which experience benefits to both lag and K, and strains which were only found to grow in media containing doxycycline. Interestingly, amongst the strains only found to grow in doxycycline were knockouts for genes involved in the oxidative

stress response (e.g. *soxS*, *sodB* and *perR*), and given that tetracycline antibiotics are known to have an antioxidant effect [29, 30] this is an intriguing finding. It is possible that by acting as an antioxidant, doxycycline alleviates the lethal impact of having these genes removed, thereby allowing growth to occur. Indeed, this antioxidant effect could play a role in the improved long-term viability induced by doxycycline, protecting against the cellular damage induced by ROS such as superoxide during starvation. Further work would be needed to elucidate this however, such as an ROS assay during starvation in the presence and absence of doxycycline. Alternatively, doxycycline could be replaced with a different antioxidant to see if a similar phenotype is achieved.

This study did of course have its limitations, primarily due to the incomplete dataset as a result of the coronavirus pandemic. Further characterisation of the remaining strains would aid in our understanding of the response to antibiotic treatment.

7.4 Nanopore sequencing can be used to effectively track adaptation during long-term infection and perform comparative genomics on clinical isolates

In chapters two-four, we explored the response to antibiotics through the use of experimental evolution in a lab environment. Whilst this work is invaluable in measuring adaptive changes under controlled conditions, microbial adaption in the human body is likely to be very different. Indeed, the mutation rate of pathogens within the body has been reported to be very low, resulting in slow rates of adaptation [84]. And yet, there are rapid rates of adaptation towards antibiotics in a laboratory environment [85, 7, 86].

We therefore sought to understand the within-host adaptation to repeated antibiotic treatment over extremely long infection time-scales. Through nanopore sequencing, we were able to track the genomic changes in a clonal population of *K.pneumoniae*

over the course of an 18 month infection. The long Nanopore reads allowed us to elucidate structural variations, such as the inclusion of a plasmid fragment in the chromosome of one isolate. Furthermore, we could reconstruct whole plasmids and track both the loss of plasmids, as well as changes in their gene content over time. These isolates were of particular interest due to the detection of carbapenem resistance, deduced in the clinical laboratory to be due to a bla_{OXA-48} gene. However, from the nanopore data this carbapenem resistance was found to be likely due to mutations in the *ompK36* porin gene and the presence of a weak bla_{OXA-1} gene. Carbapenem resistance is a growing and serious threat [66, 250, 69], and as such a better understanding of the genetic basis of resistance, as well as the evolutionary dynamics occurring during chronic infection may aid preventative measures and treatment. Future work could include the resequencing of these isolates using a short-read sequencing platform such as Illumina in order to confirm the polymorphisms identified here.

An additional *E.coli* isolate set spanning 26 months was also acquired from a patient suffering from recurrent cholangitis. Again, nanopore sequencing was carried out alongside phenotypic characterisation to identify variations in the isolates over time. In this case, the isolates represented a diverse range of *E.coli* clonal groups with varying AMR and virulence genes located both on the chromosome and on plasmids. Whether these clonal types were acquired separately over time, or if they form part of a polyclonal infection cannot be deduced from this data. This would require further work involving metagenomic sequencing, however as this was a retrospective study this was not possible. This work does demonstrate the benefits of using nanopore sequencing in complex infections, as the resistance profile could rapidly be predicted based on genomic data, including the presence of ESBL genes which can be challenging to elucidate from phenotypic data alone [326, 327].

In both of these case studies, whole genome sequencing generally proved to be an effective tool in the prediction of AMR phenotypes. However, there is still extensive work to be carried out to determine if WGS can be used as a diagnostic tool, and it

is unlikely to completely replace phenotypic tests. This is due to the inconsistencies often found between AMR genes and the microbial response to antibiotic treatment. For example, an AMR gene may be identified, but that does not necessarily mean that is being expressed, or that the pathogen is resistant to the antibiotic at clinically relevant concentrations [270].

In summary, the data presented within this thesis has revealed previously unknown, antibiotic-induced benefits to bacterial growth and viability. Furthermore, antibiotic resistance was found to be eradicate these benefits. Various possible mechanisms for this phenotype have been explored, and it is likely that a combination of metabolic changes resulting from doxycycline exposure, as well as its known antioxidant properties contribute towards growth benefits.

Additionally, nanopore sequencing has been used to track both the adaptation of carbapenem-resistant *K.pneumoniae* during a single infection, and to compare the genomes of *E.coli* isolates belonging to different clonal groups over a 26 month infection period. There is growing interest in the use of genomics to track adaptive changes occurring over the course of long-term infection, particularly genomic modifications related to antibiotic resistance. Moreover, increasing our understanding on how pathogens adapt during repeated antibiotic therapy, and how these genomic changes relate to phenotypic outcome could aid treatment. Although the data obtained from the *E.coli* isolates did not allow temporal adaptive changes to be tracked, nanopore sequencing did prove effective in determining the clonal types and characterising key genomic features such as AMR and virulence genes.

METHODS - CHAPTERS 2 AND 3

8.1 Media

Lysogeny broth (LB) was utilised here as a rich media. LB was prepared by combining 25g of high salt (10g/L) LB powder (Sigma-Aldrich) with 1L deionised (DI) water which was then autoclaved at 121°C for 20 minutes. LB agar was prepared using the same method, with the addition of 12g agar powder (Sigma-Aldrich).

Minimal media (M9) component A was prepared by combining 350g K_2HPO_4 (Sigma-Aldrich) and 100g KH_2HPO_4 (Sigma-Aldrich) in 1L DI water. Component B was prepared by combining 29.4g trisodium citrate (Fisher Scientific), 50g $(NH_4)_2SO_4$ (Sigma-Aldrich) and 10.45g $MgSO_4$ (Sigma-Aldrich) in 1L DI water. Both components A and B were autoclaved for 20 minutes at 121°C. To prepare M9, 20ml of component A and 20ml of component B were then mixed with 960ml of DI water.

Glucose stock solutions (20%) were prepared by diluting 10g glucose (Sigma-Aldrich) in 50ml DI water. Casamino acid stock solutions (10%) were prepared by diluting 5g casamino acids (Melford) in 50ml DI water. Both the glucose and casamino acid stock solutions were filter sterilised.

The M9 was supplemented with glucose (0.2% (w/v) unless otherwise stated) and 0.1% casamino acids prepared from the filter sterilised 20% and 10% stock solutions to make defined minimal media (hereafter referred to as M9CAA).

8.2 Bacterial strains

Prior to use, bacteria were grown in M9CAA for 24 hours at 30°C, shaken at 160rpm. The following bacteria strains were utilised in chapters 2-3 (table 19). The keio strains utilised in chapter 4 are displayed in figures S15-S28, and the GFP promoter strains are shown in table 1. The keio library and GFP promoter strains were received in 96-

well microplates and immediately stored at -80°C. Prior to use, a pin replicator was used to transfer a small volume of each culture into a microplate containing 150µl M9CAA within each well. The microplates were then incubated for 24 hours at 30°C and shaken at 160rpm in order to prepare overnight cultures.

Strain	Genotype	Ref
E.coli MG1655	K-12 *F- λ - ilvG0 rfb -50 rph -1*	[328]
E.coli GB(c)	MC4100 galK::CFP ampR pGW155B	[129]
E.coli MG1655Δ 1 *rrn*	MG1655 Δ rrnE	[163]
E.coli MG1655 Δ 2 *rrn*	MG1655 Δ rrnGB	[163]
E.coli MG1655 Δ 3 *rrn*	MG1655 Δ rrnGBA	[163]
E.coli MG1655 Δ 4 *rrn*	MG1655 Δ rrnGBAD	[163]
E.coli MG1655 Δ 5 *rrn*	MG1655 Δ rrnGBADH ptRNA67	[163]
E.coli MG1655 Δ 6 *rrn*	MG1655 Δ rrnGBADHB ptRNA67	[163]

Table 19: The bacterial strains used in chapters 2-4, excluding the keio and GFP strains.

8.3 CFU/OD calibration

Optical density (OD) has been used throughout this work as a proxy for cell number, however cell size can vary during different stages of growth and as such the robustness of this measurement must be tested [329, 330]. The relationship between OD and CFU/ml was therefore examined for *E.coli* MG1655 to ensure that there is a linear relationship between these two measurements. Cultures of *E.coli* MG1655 were grown for 24 hours in defined minimal media, after which 6 serial dilutions were performed and OD(600nm) reads were taken using a Tecan Spark microplate reader. To quantify CFU/ml, 10µl of diluted culture (with final dilutions of 10^{-5} and 10^{-6}) were spread onto LB agar plates and incubated at 30°C for 24 hours. The number of colonies were then counted and the following calculation was used to determine the number of cells in the original culture:

$$\text{CFU/ml} = \frac{\text{Colony number} \times \text{Dilution factor}}{\text{Volume of culture plated (10 µl)}} \quad (1)$$

The final CFU/OD calibration curve is shown in figure 74.

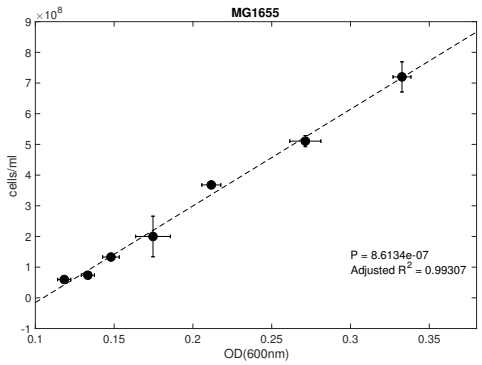

Figure 74: The calibration for OD against CFU/ml for *E.coli* MG1655. *n = 3*.

8.4 Determination of MIC

Multiple antibiotics are used within this thesis, including doxycycline (Sigma-Aldrich), erythromycin (Duchefa Biochemie), penicillin (Sigma-Aldrich) and rifampicin (Melford). The solvent and stock solution concentrations were prepared for each antibiotic according to the manufacturers instructions, as displayed in table 20. All antibiotic stock solutions were filter sterilised using a 0.22 µm filter before being frozen at -20°C. Note that rifampicin must be protected from light to avoid degradation.

Antibiotic	Solvent	Stock solution	Storage temperature
Doxycycline	DI water	5mg/ml	-20°C
Erythromycin	Pure ethanol	10mg/ml	-20°C
Rifampicin	Pure methanol	25mg/ml	-20°C
Penicillin	DI water	10mg/ml	-20°C

Table 20: Antibiotic stock solutions.

Working solutions were prepared from stock solutions by dilution in the appropriate media for that experiment (e.g. M9CAA). Linear gradients of doxycycline, ery-

thromycin, rifampicin and penicillin were then prepared in microtiter plates and diluted 1:1 in M9CAA inoculated with 1x10^6 CFU of *E.coli* MG1655 (the cell number having been calculated based on the previously shown CFU/OD calibration curve in figure 74). An additional doxycycline dose response was performed for the keio WT strain *E.coli* BW25113 (Supplementary figure S12). The microplates were incubated at 30°C, shaking at 160rpm and OD(600nm) readings were taken every 20 minutes in a Tecan Spark microplate reader. The final dose response curves are presented in supplementary figure S1, and the minimal inhibitory concentration (MIC) was determined to be the concentration of antibiotic that inhibited 99% of growth by 24hrs.

8.5 Extended growth curves and dose response curves

To test for the long-term effects of doxycycline on the growth of *E.coli*, extended dose response assays were carried out. Briefly, dilutions of doxycycline were prepared from the stock solution (0, 0.05, 0.1, 0.2, 0.3, 0.4, 0.6, 0.8 and 1mg/l) in 10ml M9CAA and inoculated with 1x10^6 cells of *E.coli* MG1655 overnight culture. 150 µl of each culture was then inoculated into a microtiter plate in triplicate and incubated at 30℃ for 72 hours. Cell density was measured as OD(600nm) every 20 minutes by a Tecan Spark plate reader.

In order to test for the robustness of the resulting phenotypes across different resource concentrations, the growth of *E.coli* MG1655 in three different doxycycline concentrations (0.2, 0.4, 0.8mg/l), as well as drug-free conditions was measured in M9CAA supplemented with different concentrations of glucose (0.2, 1 and 2mg ml $^{-1}$) in triplicate. Cell density was measured as OD(600nm) every 20 minutes for 72 hours by a Tecan Spark plate reader.

An extended dose response was also performed for the doxycycline-resistant strain *E.coli* GBc by diluting 1x10^6 cells of overnight culture into 10ml M9CAA containing 0, 0.6 or 0.8mg/l doxycycline prepared from frozen stock solution. 150 µl of each culture was then inoculated into a microtiter plate in triplicate and incubated at 30℃

for 72 hours. Cell density was measured as OD(600nm) every 20 minutes by a Tecan Spark plate reader.

The growth of the *E.coli* rrn strains were measured over an extended period of time to establish the effect of *rrn* knockouts on various growth parameters. For each *rrn* knockout strain, and the WT *E.coli* MG1655 strain, 1x10^6 cells of the respective overnight culture was inoculated into 10ml of M9CAA. Note that no antibiotic is supplemented into the media. 150 µl of each culture was then inoculated into a microtiter plate in triplicate and incubated at 30℃ for 72 hours. Cell density was measured as OD(600nm) every 20 minutes by a Tecan Spark plate reader.

Due to the long incubation period, the edge wells of the microplate were not used in order to mitigate against evaporation of media in all extended growth experiments. Growth parameters such as lag and growth rate were calculated for all growth curves as set out in section 8.6.

8.6 Quantification of growth parameters

The growth rate (r), maximum population density (K) and lag time (L) were determined by fitting both a four-parameter logistic model (equation 2) and exponential model (equation 3) to the OD growth data, using 'fitnlm' in MATLAB. In this case, B represents the estimated blank (that is the blank reading of a well containing only M9CAA) and a is a fitting parameter. $N(t)$ represents the bacterial growth over time (t). The most appropriate model was chosen based on the model with the lowest corrected Akaike Information Criterion (AICc). If nutrients are not fully depleted by the end of the measurement period, we would expect an exponential growth curve. On the other hand, if nutrients are depleted and the culture reaches stationary phase, we would anticipate that a logistic curve would be the best fit to the data.

The resource efficiency, or yield, is then estimated by dividing K by the concentration of glucose supplied in the media.

$$N(t) = B + \frac{K}{1 + a \cdot e^{-r(t-L)}} \tag{2}$$

$$N(t) = B + ae^{rt} \tag{3}$$

8.7 Long-term batch culture

In order to quantify the effects of antibiotics on the long term viability of *E.coli*, long-term batch cultures were prepared. As these cultures were to be incubated for a relatively long period of time, larger volumes of media were required to mitigate against the effects of liquid evaporation. Overnight culture of *E.coli* MG1655 was inoculated into 30ml of M9CAA (M9 supplemented with 0.2% glucose and 0.1% casamino acids) at an initial inoculum size of 1x10^6 cells/ml, as determined by the CFU/OD calibration curve shown in figure 74. Doxycycline, erythromycin, penicillin and rifampicin were then added to individual cultures at concentrations determined to inhibit 20% and 50% of growth (0.2 and 0.4mg/l for doxycycline, 2 and 5mg/ml for erythromycin, 0.125 and 0.25mg/l for penicillin and finally 0.25 and 0.5mg/l for rifampicin). Three replicates of each antibiotic condition were prepared, alongside three replicates of a drug-free control. All cultures were then incubated at 30℃ and shaken at 160rpm for 28 days without the addition of fresh media. At regular intervals (days 0, 3, 6, 8 10, 16, 20 and 28), 10μl was removed from each culture, serially diluted and spread onto LB agar plates for the purpose of colony counting and to check for contamination.

Long-term batch cultures of the doxycycline-resistant strain *E.coli* GBc were prepared in a similar way, with cultures prepared either in 30ml of drug-free M9CAA, or with the addition of doxycycline (0.2 and 0.4mg/l) in triplicate. Again, the cultures were incubated for 28 days without the addition of fresh nutrients and growth

dynamics were measured as CFU's.

To explore the role of ribosome production on long-term viability, the *E.coli rrn* knockout strains were grown in long-term batch culture without the addition of any antibiotic. Again, 1x10^6 cells of overnight culture for each of the 6 knockout strains and WT (*E.coli* MG1655) were inoculated into 30ml M9CAA in triplicate and incubated at 30℃, shaken at 160rpm. The cultures were incubated for 14 days without the addition of any fresh media or nutrient. On days 0, 1, 2, 3, 4, 5, 8 and 14, 10μl was removed from each culture, serially diluted and spread onto LB agar plates for the purpose of colony counting, and to check for contamination.

8.8 Supernatant assay

The following protocol was used to determine the effect of doxycycline on the growth of *E.coli* in spent supernatant. Firstly, *E.coli* MG1655 was inoculated into 30ml of M9CAA at an initial inoculum size of 1x10^6 cells in triplicate, as determined by the CFU/OD calibration curve. These cultures were grown at 30℃ and shaken at 160rpm for 48 hours, as it was anticipated that the majority of glucose in the media would be exhausted by this time point (as confirmed by a glucose assay, set out in section 8.9). The cultures were then centrifuged at 8,000x rpm for 3 minutes, after which the supernatant was transferred to a fresh tube and bacterial cell pellet discarded. This centrifugation step was repeated a second time to maximise the removal of intact cells from the supernatant. The supernatant was then filter sterilised using a 0.22 µm filter to remove any remaining *E.coli* cells, leaving only small molecules within the media behind.

The *E.coli* cells used to inoculate into this supernatant were then prepared as followed. Fresh overnight cultures of *E.coli* MG1655 were grown in 10ml M9CAA for 24 hours and then centrifuged at 5,000x rpm for 2 minutes. The supernatant was discarded and the bacterial pellet was resuspended in 10ml PBS (Fisher Scientific),

followed by a further centrifugation at 5,000x rpm for 2 minutes. This wash step was repeated a further two times to ensure that no glucose or component of the M9CAA was remaining in the culture. The washed *E.coli* were inoculated into 10ml x 12 of the prepared supernatant, as well as M9CAA controls at a cell density determined to be 1x10 ^{6} cells. The specific conditions and number of replicates used are detailed in table 21. 150μl of each culture was inoculated into a 96-well microplate and incubated at 30℃. Cell density was measured as OD(600nm) every 20 minutes for 72 hours in a Tecan Spark microplate reader.

Note that, due to the long incubation period, the edge wells of the microplate were not used in order to mitigate against evaporation of media in all extended growth experiments. Growth parameters such as lag and growth rate were calculated for all growth curves as set out in section 8.6.

No. replicates	Condition
3	Supernatant
3	Supernatant + 0.2mg/l doxycycline
3	Supernatant + 0.2mg ml^{-1} glucose
3	Supernatant + 0.2mg ml^{-1} glucose + 0.2mg/l doxycycline
3	M9CAA
3	M9CAA + 0.2mg/l doxycycline

Table 21: The conditions used in the supernatant assay. All were prepared in 10ml volumes and inoculated with 1x10 ^{6} cells of fresh *E.coli* overnight culture.

8.9 Glucose assay

To ensure that all of the available glucose was being exhausted from the media of starving cultures, a colourmetric glucose assay (BioVision) was used. This glucose enzyme mix oxidises any glucose in the sample, making a product that then reacts with a dye within the assay mix to produce a coloured product. This coloured product can then be detected using a microplate reader. Briefly, a standard curve was made

according to the manufacturers instructions through the serial dilution of a glucose standard (shown in figure S5) into the glucose assay master mix (glucose assay buffer, glucose probe and glucose enzyme mix). The samples were incubated for 30 minutes at 37℃ and protected from light. Absorbance was then read at 570nm in a Tecan Spark plate reader.

Samples of culture (50 µl x 3) were removed from *E.coli* MG1655 cultures at 0, 24 and 48 hours. In addition, glucose assays were performed at 0, 24 and 48 hours on cultures of *E.coli* MG1655 supplemented with 0.2 and 0.4mg/l doxycycline in order to test for the impact of doxycycline on glucose concentration over time. At each time point, 50 µl samples were loaded into a 96-well microplate, along with 50 µl of glucose assay master mix in triplicate. Note that for the initial time 0 samples, dilutions were made to ensure that the readings were in the range of the standard curve, and these dilutions were accounted for in further calculations. For the control, the sample was substituted for 50 µl of background control mix. The samples were incubated for 30 minutes at 37℃ and protected from light. Absorbance was then read at 570nm in a Tecan Spark plate reader. The readings were then compared against the standard curve to determine the concentration of glucose in the sample and the following calculation was used to determine nmol/ µl, where B is the amount of glucose in the sample well (nmol), V is the volume of sample in the well and D is the sample dilution factor used:

$$\text{Glucose concentration (nmol/ µl)} = \frac{B}{V \times D} \tag{4}$$

8.10 Whole genome sequencing of starved *E.coli* cultures

To elucidate any genomic changes occurring in populations of starving *E.coli* in the presence and absence of doxycycline, whole genome sequencing (WGS) was performed. This required the use of larger volume cultures (500ml) to facilitate the removal of culture for DNA extraction.

An overnight culture of *E.coli* MG1655 was grown in 10ml M9CAA for 24 hours at 30℃, shaken at 160rpm in triplicate. These cultures were then used to inoculate 16x 500ml M9CAA in 2L erlenmeyer flasks at a density of $1x10^6$ cells. Four cultures were left drug-free, four cultures were supplemented with 0.2mg/l doxycycline and four cultures were supplemented with 0.4mg/l doxycycline prepared from frozen stock solution (stored at -20℃). The remaining four replicates served as a control for volume loss, as no culture would be removed from these flasks but cell density would still be monitored. This is to check that growth dynamics are not substantially impacted by the frequent removal of culture. The cultures were incubated at 30℃ and shaken at 160rpm for 21 days without the addition of fresh media or nutrients. At 7 time points over the course of the 21 days (Days 1, 3, 7, 10, 15, 17 and 21), 5ml of culture was removed and centrifuged at 8,000x rpm for 3 minutes (aside from the four replicates acting as a volume control). The supernatant was removed and the bacterial pellet was stored at -80℃ in preparation for DNA extraction. At each of these time points, an additional 10 µl from each culture was removed and serially diluted before being spread onto LB agar plates for colony counting in order to calculate the CFU/ml. Four replicates of the ancestral strain (*E.coli* MG1655) were also prepared and stored as cell pellets at -80℃ in preparation for sequencing to ensure conformity between the published MG1655 reference and the strain used here.

8.11 DNA extraction

The 'GeneJet DNA purification kit' (Thermo Fisher Scientific) was used to extract DNA from the bacterial pellets that had been stored at -80℃ as per the manufacturers instructions using a silica-based spin column method. Alterations to the standard protocol included an extended incubation time at 56℃ to allow for complete cell lysis, and an additional final elution step to maximise the DNA yield. The DNA was run

on a 1% agarose gel to check that the DNA wasn't heavily fragmented, and to check for protein contamination which would appear as a smear on the gel. The DNA was then quantified with the Qubit system, using the 'Qubit high sensitivity (HS) assay' kit (Thermo Fisher Scientific) to ensure that the DNA yield was sufficient for sequencing. To concentrate the DNA, the samples were then spun on a vacuum centrifuge (SpeedVac) at 50℃ until the sample was almost entirely evaporated, followed by the addition of elution buffer to make the volume up to 10 µl. The final concentration of each DNA sample is displayed in table 22. The DNA was then stored at 4℃ in preparation for sequencing. Paired-end libraries were prepared at the 'Institute of Clinical Molecular Biology (IKMB)', Kiel University and run on the HiSeq using the Nextra library preparation protocol.

Time point	Doxycycline (mg/l)	Replicate	Volume (µl)	Concentration (ng/µl)
1	0	1	10	365.9
1	0	2	10	592.8
1	0	3	10	402.8
1	0	4	10	562.4
1	0.2	1	10	448.4
1	0.2	2	10	321.9
1	0.2	3	10	486.4
1	0.2	4	10	350.0
1	0.4	1	10	315.4
1	0.4	2	10	338.6
1	0.4	3	10	345.4
1	0.4	4	10	356.4
3	0	1	10	661.2
3	0	2	10	391.4
3	0	3	10	934.8
3	0	4	10	634.6
3	0.2	1	10	874.0
3	0.2	2	10	695.4
3	0.2	3	10	774.8
3	0.2	4	10	699.2
3	0.4	1	10	748.6
3	0.4	2	10	714.4
3	0.4	3	10	801.8
3	0.4	4	10	570.0
7	0	1	10	509.2
7	0	2	10	646.0
7	0	3	10	337.1
7	0	4	10	444.6
7	0.2	1	10	729.6
7	0.2	2	10	672.6
7	0.2	3	10	539.6
7	0.2	4	10	809.4
7	0.4	1	10	938.6
7	0.4	2	10	592.8
7	0.4	3	10	1455.4
7	0.4	4	10	1261.6
10	0	1	10	421.8
10	0	2	10	563.9
10	0	3	10	383.8
10	0	4	10	548.7
10	0.2	1	10	315.4
10	0.2	2	10	380.0
10	0.2	3	10	532.0
10	0.2	4	10	379.6
10	0.4	1	10	425.6
10	0.4	2	10	467.4
10	0.4	3	10	494.0
10	0.4	4	10	373.5
14	0	1	10	562.4
14	0	2	10	471.2
14	0	3	10	444.6
14	0	4	10	360.2
14	0.2	1	10	551.0
14	0.2	2	10	344.7
14	0.2	3	10	524.4
14	0.2	4	10	354.5
14	0.4	1	10	387.6
14	0.4	2	10	395.2
14	0.4	3	10	547.2
14	0.4	4	10	535.8
17	0	1	10	505.4
17	0	2	10	367.1
17	0	3	10	566.2
17	0	4	10	406.6
17	0.2	1	10	649.8
17	0.2	2	10	452.2
17	0.2	3	10	676.4
17	0.2	4	10	418.0
17	0.4	1	10	779.0
17	0.4	2	10	516.8
17	0.4	3	10	490.2
17	0.4	4	10	410.4
21	0	1	10	798.0
21	0	2	10	414.2
21	0	3	10	566.2
21	0	4	10	365.6
21	0.2	1	10	801.8
21	0.2	2	10	444.6
21	0.2	3	10	478.8
21	0.2	4	10	345.8
21	0.4	1	10	672.6
21	0.4	2	10	547.2
21	0.4	3	10	1037.4
21	0.4	4	10	619.4
Ancestral	-	-	10	402.8
Ancestral	-	-	10	391.4
Ancestral	-	-	10	418.0
Ancestral	-	-	10	399.0

Table 22: Concentration and volume of DNA used for sequencing.

8.12 DNA quality control, mapping and variant calling

FastQC (v 0.11) was used to assess multiple quality control parameters such as read quality and GC content. A representative example of the read quality is displayed in figure 75. Low quality reads (with a read quality below 20) were trimmed using Cutadapt (v2.10) [331]). The reads were then mapped against the previously published *E.coli* MG1655 reference genome using burrows-wheeler aligner (BWA, v0.7.4) [332] with standard parameters. The alignments were then sorted into genomic position and indexed using Samtools (v1.3.1).

To call variants such as single nucleotide polymorphisms (SNPs), initially Varscan was used (v2.4.0) [333] with a minimum average quality of 30. Additionally, variants were called using Breseq v(0.30.0) [334]. Breseq is a computational pipeline used to detect SNPs, indels and new junctions (such as those caused by the insertion of a mobile element). Breseq was run in polymorphism mode as whole population samples were sequenced rather than clones. Not only were the SNPs previously detected by Varscan confirmed by breseq, additional low frequency SNPs and indels were also identified.

The annotation files for *E.coli* MG1655 were accessed from NCBI, and these Genbank files were used to annotate the polymorphisms identified. A combination of MATLAB and python were used for the downstream analysis.

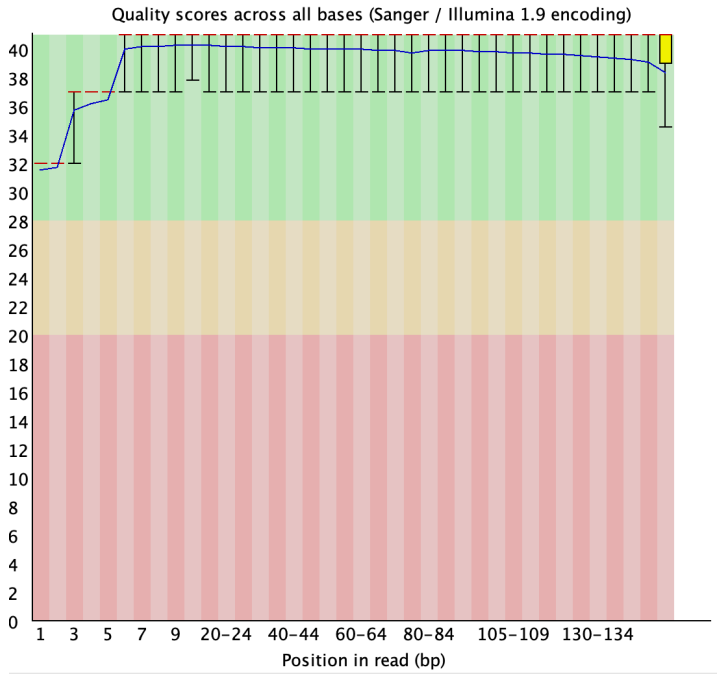

Figure 75: The Q score across all positions for the trimmed day one, 0mg/l doxycycline read. Analysed using 'FastQC'.

8.13 Measurement of promoter activity

To study the effects of doxycycline on the expression of various promoters, a library of *E.coli* MG1655 reporter strains was used in which a fast-folding GFP is fused to a full-length copy of the *E.coli* promoter in a low-copy plasmid [335]. Upon receipt of the reporter library from 'Horizon Discovery', all strains were stored at -80℃ in 96-well microplates.

The GFP reporter strains selected for this work (shown in table 1) were initially grown for 24 hours in 10ml M9CAA (30℃, 160rpm) in order to revive the cells from the frozen cultures. These cultures were then used to inoculate 150 µl of drug-free M9CAA or M9CAA containing 0.4mg/l doxycycline (preformed in triplicate). OD measurements (600nm) were taken every 20 minutes, alongside measurements of GFP fluorescence (485/520nm) in a Tecan Infinite 200 Pro. The GFP measurements were normalised to the respective OD readings for each strain to obtain GFP/OD, and the maximal GFP expression was defined as the maximum level of GFP fluorescence obtained per cell (GFP/OD). Background fluorescence was subtracted using the GFP measurements from a reporter strain with a promoterless vector (pUA66), which was supplied with the reporter library.

8.14 Growth of the keio library

The keio collection is a library of 3,985 *E.coli* BW25113 strains, each with an individual, non-essential gene knocked out. It is an invaluable resource to test for the effects of gene knockouts on growth within different conditions. Upon receipt of the keio library from 'Horizon Discovery', the strains were stored at -80℃ in 96-well microplates.

In order to measure the differences in phenotype between the keio strains in the presence and absence of doxycycline, the keio strains were first transferred with a custom 3D-printed 96-pin replicator into 96-well microplates containing 150 µl of

M9CAA within each well. These cultures were then incubated for 24 hours at 30℃, shaking at 160rpm. The cultures were then transferred using a 96-pin replicator into either a 96-well microplate containing M9CAA or a 96-well microplate containing M9CAA plus 0.4mg/l doxycycline. In order to prevent the evaporation of media during prolonged periods of incubation, 'reservoir plates' were used - these are 96-well microplates surrounded by a reservoir that is then filled with 3ml of soft agar. The cultures were then incubated at 30℃ in Tecan Spark microplate readers, with cell density measured every 20 minutes for 72 hours as OD(600nm). In total, the growth of 1,266 strains was measured in the presence and absence of 0.4mg/l doxycycline, generating 2,532 growth curves.

Data analysis was carried out in MATLAB. Briefly, the dimensionally of the data was reduced using principle component analysis (pca in MATLAB). For cluster analysis, K-means clustering was applied in MATLAB, and the optimal number of clusters for k-means analysis was calculated using 'evalclusters', again in MATLAB. As an additional clustering analysis, hierarchal clustering was performed in MATLAB using 'clustergram' to generate a heatmap with dendrograms. The COG terms were assigned to each gene using a custom python script, and the significance of COG enrichment was tested for in MATLAB using a fishers exact test (fishertest).

METHODS - CHAPTERS 5 & 6

9.1 Selection of clinical isolates and ethics

The aim of this work was to monitor the genomic and phenotypic variations in a clinical pathogen during a long period of treatment. As such, certain requirements were put in place to obtain appropriate isolates. The patient samples were selected based on the duration of infection, the number of isolates available from a single patient, and finally confirmation of a multidrug-resistant infection. Ethical clearance was obtained for the use of the samples via a verbal consent given to the patients clinician (Dr Fergus Hamilton). No further ethical clearance was required as only stored bacterial isolates were acquired (not direct patient samples possibly containing human DNA), and no identifying patient data was obtained. In addition, this was a retrospective study, and as such samples were already stored and available rather than being acquired specifically for the purpose of this study.

The following patient isolates were selected based on our criteria:

1. *K.pneumoniae* isolates (x6) spanning 18 months from a female patient. The infection was acquired in India following a hip replacement and later found to be carbapenem-resistant. The isolates were acquired from the patient and stored in Aug ’18, Sept ’18, Oct ’18, Jan ’19, March ’19 and May ’19.

2. *E.coli* isolates (x6) spanning 26 months from an elderly male patient with cholangitis. The isolates were acquired from the patient and stored on day 1, 11 months, 23 months, 24 months, 26 months and finally 26 months and 2 days into the infection. This set of samples was of particular interest due to the repeated treatment failure, as well as the reported presence of ESBL genes.

The samples were received on agar slopes and immediately stored at 4℃. A small amount of each sample was inoculated into 10ml of M9CAA (M9 supplemented with 0.2% glucose and 0.1% casamino acids) and 10ml of LB using an inoculation loop and incubated at 30℃, shaken at 160rpm for 24 hours. 1ml of each culture was frozen in 80% glycerol (Fisher Scientific) and stored at -80℃ in triplicate to preserve the samples for future use.

9.2 Automated antibiotic susceptibility testing

Automated antibiotic susceptibility testing was carried out on every isolate using the Vitek 2 automated system (bioMérieux, Marcy-létoile, France) in the clinical laboratory based at Southmead Hospital, Bristol. In addition, data obtained through disk diffusion assays was also acquired.

In addition to the AMR profiles generated by the Vitek 2, antibiotic susceptibility tests were also carried out through the broth micro-dilution method. First, antibiotic stock solutions of gentamicin (Melford), meropenem (Abcam) and ciprofloxacin (Sigma-Aldrich) were prepared according to manufactures instructions, in the solvents and concentrations displayed in table 23. All antibiotic stock solutions were filter sterilised using a 0.22 µm filter and then stored in 1ml aliquots at -20°C prior to use.

Antibiotic	Solvent	Stock solution	Storage temperature
Meropenem	DMSO	10mg/ml	-20°C
Ciprofloxacin	0.1N HCl	10mg/ml	-20°C
Gentamicin	DI water	10mg/ml	-20°C

Table 23: Antibiotic stock solutions.

Further antibiotic dilutions were made in the media to be used for growth, that is M9CAA unless otherwise stated. For the AST testing of the six *K.pneumoniae*

isolates, dilutions of gentamicin (1, 16 and 32mg/l) and meropenem (0.5, 1 and 16mg/l) were prepared, and for the six *E.coli* isolates, dilutions of gentamicin (0.5, 8 and 16mg/l) and ciprofloxacin (0.1 and 4mg/l) were prepared in 10ml M9CAA. 150 µl of each antibiotic dilution inoculated with *K.pneumoniae* or *E.coli* was then transferred to a 96-well microplate in triplicate, as well as three drug-free control controls of each isolate. The microplates were incubated at 30°C, shaking at 160rpm and optical density (OD) readings were taken every 20 minutes for 24 hours in a Tecan Spark microplate reader.

9.3 DNA extraction

Four *K.pneumoniae* isolates (the isolates obtained in August 2018, October 2018, January 2019 and May 2019) and four *E.coli* isolates (the isolates obtained on day one, month 11, month 23 and month 26 of infection) were selected for DNA sequencing. The remaining isolates are currently awaiting sequencing. All of the isolates were inoculated into 10ml M9CAA in triplicate using an inoculation loop directly from the original agar slope. The original agar slope was used in order to reduce the number of culturing steps as this could impact genomic modifications. All cultures were grown for 24 hours at 30°C, shaken at 160rpm.

The 'GeneJet DNA purification kit' (Thermo Fisher Scientific) was used to extract DNA from the bacterial pellets that had been stored at -80℃ as per the manufacturers instructions using a silica-based spin column method. Alterations to the standard protocol included an extended incubation time at 56℃ to allow for complete cell lysis, and an additional final elution step to maximise the DNA yield. The DNA was run on a 1% agarose gel to check that the DNA wasn't heavily fragmented, and to check for protein contamination which would appear as a smear on the gel. The nano drop system was also used to check DNA purity.

The DNA was then quantified with the Qubit system, using the 'Qubit high sensitivity

(HS) assay' kit (Thermo Fisher Scientific) to ensure that the DNA yield was sufficient for sequencing. To concentrate the DNA, the samples were then spun on a vacuum centrifuge (SpeedVac) at 50℃ until the sample was almost entirely evaporated, followed by the addition of elution buffer to make the volume up to 10 µl. The DNA was then stored at 4℃ in preparation for sequencing. The final concentration of DNA samples for the *K.pneumoniae* and *E.coli* isolates are displayed in tables 24 and 25.

Time point	Replicate	Volume (µl)	Concentration (ng/µl)
August 2018	1	10	223
August 2018	2	10	310
August 2018	3	10	326
October 2018	1	10	189
October 2018	2	10	192
October 2018	3	10	155
January 2019	1	10	312
January 2019	2	10	334
January 2019	3	10	192
May 2019	1	10	260
May 2019	2	10	219
May 2019	3	10	316

Table 24: Concentration and volume of DNA used for sequencing - *K.pneumoniae* isolates.

Time point	Replicate	Volume (µl)	Concentration (ng/µl)
Day one	1	10	319
Day one	2	10	270
Day one	3	10	236
11 months	1	10	148
11 months	2	10	185
11 months	3	10	216
23 months	1	10	115
23 months	2	10	134
23 months	3	10	123
26 months	1	10	261
26 months	2	10	244
26 months	3	10	222

Table 25: Concentration and volume of DNA used for sequencing - *E.coli* isolates.

9.4 Library preparation

All of the isolates were to be sequenced using Oxford Nanopore sequencing platforms. The *K.pneumoniae* isolates were sequenced using the Oxford Nanopore GridION and the *E.coli* isolates were sequenced using the Oxford Nanopore MinION. For all of the isolates, the the rapid barcoding kit (Oxford Nanopore - SQK-RBK004) was used for library preparation as this allowed 12 samples to be multiplexed onto one flow cell. The kit contains a transposase which cleaves template molecules and attaches a unique barcoded tag to each sample. The different barcoded samples can then be pooled and reads can be separated using MinKNOW software during sequencing. FLO-PRO002 flow cells were used for all sequencing runs.

9.5 Nanopore sequencing

The Oxford Nanopore GridION platform was used for the sequencing of the *K.pneumoniae* isolates through the University of Exeter sequencing service. The samples were sequenced for a total of 2 days and 15 hours using MinKNOW with high accuracy base calling. The resulting fast5 files were base called using Guppy v3.0.0 and barcodes were removed automatically. This resulted in 22.97Gb of data (3.85 million reads), with an average read length of 9.18Kb.

The Oxford Nanopore MinION platform was used for the sequencing of the *E.coli* isolates (carried out by Emily Wood). The samples were sequenced for 1 day and 12 hours using MinKNOW with high accuracy base calling. The resulting fast5 files were base called using Guppy v3.0.0 and barcodes were removed automatically. This resulted in 8.17Gb of data, equating to a total of 1.24 million reads, with an average read length of 9.22Kb. Reads were automatically de-barcoded in MinKNOW.

9.6 Genome assembly and annotation

FastQC (v0.11) was used to assess multiple quality control parameters such as read quality and GC content. Low quality reads (with a read quality below 20) were then trimmed using Cutadapt (v2.10) [331]).

The reads were assembled using both Canu v2.1.1 [336] and Flye v2.8.3 assemblers [234], with the Flye assemblies used for further downstream analysis as highly contiguous assemblies were produced. This was followed by multiple rounds of polishing with Racon v1.4.2 [337] until the assemblies could no longer be improved. Next, the genomes were annotated using both the 'Rapid Annotation using Subsystem Technology' (RAST) [338] and Prokka v1.13.4 [339].

The contigs were confirmed as being either chromosomal or plasmid using the online service mlplasmid [235], which consists of binary classifiers, outputting the probability of a contig being chromosomal or plasmid. The plasmid replicons were then confirmed using PlasmidFinder [236] which uses BLAST to compare inputted sequences to existing databases to identify replicons.

The multilocus sequence type (MLST) of the *K.pneumoniae* isolates were determined using the *Klebsiella* sequence typing tool (`http://bigsdb.pasteur.fr/klebsiella/klebsiella.html`). For the *E.coli* isolates, MLST typing was performed using MLST v.2.0 [297] and serotyping was carried out using SerotypeFinder v2.0 with standard settings [296].

9.7 AMR and virulence gene detection

The genomes were assessed for the presence of AMR genes (both chromosomal point mutations and acquired antimicrobial resistance genes) through the use of the online tool ResFinder v4.1, using the standard settings (90% threshold, 60% minimum length) [243]. ResFinder compares the inputted sequence files against databases of known AMR genes, using BLAST to generate a list of identified AMR

genes and point mutations previously found to result in resistance. Virulence genes were identified in a similar manner using VirulenceFinder v2.0 [340] with standard settings (90% threshold, 60% minimum length).

9.8 Variant calling and comparative analysis

In order to identify genomics modifications and how they change over time, sequences are first mapped to the earliest available isolate (assembled genome) using burrows-wheeler aligner (BWA) [332] with standard parameters. Alignments were sorted into genomic position and indexed using Samtools. Structural variants were called using Sniffles v1.0.7 [265], a structural variant identification tool to be used specifically with third generation sequencing (PacBio and Nanopore). Genome coverage was assessed using bedtools coverage (v 2.24.0) [341]. Direct comparisons were made between both chromosomes and plasmids using EasyFig v2.2.2 [342], a genome visualiser that produces BLAST comparisons of two or more genomic regions. A combination of MATLAB and python were used for the downstream analysis.

SUPPLEMENTARY DATA

10.1 Supplementary data for Chapter 2

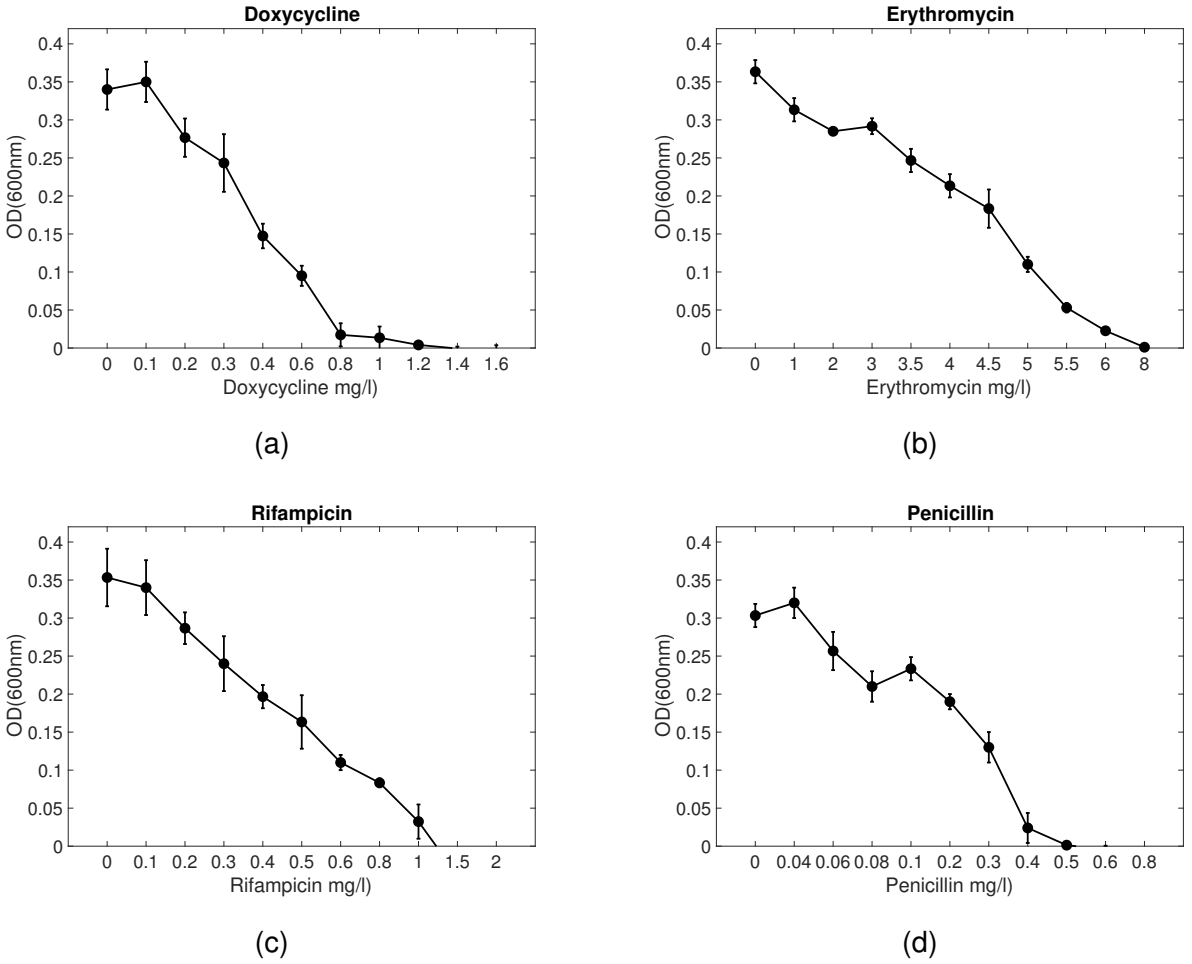

Figure S1: Dose responses of *E.coli* MG1655 against a concentration gradient of a) doxycycline, b) erythromycin, c) rifampicin and d) penicillin. *n=3*.

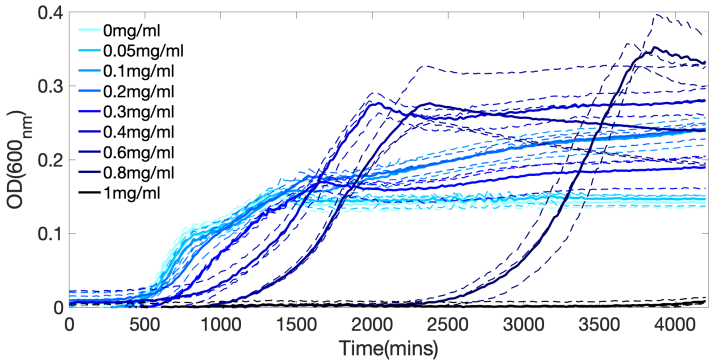

Figure S2: Raw growth curves for *E.coli* cultures exposed to a range of doxycycline concentrations over 72 hours. Higher doses of doxycycline lead to an increase in population density relative to the drug-free control over time.

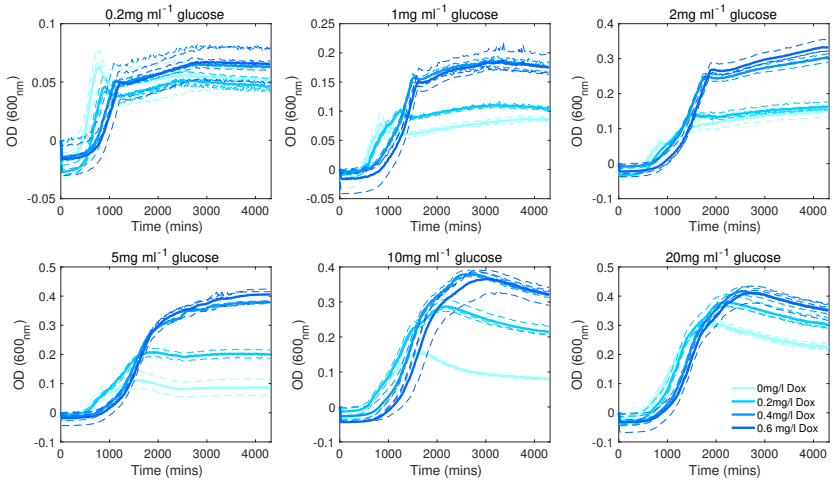

Figure S3: The raw, blank corrected growth data for populations of *E.coli* grown in varying concentrations of doxycycline (as shown by different coloured lines), across different glucose concentrations. *n=3*.

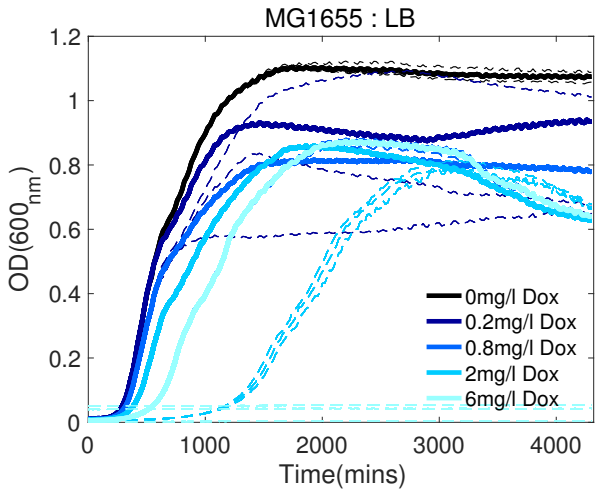

Figure S4: No overgrowth is observed with doxycycline when *E.coli* is grown in LB media.

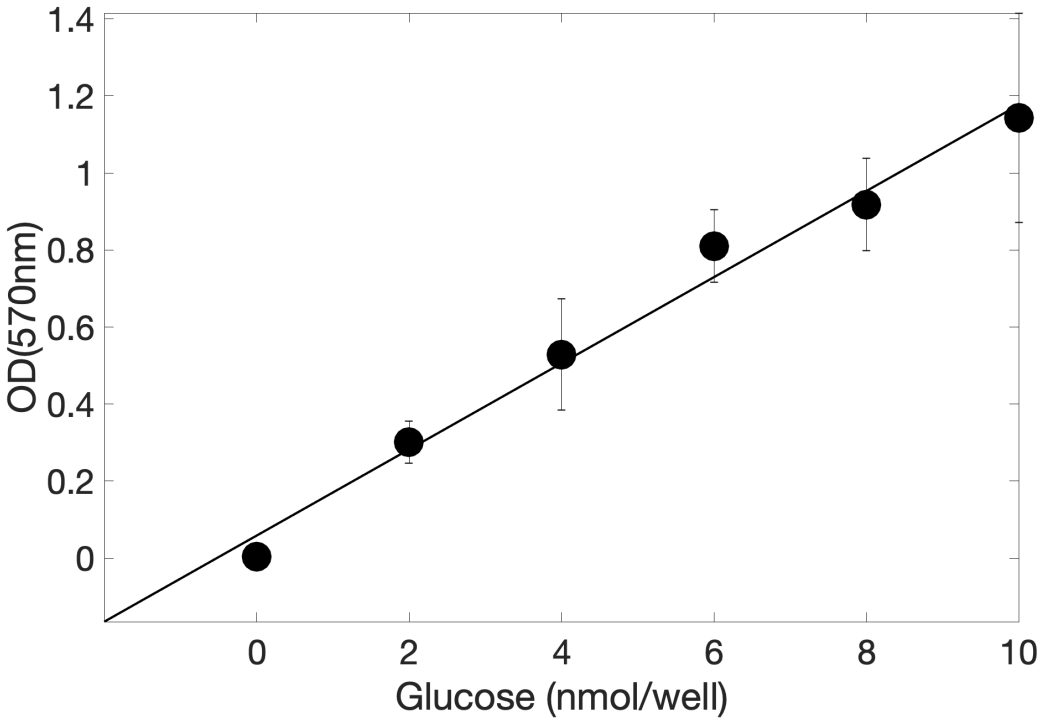

Figure S5: Standard curve for glucose concentration using a colorimetric glucose assay. Absorbance at 570nm was measured for known glucose concentrations (n=3). A linear regression was fitted to the points in order to extrapolate future glucose concentrations.

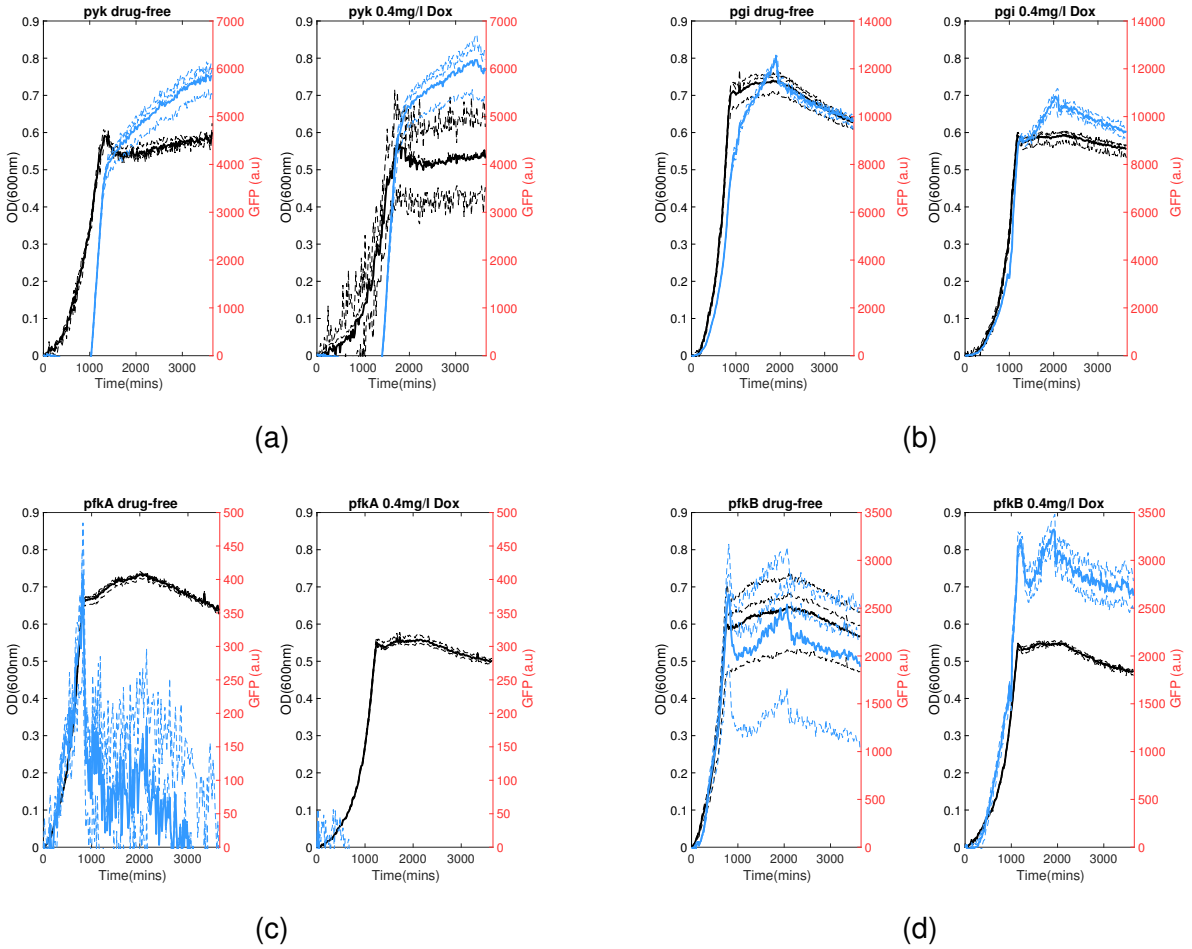

Figure S6: The growth over 72 hours of *E.coli* gfp-promoter strains (measured as OD600nm) shown on the left y axis, alongside the level of gfp expression shown on the right y axis. These strains have tagged genes involved in glycolysis. The growth of both drug-free and doxycycline-exposed cultures is shown. A relatively large amount of noise is measured at very low fluorescence measurements, for example with pfkA in drug-free conditions. *n=3*.

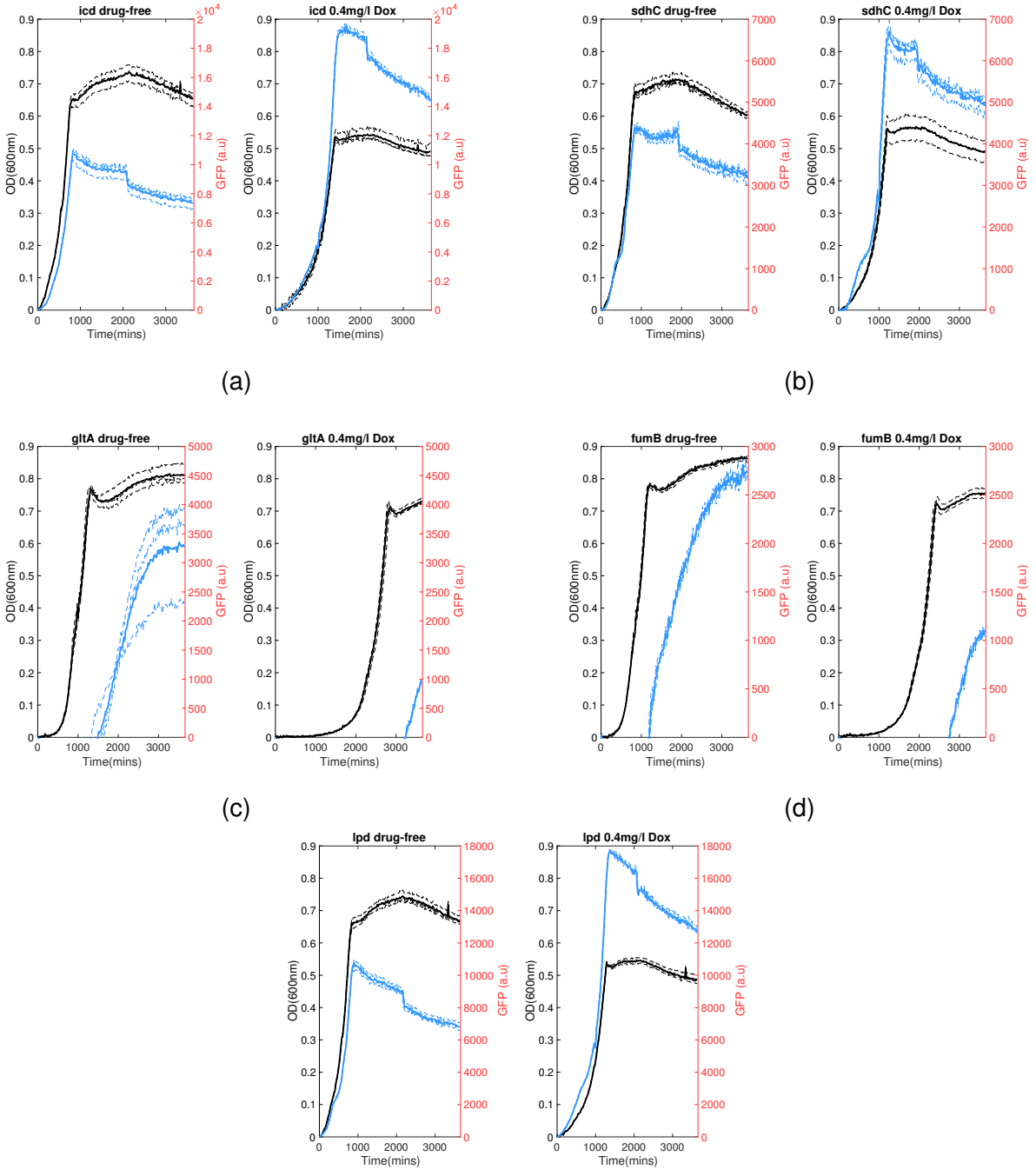

Figure S7: The growth over 72 hours of *E.coli* gfp-promoter strains (measured as OD600nm) shown on the left y axis, alongside the level of gfp expression shown on the right y axis. These strains have tagged genes involved in the TCA cycle. The growth of both drug-free and doxycycline-exposed cultures is shown. *n=3*.

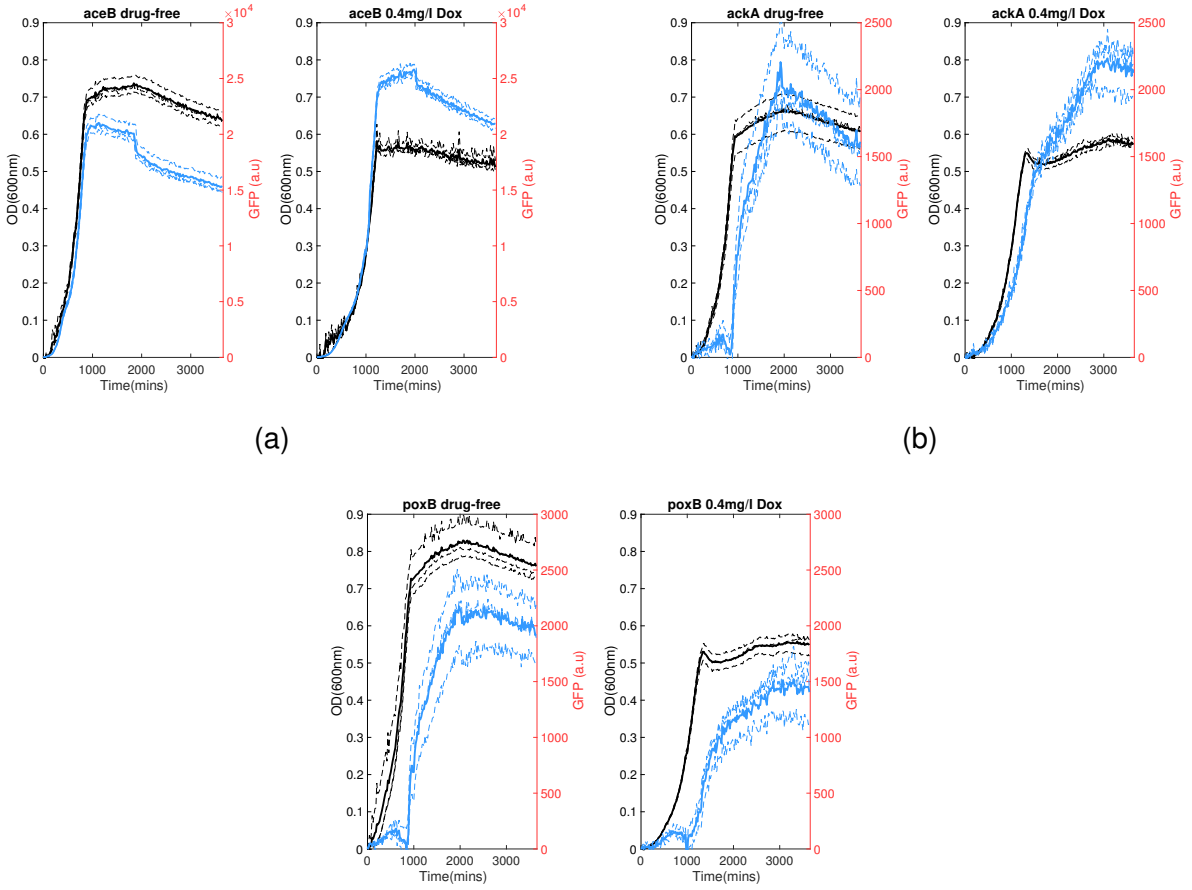

Figure S8: The growth over 72 hours of *E.coli* gfp-promoter strains (measured as OD600nm) shown on the left y axis, alongside the level of gfp expression shown on the right y axis. These strains have tagged genes involved in acetate biosynthesis/metabolism. The growth of both drug-free and doxycycline-exposed cultures is shown. *n=3*.

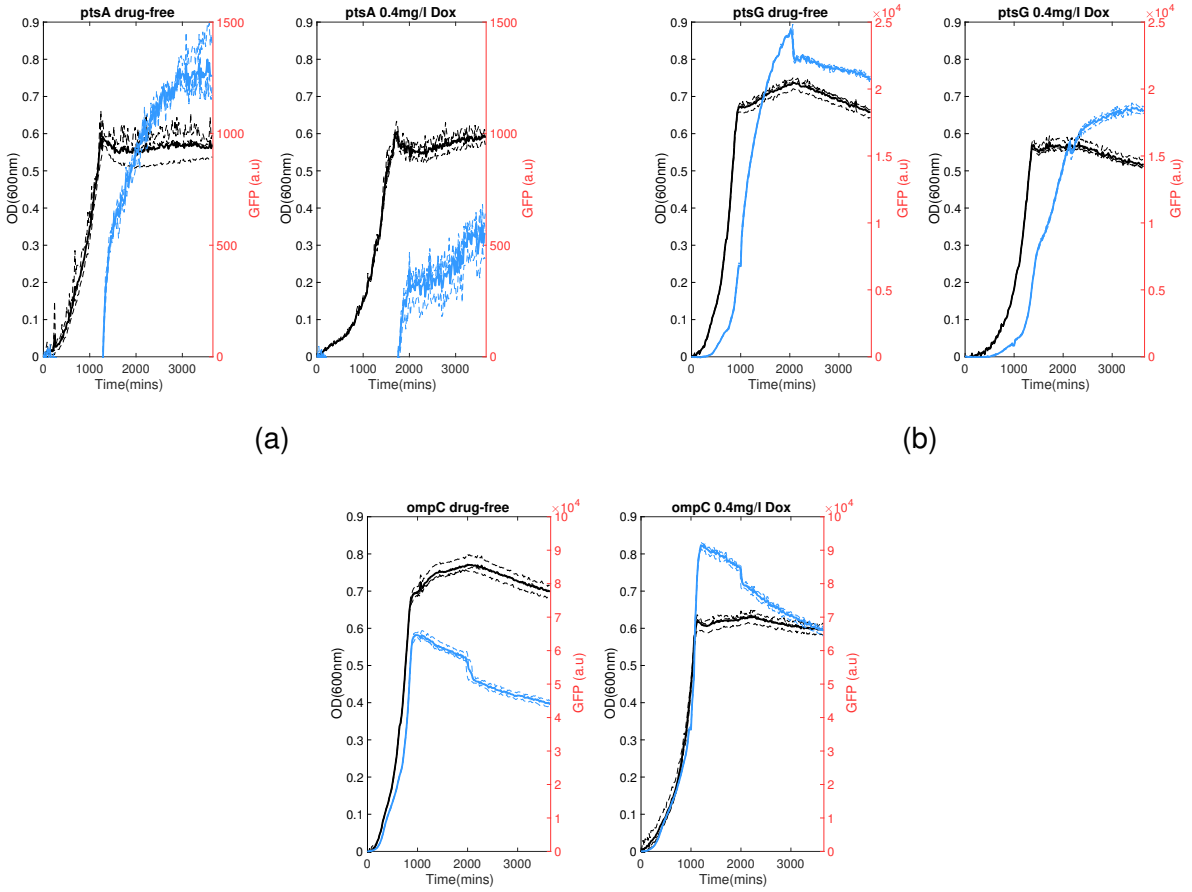

Figure S9: The growth over 72 hours of *E.coli* gfp-promoter strains (measured as OD600nm) shown on the left y axis, alongside the level of gfp expression shown on the right y axis. These strains have tagged genes involved in glucose transport. The growth of both drug-free and doxycycline-exposed cultures is shown. *n=3*.

10.2 Supplementary data for Chapter 3

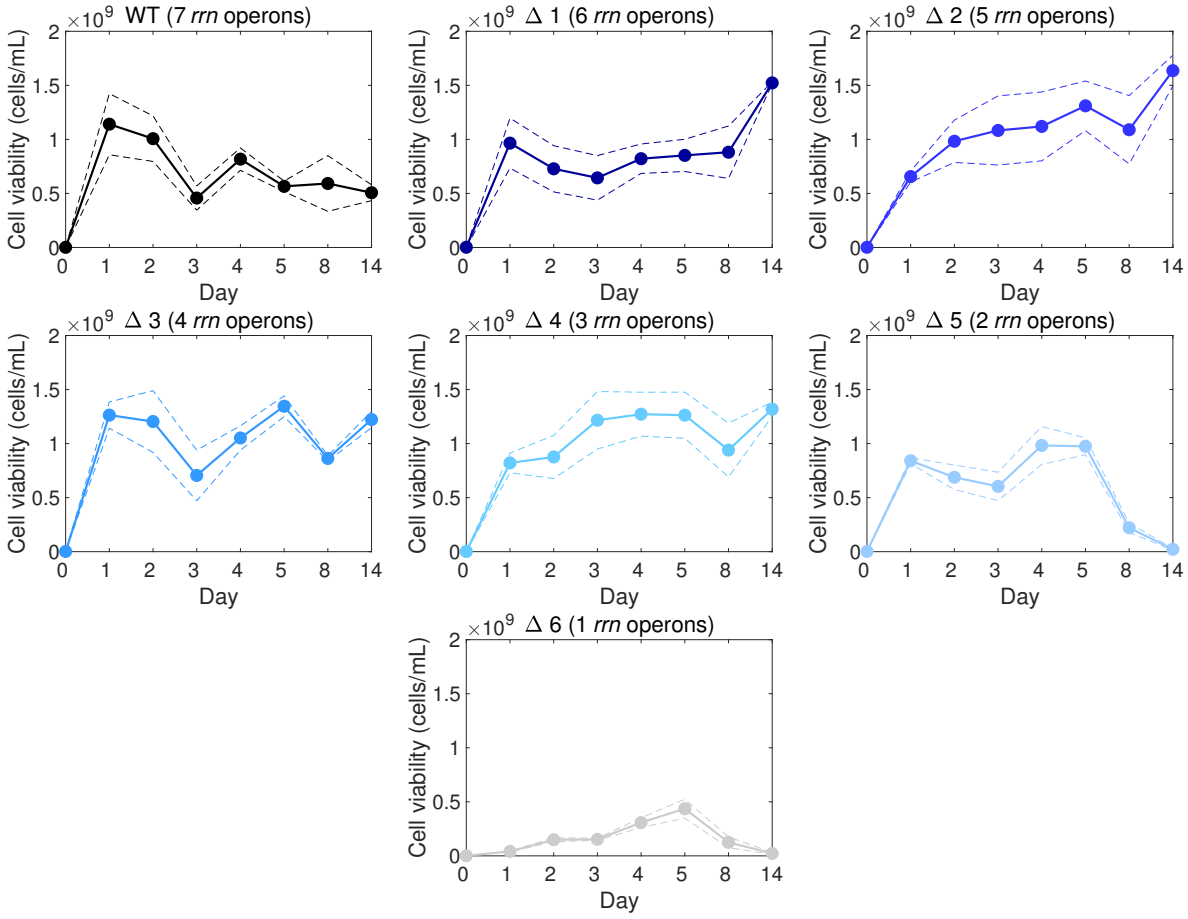

Figure S10: The growth dynamics of the *rrn* knockout strains over 14 days was measured through CFU counts at various time points. The mean is shown as a solid line, with ± estimated 95% confidence intervals (CI, 3 replicates) shown as dashed lines.

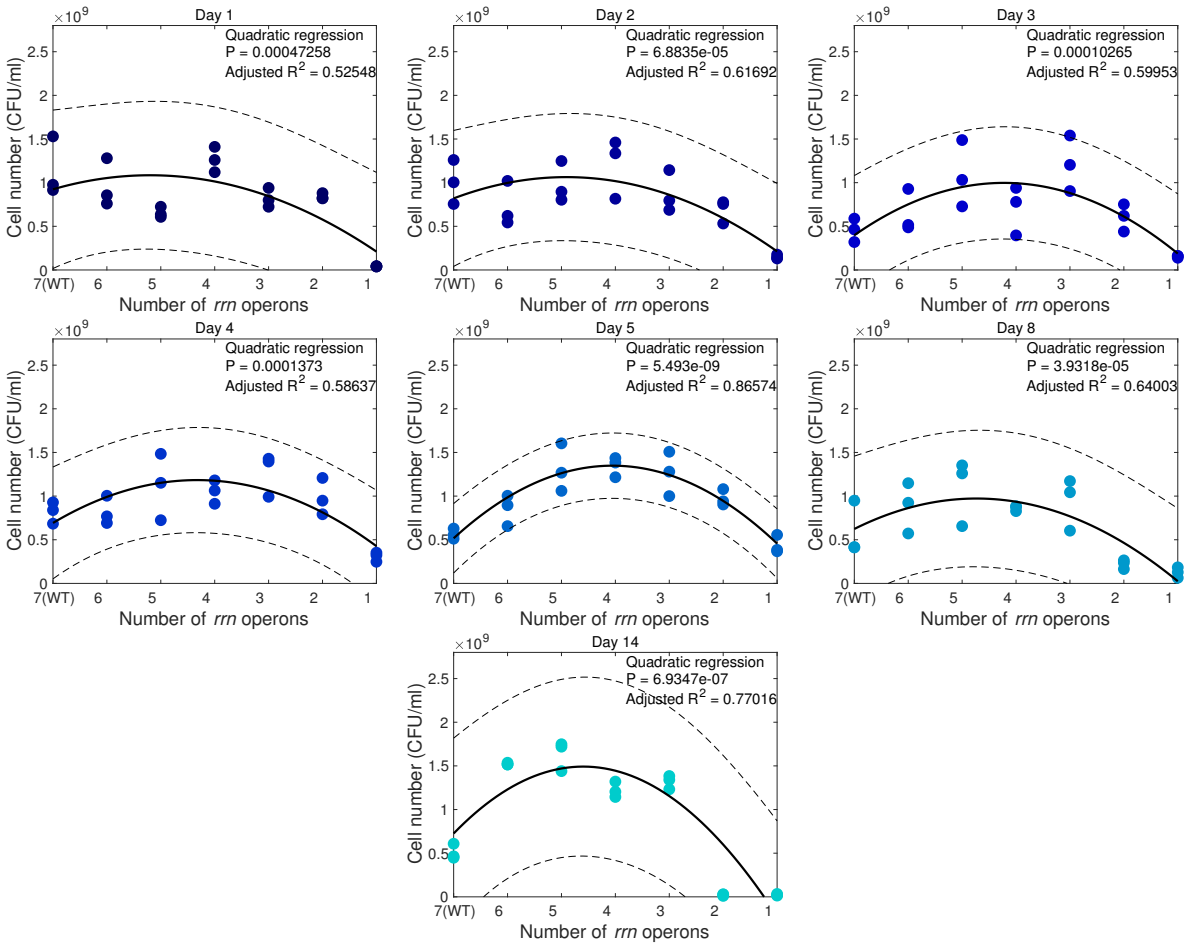

Figure S11: The optimality of *rrn* operon copy number changes over time. Unnormalised cell viability (y axis) is shown as a function of *rrn* operon number (x axis), with different subplots showing different time points. We observe a shift in the optimal *rrn* copy number to strains with fewer *rrn* operons as time progresses. Both linear and quadratic regressions were calculated, with the best fit according to the R^2 value shown. Regressions are shown as solid lines, with $\pm$ estimated 95% confidence intervals (CI, 3 replicates) shown as dashed lines.

10.3 Supplementary data for Chapter 4

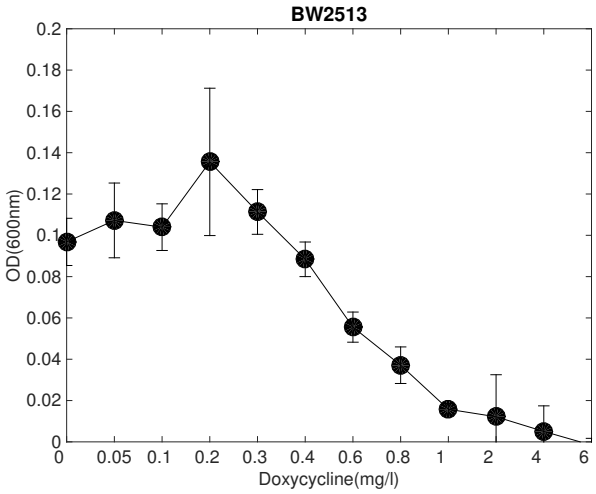

Figure S12: Dose response of *E.coli* BW2513 exposed to a dilution series of doxycycline.

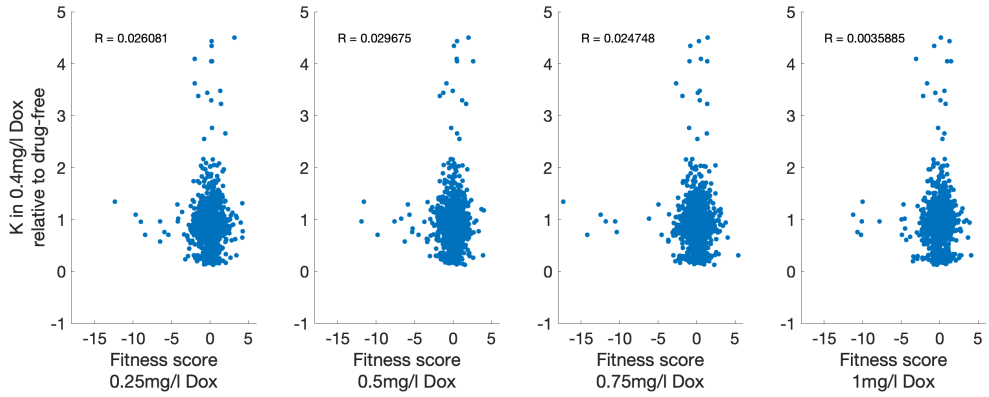

Figure S13: A scatterplot comparing the fitness scores obtained by Nichols et al. [178] for each of the keio strains in 0.25, 0.5, 0.75 and 1mg/l doxycycline against the data obtained here for K (0.4mg/l doxycycline relative to drug-free). Note the poor correlation (as shown by the correlation coefficient, or 'r' value) between K values obtained in this study and the fitness scores for each concentration of doxycycline tested by Nichols et al. It is possible that this lack of correlation is due to the different methods utilised to obtain the data, such as the use of colony size versus OD as a measure of growth, as well as the different media used.

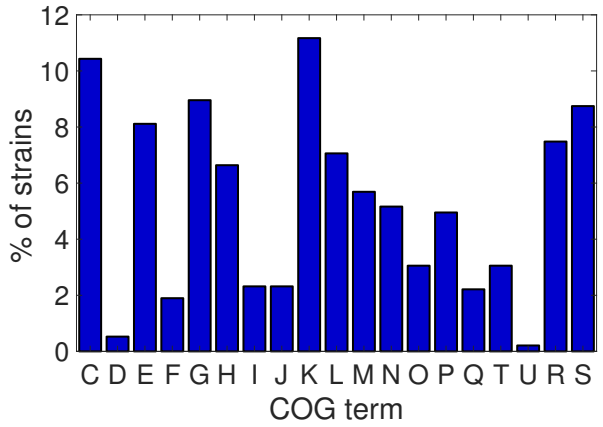

Figure S14: The percentage of knockout genes assinged to a specific COG term from the keio strains utiliised in this study.

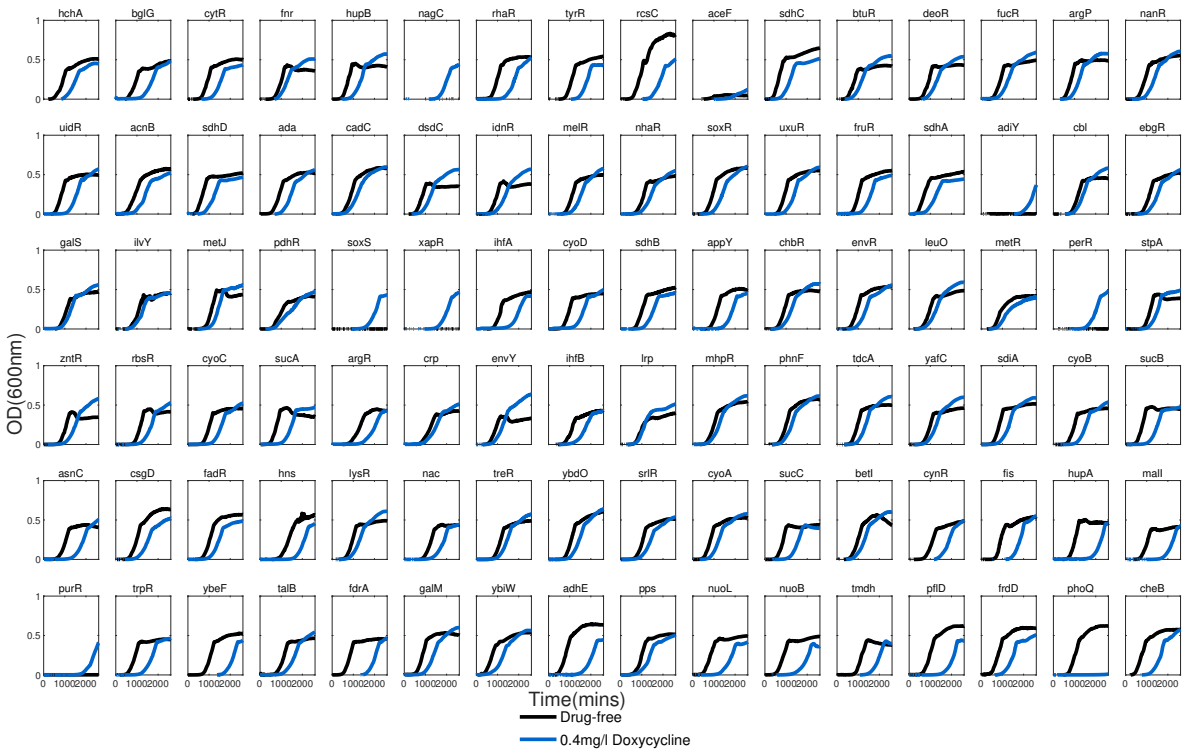

Figure S15: Growth profiles for 96 strains of the *E.coli* keio collection isolates 1-96

Figure S16: Growth profiles for 96 strains of the *E.coli* keio collection isolates 97-192

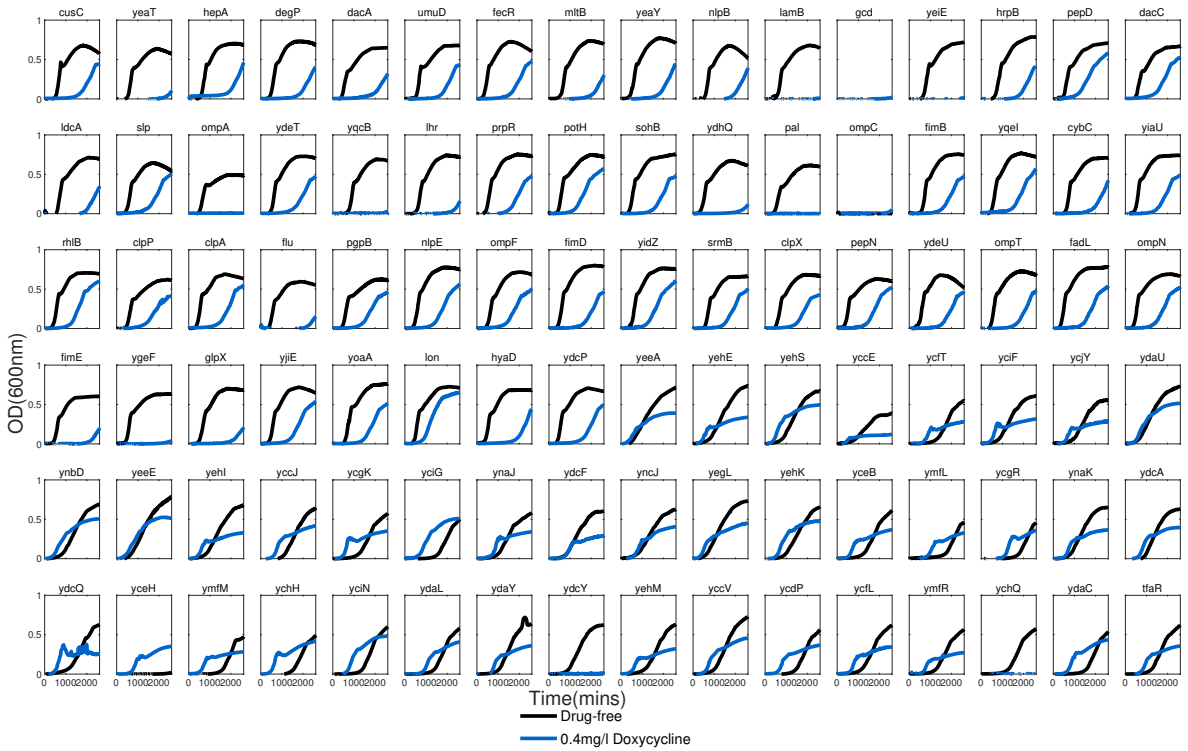

Figure S17: Growth profiles for 96 strains of the *E.coli* keio collection isolates 193-288

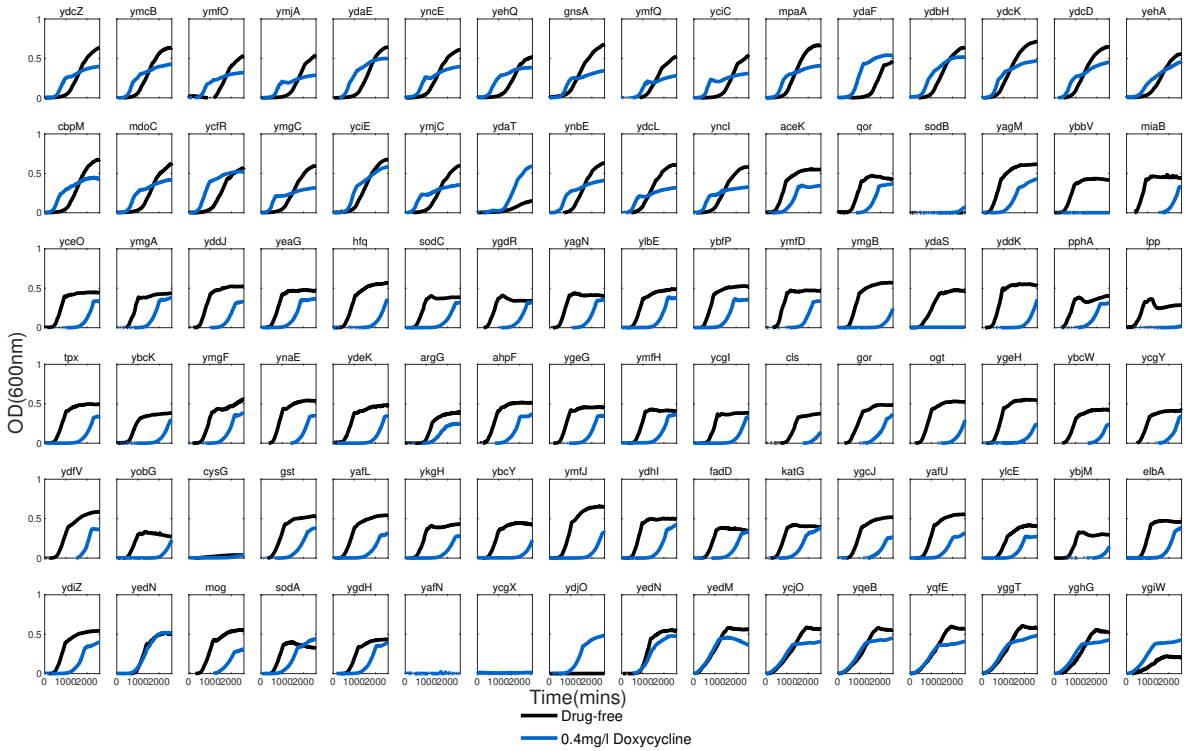

Figure S18: Growth profiles for 96 strains of the *E.coli* keio collection isolates 289-384

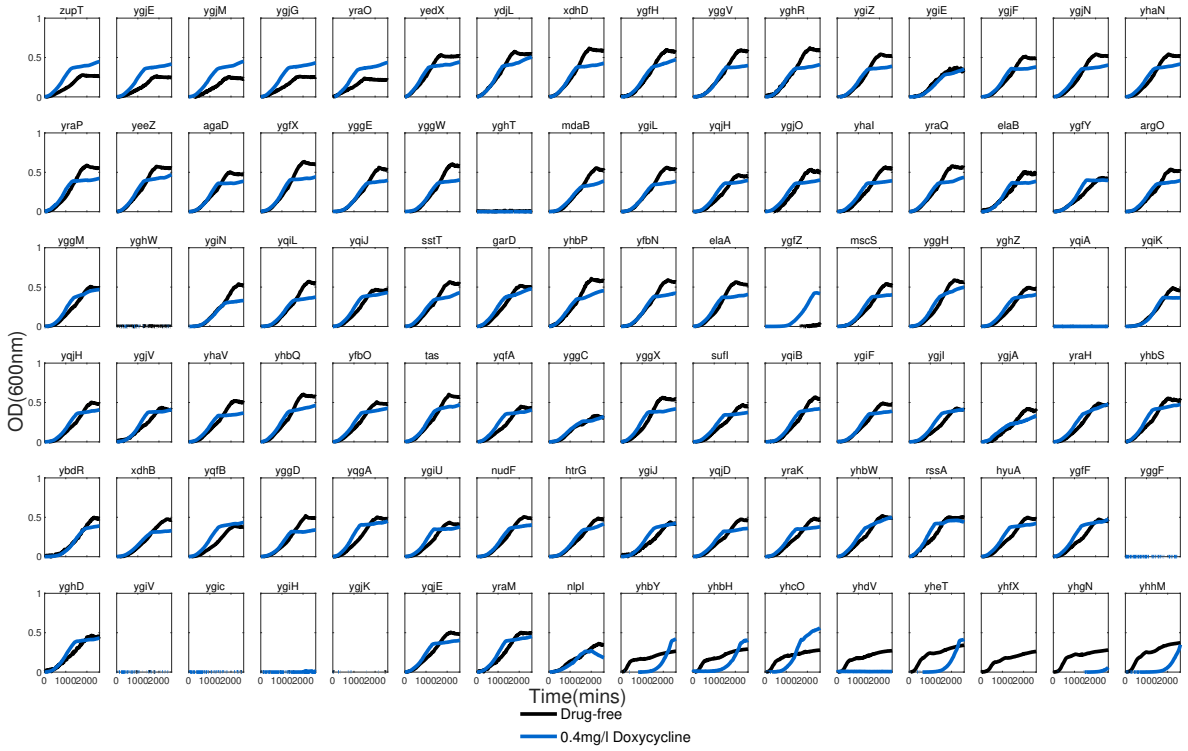

Figure S19: Growth profiles for 96 strains of the *E.coli* keio collection isolates 385-480

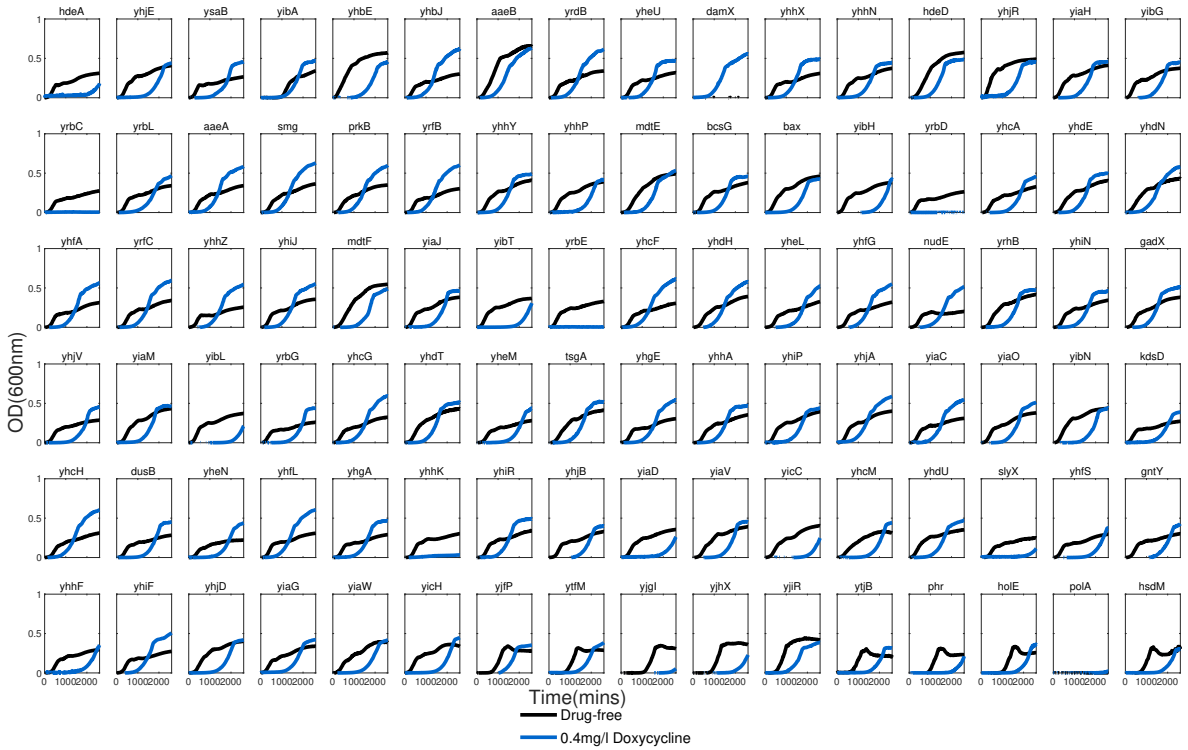

Figure S20: Growth profiles for 96 strains of the *E.coli* keio collection isolates 481-576

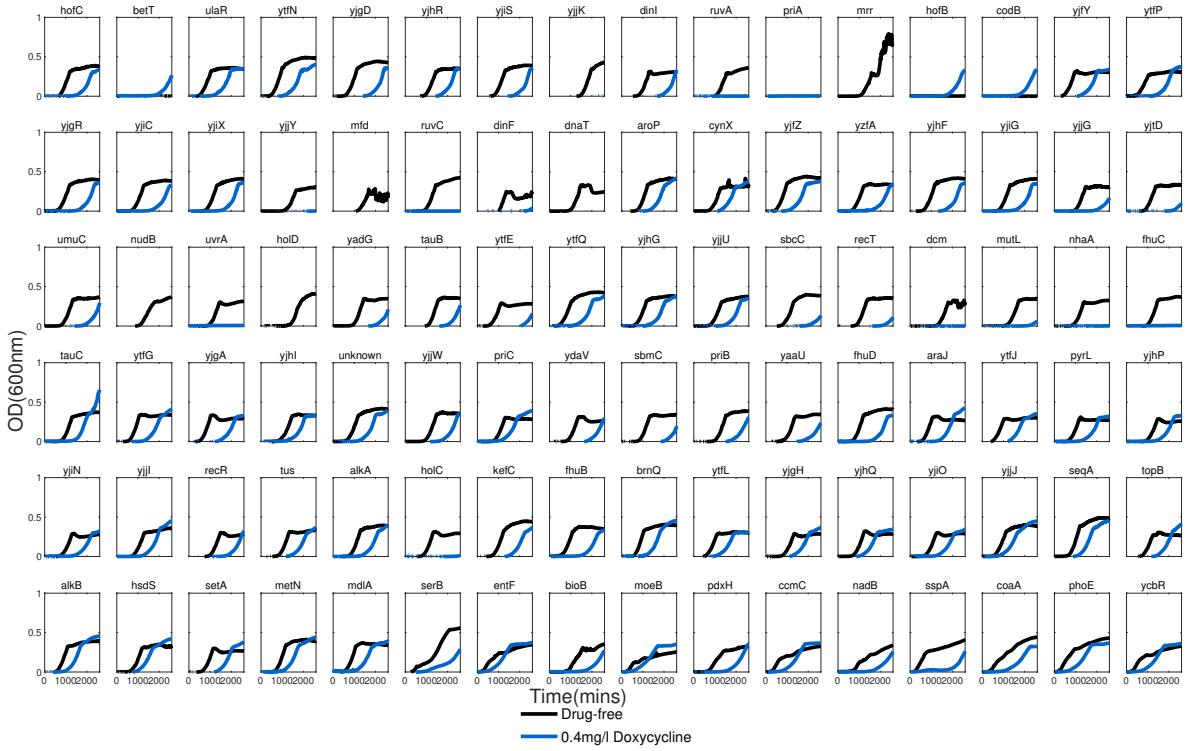

Figure S21: Growth profiles for 96 strains of the *E.coli* keio collection isolates 577-672

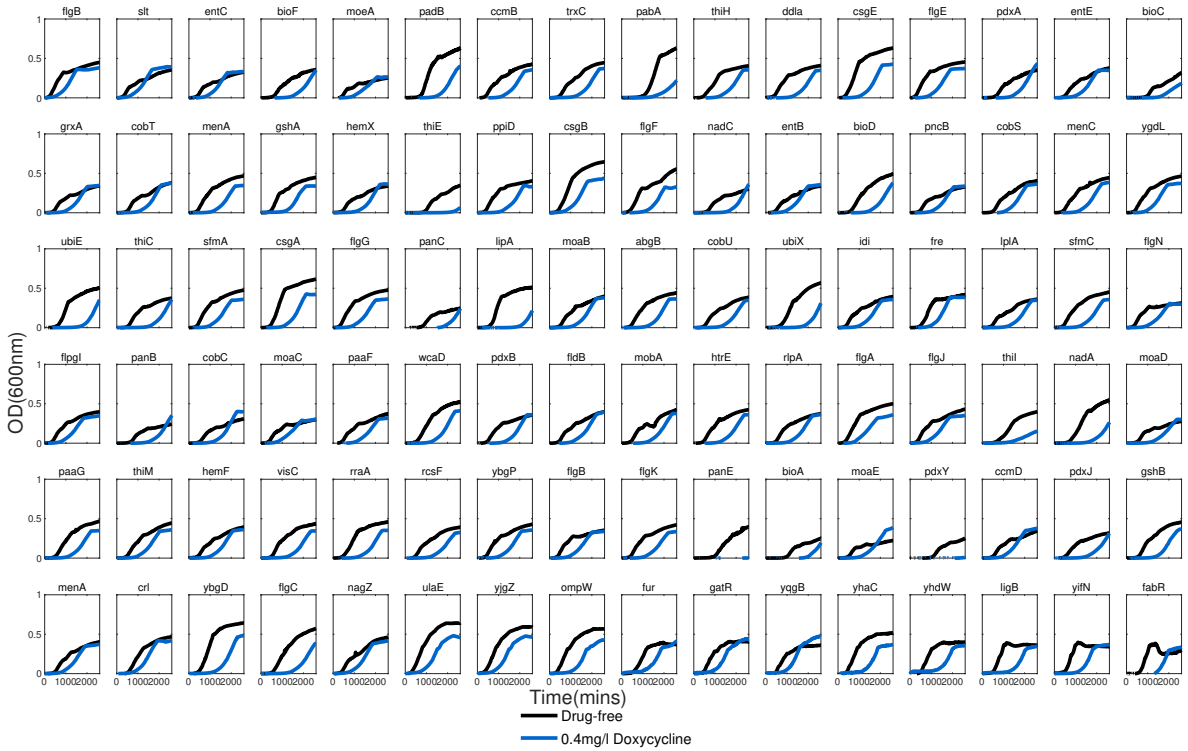

Figure S22: Growth profiles for 96 strains of the *E.coli* keio collection isolates 673-768

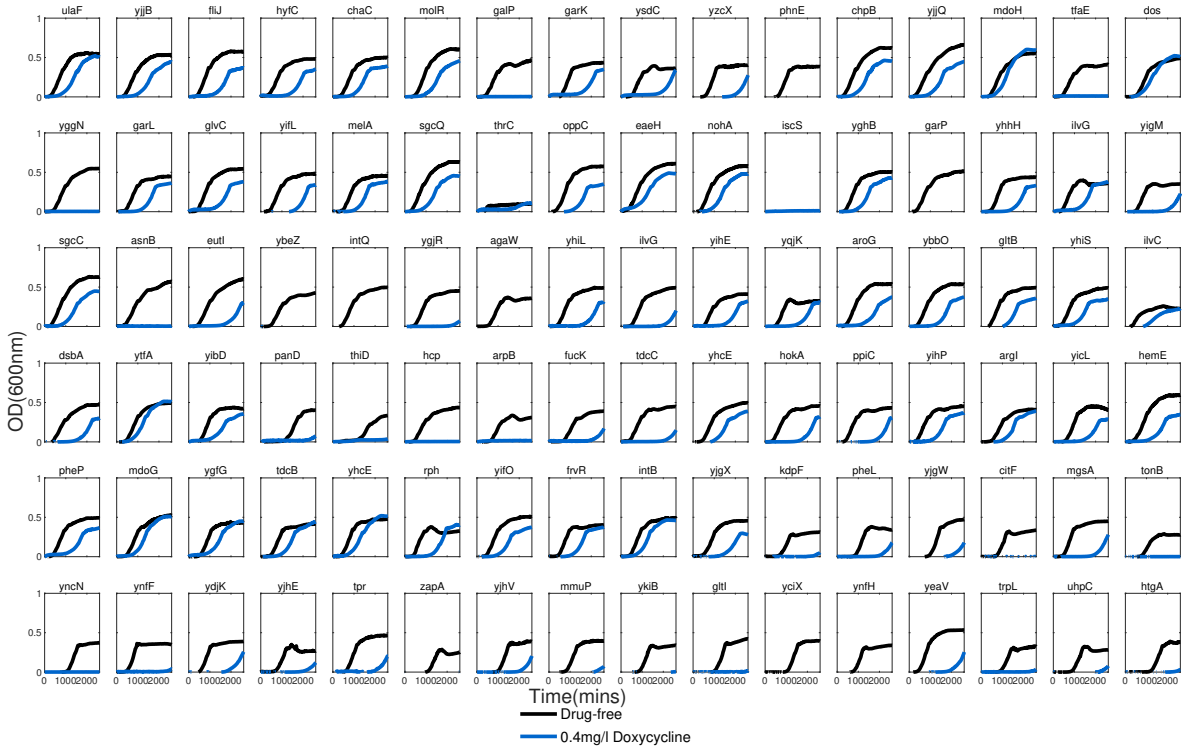

Figure S23: Growth profiles for 96 strains of the *E.coli* keio collection isolates 769-864

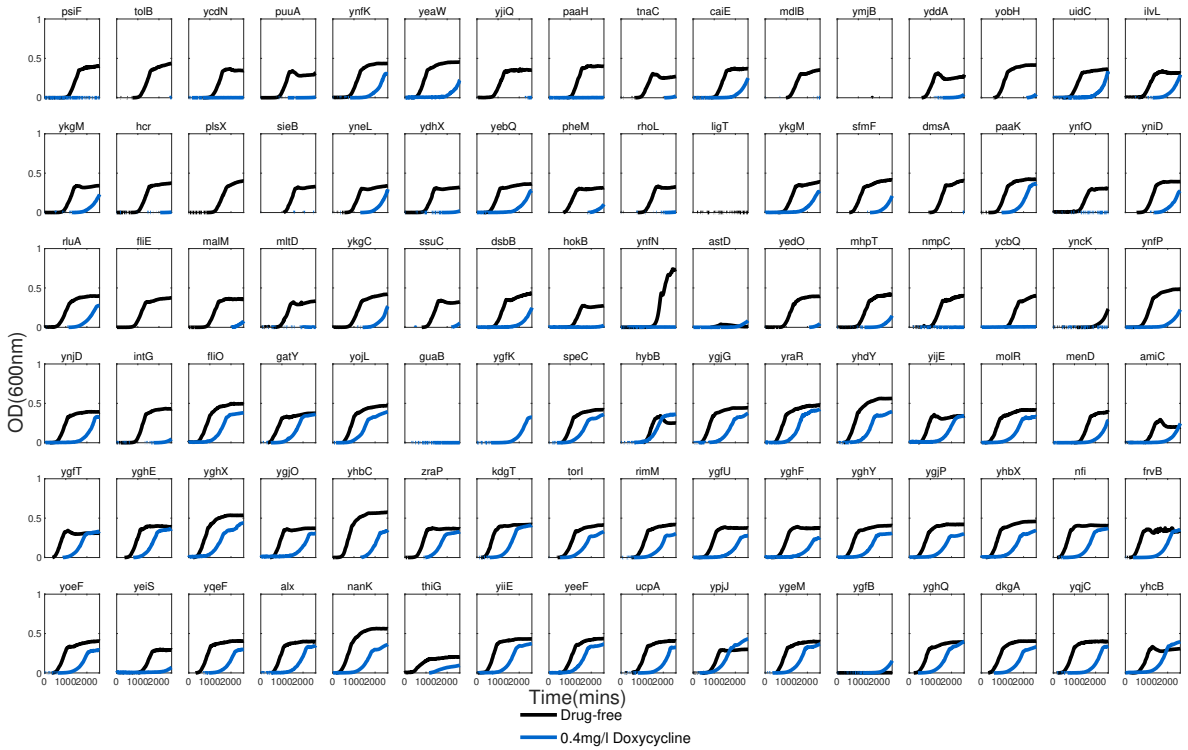

Figure S24: Growth profiles for 96 strains of the *E.coli* keio collection isolates 865-960

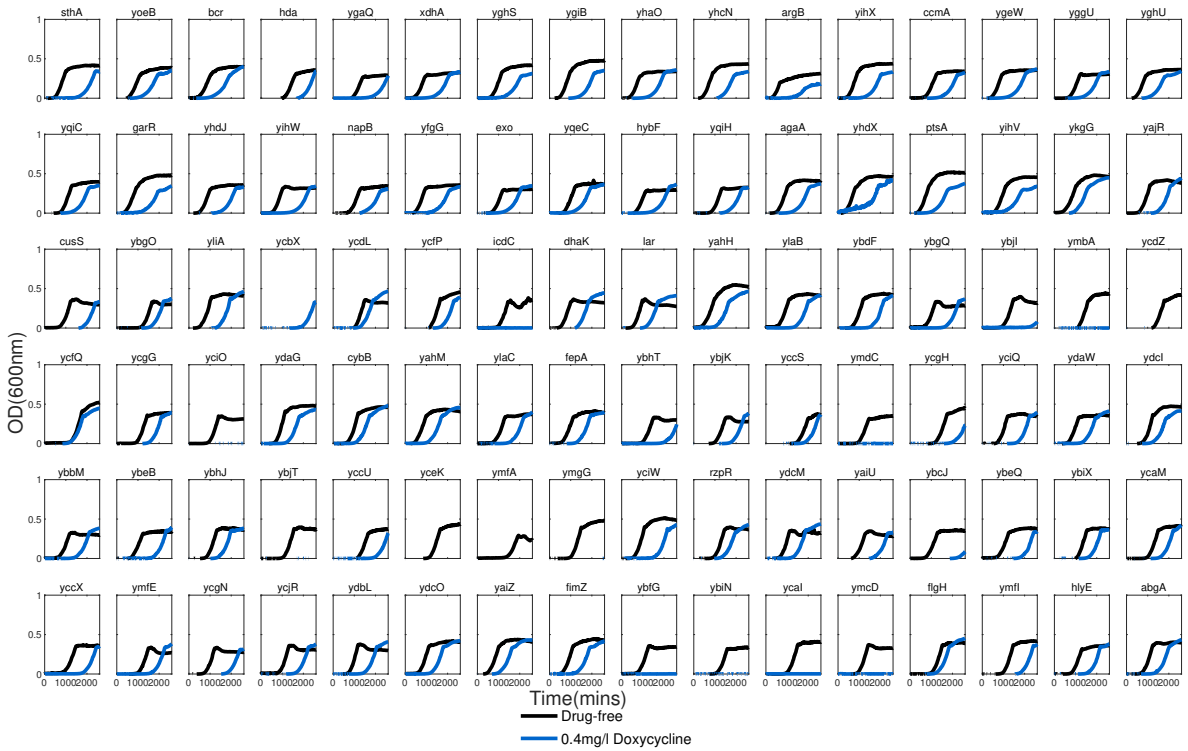

Figure S25: Growth profiles for 96 strains of the *E.coli* keio collection isolates 961-1,056

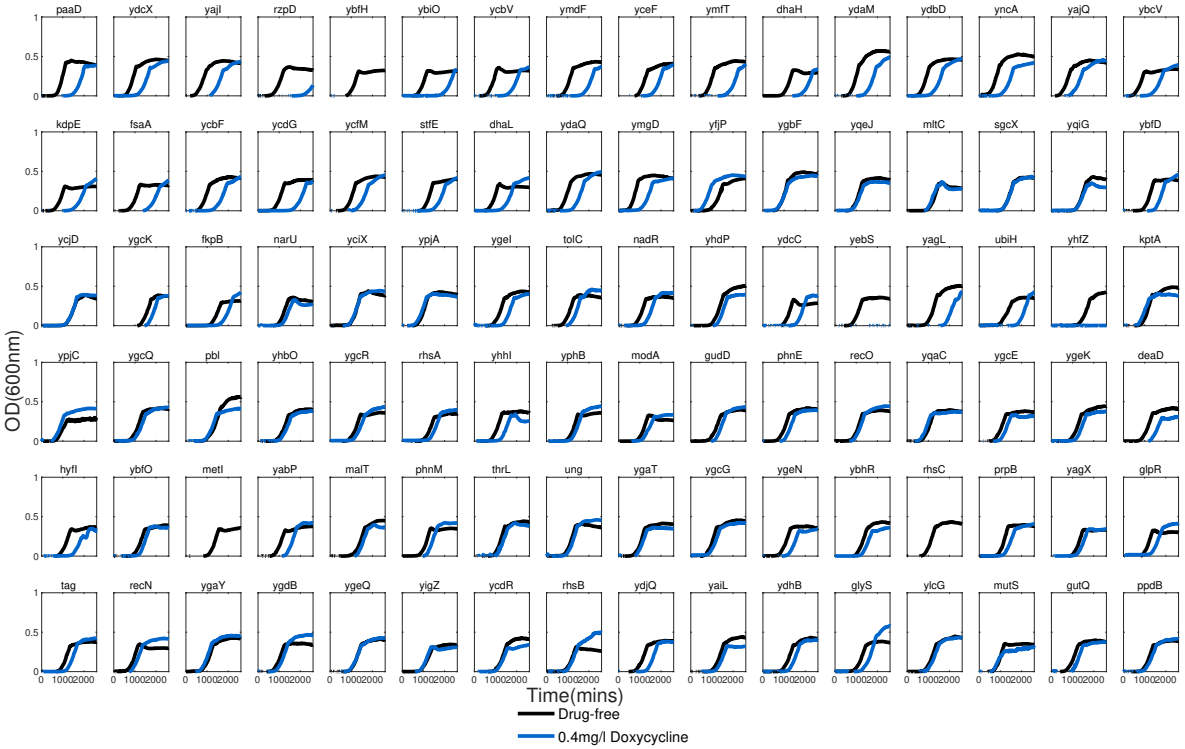

Figure S26: Growth profiles for 96 strains of the *E.coli* keio collection isolates 1,057-1,152

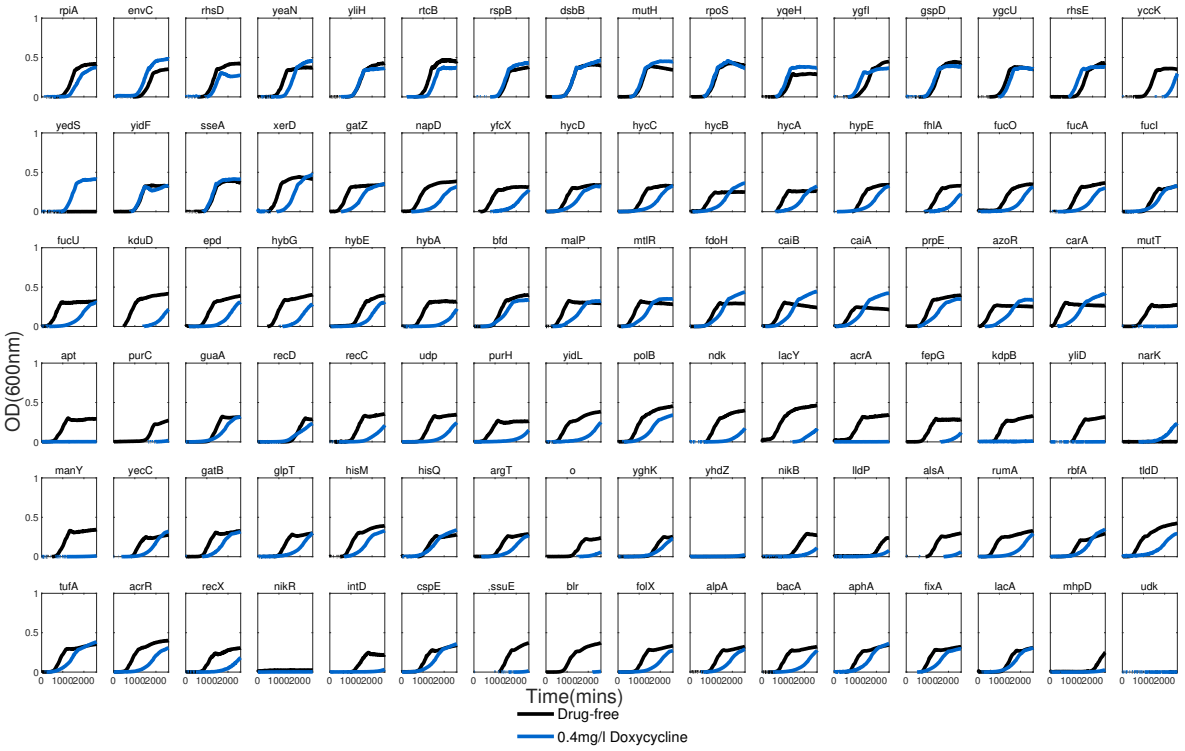

Figure S27: Growth profiles for 96 strains of the *E.coli* keio collection isolates 1,153-1,248

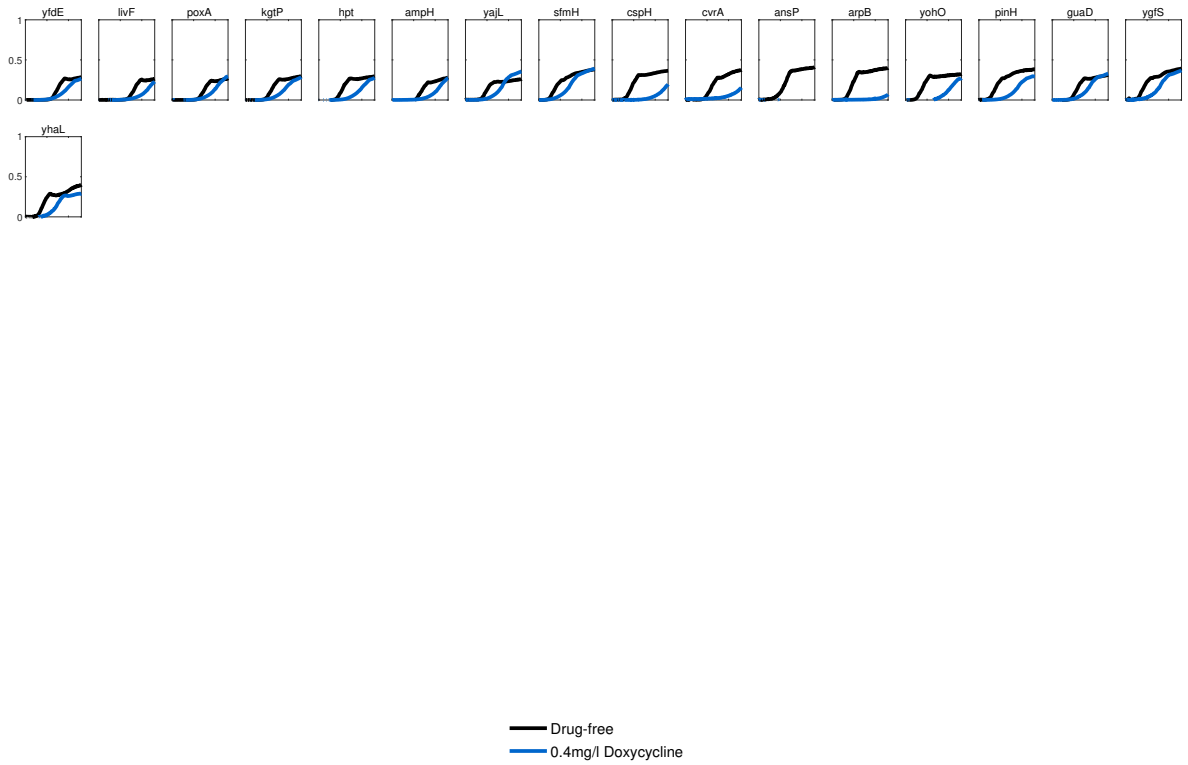

Figure S28: Growth profiles for 17 strains of the *E.coli* keio collection isolates 1,249-1,266

Gene	Function
Δ yafN	Uncharacterised protein
Δ yghW	Uncharacterised protein
Δ ygiV	Probable transcriptional regulator YgiV
Δ ygic	Putative acid–amine ligase YgiC
Δ ygjK	Glucosidase YgjK
Δ ymjB	Uncharacterised protein
Δ dppA	Periplasmic dipeptide transport protein
Δ yghT	Uncharacterized ATP-binding protein YghT
Δ yqiA	Esterase YqiA
Δ ygiH	Probable glycerol-3-phosphate acyltransferase
Δ ygjk	Glucosidase YgjK
Δ priA	Primosomal protein N
Δ guaB	Inosine-5-monophosphate dehydrogenase
Δ udk	Uridine kinase
Δ dpbA	ATP-dependent RNA helices DdpA
Δ gcd	Quinoprotein glucose dehydrogenase
Δ ompC	Outer membrane porin C precursor
Δ cysG	Siroheme synthase
Δ ycgX	Uncharacterised protein
Δ polA	DNA polymerase I
Δ iscC	Thiamine biosynthesis
Δ yhdZ	ATP-binding cassette domain-containing protein
Δ nikR	DNA-binding transcriptional repressor

Table S1: Keio gene knockout strains that failed to grow in either doxycycline or drug-free media.

Gene	Function	Gene	Function
Δ citA	Histidine kinase	Δ trpL	trp operon leader peptide
Δ PhoP	Transcriptional regulatory protein PhoP	Δ ntgA	Uncharacterised protein
Δ ppdD	PpdD protein	Δ psiF	Phosphate starvation-inducible protein PsiF
Δ rseA	Anti-sigma-E factor RseA	Δ tolB	Tol-Pal system protein TolB precurser
Δ lamB	Maltoporin precursor	Δ ycdN	Putative inactive ferrous iron permease EfeU
Δ yeiE	Uncharacterised protein	Δ puuA	Gamma-glutamylputrescine synthetase
Δ yqcB	tRNA pseudouridine synthase C	Δ yjiQ	Putative inactive recombination-promoting nuclease-like protein YjiQ
Δ ompA	Outer membrane protein A	Δ paaH	3-hydroxyadipyl-CoA dehydrogenase
Δ pal	Peptidoglycan-associated lipoprotein	Δ tnaC	Tryptophanase operon leader peptide
Δ yqeF	Uncharacterised protein	Δ mdlB	Multidrug resistance-like ATP-binding protein MdlB
Δ ydcY	Pyruvate formate-lyase 1-activating enzyme	Δ yddA	ABC transporter ATP-binding protein
Δ ychQ	Predicted transcriptional regulator	Δ yobH	Uncharacterised protein
Δ ybbV	Uncharacterized protein	Δ hcr	HCP oxidoreductase
Δ ydaS	Uncharacterized protein	Δ plsX	Phosphate acyltransferase
Δ yhdV	Uncharacterised protein	Δ sieB	Superinfection exclusion protein B
Δ yhfX	Uncharacterised protein	Δ rhoL	rho operon leader peptide
Δ yrbC	Uncharacterised protein	Δ yhdX	Uncharacterised protein
Δ yrbD	Intermembrane phospholipid transport system binding protein MlaD	Δ dmsA	Dimethyl sulfoxide reductase DmsA
Δ yrbE	Intermembrane phospholipid transport system permease protein MlaE	Δ ynfO	Uncharacterized protein
Δ yjjK	Energy-dependent translational throttle protein EttA	Δ fliE	Flagellar hook-basal body complex protein FliE
Δ yhhK	PanD regulatory factor	Δ mltD	Membrane-bound lytic murein transglycosylase D
Δ ruvA	Holiday junction ATP-dependent DNA helicase	Δ hokB	Toxic protein HokB
Δ mrr	Mrr restriction system protein	Δ ynfN	Uncharacterized protein
Δ yjjY	Uncharacterized protein	Δ yedO	Uncharacterised protein
Δ mfD	Transcriptional repair coupling factor	Δ nmpC	Putative outer membrane porin protein NmpC
Δ ruvC	Crossover junction endodeoxyribonuclease	Δ ycbQ	Fimbrial subunit ElfA
Δ dnaT	Primosomal protein 1	Δ yncK	IS609 transposase
Δ nudB	Dihydroneopterin triphosphate	Δ intG	Uncharacterised protein
Δ uvrA	UvrABC system protein A	Δ rcdC	Uncharacterised protein
Δ holD	DNA polymerase III subunit psi	Δ icdC	Uncharacterised protein
Δ dcm	tRNA sulfurtransferase	Δ ymbA	Uncharacterised protein
Δ nhaA	Na(+)/H(+) antiporter NhaA	Δ ycdZ	Inner membrane protein YcdZ
Δ fhuC	Iron(3+)-hydroxamate import ATP-binding protein	Δ yciO	Uncharacterised protein
Δ holC	DNA polymerase III subunit chi	Δ ymdC	Cardiolipin synthase C
Δ panE	2-dehydropantoate 2-reductase	Δ ycjT	Kojibiose phosphorylase
Δ galP	Galactose-proton symporter	Δ yceK	Uncharacterized protein
Δ phnE	Putative cryptic phosphonate transport system permease protein PhnE2	Δ ymfA	Inner membrane protein YmfA
Δ tfaE	Predicted tail fibre assembly protein	Δ ymgG	UPF0757 protein YmgG
Δ yggN	Uncharacterized protein	Δ ybfG	Uncharacterized protein
Δ garP	Probable galactarate transporter	Δ ybiN	Ribosomal RNA large subunit methyltransferase F
Δ agaW	PTS-system	Δ ycaI	Uncharacterized protein
Δ asnB	Asparagine synthetase B	Δ ymcD	Threonine-rich inner membrane protein GfcA
Δ ybeZ	Endoribonuclease YbeY	Δ ybfH	Uncharacterized transporter YbhF
Δ intQ	Putative defective protein IntQ	Δ yebS	Intermembrane transport protein YebS
Δ thiD	Hydoxymethlypyrimidine/phosphomethylpyrimidine kinase	Δ rhsC	Protein RhsC
Δ hcp	Hydroxylamine reductase	Δ metI	D-methionine transport system permease protein
Δ arpB	Uncharacterised protein	Δ mktT	Uncharacterised protein
Δ citF	Citrate lyase alpha chain	Δ apt	Adenine phosphoribosyltransferase
Δ tonB	Protein TonB	Δ purC	Phosphoribosylaminoimidazole-succinocarboxamide synthase
Δ yncN	Uncharacterized protein	Δ acrA	Multidrug efflux pump subunit AcrA
Δ ynfF	Uncharacterised protein	Δ kdpB	Potassium-transporting ATPase ATP-binding subunit
Δ zapA	Cell division protein ZapA	Δ yliD	Glutathione transport system permease protein GsiD
Δ ykiB	Uncharacterised protein	Δ manY	PTS system mannose-specific EIIC component
Δ gltI	Glutamate/aspartate import solute-binding protein	Δ intD	Prophage DLP12 integrase
Δ yciX	Uncharacterized protein	Δ ssuE	FMN reductase (NADPH)
Δ ynfH	Oxidoreductase	Δ blr	Blr protein
Δ ansP	L-asparagine permease	Δ mhpD	2-keto-4-pentenoate hydratase

Table S2: Keio gene knockout strains that only grew in drug-free media, not in the presence of doxycycline.

Genes	Functions
Δ nagC	N-acetylglucosamine repressor
Δ adiY	HTH-type transcriptional regulator AdiY
Δ soxS	Regulatory protein SoxS
Δ xapR	HTH-type transcriptional regulator XapR
Δ perR	HTH-type transcriptional regulator PerR
Δ purR	HTH-type transcriptional repressor PurR
Δ yceH	Uncharacterised protein
Δ sodB	Superoxide dismutase [Fe]
Δ ydjO	Uncharacterised protein
Δ ygfZ	tRNA-modifying protein
Δ damX	Cell division protein DamX
Δ betT	High-affinity choline transport protein
Δ hofB	Protein transport protein HofB homolog
Δ codB	Cytosine permease
Δ ygfK	Uncharacterised protein
Δ ygfB	Uncharacterised protein
Δ ycbX	Sulfite reductase [NADPH] flavoprotein alpha-component
Δ yedS	Putative outer membrane protein
Δ narK	Nitrate/nitrite transporter NarK

Table S3: Keio gene knockout strains that grew only in media containing doxycycine, but not in drug-free media.

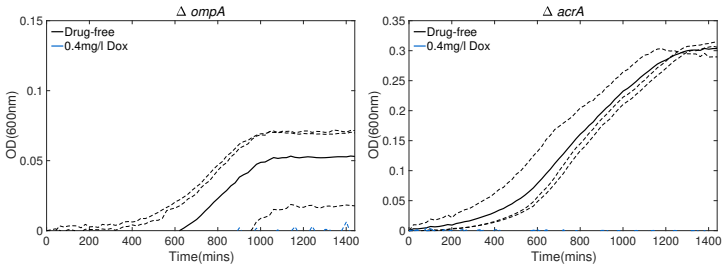

(a) (b)

Figure S29: Replicates of keio strains found to be hypersensitive to doxycycline relative to drug-free conditions. *n=3*

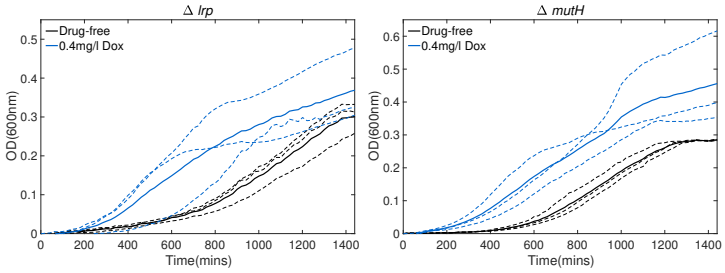

(a) (b)

Figure S30: Replicates of keio super strains - strains found to have a shorter lag and also larger K with doxycycline relative to drug-free conditions. *n=3*.

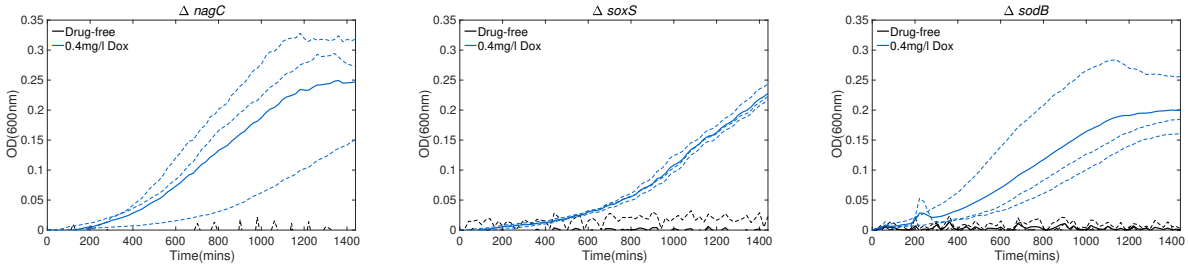

(a) (b) (c)

Figure S31: Replicates of keio strains that only grow in the presence of doxycycline. *n=3*

10.4 Supplementary data for Chapter 5

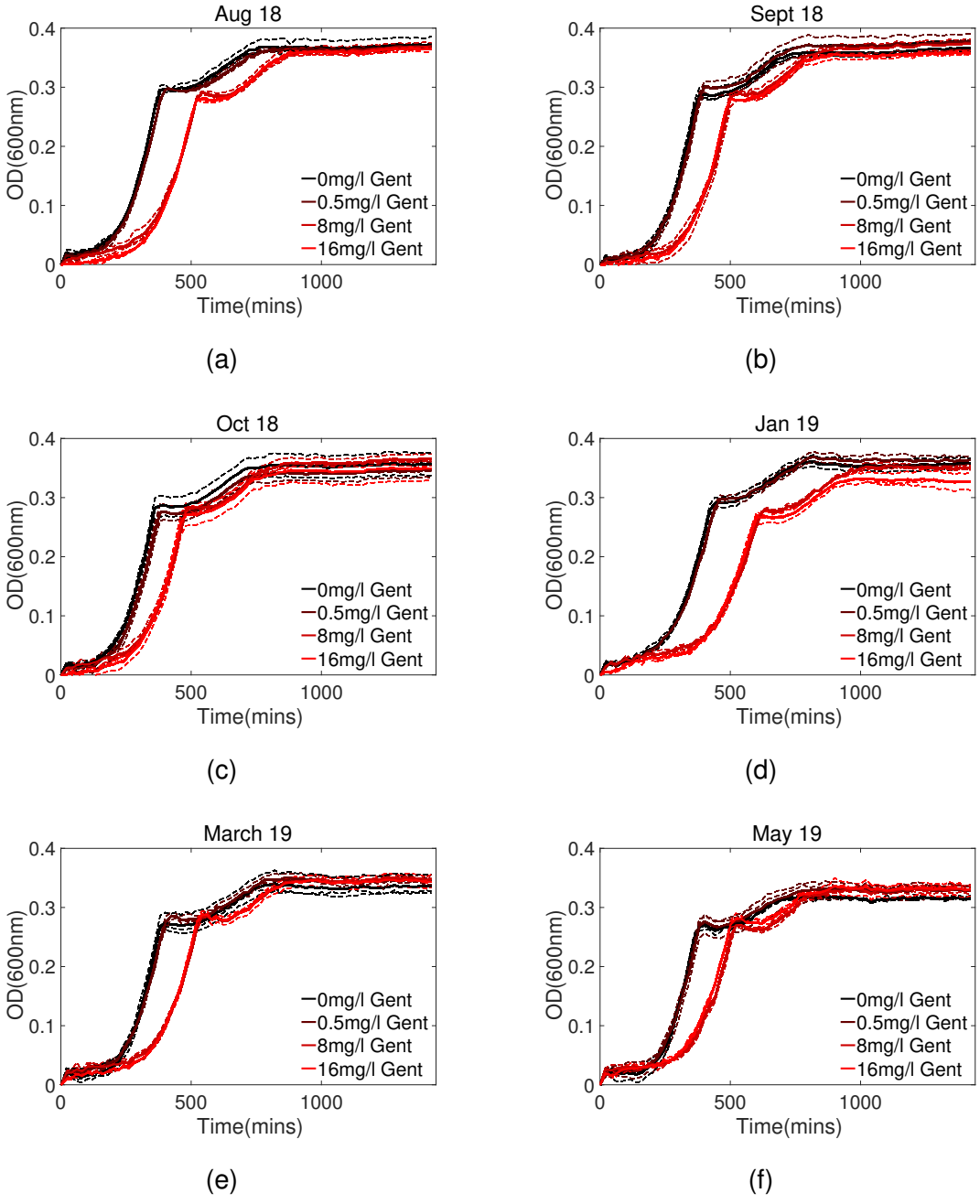

Figure S32: The growth of the six *K.pneumoniae* isolates in response to Gentamcin over 24 hours. Every strain was found to grow up to 16mg/l of gentamicin, in disagreement with the clinical data. Growth was measured as OD_{600nm}. *n=3*

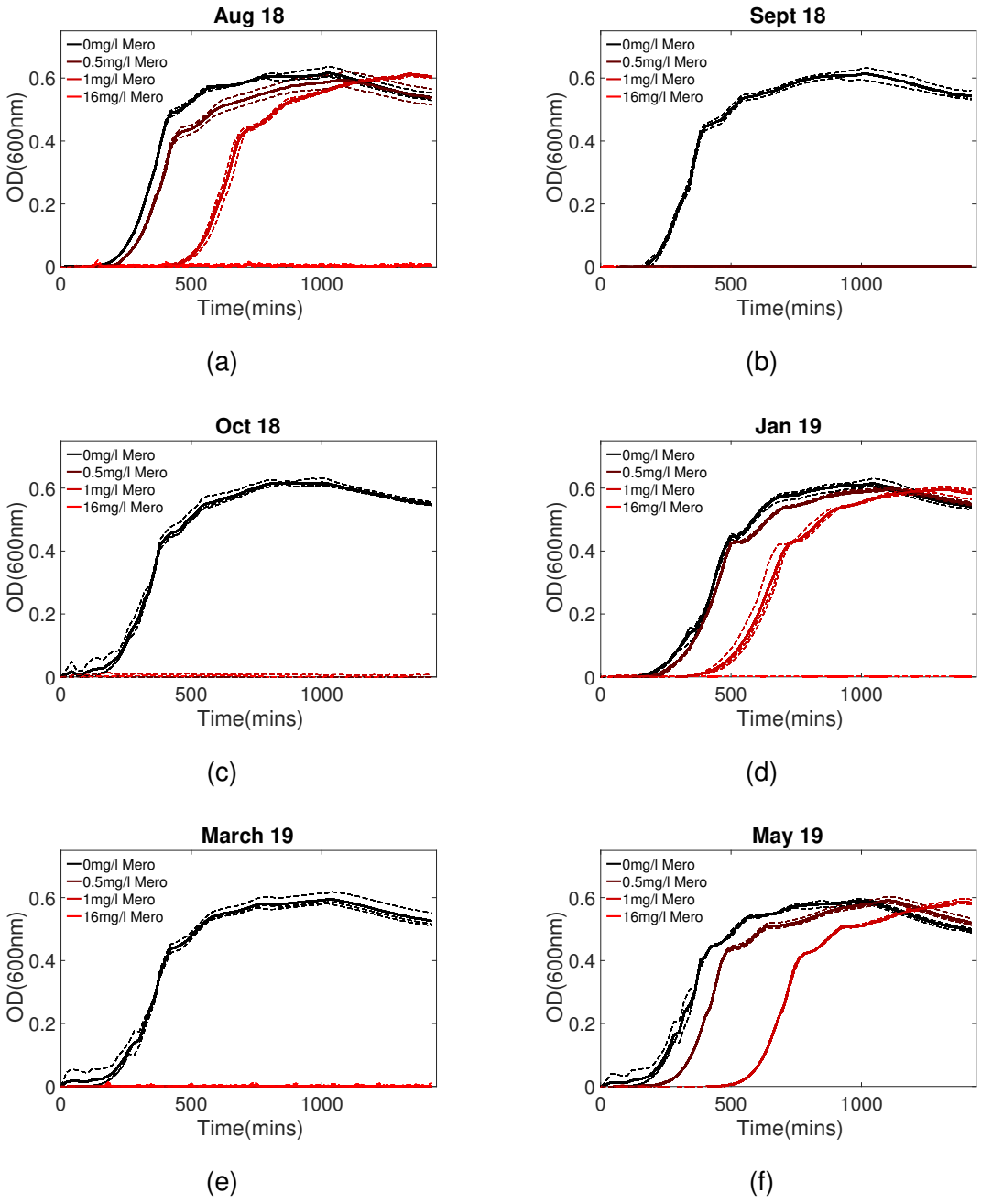

Figure S33: The growth of the six *K.pneumoniae* isolates in response to Meropenem over 24 hours. Whilst the isolates form August 2018, January 2019 and May 2019 all grow up to 1mg/l meropenem, the isolates from September 2018, October 2018 and March 2019 were only able to grow in drug-free conditions. In the strains that grow in meropenem, lag time is extended relative to the drug-free populations, but the final population density is not reduced. Growth was measured as OD_{600nm}. *n=3*

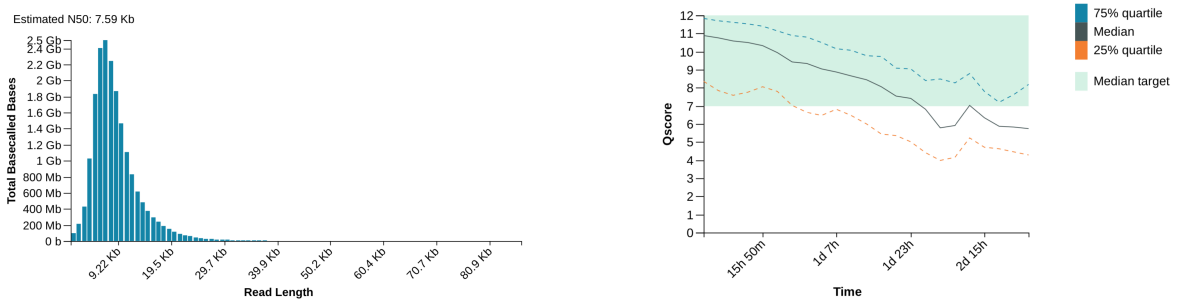

(a) (b)

Figure S34: The distribution of read lengths (a) and changes in Qscore (b) from a 40 hour GridION sequence run with 12 multiplexed *K.pneumoniae* samples.

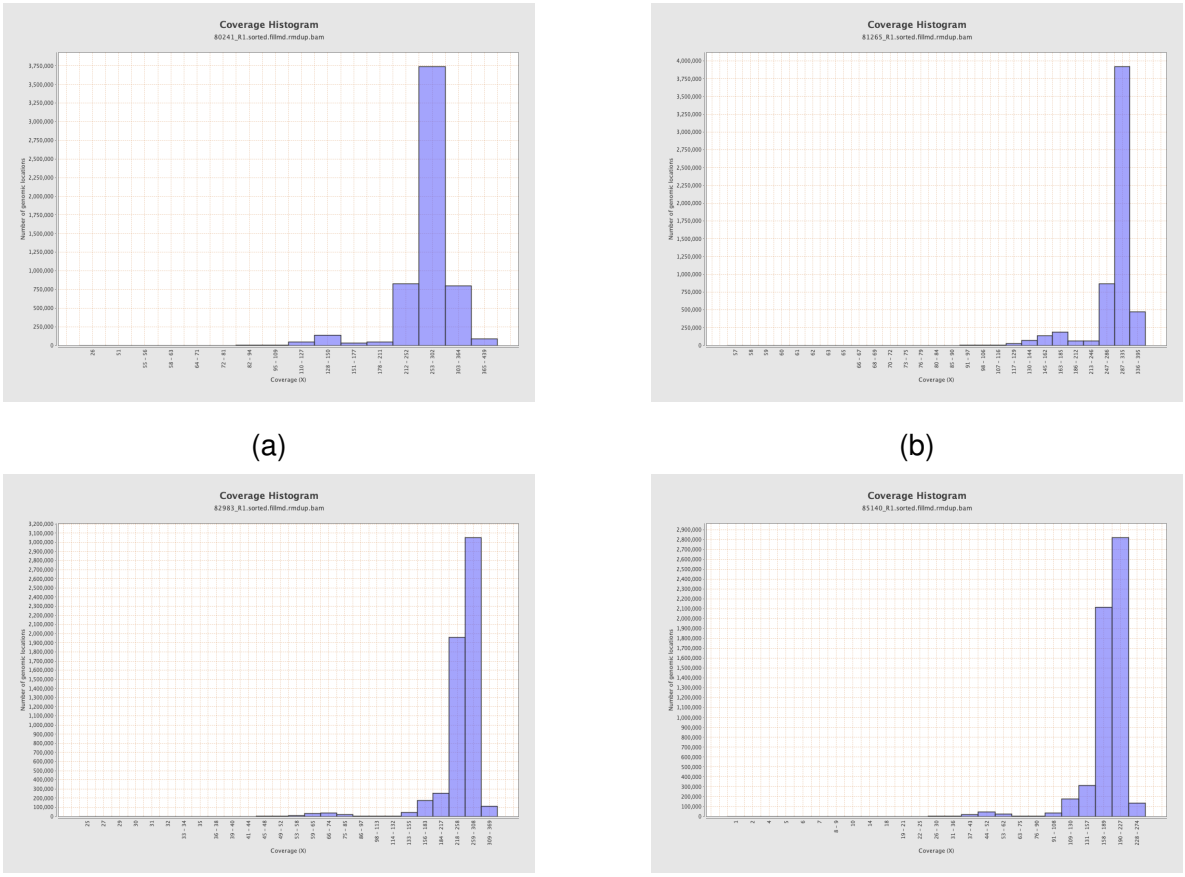

(a) (b)

(c) (d)

Figure S35: Histograms showing the distribution of coverage across genomic locations in the isolates KP1 (a), KP2 (b), KP3 (c) and KP4 (d). Obtained using qualimap.

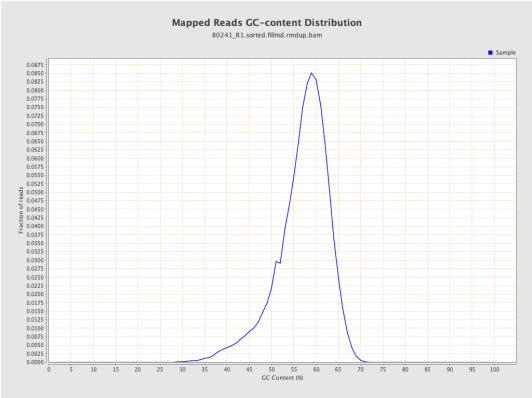

(a)

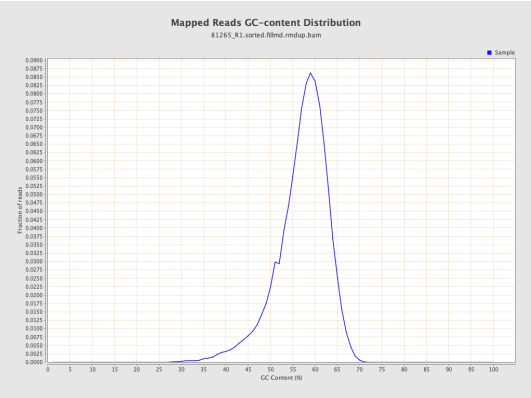

(b)

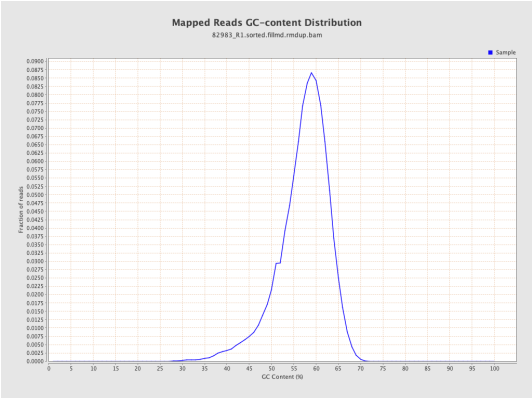

(c)

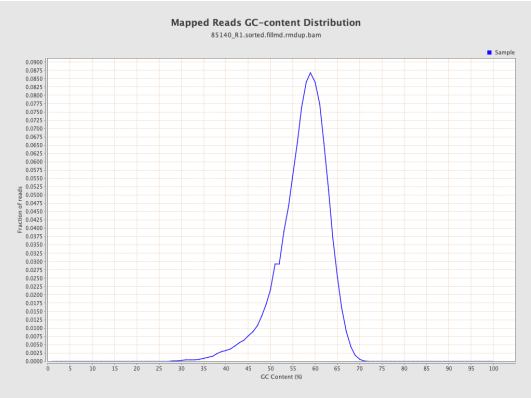

(d)

Figure S36: Histograms showing the distribution of GC content across all mapped reads in the isolates KP1 (a), KP2 (b), KP3 (c) and KP4 (d). Obtained using qualimap.

Antimicrobial	Class	WGS predicted phenotype	Genetic background
ciprofloxacin	fluoroquinolone	Resistant	oqxB oqxA aac(6)-Ib-cr
nalidixic acid	fluoroquinolone	Resistant	oqxB oqxA
chloramphenicol	phenicol	Resistant	catB3 catA1
netilmicin	aminoglycoside	Resistant	armA aac(6)-Ib-cr
dibekacin	aminoglycoside	Resistant	aac(6)-Ib-cr
sisomicin	aminoglycoside	Resistant	aac(6)-Ib-cr
isepamicin	aminoglycoside	Resistant	armA
streptomycin	aminoglycoside	Resistant	aadA2
tobramycin	aminoglycoside	Resistant	armA aac(6)-Ib-cr
amikacin	aminoglycoside	Resistant	armA aac(6)-Ib-cr
gentamicin	aminoglycoside	Resistant	armA
erythromycin	macrolide	Resistant	mph(E) msr(E)
azithromycin	macrolide	Resistant	msr(E)
sulfamethoxazole	folate pathway antagonist	Resistant	sul1
trimethoprim	folate pathway antagonist	Resistant	dfrA14 dfrA1 dfrA12
pristinamycin ia	streptogramin b	Resistant	msr(E)
virginiamycin s	streptogramin b	Resistant	msr(E)
quinupristin	streptogramin b	Resistant	msr(E)
tetracycline	tetracycline	Resistant	tet(D)
doxycycline	tetracycline	Resistant	tet(D)
ceftazidime	beta-lactam	Resistant	blaCTX-M-15 blaSHV-106
ampicillin	beta-lactam	Resistant	blaOXA-1 blaTEM-1A blaCTX-M-15 blaSHV-106
cephalothin	beta-lactam	Resistant	blaTEM-1A
amoxicillin	beta-lactam	Resistant	blaOXA-1 blaTEM-1A blaCTX-M-15 blaSHV-106
piperacillin	beta-lactam	Resistant	blaOXA-1 blaTEM-1A blaCTX-M-15 blaSHV-106
aztreonam	beta-lactam	Resistant	blaCTX-M-15 blaSHV-106
cefotaxime	beta-lactam	Resistant	blaCTX-M-15 blaSHV-106
cefepime	beta-lactam	Resistant	blaOXA-1blaCTX-M-15 blaSHV-106
amoxicillin+clavulanic acid	beta-lactam	Resistant	blaOXA-1
ticarcillin	beta-lactam	Resistant	blaTEM-1A blaCTX-M-15 blaSHV-106
ceftriaxone	beta-lactam	Resistant	blaCTX-M-15 blaSHV-106
piperacillin+tazobactam	beta-lactam	Resistant	blaOXA-1
fosfomycin	fosfomycin	Resistant	fosA
spectinomycin	aminocyclitol	Resistant	aadA2
cephalosporins	under_development	Resistant	ompK36 (p.L191S)
fluoroquinolone	under_development	Resistant	aac(6)-Ib-cr
carbapenem	under_development	Resistant	ompK36

Table S4: **KP1 (August 2018)** - Resistance phenotypes predicted from whole genome sequence data by ResFinder.

Antimicrobial	Class	WGS predicted phenotype	Genetic background
ciprofloxacin	fluoroquinolone	Resistant	aac(6)-Ib-cr oqxB oqxA
nalidixic acid	fluoroquinolone	Resistant	oqxB oqxA
chloramphenicol	phenicol	Resistant	catB3 catA1
netilmicin	aminoglycoside	Resistant	armA aac(6)-Ib-cr
dibekacin	aminoglycoside	Resistant	aac(6)-Ib-cr
sisomicin	aminoglycoside	Resistant	aac(6)-Ib-cr
isepamicin	aminoglycoside	Resistant	armA
streptomycin	aminoglycoside	Resistant	aadA2
tobramycin	aminoglycoside	Resistant	armA aac(6)-Ib-cr
amikacin	aminoglycoside	Resistant	armA aac(6')-Ib-cr
gentamicin	aminoglycoside	Resistant	armA
erythromycin	macrolide	Resistant	msr(E) mph(E)
azithromycin	macrolide	Resistant	msr(E)
sulfamethoxazole	folate pathway antagonist	Resistant	sul1
trimethoprim	folate pathway antagonist	Resistant	dfrA12 dfrA14 dfrA1
pristinamycin ia	streptogramin b	Resistant	msr(E)
virginiamycin s	streptogramin b	Resistant	msr(E)
quinupristin	streptogramin b	Resistant	msr(E)
tetracycline	tetracycline	Resistant	tet(D)
doxycycline	tetracycline	Resistant	tet(D)
ceftazidime	beta-lactam	Resistant	blaSHV-106 blaCTX-M-15
ampicillin	beta-lactam	Resistant	blaOXA-1 blaTEM-1A blaSHV-106 blaCTX-M-15
cephalothin	beta-lactam	Resistant	blaTEM-1A
amoxicillin	beta-lactam	Resistant	blaOXA-1 blaTEM-1A blaSHV-106 blaCTX-M-15
piperacillin	beta-lactam	Resistant	blaOXA-1 blaTEM-1A blaSHV-106 blaCTX-M-15
aztreonam	beta-lactam	Resistant	blaSHV-106 blaCTX-M-15
cefotaxime	beta-lactam	Resistant	blaSHV-106 blaCTX-M-15
cefepime	beta-lactam	Resistant	blaOXA-1 blaSHV-106 blaCTX-M-15
amoxicillin+clavulanic acid	beta-lactam	Resistant	blaOXA-1
ticarcillin	beta-lactam	Resistant	blaTEM-1A blaSHV-106 blaCTX-M-15
ceftriaxone	beta-lactam	Resistant	blaSHV-106 blaCTX-M-15
piperacillin+tazobactam	beta-lactam	Resistant	blaOXA-1
fosfomycin	fosfomycin	Resistant	fosA
spectinomycin	aminocyclitol	Resistant	aadA2
cephalosporins	under_development	Resistant	ompK36
fluoroquinolone	under_development	Resistant	aac(6)-Ib-cr
carbapenem	under_development	Resistant	ompK36 ompK37

Table S5: **KP2 (Oct 2018)** - Resistance phenotypes predicted from whole genome sequence data by ResFinder.

Antimicrobial	Class	WGS-predicted phenotype	Genetic background
ciprofloxacin	fluoroquinolone	Resistant	oqxA oqxB aac(6)-Ib-cr
nalidixic acid	fluoroquinolone	Resistant	oqxA oqxB
chloramphenicol	phenicol	Resistant	catB3
netilmicin	aminoglycoside	Resistant	armA aac(6)-Ib-cr
dibekacin	aminoglycoside	Resistant	aac(6)-Ib-cr
sisomicin	aminoglycoside	Resistant	aac(6)-Ib-cr
isepamicin	aminoglycoside	Resistant	armA
streptomycin	aminoglycoside	Resistant	aadA2
tobramycin	aminoglycoside	Resistant	armA aac(6)-Ib-cr
amikacin	aminoglycoside	Resistant	armA aac(6)-Ib-cr
gentamicin	aminoglycoside	Resistant	armA
erythromycin	macrolide	Resistant	msr(E) mph(E)
azithromycin	macrolide	Resistant	msr(E)
sulfamethoxazole	folate pathway antagonist	Resistant	sul1
trimethoprim	folate pathway antagonist	Resistant	dfrA1 dfrA12 dfrA14
pristinamycin ia	streptogramin b	Resistant	msr(E)
virginiamycin s	streptogramin b	Resistant	msr(E)
quinupristin	streptogramin b	Resistant	msr(E)
tetracycline	tetracycline	Resistant	tet(D)
doxycycline	tetracycline	Resistant	tet(D)
ceftazidime	beta-lactam	Resistant	blaSHV-106 blaCTX-M-15
ampicillin	beta-lactam	Resistant	blaTEM-1A blaSHV-106 blaOXA-1 blaCTX-M-15
cephalothin	beta-lactam	Resistant	blaTEM-1A
amoxicillin	beta-lactam	Resistant	blaTEM-1A blaSHV-106 blaOXA-1 blaCTX-M-15
piperacillin	beta-lactam	Resistant	blaTEM-1A blaSHV-106 blaOXA-1 blaCTX-M-15
aztreonam	beta-lactam	Resistant	blaSHV-106 blaCTX-M-15
cefotaxime	beta-lactam	Resistant	blaSHV-106 blaCTX-M-15
cefepime	beta-lactam	Resistant	blaSHV-106 blaOXA-1 blaCTX-M-15
amoxicillin+clavulanic acid	beta-lactam	Resistant	blaOXA-1
ticarcillin	beta-lactam	Resistant	blaTEM-1A blaSHV-106 blaCTX-M-15
ceftriaxone	beta-lactam	Resistant	blaSHV-106 blaCTX-M-15
piperacillin+tazobactam	beta-lactam	Resistant	blaOXA-1
fosfomycin	fosfomycin	Resistant	fosA
spectinomycin	aminocyclitol	Resistant	aadA2
cephalosporins	under_development	Resistant	ompK36
fluoroquinolone	under_development	Resistant	aac(6)-Ib-cr
carbapenem	under_development	Resistant	ompK37 ompK36

Table S6: **KP3 (Jan 2019)** - Resistance phenotypes predicted from whole genome sequence data by ResFinder.

Antimicrobial	Class	WGS-predicted phenotype	Genetic background
ciprofloxacin	fluoroquinolone	Resistant	aac(6)-Ib-cr oqxB oqxA
nalidixic acid	fluoroquinolone	Resistant	oqxB oqxA
chloramphenicol	phenicol	Resistant	catB3
netilmicin	aminoglycoside	Resistant	aac(6)-Ib-cr armA
dibekacin	aminoglycoside	Resistant	aac(6)-Ib-cr
sisomicin	aminoglycoside	Resistant	aac(6)-Ib-cr
isepamicin	aminoglycoside	Resistant	armA
streptomycin	aminoglycoside	Resistant	aadA2
tobramycin	aminoglycoside	Resistant	aac(6)-Ib-cr armA
amikacin	aminoglycoside	Resistant	aac(6)-Ib-cr armA
gentamicin	aminoglycoside	Resistant	armA
erythromycin	macrolide	Resistant	msr(E) mph(E)
azithromycin	macrolide	Resistant	msr(E)
sulfamethoxazole	folate pathway antagonist	Resistant	sul1
trimethoprim	folate pathway antagonist	Resistant	dfrA12 dfrA14 dfrA1
pristinamycin ia	streptogramin b	Resistant	msr(E)
virginiamycin s	streptogramin b	Resistant	msr(E)
quinupristin	streptogramin b	Resistant	msr(E)
tetracycline	tetracycline	Resistant	tet(D)
doxycycline	tetracycline	Resistant	tet(D)
ceftazidime	beta-lactam	Resistant	blaSHV-106 blaCTX-M-15
ampicillin	beta-lactam	Resistant	blaTEM-1A blaOXA-1 blaSHV-106 blaCTX-M-15
cephalothin	beta-lactam	Resistant	blaTEM-1A
piperacillin	beta-lactam	Resistant	blaTEM-1A blaOXA-1 blaSHV-106 blaCTX-M-15
aztreonam	beta-lactam	Resistant	blaSHV-106 blaCTX-M-15
cefotaxime	beta-lactam	Resistant	blaSHV-106 blaCTX-M-15
cefepime	beta-lactam	Resistant	blaOXA- blaSHV-106 blaCTX-M-15
amoxicillin+clavulanic acid	beta-lactam	Resistant	blaOXA-1
ticarcillin	beta-lactam	Resistant	blaTEM-1A blaSHV-106 blaCTX-M-15
ceftriaxone	beta-lactam	Resistant	blaSHV-106 blaCTX-M-15
piperacillin+tazobactam	beta-lactam	Resistant	blaOXA-1
fosfomycin	fosfomycin	Resistant	fosA
spectinomycin	aminocyclitol	Resistant	aadA2
cephalosporins	under_development	Resistant	ompK36 ompK36
fluoroquinolone	under_development	Resistant	aac(6)-Ib-cr

Table S7: **KP3 (May 2019)** - Resistance phenotypes predicted from whole genome sequence data by ResFinder.

10.5 Supplementary data for Chapter 6

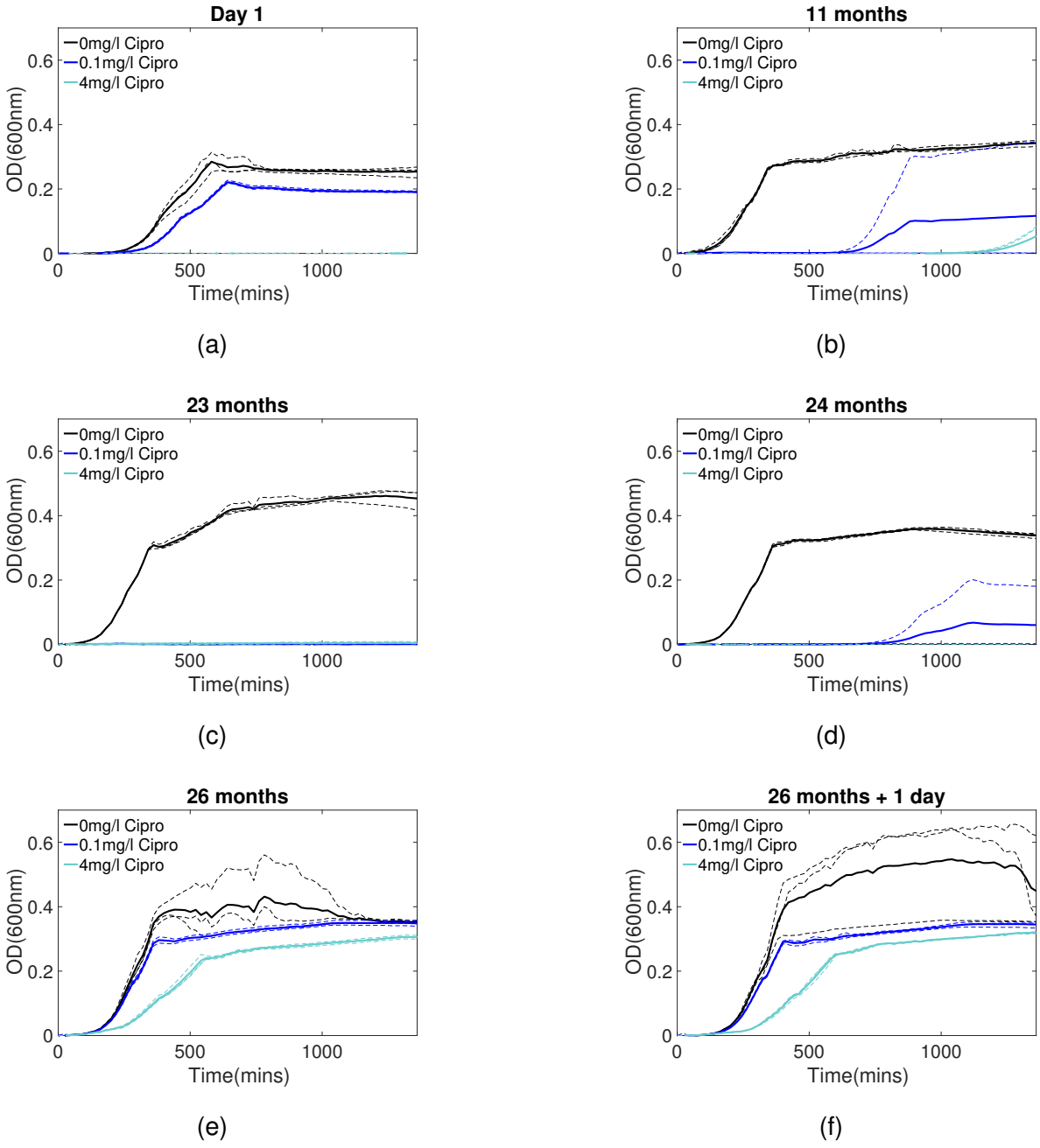

Figure S37: The growth of the six *E.coli* isolates in response to ciprofloxacin over 24 hours. Growth was measured as OD_{600nm}. *n=3*

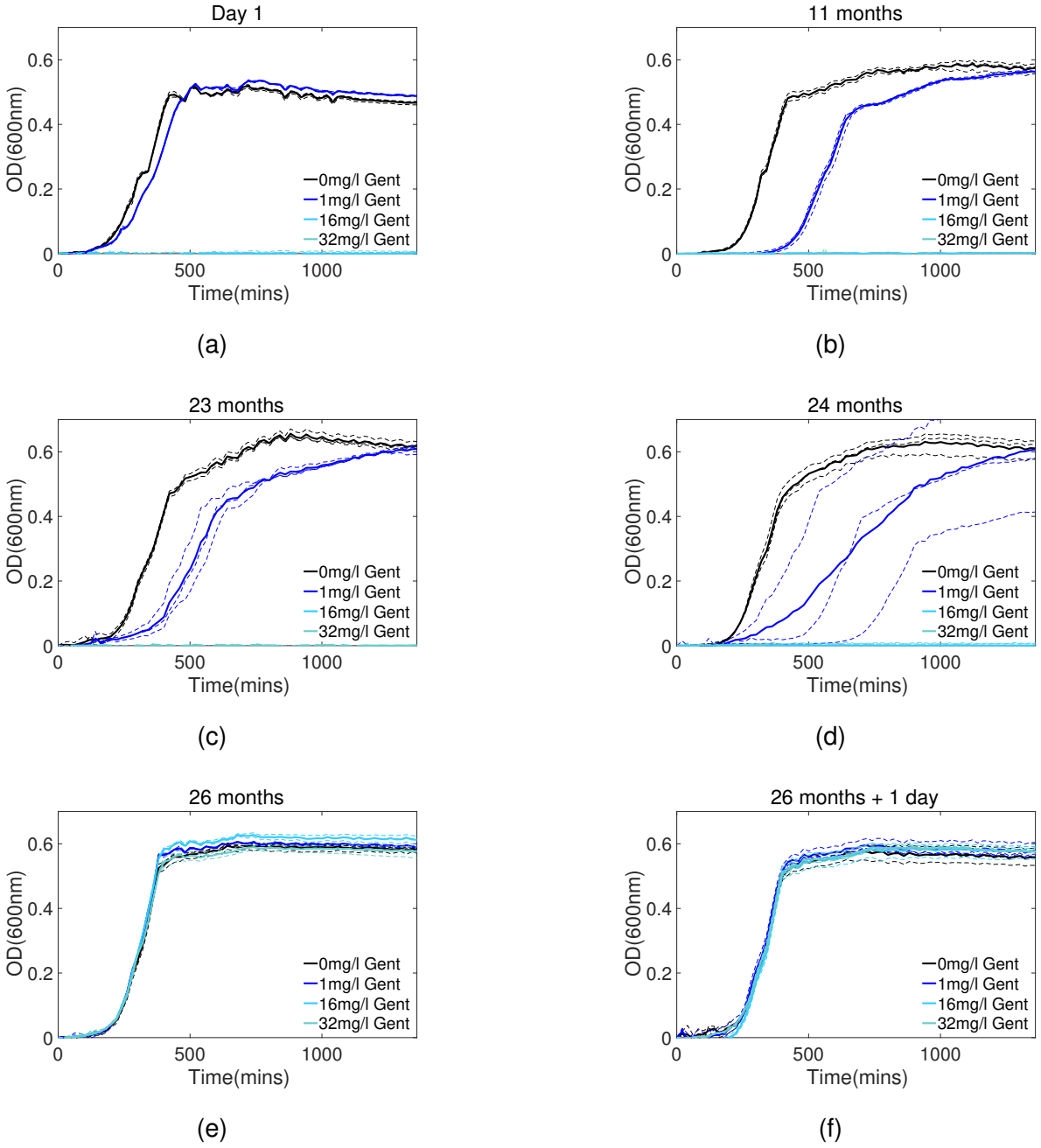

Figure S38: The growth of the six *E.coli* isolates in response to genatmicin over 24 hours. Growth was measured as OD_{600nm}. *n=3*.

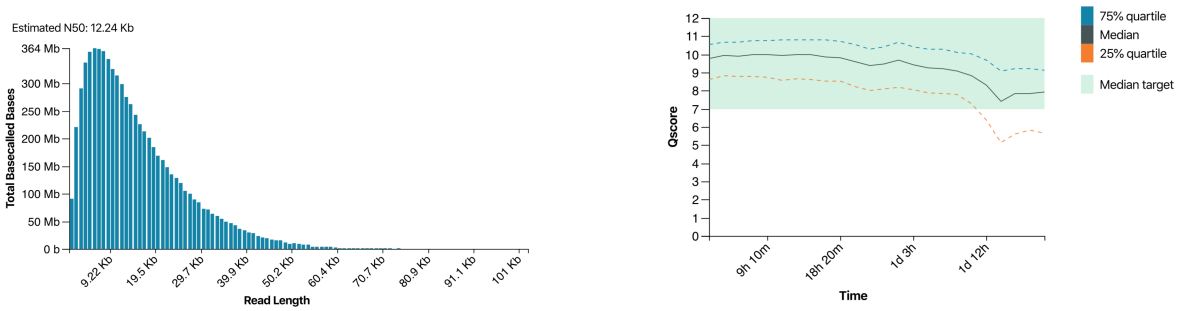

(a) (b)

Figure S39: The distribution of read lengths (a) and changes in Qscore (b) from a 40 hour minION sequence run with 12 multiplexed *E.coli* samples.

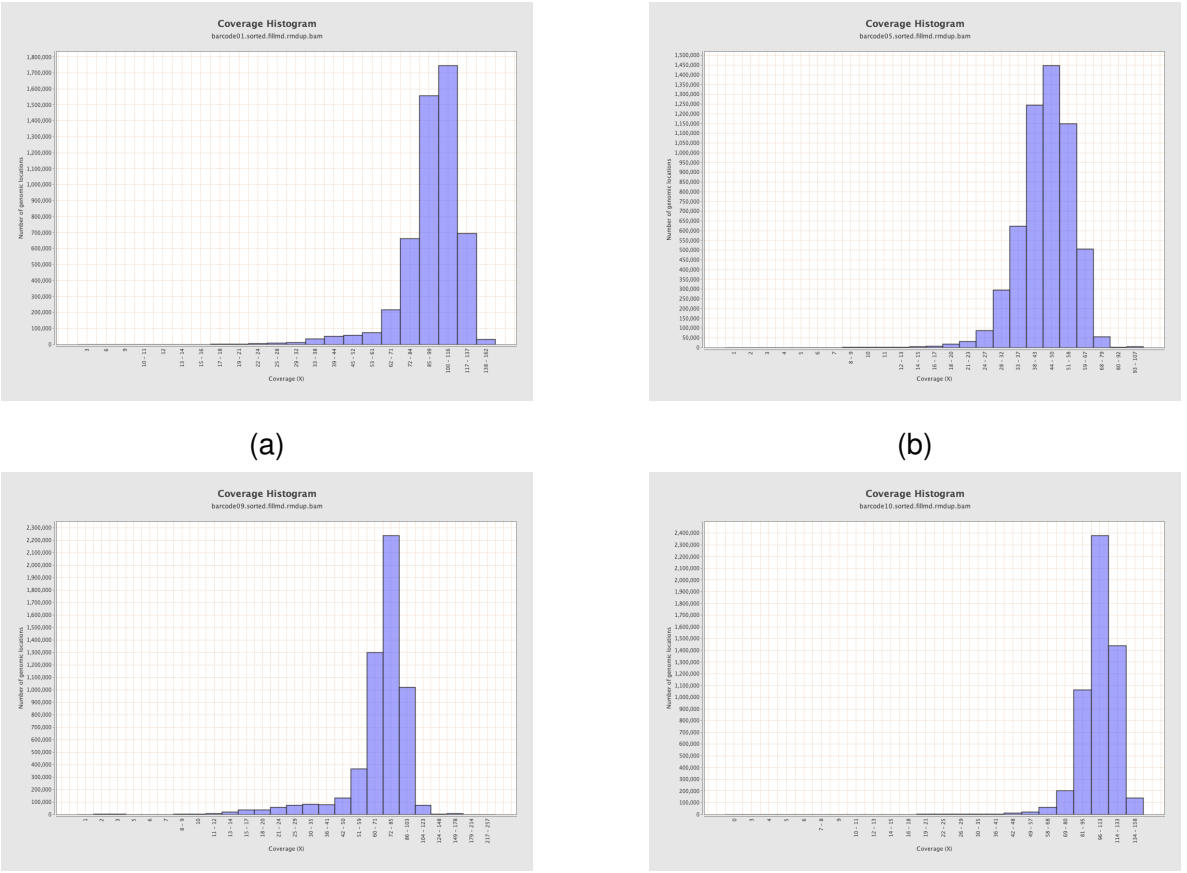

(a) (b)

(c) (d)

Figure S40: Histograms showing the distribution of coverage across genomic locations in the isolates EC1 (a), EC2 (b), EC3 (c) and EC4 (d). Obtained using qualimap.

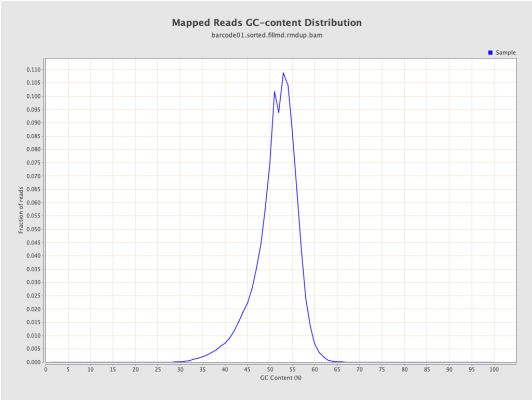

(a)

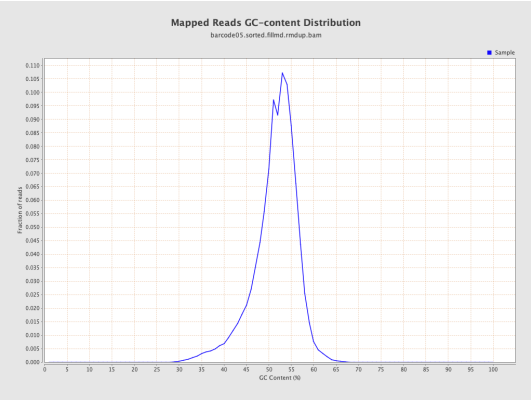

(b)

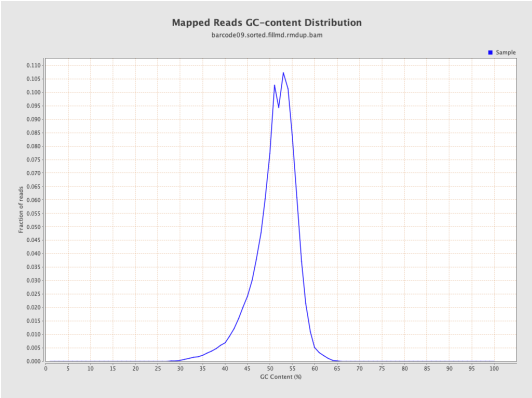

(c)

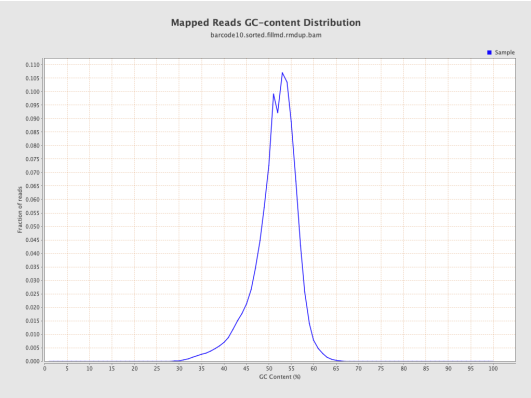

(d)

Figure S41: Histograms showing the distribution of GC content across all mapped reads in the isolates EC1 (a), EC2 (b), EC3 (c) and EC4 (d). Obtained using qualimap.

Antimicrobial	Class	WGS-predicted phenotype	Genetic background
ceftazidime	beta-lactam	Resistant	ampC-promoter (g.-42C>T)
piperacillin	beta-lactam	Resistant	ampC-promoter (g.-42C>T)
amoxicillin+clavulanic acid	beta-lactam	Resistant	ampC-promoter (g.-42C>T)
cefoxitin	beta-lactam	Resistant	ampC-promoter (g.-42C>T)
cefotaxime	beta-lactam	Resistant	ampC-promoter (g.-42C>T)

Table S8: **EC1 (Day 1)** - Resistance phenotypes predicted from whole genome sequence data by ResFinder.

Antimicrobial	WGS-predicted phenotype	Class	Genetic background
streptomycin	aminoglycoside	Resistant	aadA1
cephalothin	beta-lactam	Resistant	blaTEM-1C
piperacillin	beta-lactam	Resistant	blaTEM-1C
ampicillin	beta-lactam	Resistant	blaTEM-1C
ticarcillin	beta-lactam	Resistant	blaTEM-1C
amoxicillin	beta-lactam	Resistant	blaTEM-1C
tetracycline	tetracycline	Resistant	tet(A)
doxycycline	tetracycline	Resistant	tet(A)
spectinomycin	aminocyclitol	Resistant	aadA1
trimethoprim	folate pathway antagonist	Resistant	dfrA1
sulfamethoxazole	folate pathway antagonist	Resistant	sul1

Table S9: **EC2 (11 Months)** - Resistance phenotypes predicted from whole genome sequence data by ResFinder.

Antimicrobial	Class	WGS-predicted phenotype	Genetic background
spectinomycin	aminocyclitol	Resistant	aadA1
trimethoprim	folate pathway antagonist	Resistant	dfrA1
sulfamethoxazole	folate pathway antagonist	Resistant	sul2
piperacillin	beta-lactam	Resistant	blaTEM-1B
ampicillin	beta-lactam	Resistant	blaTEM-1B
ticarcillin	beta-lactam	Resistant	blaTEM-1B
cephalothin	beta-lactam	Resistant	blaTEM-1B
amoxicillin	beta-lactam	Resistant	blaTEM-1B
doxycycline	tetracycline	Resistant	tet(B) tet(A)
minocycline	tetracycline	Resistant	tet(B)
tetracycline	tetracycline	Resistant	tet(B) tet(A)
streptomycin	aminoglycoside	Resistant	aph(6)-Id aph(3)-Ib aadA1

Table S10: **EC3 (23 Months)** - Resistance phenotypes predicted from whole genome sequence data by ResFinder.

Antimicrobial	Class	WGS-predicted phenotype	Genetic background
doxycycline	tetracycline	Resistant	tet(A)
tetracycline	tetracycline	Resistant	tet(A)
ceftriaxone	beta-lactam	Resistant	blaCTX-M-1
cefepime	beta-lactam	Resistant	blaCTX-M-1
ticarcillin	beta-lactam	Resistant	blaCTX-M-1
piperacillin	beta-lactam	Resistant	blaCTX-M-1
aztreonam	beta-lactam	Resistant	blaCTX-M-1
ceftazidime	beta-lactam	Resistant	blaCTX-M-1
amoxicillin	beta-lactam	Resistant	blaCTX-M-1
ampicillin	beta-lactam	Resistant	blaCTX-M-1
cefotaxime	beta-lactam	Resistant	blaCTX-M-1
sulfamethoxazole	folate pathway antagonist	Resistant	sul2

Table S11: **EC4 (26 Months)** - Resistance phenotypes predicted from whole genome sequence data by ResFinder.

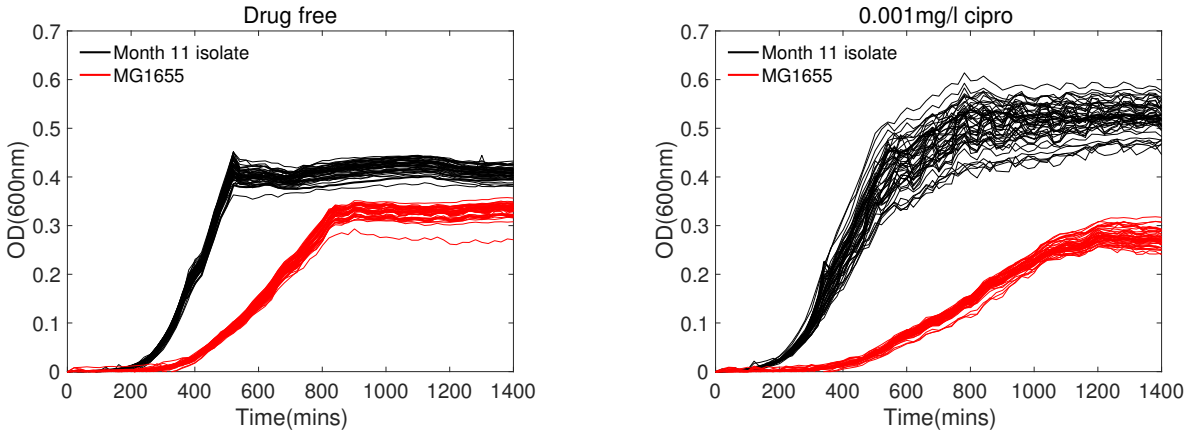

(a) (b)

Figure S42: There is little variation in growth between replicates with both *E.coli* isolates EC2 (Month 11) and MG1655 in the absence of antibiotic. However, with 0.001mg/l ciprofloxacin, there is variation in the growth curves of isolate EC2 but not MG1655. This variation was confirmed to be due to filamentation in the presence of ciprofloxacin through microscopy.

References

[1] Bush, K., et al.: Tackling antibiotic resistance. *Nat Rev Microbiol* **9(12)**, 894–6 (2011)

[2] Heras-Canas, V., et al.: Antibiotic activity and concentrations in clinical samples from patients with chronic bacterial prostatitis. *Actas Urol Esp* **41(10)**, 631–38 (2017)

[3] Taccetti, G., et al.: Early antibiotic treatment for *Pseudomonas aeruginosa* eradication in patients with cystic fibrosis: a randomised multicentre study comparing two different protocols. *Thorax*. **67(10)**, 853–9 (2012)

[4] Ferrer, R., et al.: Empiric antibiotic treatment reduces mortality in severe sepsis and septic shock from the first hour: results from a guideline-based performance improvement program. *Crit Care Med.* **42(8)**, 1749–55 (2014)

[5] Lobritz, M., et al.: Antibiotic efficacy is linked to bacterial cellular respiration. *Proc Natl Acad Sci U S A.* **112(27)**, 8173–80 (2015)

[6] Chopra, I., Roberts, M.: Tetracycline antibiotics: mode of action, applications, molecular biology and epidemiology of bacterial resistance. *Microbiology and Molecular Biology Reviews* **65(2)**, 232–60 (2001)

[7] Reding-Roman, C., et al.: The unconstrained evolution of fast and efficient antibiotic-resistant bacterial genomes. *Nature Ecology and Evolution* **1**, 0050 (2017)

[8] Lin, X., Kan, L., Peng, X.: Fluctuation of multiple metabolic pathways is required for *Escherichia coli* in response to chlortetracycline stress. *Mol Biosyst* **10(4)**, 901–8 (2014)

[9] Bisellia, E., Schink, J., Gerland, U.: Slower growth of *Escherichia coli* leads to longer survival in carbon starvation due to a decrease in the maintenance rate. *Mol Syst Biol* p. e9478 (2020)

[10] Ghoul, M., Mitri, S.: The ecology and evolution of microbial competition. *Trends Microbiol* **24(10)**, 833–45 (2016)

[11] Slattery, M., Rajbhandari, I., Wesson, K.: Competition-mediated antibiotic induction in the marine bacterium *Streptomyces tenjimariensis*. *Microb Ecol*. **41(2)**, 90–6 (2001)

[12] Lee, N., et al.: Iron competition triggers antibiotic biosynthesis in *Streptomyces coelicolor* during coculture with *Myxococcus xanthus*. *ISME J* **14(5)**, 1111–24 (2020)

[13] Romero, D., Traxler, M., Lopez, D., Kotler, R.: Antibiotics as signal molecules. *Chemical reviews* **111(9)**, 5492–505 (2011)

[14] Price-Whelan, A., Dietrich, L., Newman, D.: Rethinking 'secondary' metabolism: physiological roles for phenazine antibiotics. *Nat Chem Biol* **2(2)**, 71–8 (2006)

[15] Stanton, I., et al.: Evolution of antibiotic resistance at low antibiotic concentrations including selection below the minimal selective concentration. *Commun Biol* **3(1)**, 467 (2020)

[16] Gullberg, E., et al.: Selection of resistant bacteria at very low antibiotic concentrations. *PLoS Pathog* **7(7)**, e1002,158 (2011)

[17] Linares, J., et al.: Antibiotics as intermicrobial signaling agents instead of weapons. *PNAS* **103(51)**, 19,484–9 (2006)

[18] Rachid, S., et al.: Effect of subinhibitory antibiotic concentrations on polysaccharide intercellular adhesin expression in biofilm-forming *Staphylococcus epidermidis*. *Antimicrob Agents Chemother* **44(12)**, 3357–63 (2000)

[19] Wang, D., Lin, Z.: An analogous wood barrel theory to explain the occurrence of hormesis: A case study of sulfonamides and erythromycin on *Escherichia coli* growth. *PLoS One* **12(7)**, e0181,321 (2017)

[20] Migliore, L., Rotini, A., Thaller, M.: Low doses of tetracycline trigger the *E. coli* growth: A case of hormetic response. *Dose Response* **11(4)**, 550–7 (2013)

[21] Grossman, T.: Tetracycline antibiotics and resistance. *Cold Spring Harb Perspect Med* **6(4)**, a025,387 (2016)

[22] Nguyen, F., et al.: Tetracycline antibiotics and resistance mechanisms. *Biol Chem*. **395(5)**, 559–75 (2014)

[23] Pankey, G., Sabath, L.: Clinical relevance of bacteriostatic versus bactericidal mechanisms of action in the treatment of gram-positive bacterial infections. *Clinical Infectious Diseases* **38(6)**, 864–70 (2004)

[24] Yang, Y., et al.: Changes in the carbon metabolism of escherichia coli during the evolution of doxycycline resistance. *Front Microbiol.* **10**, 2506 (2019)

[25] Ahler, E., et al.: Doxycycline alters metabolism and proliferation of human cell lines. *PLoS One* **8(5)**, e64,561 (2013)

[26] Petovari, G., et al.: Targeting cellular metabolism using rapamycin and/or doxycycline enhances anti-tumour effects in human glioma cells. *Cancer Cell Int.* **18**, 211 (2018)

[27] Oxenkrug, G., et al.: Minocycline effect on life and health span of drosophila melanogaster. *Aging Dis.* **3(5)**, 352–9 (2012)

[28] Houtkooper, R., et al.: Mitonuclear protein imbalance as a conserved longevity mechanism. *Nature* **497(7450**, 451–7 (2013)

[29] Kladna, A., et al.: Evaluation of the antioxidant activity of tetracycline antibiotics in vitro. *Luminescence.* **249-55**, 249–55 (2012)

[30] Clemens, D., et al.: Novel antioxidant properties of doxycycline. *Int J Mol Sci.* **19(12)**, 4078 (2018)

[31] Griffin, M., et al.: Tetracyclines: a pleitropic family of compounds with promising therapeutic properties. review of the literature. *Am J Physiol Cell Physiol* **299(3)**, 539–48 (2010)

[32] Garrido-Mesa, N., Zarzuelo, A., Galvez, J.: Minocycline: far beyond an antibiotic. *Br J Pharmacol.* **169(2)**, 337–52 (2013)

[33] Stokes, J., Lopatkin, A., Lobritz, M., Collins, J.: Bacterial metabolism and antibiotic efficacy. *Cell Metab* **30(2)**, 251–59 (2019)

[34] Kohanski, M., et al.: A common mechanism of cellular death induced by bactericidal antibiotics. *Cell.* **130(5)**, 797–810 (2007)

[35] Hong, Y., et al.: Post-stress bacterial cell death mediated by reactive oxygen species. *Proc. Natl. Acad. Sci.* **116**, 10,064–71 (2019)

[36] Wood, T., et al.: Bacterial persister cell formation and dormancy. *Appl Environ Microbiol* **79(23)**, 7116–21 (2013)

[37] Lopatkin, A., et al.: Clinically relevant mutations in core metabolic genes confer antibiotic resistance. *Science* **371**, 6531 (2021)

[38] Gil-Gil, T., et al.: The inactivation of enzymes belonging to the central carbon metabolism is a novel mechanism of developing antibiotic resistance. *mSystems* **5(3)**, e00,282–20 (2020)

[39] Martinez, J., et al.: Metabolic regulation of antibiotic resistance. *FEMS Microbiol Rev* **35(5)**, 768–89 (2011)

[40] Lo-Ten-Foe, J., et al.: Comparative evaluation of the vitek 2, disk diffusion, etest, broth microdilution, and agar dilution susceptibility testing methods for colistin in clinical isolates, including heteroresistant *Enterobacter cloacae* and *Acinetobacter baumannii* strains. *Antimicrob Agents Chemother* **51(10)**, 3726–30 (2007)

[41] Andersson, D., Hughes, D.: Effects of antibiotic resistance on bacterial fitness, virulence, and transmission. *ASM Press* pp. 307–18 (2007)

[42] Lenski, R., Mongold, J., Sniegowski, P.: Evolution of competitive fitness in experimental populations of *E. coli*: what makes one genotype a better competitor than another. *Antonie Van Leeuwenhoek* **73(1)**, 35–47 (1998)

[43] Papadopoulos, D., Schneider, D., Meier-Eiss, J.: Genomic evolution during a 10,000-generation experiment with bacteria. *Proc Natl Acad Sci U S A* **96(7)**, 3807–12 (1999)

[44] Lenski, R., Travisano, M.: Dynamics of adaptation and diversification: a 10,000-generation experiment with bacterial populations. *Proc Natl Acad Sci U S A* **91(15)**, 6808–14 (1994)

[45] Bergkessel, M., Basta, D., Newman, D.: The physiology of growth arrest: uniting molecular and environmental biology. *Nature Reviews Microbiology* **14(9)**, 549–62 (2016)

[46] Stocker, R.: Marine microbes see a sea of gradients. *Science* **338(6107)**, 628–33 (2012)

[47] Morita, R.: Bacteria in oligotrophic environments: Starvation survival lifestyle. *Springer* (1997)

[48] Navarro-Llorens, J., Tormo, A., Martinez-Garia, E.: Stationary phase in gram-negative bacteria. *FEMS Microbiology Reviews* **34(4)**, 476–95 (2010)

[49] Wortel, M., et al.: Metabolic enzyme cost explains variable trade-offs between microbial growth rate and yield. *PLoS Comput Biol* **14(2)**, e1006,010 (2018)

[50] Basan, M., et al.: Overflow metabolism in *Escherichia coli* results from efficient proteome allocation. *Nature* **528(7580)**, 99–104 (2015)

[51] Zarrinpar, A., Chaix, A., Yooseph, S., Panda, S.: Diet and feeding pattern affect the diurnal dynamics of the gut microbiome. *Cell Metab* **20(6)**, 1006–17 (2014)

[52] Hibbing, M., Fuqua, C., Parsek, M., Peterson, S.: Bacterial competition: surviving and thriving in the microbial jungle. *Nature reviews. Microbiology* **8(1)**, 15–25 (2010)

[53] Rozwandowicz, M., Brouwer, M., Fischer, J.: Plasmids carrying antimicrobial resistance genes in *Enterobacteriaceae*. *J Antimicrob Chemother.* **73(5)**, 1121–37 (2018)

[54] Mathers, A., Peirano, G., Pitout, J.: The role of epidemic resistance plasmids and international high-risk clones in the spread of multidrug-resistant *Enterobacteriaceae. Clin Microbiol Rev.* **28(3)**, 565–91 (2015)

[55] Poole, K.: Efflux pumps as antimicrobial resistance mechanisms. *Ann Med* **39(3)**, 162–76 (2007)

[56] Ghafourian, S., Sadeghifard, N., Soheili, S., Sekawi, Z.: Extended spectrum beta-lactamases: Definition, classification and epidemiology. *Curr Issues Mol Biol* **17**, 11–21 (2015)

[57] Choi, U., Lee, C.: Distinct roles of outer membrane porins in antibiotic resistance and membrane integrity in *Escherichia coli. Front Microbiol.* **10**, 953 (2019)

[58] Bush, K.: Past and present perspectives on β-lactamases. *Antimicrob Agents Chemother.* **62(10)**, e01,076–18 (2018)

[59] Benz, F., et al.: Plasmid- and strain-specific factors drive variation in esbl-plasmid spread in vitro and in vivo. *ISME J* (2020)

[60] Bradford, P.: Extended-spectrum beta-lactamases in the 21st century: characterization, epidemiology, and detection of this important resistance threat. *Clin Microbiol Rev*. **14(4)**, 933–51 (2001)

[61] Pitton, J.: Mechanisms of bacterial resistance to antibiotics. *Review of Physiology* pp. 15–93 (1972)

[62] Liakopoulos, A., Mevius, D., Ceccarelli, D.: A review of shv extended-spectrum *Front Microbiol.* **7**, 1374 (2016)

[63] Canton, R., Gonzalez-Alba, J., Galan, J.: Ctx-m enzymes: Origin and diffusion. *Front Microbiol.* **3**, 110 (2012)

[64] Hedges, R., Datta, N., Kontomichalou, P., Smith, J.: Molecular specificities of r factor-determined β-lactamases: correlation with plasmid compatibility. *J. Bacteriol.* **117**, 56–62 (1974)

[65] Sawa, T., Kooguchi, K., Moriyama, K.: Molecular diversity of extended-spectrum β-lactamases and carbapenemases, and antimicrobial resistance. *J Intensive Care.* **8**, 13 (2020)

[66] Nordmann, P., Poirel, L.: The difficult-to-control spread of carbapenemase producers among enterobacteriaceae worldwide. *Clin Microbiol Infect.* **20(9)**, 821–30 (2014)

[67] Yigit, H., et al.: Novel carbapenem-hydrolyzing beta-lactamase, kpc-1, from a carbapenem-resistant strain of *Klebsiella pneumoniae*. *Antimicrob Agents Chemother* **45(4)**, 1151–61 (2001)

[68] van Duin, D., Doi, Y.: The global epidemiology of carbapenemase-producing *Enterobacteriaceae*. *Virulence.* **8(4)**, 460–9 (2017)

[69] Arnold, S., et al.: Emergence of *Klebsiella pneumoniae* carbapenemase-producing bacteria. *South Med J* **104(1)**, 40–5 (2011)

[70] Logan, L., Weinstein, R.: The epidemiology of carbapenem-resistant enterobacteriaceae: The impact and evolution of a global menace. *J Infect Dis.* **215**, 28–36 (2017)

[71] Lauretti, L., Riccio, M., Mazzariol, A.: Cloning and characterization of blavim, a new integron-borne metallo-β-lactamase gene from a *Pseudomonas aeruginosa* clinical isolate. *Antimicrob Agents Chemother* **43**, 1584–90 (1999)

[72] Yong, D., Toleman, M., Giske, C.: Characterization of a new metallo-β-lactamase gene, blandm-1, and a novel erythromycin esterase gene carried on a unique genetic structure in *Klebsiella pneumoniae* sequence type 14 from india. *Antimicrob Agents Chemother* **53**, 5046–54 (2009)

[73] Tzouvelekis, L., Markogiannakis, A.: Carbapenemases in *Klebsiella pneumoniae* and other *Enterobacteriaceae*: an evolving crisis of global dimensions. *Clin Microbiol Rev.* **25(4)**, 682–707 (2012)

[74] Antunes, N., Lamoureaux, T., Toth, M.: Class d β-lactamases: are they all carbapenemases? *Antimicrob Agents Chemother.* **58(4)**, 2119–25 (2014)

[75] Poirel, L., Potron, A., Nordmann, P.: Oxa-48-like carbapenemases: the phantom menace. *J Antimicrob Chemother* **67(7)**, 1597–606 (2012)

[76] Tsai, Y., et al.: *Klebsiella pneumoniae* outer membrane porins ompk35 and ompk36 play roles in both antimicrobial resistance and virulence. *Antimicrob Agents Chemother.* **55(4)**, 1485–93 (2011)

[77] Wong, J., et al.: Ompk36-mediated carbapenem resistance attenuates st258 *Klebsiella pneumoniae* in vivo. *Nat Commun.* **10(1)**, 3957 (2019)

[78] Hamzaoui, Z., et al.: Role of association of ompk35 and ompk36 alteration and blaesbl and/or blaampc genes in conferring carbapenem resistance among non-carbapenemase-producing *Klebsiella pneumoniae*. *Int J Antimicrob Agents*. **52(6)**, 898–905 (2018)

[79] Snitkin, E., et al.: Tracking a hospital outbreak of carbapenem-resistant klebsiella pneumoniae with whole-genome sequencing. *Sci Transl Med* **4(148)**, 148ra116 (2012)

[80] Gorrie, C., et al.: Antimicrobial-resistant *Klebsiella pneumoniae* carriage and infection in specialized geriatric care wards linked to acquisition in the referring hospital. *Clin Infect Dis*. **67(2)**, 161–70 (2018)

[81] Charre, C., et al.: Evaluation of ngs-based approaches for sars-cov-2 whole genome characterisation. *Virus Evolution* **6(12)** (2020)

[82] Comas, I., et al.: Whole-genome sequencing of rifampicin-resistant *Mycobacterium tuberculosis* strains identifies compensatory mutations in rna polymerase genes. *Nat Genet* **44(1)**, 106–10 (2011)

[83] Blair, J., et al.: Acrb drug-binding pocket substitution confers clinically relevant resistance and altered substrate specificity. *Proc Natl Acad Sci U S A* **112(11)**, 3511–6 (2015)

[84] Wylie, K., Wylie, T., Minx, P., Rosen, D.: Sequencing of *Klebsiella pneumoniae* isolates to track strain progression in a single patient with recurrent urinary tract infection. *Front Cell Infect Microbiol.* **9(14)** (2019)

[85] Fuentes-Hernandez, A., et al.: Using a sequential regimen to eliminate bacteria at sublethal antibiotic dosages. *PLoS Biol.* **13(4)**, e1002,104 (2015)

[86] Baym, M., et al.: Spatiotemporal microbial evolution on antibiotic landscapes. *Science*. **353(6304)**, 1147–51 (2016)

[87] Yen, P., Papin, J.: History of antibiotic adaptation influences microbial evolutionary dynamics during subsequent treatment. *PLoS Biol* **15(8)**, e2001,586 (2017)

[88] Muller, M., dela Pena, A., Derendorf, H.: Issues in pharmacokinetics and pharmacodynamics of anti-infective agents: distribution in tissue. *Antimicrob Agents Chemother.* **48(5)**, 1441–1453 (2004)

[89] Greulich, P., Scott, M., Evans, M., Allen, R.: Growth-dependent bacterial susceptibility to ribosome-targeting antibiotics. *Mol Syst Biol* **11(3)**, 796 (2015)

[90] Nemeth, J., Oesch, G., Kuster, S.: Bacteriostatic versus bactericidal antibiotics for patients with serious bacterial infections: systematic review and meta-analysis. *J Antimicrob Chemother* **70(2)**, 382–95 (2015)

[91] Moller, T., et al.: Global responses to oxytetracycline treatment in tetracycline-resistant *Escherichia coli*. *Sci Rep* **10(1)**, 8438 (2020)

[92] Moullan, N., et al.: Tetracyclines disturb mitochondrial function across eukaryotic models: A call for caution in biomedical research. *Cell Rep* **10(10)**, 1681–91 (2015)

[93] Lee, G., Lim, J., Hyun, S.: Minocycline treatment increases resistance to oxidative stress and extends lifespan in drosophila via foxo. *Oncotarget* **8(50)**, 87,878–90 (2017)

[94] Farrell, M., Finkel, S.: The growth advantage in stationary-phase phenotype conferred by rpos mutations is dependent on the ph and nutrient environment. *J Bacteriol* **185(24)**, 7044–52 (2003)

[95] Ying, B., Honda, T., Tsuru, S.: Evolutionary consequence of a trade-off between growth and maintenance along with ribosomal damages. *PLoS One* **10(8)**, e0135,639 (2015)

[96] Rice, K., Bayles, K.: Molecular control of bacterial death and lysis. *Microbiol Mol Biol Rev* **27(1)**, 85–109 (2008)

[97] Cuny, C., et al.: Investigation of the first events leading to loss of culturability during *Escherichia coli* starvation: future nonculturable bacteria form a subpopulation. *J Bacteriol* **187(7)**, 2244–8 (2005)

[98] Biselli, E., Schink, S., Gerland, U.: Slower growth of *Escherichia coli* leads to longer survival in carbon starvation due to a decrease in the maintenance rate. *Mol Syst Biol.* **16(6)**, e9478 (2020)

[99] Pletnev, P., et al.: Survival guide: *Escherichia coli* in the stationary phase. *Acta Naturae* **7(4)**, 22–33 (2015)

[100] Zundel, M., Basturea, G., Deutscher, M.: Initiation of ribosome degradation during starvation in *Escherichia coli*. *RNA* **15(5)**, 977–83 (2009)

[101] Reeve, C., Amy, P., Matin, A.: Role of protein synthesis in the survival of carbon-starved *Escherichia coli* k-12. *J Bacteriol* **160(4)**, 1041–1046 (1984)

[102] Nicholson, W., Munakata, N., Horneck, G., Melosh, H., Setlow, P.: Resistance of bacillus endospores to extreme terrestrial and extraterrestrial environments. *Microbiol Mol Biol Rev* **64(3)**, 548–72 (2000)

[103] Vreeland, R., Rosenzweig, W., Powers, D.: Isolation of a 250 million-year-old halotolerant bacterium from a primary salt crystal. *Nature* **407**, 897–900 (2000)

[104] Kram, K., Finkel, S.: Culture volume and vessel affect long-term survival, mutation frequency, and oxidative stress of *Escherichia coli. Applied Environmental Microbiology* **80(5)**, 1732–8 (2014)

[105] Bergman, J., Wrande, M., Hughes, D.: Acetate availability and utilization supports the growth of mutant sub-populations on aging bacterial colonies. *PLoS One* **9(10)**, e109,255 (2014)

[106] Schink, S., et al.: Death rate of *E. coli* during starvation is set by maintenance cost and biomass recycling. *Cell Systems* **9**, 64–73 (2019)

[107] Takano, S., et al.: Density-dependent recycling promotes the long-term survival of bacterial populations during periods of starvation. *mBio* **8**, e02,336–16 (2017)

[108] Zinser, E., Kolter, R.: *E. coli* evolution during stationary phase. *Res Microbiol* **155**, 328–36 (2004)

[109] Zinser, E., Kolter, R.: Mutations enhancing amino acid catabolism confer a growth advantage in stationary phase. *J Bacteriol* **181**, 5800–7 (1999)

[110] Zinser, E., Kolter, R.: Prolonged stationary phase incubation selects for lrp mutants in *E. coli* k-12. *J. Bacteriol* **182**, 4361–5 (2000)

[111] Wayne, P.: Standards for antimicrobial susceptibility testing. 30th ed. clsi supplement. clsi document m100. *Clinical and Laboratory Standards Institute* (2020)

[112] Hewlett, M.: The evolution of resistance to multidrug antibiotic therapies. (2015)

[113] Bohannan, B., et al.: Trade-offs and coexistence in microbial microcosms. *Antonie Van Leeuwenhoek* **81(1-4)**, 107–15 (2002)

[114] Maharjan, R., et al.: The form of a trade-off determines the response to competition. *Ecol Lett.* **16(10)**, 1267–76 (2013)

[115] Mori, M., Marinari, E., De Martino, A.: A yield-cost tradeoff governs *Escherichia coli's* decision between fermentation and respiration in carbon-limited growth. *NPJ Syst Biol Appl* **1**, 16 (2019)

[116] Pfeiffer, T., Schuster, S., Bonhoeffer, S.: Cooperation and competition in the evolution of atp-producing pathways. *Science* **292(5516)**, 504–7 (2001)

[117] Szenk, M., Dill, K., de Graff, A.: Why do fast-growing bacteria enter overflow metabolism? testing the membrane real estate hypothesis. *Cell Syst* **5(2)**, 95–104 (2017)

[118] Li, Z., Nimtz, M., Rinas, U.: The metabolic potential of *Escherichia coli* bl21 in defined and rich medium. *Microb Cell Fact* **13(1)**, 45 (2014)

[119] Sezonov, G., Joseleau-Petit, D., D'Ari, R.: *Escherichia coli* physiology in luria-bertani broth. *J Bacteriol* **189(23)**, 8746–9 (2007)

[120] Bosdriesz, E., Molenaar, D., Teusink, B., Bruggeman, F.: How fast-growing bacteria robustly tune their ribosome concentration to approximate growth-rate maximization. *FEBS J* **282(10)**, 2029–44 (2015)

[121] Serbanescu, D., Ojkic, N., Banerjee, S.: Nutrient-dependent trade-offs between ribosomes and division protein synthesis control bacterial cell size and growth. *Cell Rep* **32(12)**, 108,183 (2020)

[122] Jaishankar, J., Srivastava, P.: Molecular basis of stationary phase survival and applications. *Front Microbiol* **16(8)**, 2000 (2017)

[123] Fessler, M., et al.: Short-term kinetics of rrna degradation in *Escherichia coli* upon starvation for carbon, amino acid or phosphate. *Mol Microbiol* **113(5)**, 951–63 (2020)

[124] Tipper, D.: Mode of action of beta-lactam antibiotics. *Pharmacol Ther* **27(1)**, 1–35 (1985)

[125] Campbell, E., et al.: Structural mechanism for rifampicin inhibition of bacterial rna polymerase. *Cell.* **104(6)**, 901–12 (2001)

[126] de Cristobal, R., Vincent, P., Salomon, R.: Multidrug resistance pump acrab-tolc is required for high-level, tet(a)-mediated tetracycline resistance in *Escherichia coli*. *J Antimicrob Chemother* **58(1)**, 31–36 (2006)

[127] Speer, B., Shoemaker, N., Salyers, A.: Bacterial resistance to tetracycline: mechanisms, transfer, and clinical significance. *Clin Microbiol Rev* **5(4)**, 387–399 (1992)

[128] Connell, S., Tracz, D., Nierhaus, K., Taylor, D.: Ribosomal protection proteins and their mechanism of tetracycline resistance. *Antimicrob Agents Chemother.* **47(12)**, 3675–3681 (2003)

[129] Chait, R., et al.: A differential drug screen for compounds that select against antibiotic resistance. *PLoS One* **5(12)**, e15,179 (2010)

[130] Whittle, G., et al.: Identification of a new ribosomal protection type of tetracycline resistance gene, tet(36), from swine manure pits. *Appl Environ Microbiol* **69(7)**, 4151–4158 (2003)

[131] Phaiboun, A., Zhang, Y., Park, B., Kim, M.: Survival kinetics of starving bacteria is biphasic and density-dependent. *PLoS Comput Biol* **11**, e1004,198 (2015)

[132] Finkel, S.: Long-term survival during stationary phase: evolution and the gasp phenotype. *Nat Rev Microbiol* **4**, 113–20 (2006)

[133] Zambrano, M., et al.: Microbial competition: *Escherichia coli* mutants that take over stationary phase cultures. *Science* **259**, 1757–60 (1993)

[134] Monod, J.: The growth of bacterial cultures. *Annual Review in Microbiology* **3**, 349–71 (1949)

[135] Inada, T., Kimata, K., Aiba, H.: Mechanism responsible for glucose-lactose diauxie in *Escherichia coli*: challenge to the camp model. *Genes to Cells* **1**, 293–301 (1996)

[136] Bruckner, R., Titgemeyer, F.: Carbon catabolite repression in bacteria: choice of the carbon source and autoregulatory limitation of sugar utilization. *FEMS Microbiology Letters* **209**, 141–8 (2002)

[137] Enjalbert, B., et al.: Acetate exposure determines the diauxic behavior of *Escherichia coli* during the glucose-acetate transition. *J Bacteriol* **197(19)**, 3173–81 (2015)

[138] Zaslaver, A., et al.: A comprehensive library of fluorescent transcriptional reporters for *Escherichia coli*. *Nat Methods* **3(8)**, 623–8 (2006)

[139] Bremer, H., Dennis, P.: Modulation of chemical composition and other parameters of the cell by growth rate. in: *Escherichia coli* and *Salmonella typhimurium*. *Cellular and Molecular Biology* **2**, 1553–69 (1996)

[140] Li, L., et al.: The transcriptomic signature of tigecycline in *Acinetobacter baumannii*. *Front Microbiol* (2020)

[141] Mitosch, K., Rieckh, G., Bollenbach, T.: Noisy response to antibiotic stress predicts subsequent single-cell survival in an acidic environment. *Cell Syst* **4(4)**, 393–403 (2017)

[142] Kornberg, H.: The role and control of the glyoxylate cycle in *Escherichia coli*. *Biochem J* **99(1)**, 1–11 (1966)

[143] Dolan, S., Welch, M.: The glyoxylate shunt, 60 years on. *Annu Rev Microbiol.* **(72)**, 309–30 (2018)

[144] Clark, D., Cronan, J.: Two-carbon compounds and fatty acids as carbon sources. *EcoSal Plus* **1(2)** (2005)

[145] Bernal, V., Castano-Cerezo, S., Canovas, M.: Acetate metabolism regulation in *Escherichia coli*: carbon overflow, pathogenicity, and beyond. *Appl Microbiol Biotechnol.* **100(21)**, 8985–9001 (2016)

[146] Jung, H., et al.: Metabolic perturbations in mutants of glucose transporters and their applications in metabolite production in *Escherichia coli*. *Microb Cell Fact*. **8(1)**, 170 (2019)

[147] Liu, X., Ferenci, T.: An analysis of multifactorial influences on the transcriptional control of ompf and ompc porin expression under nutrient limitation. *Microbiology* **147**, 2981–9 (2001)

[148] Ferenci, T., Phan, K.: How porin heterogeneity and trade-offs affect the antibiotic susceptibility of gram-negative bacteria. *Genes* **6(4)**, 1113–24 (2015)

[149] Ferenci, T.: Maintaining a healthy spanc balance through regulatory and mutational adaptation. *Mol Microbiol*. **57(1)**, 1–8 (2005)

[150] Escalante, A., Salinas Cervantes, A.: Current knowledge of the *Escherichia coli* phosphoenolpyruvate-carbohydrate phosphotransferase system: peculiarities of regulation and impact on growth and product formation. *Appl Microbiol Biotechnol* **94(6)**, 1483–94 (2012)

[151] Kimata, K., Tanaka, Y., Inada, T., Aiba, H.: Expression of the glucose transporter gene, ptsg, is regulated at the mrna degradation step in response to glycolytic flux in *Escherichia coli. EMBO J* **20(13)**, 3587–95 (2001)

[152] Avrani, S., Bolotin, E., Katz, S., Hershberg, R.: Rapid genetic adaptation during the first four months of survival under resource exhaustion. *Mol Biol Evol.* **34(7)**, 1758–69 (2017)

[153] Kram, K., Finkel, S.: Rich medium composition affects *Escherichia coli* survival, glycation, and mutation frequency during long-term batch culture. *Appl Environ Microbiol*. **81(13)**, 4442–50 (2015)

[154] Freddolino, P., Amini, S., Tavazoie, S.: Newly identified genetic variations in common *Escherichia coli* mg1655 stock cultures. *J Bacteriol.* **194(2)**, 303–6 (2012)

[155] Faure, D., et al.: Genomic changes arising in long-term stab cultures of *Escherichia coli*. *J Bacteriol.* **186**, 6437–42 (2004)

[156] Kinnersley, M., Holben, W., Rosenzweig, F.: *E unibus plurum*: genomic analysis of an experimentally evolved polymorphism in *Escherichia coli*. *PLoS Genet* **5**, e1000,713 (2009)

[157] Koo, M., et al.: A reducing system of the superoxide sensor soxr in *Escherichia coli*. *EMBO J.* **22(11)**, 2614–2622 (2003)

[158] McDougald, D., et al.: Defences against oxidative stress during starvation in bacteria. *Antonie Van Leeuwenhoek* **81(1-4)**, 3–13 (2002)

[159] Zorraquino, V., Kim, M., Rai, N., Tagkopoulos, I.: The genetic and transcriptional basis of short and long term adaptation across multiple stresses in *Escherichia coli. Mol Biol Evol* **34(3)**, 707–17 (2017)

[160] Kryazhimskiy, S., Plotkin, J.: The population genetics of dn/ds. *PLoS Genet* **4(12)**, e1000,304 (2008)

[161] Conrad, T., et al.: Rna polymerase mutants found through adaptive evolution reprogram *Escherichia coli* for optimal growth in minimal media. *PNAS* **107(47)**, 20,500–5 (2010)

[162] Melnyk, A., Wong, A., Kassen, R.: The fitness costs of antibiotic resistance mutations. *Evol Appl* **8(3)**, 273–83 (2015)

[163] Bollenbach, T., Quan, S., Chait, R., Kishony, R.: Non-optimal microbial responses to antibiotics underlies suppressive drug interactions. *Cell* **139(4)**, 707–18 (2009)

[164] Maeda, M., Shimada, T., Ishihama, A.: Strength and regulation of seven rrna promoters in *Escherichia coli. PLoS One*. **10(12)**, e0144,697 (2015)

[165] Molenaar, D., van Berlo, R., de Ridder, D., Teusink, B.: Shifts in growth strategies reflect tradeoffs in cellular economics. *Molecular Systems Biology* **5(323)** (2009)

[166] Dai, X., Zhu, M.: Coupling of ribosome synthesis and translational capacity with cell growth. *Trends Biochem Sci*. **45(8)**, 681–92 (2020)

[167] Paul, B., et al.: rrna transcription in *Escherichia coli*. Annu Rev Genet **38**, 749–70 (2004)

[168] Stevenson, B., Schmidt, T.: Life history implications of rrna gene copy number in *Escherichia coli*. *Appl Environ Microbiol* **70(11)**, 6670–7 (2004)

[169] Condon, C., et al.: rrna operon multiplicity in *Escherichia coli* and the physiological implications of *rrn* inactivation. J Bacteriol **177(14)**, 4152–6 (1995)

[170] Gyorfy, Z., et al.: Engineered ribosomal rna operon copy-number variants of *E. coli* reveal the evolutionary trade-offs shaping rrna operon number. *Nucleic Acids Res* **43(3)**, 1783–1794 (2015)

[171] Lovmar, M., Ehrenberg, M.: Rate, accuracy and cost of ribosomes in bacterial cells. *Biochimie* **88(8)**, 951–61 (2006)

[172] Li, L., et al.: Insight into synergetic mechanisms of tetracycline and the selective serotonin reuptake inhibitor, sertraline, in a tetracycline-resistant strain of *Escherichia coli*. *J. Antibio.* **70**, 944–53 (2017)

[173] Roller, B., Stoddard, S., Schmidt, T.: Exploiting rrna operon copy number to investigate bacterial reproductive strategies. *Nat Microbiol.* **1(11)**, 16,160 (2016)

[174] Klappenbach, J., Dunbar, J., Schmidt, T.: rrna operon copy number reflects ecological strategies of bacteria. *Appl Environ Microbiol.* **66(4)**, 1328–1333 (2000)

[175] Baba, T., et al.: Construction of *Escherichia coli* k-12 in-frame, single-gene knockout mutants: the keio collection. *Mol Syst Biol* **2** (2006)

[176] Cao, H., Butler, K., Hossain, M., Lewis, J.: Variation in the fitness effects of mutations with population density and size in *Escherichia coli*. *PLoS One* **9(8)**, e105,369 (2014)

[177] Liu, A., et al.: Antibiotic sensitivity profiles determined with an *Escherichia coli* gene knockout collection: generating an antibiotic bar code. *Antimicrob Agents Chemother* **54(4)**, 1393–1403 (2010)

[178] Nichols, R., et al.: Phenotypic landscape of a bacterial cell. *Cell* **144(1)**, 143–56 (2011)

[179] Mateus, A., et al.: The functional proteome landscape of *Escherichia coli*. *Nature* **588(7838)**, 473–8 (2020)

[180] Tatusov, R., Galperin, M., Natale, D., Koonin, E.: The cog database: a tool for genome-scale analysis of protein functions and evolution. *Nucleic Acids Res* **28(1)**, 33–36 (2000)

[181] Levin, B., et al.: A numbers game: Ribosome densities, bacterial growth, and antibiotic-mediated stasis and death. *mBio* **8(1)**, e02,253–16 (2017)

[182] Price, M., et al.: Mutant phenotypes for thousands of bacterial genes of unknown function. *Nature* **557(7706)**, 503–509 (2018)

[183] Joyce, A., et al.: Experimental and computational assessment of conditionally essential genes in *Escherichia coli*. *J Bacteriol* **188(23)**, 8259–71 (2006)

[184] Guzman, G., et al.: Reframing gene essentiality in terms of adaptive flexibility. *BMC Syst Biol* **12(1)**, 143 (2018)

[185] Kroner, G., Wolfe, M., Freddolino, P.: *Escherichia coli* lrp regulates one-third of the genome via direct, cooperative, and indirect routes. *J Bacteriol.* **201(3)**, e00,411–18 (2019)

[186] Harris, R., et al.: Mismatch repair protein mutl becomes limiting during stationary-phase mutation. *Genes Dev.* **11(18)**, 2426–37 (1997)

[187] Perez, A., et al.: Effect of transcriptional activators soxs, roba, and rama on expression of multidrug efflux pump acrab-tolc in *Enterobacter cloacae*. *Antimicrob Agents Chemother.* **56(12)**, 6256–66 (2012)

[188] Dubbs, J., Mongkolsuk, S.: Peroxide-sensing transcriptional regulators in bacteria. *J Bacteriol.* **194(20)**, 5495–5503 (2012)

[189] Dukan, S., Nystrom, T.: Oxidative stress defense and deterioration of growth-arrested *Escherichia coli* cells. *J Biol Chem.* **274(37)**, 26,027–32 (1999)

[190] Chung, P.: The emerging problems of *Klebsiella pneumoniae* infections: carbapenem resistance and biofilm formation. *FEMS Microbiol Lett.* **363(20)** (2016)

[191] Xu, M.: Bloodstream infections caused by *Klebsiella pneumoniae*: prevalence of blakpc, virulence factors and their impacts on clinical outcome. *BMC Infect Dis.* **18(1)**, 368 (2018)

[192] PHE.: Annual epidemiological commentary: Gram-negative bacteraemia, mrsa bacteraemia, mssa bacteraemia and *C. difficile* infections, up to and including financial year april 2017 to march 2018. (2018)

[193] WHO.: Global priority list of antibiotic-resistant bacteria to guide. research, discovery, and development of new antibiotics. (2017)

[194] Alizadeh, N., et al.: Evaluation of resistance mechanisms in carbapenem-resistant *Enterobacteriaceae*. *Infect Drug Resist* **13**, 1377–85 (2020)

[195] Findlay, J., et al.: Characterization of carbapenemase-producing *Enterobacteriaceae* in the west midlands region of england: 2007-14. *Journal of Antimicrobial Chemotherapy* **72(4)**, 1054–62 (2017)

[196] Pulzova, L., Navratilova, L., Comor, L.: Alterations in outer membrane permeability favor drug-resistant phenotype of *Klebsiella pneumoniae*. *Microb Drug Resist.* **23(4)**, 413–20 (2017)

[197] Ruiz, E., et al.: Acquisition of carbapenem resistance in multiresistant *Klebsiella pneumoniae* strains harbouring blactx-m-15, qnrs1 and aac(6')-ib-cr genes. *J Med Microbiol.* **61(5)**, 672–7 (2012)

[198] Bartolini, A., Frasson, I., Cavallaro, A.: Comparison of phenotypic methods for the detection of carbapenem non-susceptible *Enterobacteriaceae*. *Gut Pathog* **6**, 13 (2014)

[199] Rechenchoski, D., et al.: Antimicrobial activity evaluation and comparison of methods of susceptibility for *Klebsiella pneumoniae* carbapenemase (kpc)-producing enterobacter spp. isolates. *Braz J Microbiol.* **48(3)**, 509–14 (2017)

[200] Lat, A., Clock, S., Wu, F.: Comparison of polymyxin b, tigecycline, cefepime, and meropenem mics for kpc-producing *Klebsiella pneumoniae* by broth microdilution, vitek 2, and etest. *J Clin Microbiol.* **49**, 1795–8 (2011)

[201] Bulik, C., et al.: Comparison of meropenem mics and susceptibilities for carbapenemase-producing *Klebsiella pneumoniae* isolates by various testing methods. *J Clin Microbiol* **48(7)**, 2402–6 (2010)

[202] Ruppe, E., et al.: Investigating hospital outbreaks of kpc-producing *Klebsiella pneumoniae* with whole-genome sequencing. *Clin Microbiol Infect* **23(7)**, 470–5 (2017)

[203] Perdigao, J., et al.: Whole-genome sequencing resolves a polyclonal outbreak by extended-spectrum beta-lactam and carbapenem-resistant *Klebsiella pneumoniae* in a portuguese tertiary-care hospital. *Microb Genom* (2020)

[204] Smith, D., et al.: Persistent colonization and the spread of antibiotic resistance in nosocomial pathogens: resistance is a regional problem. *Proc Natl Acad Sci U S A.* **101(10)**, 3709–14 (2004)

[205] Hassan, M., et al.: Contamination of hospital surfaces with respiratory pathogens in bangladesh. *PLoS One.* **14(10)**, e0224,065 (2019)

[206] Weber, D., et al.: Role of hospital surfaces in the transmission of emerging health care-associated pathogens: norovirus, clostridium difficile, and acinetobacter species. *Am J Infect Control.* **38(5)**, S25–33. (2010)

[207] Huang, T., et al.: Copy number change of the ndm-1 sequence in a multidrug-resistant *Klebsiella pneumoniae* clinical isolate. *PLoS One.* **8(4)**, e62,774. (2013)

[208] Schechter, L., et al.: Extensive gene amplification as a mechanism for piperacillin-tazobactam resistance in *Escherichia coli. mBio* **9(2)**, e00,583–18 (2018)

[209] Pereira, C., et al.: The highly dynamic nature of bacterial heteroresistance impairs its clinical detection. *Commun Biol.* **4(1)**, 521. (2021)

[210] Nicoloff, H.: The high prevalence of antibiotic heteroresistance in pathogenic bacteria is mainly caused by gene amplification. *Nat Microbiol* **4**, 504–14 (2019)

[211] Belikova, D., et al.: Gene accordions cause genotypic and phenotypic heterogeneity in clonal populations of staphylococcus aureus. *Nat Commun* **11(1)**, 3526 (2020)

[212] Elliott, K., Cuff, L., Neidle, E.: Copy number change: evolving views on gene amplification. *Future Microbiol* **8(7)**, 887–99 (2013)

[213] Laehnemann, D., et al.: Genomics of rapid adaptation to antibiotics: convergent evolution and scalable sequence amplification. *Genome Biol Evol.* **6(6)**, 1287–301 (2014)

[214] Godfroid, M., et al.: Insertion and deletion evolution reflects antibiotics selection pressure in a *Mycobacterium tuberculosis* outbreak. *PLoS Pathog.* **16(9)**, e1008,357 (2020)

[215] Martinez, E., Holmes, N., Jelfs, P., Sintchenko, V.: Genome sequencing reveals novel deletions associated with secondary resistance to pyrazinamide in mdr *Mycobacterium tuberculosis. J Antimicrob Chemother.* **70(9)**, 2511–4 (2015)

[216] Forde, B., et al.: Population dynamics of an *Escherichia coli* st131 lineage during recurrent urinary tract infection. *Nat Commun.* **10(1)**, 3643 (2019)

[217] Ferrari, C., et al.: Multiple *Klebsiella pneumoniae* kpc clones contribute to an extended hospital outbreak. *Front Microbiol.* **10**, 2767 (2019)

[218] Chen, S.: Genomic diversity and fitness of *E. coli* strains recovered from the intestinal and urinary tracts of women with recurrent urinary tract infection. *Sci Transl Med* **5(184)**, 184ra60 (2013)

[219] Arredondo-Alonso, S., Willems, R., van Schaik, W., Schurch, A.: On the (im)possibility of reconstructing plasmids from whole-genome short-read sequencing data. *Microb Genom* **3(10)**, e000,128 (2017)

[220] de Sanctis, J., et al.: Complex prosthetic joint infections due to carbapenemase-producing *Klebsiella pneumoniae*: a unique challenge in the era of untreatable infections. *Int J Infect Dis.* **25**, 73–8 (2014)

[221] Michalik, S.: How does vitek 2 generate mic values? URL : `https://www.biomerieux-microbio.com/education/how-does-vitek-2-generate-mic-values/` (2017)

[222] Vitek 2 ast cards. URL : `https://www.biomerieux.co.uk/product/vitek-2-ast-cards`

[223] Krause, K., Serio, A., Kane, T., Connolly, L.: Aminoglycosides: An overview. *Cold Spring Harb Perspect Med* **6(6)**, a027,029 (2016)

[224] Papp-Wallace, K., Endimiani, A., Taracila, M., Bonomo, R.: Carbapenems: past, present, and future. *Antimicrob Agents Chemother* **55(11)**, 4943–60 (2011)

[225] Tan, T., Ng, S.: Comparison of etest, vitek and agar dilution for susceptibility testing of colistin. *Clin Microbiol Infect* **13(5)**, 541–4 (2007)

[226] Cury, A., Girardello, R., Duarte, A., Rossi, F.: Kpc-producing *Enterobacterales* with uncommon carbapenem susceptibility profile in vitek 2 system. *Int J Infect Dis* **93**, 118–20 (2020)

[227] Lee, S., et al.: Comparison of the vitek 2, microscan, and etest methods with the agar dilution method in assessing colistin susceptibility of bloodstream isolates of acinetobacter species from a korean university hospital. *J Clin Microbiol* **51(6)**, 1924–6 (2013)

[228] Lo-Ten-Foe, J., de Smet, A., Diederen, B., Kluytmans, J., van Keulen, P.: Comparative evaluation of the vitek 2, disk diffusion, etest, broth microdilution, and agar dilution susceptibility testing methods for colistin in clinical isolates, including heteroresistant *Enterobacter cloacae* and *Acinetobacter baumannii* strains. *Antimicrob Agents Chemother* **51(10)**, 3726–30 (2007)

[229] Gonzalez-Escalona, N., Allard, M., Brown, E., Sharma, S., Hoffmann, M.: Nanopore sequencing for fast determination of plasmids, phages, virulence markers, and antimicrobial resistance genes in shiga toxin-producing *Escherichia coli*. *PLoS One* **14(7)**, e0220,494 (2019)

[230] Brinda, K., et al.: Rapid inference of antibiotic resistance and susceptibility by genomic neighbour typing. *Nat Microbiol.* **5(3)**, 455–64 (2020)

[231] Diancourt, L., et al.: Multilocus sequence typing of *Klebsiella pneumoniae* nosocomial isolates. *J. Clin. Microbiol.* **43**, 4178–82 (2005)

[232] Marsh, J., et al.: Evolution of outbreak-causing carbapenem-resistant klebsiella pneumoniae st258 at a tertiary care hospital over 8 years. *mBio* **10(5)**, e01,945–19 (2019)

[233] Diestra, K., et al.: Multiclonal epidemic of *Klebsiella pneumoniae* isolates producing dha-1 in a spanish hospital. *Clin Microbiol Infect* **17(7)**, 1032–6 (2010)

[234] Kolmogorov, M., Yuan, J., Lin, Y., Pevzner, P.: Assembly of long, error-prone reads using repeat graphs. *Nat Biotechnol* **37(5)**, 540–6 (2019)

[235] Arredondo-Alonso, S., et al.: mlplasmids: a user-friendly tool to predict plasmid- and chromosome-derived sequences for single species. *Microb Genom* **4(11)**, e000,224 (2018)

[236] Carattoli, A., et al.: In silico detection and typing of plasmids using plasmidfinder and plasmid multilocus sequence typing. *Antimicrob Agents Chemother* **58(7)**, 3895–903 (2014)

[237] Bi, D., et al.: In silico typing and comparative genomic analysis of incfiik plasmids and insights into the evolution of replicons, plasmid backbones, and resistance determinant profiles. *Antimicrob Agents Chemother* **62(10)**, e00,764–18 (2018)

[238] Osborn, A., et al.: Mosaic plasmids and mosaic replicons: evolutionary lessons from the analysis of genetic diversity in incfii-related replicons. *Microbiology* **146**, 2267–75 (2000)

[239] Villa, L., et al.: Complete sequencing of an inch plasmid carrying the blandm-1, blactx-m-15 and qnrb1 genes. *Antimicrob Chemother.* **67(7)**, 71,645–50 (2012)

[240] Okonechnikov, K., Cones, A., Garcia-Alcalde, F.: Qualimap 2: advanced multi-sample quality control for high-throughput sequencing data. *Bioinformatics* (2015)

[241] Kamruzzaman, M., Iredell, J.: Crispr-cas system in antibiotic resistance plasmids in *Klebsiella pneumoniae*. *Front Microbiol* p. 2934 (2020)

[242] San Millan, A., MacLean, R.: Fitness costs of plasmids: a limit to plasmid transmission. *Microbiol Spectr* **5(5)** (2017)

[243] Bortolaia, V., et al.: Resfinder 4.0 for predictions of phenotypes from genotypes. *Journal of Antimicrobial Chemotherapy* **dkaa345** (2020)

[244] Poirel, L., Naas, T., Nordmann, P.: Diversity, epidemiology, and genetics of class d beta-lactamases. *Antimicrob Agents Chemother* **54(1)**, 24–38 (2010)

[245] Poirel, L., Revathi, G., Bernabeu, S.: Detection of ndm-1- producing *Klebsiella pneumoniae* in kenya. *Antimicrob Agents Chemother* **55**, 934–6 (2011)

[246] Sugumar, M., Kumar, K., Manoharan, A.: Detection of oxa-1 β-lactamase gene of *Klebsiella pneumoniae* from blood stream infections (bsi) by conventional pcr and in-silico analysis to understand the mechanism of oxa mediated resistance. *PLoS One*. **9(3)**, e91,800 (2014)

[247] Lehtinen, S., Huisman, J., Bonhoeffer, S.: Evolutionary mechanisms that determine which bacterial genes are carried on plasmids. *Evol Lett.* **5(3)**, 290–301 (2021)

[248] Svara, F., Rankin, D.: The evolution of plasmid-carried antibiotic resistance. *BMC Evol Biol.* **130**, 11 (2011)

[249] Lunha, K., et al.: High-level carbapenem-resistant oxa-48-producing *Klebsiella pneumoniae* with a novel ompk36 variant and low-level, carbapenem-resistant, non-porin-deficient, oxa-181-producing *Escherichia coli* from thailand. *Diagn Microbiol Infect Dis* **85(2)**, 221–6 (2016)

[250] Pfeifer, Y., Cullik, A., Witte, W.: Resistance to cephalosporins and carbapenems in gram-negative bacterial pathogens. *J Med Microbiol*. **300(6)**, 371–9 (2010)

[251] Durand-Reville, T., et al.: Kinetics of avibactam inhibition against class a, c, and d β-lactamases. *J Biol Chem*. **288(39)**, 27,960–71 (2013)

[252] Nelson, K., et al.: Resistance to ceftazidime-avibactam is due to transposition of kpc in a porin-deficient strain of *Klebsiella pneumoniae* with increased efflux activity. *Antimicrob Agents Chemother*. **61(10)**, e00,989–17 (2017)

[253] Babini, G., Livermore, D.: Are shv beta-lactamases universal in *Klebsiella pneumoniae*? *Antimicrob Agents Chemother.* **44(8)**, 2230 (2000)

[254] Kim, Y., Tae-Un, K., Hyung-Suk, B.: Characterization of extended spectrum β-lactamase genotype tem, shv, and ctx-m producing *Klebsiella pneumoniae* isolated from clinical specimens in korea. *J Microbiol Biotechnol* **16**, 889–95 (2006)

[255] Livermore, D., et al.: Oxa-1 β-lactamase and non-susceptibility to penicillin β-lactamase inhibitor combinations among esbl-producing *Escherichia coli*. *Antimicrob Chemother.* **74(2)**, 326–33 (2019)

[256] Ehmann, D., et al.: Kinetics of avibactam inhibition against class a, c, and d β-lactamases. *J Biol Chem* **288**, 27,960–71 (2013)

[257] Aktas, Z., Kayacan, C., Oncul, O.: In vitro activity of avibactam (nxl104) in combination with β-lactams against gram-negative bacteria, including oxa-48 β-lactamase-producing *Klebsiella pneumoniae. Int J Antimicrob Agents* **39**, 86–9 (2012)

[258] Vernet, V., et al.: Virulence factors (aerobactin and mucoid phenotype) in *Klebsiella pneumoniae* and *Escherichia coli* blood culture isolates. *FEMS Microbiol Lett* **130(1)**, 51–7 (1995)

[259] Joensen, K., et al.: Real-time whole-genome sequencing for routine typing, surveillance, and outbreak detection of verotoxigenic *Escherichia coli*. *J Clin Microbiol* **52(5)**, 1501–10 (2014)

[260] Russo, T., et al.: Aerobactin mediates virulence and accounts for increased siderophore production under iron-limiting conditions by hypervirulent (hypermucoviscous) *Klebsiella pneumoniae*. *Infect Immun.* **82(6)**, 2356–67 (2014)

[261] Montenegro, M., et al.: trat gene sequences, serum resistance and pathogenicity-related factors in clinical isolates of *Escherichia coli* and other gram-negative bacteria. *J Gen Microbiol.* **131(6)**, 1511–21 (1985)

[262] Hjort, K., Nicoloff, H., Andersson, D.: Unstable tandem gene amplification generates heteroresistance (variation in resistance within a population) to colistin in *Salmonella enterica*. *Mol Microbiol* **102(2)**, 274–89 (2016)

[263] Hastings, P., et al.: Mechanisms of change in gene copy number. *Nat Rev Genet.* **10(8)**, 551–64 (2009)

[264] Nazir, A., et al.: Structural genomics of repa, repb 1-carrying incfib family pa1705-qnrs, p911021-teta, and p1642-teta, multidrug-resistant plasmids from *Klebsiella pneumoniae*. *Infection and Drug Resistance* **13**, 1889–1903 (2020)

[265] Sedlazeck, F., et al.: Accurate detection of complex structural variations using single-molecule sequencing. *Nat Methods* **15(6)**, 461–68 (2018)

[266] Turton, J., et al.: Clonal expansion of *Escherichia coli* st38 carrying a chromosomally integrated oxa-48 carbapenemase gene. *J Med Microbiol* **65(6)**, 538–46 (2016)

[267] Carroll, A., Wong, A.: Plasmid persistence: costs, benefits, and the plasmid paradox. *Can J Microbiol.* **64(5)**, 293–304 (2018)

[268] Mathers, A., et al.: Chromosomal integration of the *Klebsiella pneumoniae* carbapenemase gene, blakpc, in *Klebsiella* species is elusive but not rare. *Antimicrob Agents Chemother.* **61(3)**, e01,823–16 (2017)

[269] Wang, G., Song, G., Xu, Y.: Association of crispr/cas system with the drug resistance in *Klebsiella pneumoniae. Infect Drug Resist.* **13**, 1929–35 (2020)

[270] Piddock, L.: Assess drug-resistance phenotypes, not just genotypes. *Nat Microbiol* **1**, 16,120 (2016)

[271] Katouli, M.: Population structure of gut *Escherichia coli* and its role in development of extra-intestinal infections. *Iran J Microbiol* **(2)**, 59–72 (2010)

[272] Manges, A., et al.: Global extraintestinal pathogenic *Escherichia coli* (expec) lineages. *Clin Microbiol Rev.* **32(3)**, e00,135–18 (2019)

[273] Sarowska, J., et al.: Virulence factors, prevalence and potential transmission of extraintestinal pathogenic *Escherichia coli* isolated from different sources: recent reports. *Gut Pathog* **11(10)** (2019)

[274] Decano, A., et al.: Complete assembly of *Escherichia coli* sequence type 131 genomes using long reads demonstrates antibiotic resistance gene variation within diverse plasmid and chromosomal contexts. *mSphere* **4(3)**, e00,130–19 (2019)

[275] Poolman, J., Wacker, M.: Extraintestinal pathogenic *Escherichia coli*, a common human pathogen: Challenges for vaccine development and progress in the field. *J Infect Dis* **213(1)**, 6–13 (2016)

[276] Baraniak, A., et al.: Evolution of tem-type extended-spectrum beta-lactamases in clinical *Enterobacteriaceae* strains in poland. *Antimicrob Agents Chemother* **49(5)**, 1872–80 (2005)

[277] Drawz, S., Bonomo, R.: Three decades of beta-lactamase inhibitors. *Clin Microbiol Rev* **23(1)**, 160–201 (2010)

[278] Carattoli, A.: Resistance plasmid families in *Enterobacteriaceae*. *Antimicrob Agents Chemother* **53**, 2227–38 (2009)

[279] Rodriguez, I., et al.: Chromosomal location of blactx-m genes in clinical isolates of *Escherichia coli* from germany, the netherlands and the uk. *Int J Antimicrob Agents* **43**, 553–7 (2014)

[280] Hirai, I., et al.: Detection of chromosomal blactx-m-15 in *Escherichia coli* o25b-b2-st131 isolates from the kinki region of japan. *Int J Antimicrob Agents* **42**, 500–6 (2013)

[281] Guenther, S., et al.: Chromosomally encoded esbl genes in *Escherichia coli* of st38 from mongolian wild birds. *J Antimicrob Chemother* **72(5)**, 1310–13 (2017)

[282] Anes, J., McCusker, M., Fanning, S.: The ins and outs of rnd efflux pumps in *Escherichia coli. Front Microbiol.* **6**, 587 (2015)

[283] Stojkovic, V., et al.: Antibiotic resistance evolved via inactivation of a ribosomal rna methylating enzyme. *Nucleic Acids Res.* **44(18)**, 8897–907 (2016)

[284] Hagel, S., et al.: Esbl colonization and acquisition in a hospital population: The molecular epidemiology and transmission of resistance genes. *PLoS One.* **14(1)**, e0208,505 (2019)

[285] Oteo, J., et al.: Extended-spectrum-β-lactamase-producing *Escherichia coli* as a cause of pediatric infections: report of a neonatal intensive care unit outbreak due to a ctx-m-14-producing strain. *Antimicrob Agents Chemother.* **56(1)**, 54–8 (2012)

[286] Levert, M.: Molecular and evolutionary bases of within-patient genotypic and phenotypic diversity in *Escherichia coli* extraintestinal infections. *PLoS Pathog* **6(9)**, e1001,125 (2010)

[287] Sokal, A., et al.: Acute cholangitis: Diagnosis and management. *J Visc Surg* **156(6)**, 515–25 (2019)

[288] Rodriguez-Villodres, A., et al.: Phylogeny, resistome, and virulome of escherichia coli causing biliary tract infections. *J Clin Med.* **8(12)**, 2118 (2019)

[289] Chetlin, S., Elliott, D.: Biliary bacteremia. *Arch Surg.* **102**, 303–7 (1971)

[290] Sinanan, M.: Acute cholangitis. *Infect Dis Clin North Am* **6**, 571–99 (1992)

[291] Ahmed, M.: Acute cholangitis - an update. *World J Gastrointest Pathophysiol* **9(1)**, 1–7 (2018)

[292] Melzer, M., et al.: Biliary tract infection and bacteraemia: presentation, structural abnormalities, causative organisms and clinical outcomes. *Postgrad Med J* **83(986)**, 773–6 (2007)

[293] Spanu, T., et al.: Evaluation of the new vitek 2 extended-spectrum beta-lactamase (esbl) test for rapid detection of esbl production in *Enterobacteriaceae* isolates. *J Clin Microbiol.* **44(9)**, 3257–62 (2006)

[294] Aldred, K., Kerns, R., Osheroff, N.: Mechanism of quinolone action and resistance. *Biochemistry* **53(510)**, 1565–74 (2014)

[295] Roberts, L., et al.: Intensive infection control responses and whole genome sequencing to interrupt and resolve widespread transmission of oxa-181 *Escherichia coli* in a hospital setting. *bioRxiv* p. 850628 (2019)

[296] Joensen, K., Tetzschner, A., Iguchi, A., Aarestrup, F., Scheutz, F.: Rapid and easy in silico serotyping of *Escherichia coli* isolates by use of whole-genome sequencing data. *J Clin Microbiol* **53(8)**, 2410–26 (2015)

[297] Larsen, M., et al.: Multilocus sequence typing of total genome sequenced bacteria. *J. Clin. Micobiol* **50(4)**, 1355–61 (2012)

[298] Rogers, B., Doi, Y.: Who is leading this dance? understanding the spread of *Escherichia coli* sequence type 131. *Gut Pathog* **34**, 370–2 (2013)

[299] Day, M., et al.: Diversity of sts, plasmids and esbl genes among *Escherichia coli* from humans, animals and food in germany, the netherlands and the uk. *J Antimicrob Chemother.* **71(5)**, 1178–82 (2016)

[300] Timofte, D., et al.: Detection and molecular characterization of *Escherichia coli* ctx-m-15 and *Klebsiella pneumoniae* shv-12 β-lactamases from bovine mastitis isolates in the united kingdom. *Antimicrob Agents Chemother* **58**, 789–94 (2014)

[301] Guillouzouic, A., et al.: Mlst typing of *Escherichia coli* isolates overproducing ampc β-lactamase. *J Antimicrob Chemother* **63**, 1290–2 (2009)

[302] Valat, C.: Pathogenic *Escherichia coli* in dogs reveals the predominance of st372 and the human-associated st73 extra-intestinal lineages. *Front Microbiol* **11**, 580 (2020)

[303] Shahada, F., et al.: Distribution of extended-spectrum cephalosporin resistance determinants in *Salmonella enterica* and *Escherichia coli* isolated from broilers in southern japan. *Poult Sci.* **92(6)**, 1641–9 (2013)

[304] Wang, J., et al.: Molecular characterization of bla esbl-harboring conjugative plasmids identified in multi-drug resistant *Escherichia coli* isolated from food-producing animals and healthy humans. *Front Microbiol* **4(188)** (2013)

[305] Hansen, K., et al.: Host-specific patterns of genetic diversity among inci1-iy and inck plasmids encoding cmy-2 β-lactamase in *Escherichia coli* isolates from humans, poultry meat, poultry, and dogs in denmark. *Appl Environ Microbiol.* **82(15)**, 4705–14 (2016)

[306] Fagerstrom, A., et al.: Comparative distribution of extended-spectrum beta-lactamase-producing *Escherichia coli* from urine infections and environmental waters. *PLoS One* **14(11)**, e0224,861 (2019)

[307] Knudsen, P., et al.: Transfer of a bla ctx-m-1-carrying plasmid between different *Escherichia coli* strains within the human gut explored by whole genome sequencing analyses. *Sci Rep* **8(1)**, 280 (2018)

[308] Ogura, Y., et al.: Comparative genomics reveal the mechanism of the parallel evolution of o157 and non-o157 enterohemorrhagic *Escherichia coli*. *Proc Natl Acad Sci U S A* **106**, 17,939–44 (2009)

[309] Kao, C., et al.: Comparative genomics of *Escherichia coli* sequence type 219 clones from the same patient: Evolution of the inci1 blacmy-carrying plasmid in vivo. *Front Microbiol.* **9**, 1518 (2018)

[310] Allen, R., et al.: Associations among antibiotic and phage resistance phenotypes in natural and clinical *Escherichia coli* isolates. *mBio* **8(5)**, e01,341–17 (2017)

[311] Edgar, R., Bibi, E.: Mdfa, an *Escherichia coli* multidrug resistance protein with an extraordinarily broad spectrum of drug recognition. *J Bacteriol* **179(9)**, 2274–80 (1997)

[312] Caroff, N., Espaze, E., Berard, I., Richet, H., Reynaud, A.: Mutations in the ampc promoter of *Escherichia coli* isolates resistant to oxyiminocephalosporins without extended spectrum beta-lactamase production. *FEMS Microbiol Lett* **173(2)**, 459–65 (1999)

[313] Jacoby, G.: Ampc beta-lactamases. *Clin Microbiol Rev.* **22(1)**, 161–82 (2009)

[314] Berrazeg, M., et al.: Mutations in b-lactamase ampc increase resistance of *Pseudomonas aeruginosa* isolates to antipseudomonal cephalosporins. *Antimicrob Agents Chemother* **59(10)**, 6248–55 (2015)

[315] Skold, O.: Sulfonamide resistance: mechanisms and trends. *Drug Resist Updat* **3**, 155–60 (2000)

[316] Kaper, J., Nataro, J., Mobley, H.: Pathogenic *Escherichia coli*. *Nat Rev Microbiol.* **2(2)**, 123–40 (2004)

[317] Miajlovic, H., Smith, S.: Bacterial self-defence: how *Escherichia coli* evades serum killing. *FEMS Microbiology Letters* **1(354)**, 1–9 (2014)

[318] Jaureguy, F., et al.: Host and bacterial determinants of initial severity and outcome of *Escherichia coli* sepsis. *J Clin Microbiol.* **13(9)**, 854–62 (2007)

[319] Mora-Rillo, M., et al.: Impact of virulence genes on sepsis severity and survival in *Escherichia coli* bacteremia. *Virulence* **6(1)**, 93–100 (2015)

[320] Moss, E., Maghini, D., Bhatt, A.: Complete, closed bacterial genomes from microbiomes using nanopore sequencing. *Nat Biotechnol.* **38(6)**, 701–7 (2020)

[321] Orr, J., Christensen, D., Wolfe, A., Rao, C.: Extracellular acidic ph inhibits acetate consumption by decreasing gene transcription of the tricarboxylic acid cycle and the glyoxylate shunt. *J Bacteriol.* **201(2)**, e00,410–18 (2018)

[322] Abrudan, M., et al.: Socially mediated induction and suppression of antibiosis during bacterial coexistence. *Proc Natl Acad Sci U S A.* **112(35)**, 11,054–9 (2015)

[323] Chao, L., Levin, B.: Structured habitats and the evolution of anticompetitor toxins in bacteria. *Proc Natl Acad Sci U S A.* **78(10)**, 6324–8 (1981)

[324] Nev, O., Jepson, A., Beardmore, R., Gudelj, I.: Predicting community dynamics of antibiotic-sensitive and -resistant species in fluctuating environments. *J R Soc Interface* **16(166)** (2020)

[325] Davies, N., Flasche, S., Jit, M., Atkins, K.: Within-host dynamics shape antibiotic resistance in commensal bacteria. *Nat Ecol Evol.* **3(3)**, 440–9 (2019)

[326] Sageerabanoo, S., Malini, A., Mangaiyarkarasi, T., Hemalatha, G.: Phenotypic detection of extended spectrum β-lactamase and amp-c β-lactamase producing clinical isolates in a tertiary care hospital: A preliminary study. *J Nat Sci Biol Med.* **6(2)**, 383–7 (2015)

[327] Garrec, H., et al.: Comparison of nine phenotypic methods for detection of extended-spectrum beta-lactamase production by enterobacteriaceae. *J Clin Microbiol.* **49(3)**, 1048–57 (2011)

[328] Blattner, F., et al.: The complete genome sequence of *Escherichia coli*k-12. *Science* **277**, 1453–62 (1997)

[329] Makinoshima, H., et al.: Growth phase-coupled alterations in cell structure and function of *Escherichia coli*. *J Bacteriol.* **185(4)**, 1338–45 (2003)

[330] Nystrom, T.: Stationary-phase physiology. *Annu Rev Microbiol.* **58**, 161–81 (2004)

[331] Martin, M.: Cutadapt removes adapter sequences from high-throughput sequencing reads. *EMBnet.journal* **17(1)**, 10–12 (2011)

[332] Li, H., Durbin, R.: Fast and accurate short read alignment with burrows-wheeler transform. *Bioinformatics* **25**, 1754–60 (2009)

[333] Koboldt, D., et al.: Varscan: variant detection in massively parallel sequencing of individual and pooled samples. *Bioinformatics* **25(17)**, 2283–5 (2009)

[334] Deatherage, D., Barrick, J.: Identification of mutations in laboratory-evolved microbes from next-generation sequencing data using breseq. *Methods Mol. Biol* **1151**, 165–88 (2014)

[335] Zaslaver, A., et al.: Just-in-time transcription program in metabolic pathways. *Nature Genetics* **36**, 486–91 (2004)

[336] Koren, S., et al.: Canu scalable and accurate long-read assembly via adaptive k-mer weighting and repeat separation. *Genome Res* **27(5)**, 722–36 (2017)

[337] Vaser, R., et al.: Fast and accurate de novo genome assembly from long uncorrected reads. *Genome Res* **27(5)**, 722–36 (2017)

[338] Aziz, R., et al.: The rast server rapid annotations using subsystems technology. *BMC Genomics*. **9**, 75 (2008)

[339] Seemann, T.: Prokka: rapid prokaryotic genome annotation. *Bioinformatics* **30(14)**, 2068–9 (2014)

[340] Malberg-Tetzschner, A., et al.: In silico genotyping of *Escherichia coli* isolates for extraintestinal virulence genes by use of whole-genome sequencing data. *J Clin Microbiol.* **58(10)**, :e01,269–20 (2020)

[341] Aaron, R., et al.: Bedtools: a flexible suite of utilities for comparing genomic features. *Bioinformatics* **6(15)**, 841–2 (2010)

[342] Sullivan, M., Petty, N., Beatson, S.: Easyfig: a genome comparison visualizer. *Bioinformatics.* **27(7)**, 1009–10 (2011)